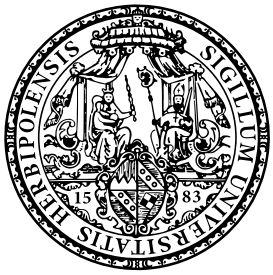

Replica Symmetry Breaking at Low Temperatures

Dissertation

zur Erlangung des
naturwissenschaftlichen Doktorgrades
der Julius-Maximilians-Universität Würzburg

vorgelegt von
Manuel J. Schmidt
aus Schwemmelsbach in Bayern

Würzburg, 2008

Eingereicht am 27. Juni 2008

bei der Fakultät für Physik und Astronomie

Gutachter der Dissertation:

1. Gutachter: Prof. Dr. Reinhold Oppermann

2. Gutachter: Prof. Dr. Björn Trauzettel

3. Gutachter: Prof. Dr. Cirano de Dominicis

Prüfer im Promotionskolloquium:

1. Prüfer: Prof. Dr. Reinhold Oppermann

2. Prüfer: Prof. Dr. Björn Trauzettel

3. Prüfer: Prof. Dr. Laurens W. Molenkamp

Tag des Promotionskolloquiums: 01.12.2008

Doktorurkunde ausgehändigt am: ....

to Elisabeth

Contents

1 Introduction **1**
- 1.1 Historical overview . . . 1
- 1.2 Modern applications in computer sciences . . . 3
  - 1.2.1 Computational complexity in optimization problems . . . 3
  - 1.2.2 Error-correcting codes . . . 4
  - 1.2.3 Neural networks . . . 5
- 1.3 Ergodicity breaking . . . 5
  - 1.3.1 Quenched disorder vs. annealed disorder . . . 6
  - 1.3.2 Replica trick . . . 6
- 1.4 Mean-field theory: from ferromagnetism to RSB . . . 7

2 Formalism at finite RSB **11**
- 2.1 The free energy in replica formalism . . . 12
  - 2.1.1 General formulation . . . 12
  - 2.1.2 Special case: Ising spin glass . . . 14
  - 2.1.3 Special case: (Quasi-)isotropic n-component spin glass . . . 15
- 2.2 The replica symmetric approximation . . . 16
  - 2.2.1 Special case: Ising spin glass . . . 18
  - 2.2.2 Special case: Quasi-isotropic n-component spin glass . . . 18
- 2.3 Parisi RSB . . . 19
  - 2.3.1 Ising spin glass (n=1) with finite J_0 and finite external field . . . 22
  - 2.3.2 The quasi-isotropic n-component spin glass . . . 24
  - 2.3.3 h-field integration . . . 25
- 2.4 Low temperature formalism . . . 26
  - 2.4.1 Parameter rescaling . . . 27
  - 2.4.2 Asymptotic renormalization group . . . 29
  - 2.4.3 The kernel correction function for an Ising spin glass . . . 30
  - 2.4.4 The kernel correction function at $T = 0$ for general n . . . 31
- 2.5 Observables in the replica formalism . . . 31
  - 2.5.1 Free/internal energy and entropy . . . 31
  - 2.5.2 Magnetic observables . . . 33
  - 2.5.3 Zero temperature and zero external field . . . 36

3 Analysis of the RS saddle point **39**
- 3.1 The Ising spin glass . . . 39
- 3.2 Isotropic n-component spin glass . . . 42

4 Results and discussion at finite order of RSB **45**
- 4.1 Analysis of thermodynamic observables . . . 45
  - 4.1.1 Free energy, internal energy and entropy . . . 46
  - 4.1.2 Magnetic susceptibilities . . . 51
  - 4.1.3 Connection to systems of finite size . . . 52
- 4.2 The order function . . . 53
  - 4.2.1 $q(a)$ at zero temperature and zero field . . . 54
  - 4.2.2 $q(a)$ at finite temperatures . . . 58

4.2.3 $q(a)$ at finite external fields . . . 60
4.3 Discreteness at zero temperature . . . 62
4.3.1 Discrete spectra in the block size ratios . . . 63
4.3.2 Two scales for the order function at zero temperature . . . 64
4.3.3 Criticality of the block size ratios . . . 66
4.4 Scaling analysis . . . 66
4.4.1 PaT-scaling . . . 67
4.4.2 Scaling in the continuous limit near $h = 0$, $T = 0$ . . . 68
4.4.3 Unified scaling at finite RSB . . . 69

5 Continuous RSB **73**
5.1 The continuous RSB transition of ker$\mathcal{C}$ . . . 73
5.2 Continuous RSB at finite temperatures . . . 75
5.3 The proper zero temperature continuous theory . . . 76
5.3.1 Replacement of the initial condition . . . 76
5.3.2 Solving the differential equations . . . 79
5.3.3 The fixed point at $a = \infty$ . . . 81
5.4 Sommers-Dupont Ansatz . . . 82
5.4.1 The method of functional Lagrange-multipliers . . . 82
5.4.2 The continuous self-consistency equations . . . 82
5.4.3 Self-consistence at $a = \infty$ . . . 83
5.4.4 Self-consistence in the full continuous a interval . . . 85
5.4.5 Relation to Pankov scaling . . . 86

6 Conclusion and outlook **87**

Acknowledgments **91**

A Proofs and derivations **93**
A.1 Steepest descent and replica limit . . . 93
A.2 First integration in the recursion sequence . . . 94
A.3 Irrelevance of the kernel normalization . . . 95
A.4 Asymptotic regime of the recursion relations . . . 95
A.5 Evaluation of replica sums . . . 96
A.6 The trace term in the entropy . . . 97

B The temperature dependence of $A(T)$ **99**

C Definitions and conventions **103**
C.1 Gaussian integral operators . . . 103
C.2 Parisi block size parameters and matrix elements . . . 104

D Numerics of the finite RSB formalism **105**
D.1 The program suite . . . 105
D.2 High precision arithmetics . . . 106

Bibliography **107**

Chapter 1

Introduction

Spin glass science is a relatively mature field of research and much work has been invested to experimentally investigate, as well as to theoretically model and understand the intriguing properties of this magnetically (dis)ordered[1] phase at low temperatures. However, up to now, many fundamental questions, e.g. what are the critical dimensions and what happens in finite-dimensional spin glasses, remain unanswered. Already at the beginning of the theoretical investigations it turned out that even the classical mean-field theory of a spin glass is technically and conceptually highly nontrivial, and its correct treatment requires a powerful tool, known as replica symmetry breaking (RSB). While researchers have gained some insight into the physics of RSB, meanwhile, the question of its relevance in finite-dimensional spin glasses is still hotly debated and no satisfactory theory which extends the mean-field model to finite dimensionality has been found, yet.

RSB as a fundamental issue in replica theory, however, has proved important in lots of other fields of physical and even of interdisciplinary research. Thus, it is important to gain a deeper understanding of RSB, to enlarge the tool kit of treating RSB and to extend the concept of RSB to more advanced situations beyond the simple model in which it has been discovered. My work focusses on the latter two points: a new formulation of the low-temperature theory has been developed which, for the first time, allows a $T = 0$ treatment of the Parisi-RSB[2] directly in the physical limit of infinite order of RSB. Further, this theory is extended from a pure classical Ising theory to general n-component spin systems with the aim of being able to generalize the concepts, developed in the present work, to quantum spin glasses.

Before going *in medias res*, however, I want to appropriately introduce the reader to the field of spin glass physics - the field in which RSB is rooted - beginning with a historical overview which focusses on the starting time in the 1970's and on the puzzles, physicists had to deal with during the first decade. After that, as an example for the interdisciplinary relevance, some applications of spin glass theory to computer sciences are shortly reviewed. Both the historical and the computer sciences overview are by no means complete - the sheer amount of work one finds in the literature is overwhelming - but should give the reader a good idea of what has been going on for the last three decades. Further, the point of ergodicity breaking must be raised in the introduction because of its importance for understanding the concept of replica theory. Finally, on the basis of a simple model of an Ising ferromagnet, the concepts and notations used throughout this thesis are introduced so that also the non-expert reader is able to understand the most important points of the discussion.

1.1 Historical overview

The year 1972 can be titled the starting year of spin glass research. The kick-off was an experimental investigation of the magnetic properties of Gold-Iron alloys at low temperatures [CM72]. Although these alloys were well investigated materials at that time, the sharp cusp in the magnetic susceptibility at low fields, which we now know is characteristic for spin glasses, has been measured for the first time and suggested the existence of a novel kind of phase transition. Though the idea of a phase characterized by frozen random spin configurations raised two years earlier in a seminal theoretical work of the later winner of the Nobel

[1] Whether the phase is ordered or disordered depends on the point of view: a characteristic autocorrelation time is large, or even infinite in spin glasses, while the orientations of the magnetic moments are random and thus don't give rise to a finite magnetization.

[2] By transforming to a different gauge, the theory has been treated by Sommers and Dupont at $T = 0$ directly [SD84].

Prize, Philip W. Anderson [And70], some details of the experiments, e.g. the sharpness of the cusp or the negative Néel temperature θ, could not be explained within available theories: the concept of a spin glass at that time rather suggested a distribution of freezing temperatures which contradicted the sharp cusp in the susceptibility measured in experiment, while, on the other hand, the negative θ contradicted an antiferromagnetic interpretation of the measurements. On that account, the authors of [CM72] ended up with the conclusion that they "do not yet have a model which can describe the antiferromagnetic ordering[3] with sharp transitions and negative values of θ".

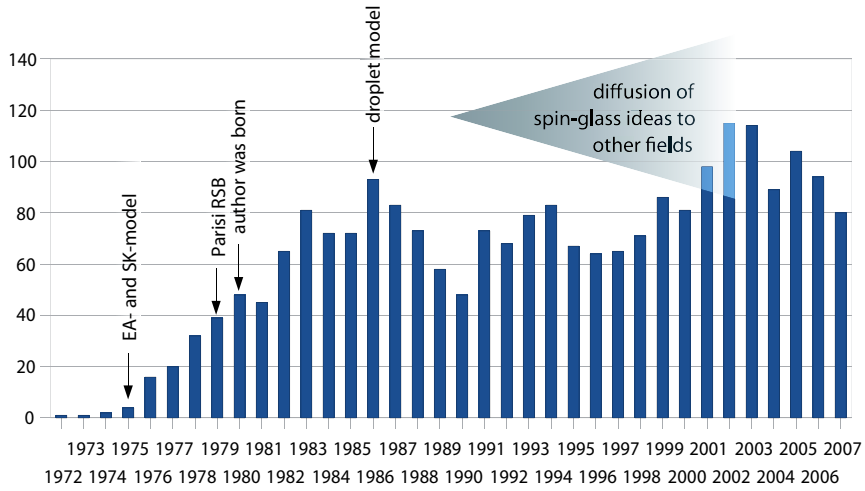

Fig. 1.1: Number of publications per year in all APS journals with *spin glass* in title or abstract from 1972 to 2007 (source: http://prola.aps.org). The most significant events during the first 15 years of spin glass research have been marked.

Three years later, in 1975, Edwards and Anderson came up with the first theoretical approach, based on random coupling of classical spins on a lattice [EA75], which could explain the susceptibility cusp in a spin glass material. From a theorists view, this celebrated Edwards-Anderson (EA) model was the foundation of the rapidly evolving field of spin glass research (see Fig. 1.1). Within the EA model, the experimentally observed sharp cusp of the magnetic susceptibility as well as the rounding of this cusp at non-zero external fields could be explained, and this was strong evidence for the principal validity of the EA spin glass concept.

Only shortly after the EA model has been proposed, David Sherrington and Scott Kirkpatrick (SK) investigated the mean-field theory of the EA model by explicitly assuming infinite range random interaction between spins [SK75]. They titled their work *Solvable model of a spin glass*, assuming that the approximation of infinite range interactions was sufficient for rendering the theory simple. They pointed out, however, that their treatment of the model was plagued by a negative entropy in the zero temperature limit, which indicated that something must be wrong with their type of analysis, based on the replica formalism. In 1977 then, a work, titled *Solution of 'Solvable model of a spin glass'* appeared [TAP77] in which the authors resort to a diagrammatic analysis of the SK-model and showed how to construct a consistent mean-field theory without the use of replicas. This theory is now known as TAP theory. The explicit analysis of the TAP equations, however, was cumbersome and comprised virtually no advantage.

In 1979, an extension to the SK-analysis appeared which allowed a consistent mean-field treatment within replica theory. Giorgio Parisi postulated a hierarchical scheme for a specific replica matrix [Par79] and derived an approximate formalism which becomes exact near the spin glass freezing temperature T_C. This hierarchical scheme, known as replica symmetry breaking (RSB) has been extended to $T < T_C$ later. The proper treatment of Parisi RSB at exactly $T = 0$, however, has not been understood for decades. Parisis RSB scheme has only been a proposition in 1979 in the sense that he didn't prove or derive this scheme. It just turned out that this scheme solves the inconsistencies of the SK-analysis. In fact, it took more than 25 years to rigorously prove that RSB yields the proper free energy [Tal06]. Nevertheless, though the form of the solution is well known and understood (it is an *order function* instead of an order parameter), numerically[4] finding the solution explicitly is still a nontrivial task; one must solve a self-consistency problem

[3] "Antiferromagnetic ordering" was synonymous for magnetic ordering without finite magnetic moment at that time.
[4] An approximate analytical solution is only possible for temperatures near the transition temperature.

which involves either a partial differential equation or many recursion equations. RSB theory, although it is a mean-field type theory, has been, and still is, a complicated business.

The main problem of RSB at the beginning of the 1980's was the lack of a proper physical interpretation of the hierarchical scheme of an infinite number of order parameters, which can be expressed as an *order function* $q(x)$. Progress on this issue happened in two different directions. In 1981, an alternative pseudo-dynamic theory has been developed by Sompolinsky [Som81, SZ81] which leads to the same formalism as the Parisi RSB, but without using the replica-formalism. Sompolinsky supplied an interpretation of $q(x)$ as an autocorrelation function parametrized by diverging relaxation times. Another appealing interpretation has been given three years later by M. Mezard et al. [MPS84]. Stimulated by the discovery of an ultrametric structure in the space of possible spin configurations, they directly translated the hierarchical structure of the Parisi Ansatz to a phase space property, namely the tree-like ordering of spin states. Up to today, ultrametricity is regarded as an important indication of RSB physics which is often used to identify mean-field like behavior e.g. in numerical simulations of finite range models [CGG07].

RSB is a mean-field theory and as such it is *a priori* only valid for infinite dimensions or infinite range interactions. The relevance of RSB in real spin glasses at finite dimensions and with short range interactions, however, was strongly questioned in 1986 as the so called *droplet model* was proposed by Fisher and Huse [FH86]. Since this time the two concepts - RSB with ultrametricity and the droplet picture - have been the two competing scenarios for real spin glasses. Up to now, none of the two scenarios could be proven true or false and so the debate about their domains of validity will probably go on for some time.

In the late 1980's the basic concepts in spin glass theory were settled and sufficiently scrutinized so that physicists thought about new applications to other fields. Over the years, many interesting topics in which RSB plays an important role have been investigated. They range from general glassy systems in physics, like e.g. the Coulomb-glass [MP01] or the structural glass [RV00, Sch03], over biophysical subjects as protein folding [RS94] to modern applications in computer science. Therefore, even if it turned out that it was irrelevant in real finite-dimensional spin glasses, there are many other reasons to investigate the beautiful complexity of replica symmetry breaking.

1.2 Modern applications in computer sciences

In order to further stress the interdisciplinary relevance of this work, I want to mention shortly three specific topics in computer sciences which are directly connected to models and methods which have their origin in spin glass theory.

1.2.1 Computational complexity in optimization problems

In computer science, the theory of computational complexity examins the cost (the amount of running time or memory) for solving a specific problem on a computer. A typical question to be answered in this context is: *Given a problem of size N, how do the resources, required for solving this problem on a deterministic computer, grow when increasing N?* The answers to such questions define several complexity classes; the two most important will be shortly described here[5]. The cost can grow polynomially (class P) on a deterministic computer or the cost can grow polynomially on a non-deterministic computer (class NP). Non-deterministic computers, however, are not directly available. They can only be simulated by deterministic computers in exponential time. Thus, in reality, NP means that the cost grows faster than polynomially with N, i.e. it grows exponentially in the worst case. As a result those problems are hard to treat numerically for large N, even with the best known algorithms[6]. Famous NP problems are, e.g., the Traveling Salesman Problem [GP06] or the Graph Coloring Problem [Wes96]. Interestingly, however, *all* members of the NP class are reducible to some specific NP problems, the totality of which defines the NP-complete complexity class - a subclass of NP. This means that if one finds an efficient algorithm for solving an NP-complete problem, this algorithm can be applied to all other NP problems, because all NP problems are mapable to an NP-complete problem in polynomial time.

[5] An extensive introduction to computational complexity with all complexity classes can be found in [Pap94].

[6] Though it is a general consensus between computer scientists that there exists no algorithm which solves an NP problem in polynomial time (this would be regarded as an efficient algorithm), this statement has not been rigorously proven. This proof (or the opposite) is one of the big tasks of complexity theory and one can earn 10^6\$ when solving it; the Clay Mathematics Institute stated P $\stackrel{?}{=}$ NP as one of the seven millennium problems.

One of the most famous members of the NP-complete class is the *Boolean satisfiability problem* (SAT) [GJ79]. It is especially interesting for theoretical physicists because it exhibits striking similarities to many-particle systems and even shows a phase transition [FA86, MZK99]. The driving parameter of this transition is the ratio $\alpha = \frac{M}{N}$ where M is the number of clauses which must be satisfied and N is the number of variables[7]. For small α, all clauses can be satisfied (SAT phase) while for $\alpha > \alpha_c$, the UNSAT phase is entered in which it is not possible to fulfill all clauses. This phase transition has several unexpected properties; e.g. the entropy (the number of solutions) is finite directly at the transition $\alpha = \alpha_c$ so that the UNSAT phase is not entered due to the successive vanishing of solutions but due to the appearance of a few unsatisfiable clauses which contradict a frozen 'backbone' of variables [MZK99].

The mapping of the SAT problem to a spin glass model [MZ96, MZ97, FA86] provided considerable insight to practical computational complexity in that problems which are computationally hard in the worst case need not necessarily be hard in the typical cases. Deep in the SAT phase ($\alpha \ll \alpha_c$), for instance, it is possible to find one solution of a typical SAT problem in polynomial time, while deep in the UNSAT phase ($\alpha \gg \alpha_c$) it is possible to efficiently verify the unsatisfiability. The density of untractable (i.e. inefficiently tractable) SAT problems is very low in these regions. Near the SAT↔UNSAT phase transition, however, the untractability density increases and one typically needs exponential time to solve the problem of finding a solution or of excluding the existence of a solution.

The mappings to statistical physics of the SAT and especially the 3-SAT problem[8] have been investigated by means of the replica formalism [MZ96, MZ97, CLP02] which is also used in the present work. The replica symmetric treatment of the model leads to a qualitatively proper picture of the important physics, but predicted the wrong critical number of clauses $\alpha_c \cdot N$. A replica symmetric treatment is not able to properly respect the large number of solutions in the SAT phase as well as the large number configurations with an equal number of unsatisfied clauses in the UNSAT phase. For a proper quantitative description the replica symmetry must be broken [MPRT04, MPZ02].

1.2.2 Error-correcting codes

Data storage has been important for mankind since the cognitive skills of the first human beings had sufficiently formed so that they were able to transfer information to their fellows. Probably the first forms of data storage on earth, we know of today, are cave paintings. Though the painters did certainly not care about *reliable* data storage over 30000 years ago, they obviously did a remarkably good job in conserving their creations over time. Today the reliability of stored data is somewhat more complex. If we are talking about data storage, we typically mean things like hard drives, DVDs or RAM in computers, and certainly, due to the digital form of the data, it is rather imporant to think about the reliability of those media and the robustness of our data with respect to perturbations. Also, and maybe this is even more important, in digital telecommunication one needs effective (and of course also efficient) methods to deal with the perturbations which are imposed on the transfered data by a noisy communication channel. Correcting or even just identifying errors in a stream of zeros and ones, however, is nearly impossible, because some additional information about the data would be needed for this task. A simple example for such an additional information would be a parity bit[9]. In general, one must introduce redundancy in the data, stored on a non-reliable disk or transmitted through some communication channel, in order to be able to restore the original data in the end. This is done by creating codewords for the data according to some definite rules which are called *error-correcting codes* (ECC)[10].

Information theory has produced a great variety of such ECC which answer the question: *I have received a codeword with M bits and some of them are maybe wrong*[11]*. I know that the size of the original message is $N < M$ and I know how the sender coded his message into the M bits. What was the original message?* Interestingly, some of the codes say that one must construct a Hamiltonian H_c from the received data. The ground state of H_c is then the most probable sequence of the original data. The important point for physicists is that the model defined by H_c is spin-glass-like and so ECC is a topic which is also of interest to the spin

[7] N also defines the size of the problem, mentioned above.

[8] K-SAT means that one OR clause contains exactly K literals.

[9] Say, the data stream is divided in blocks of 8 bits. Then, after each block, the sender can transmit a parity bit which is 1 if there has been an even number of 1's in the data block and zero otherwise. Thus, the receiver has a simple check whether the block arrived correctly or not.

[10] A parity bit, however, is typically not error correcting but only error detecting.

[11] Of course, the receiver does not know whether a given bit is wrong or not. If he knew it, e.g. by analyzing the medium on which it was stored, a good choice for an ECC would be a raptor code [Sho06].

glass community. The analysis of those Hamiltonians with the help of the tools of many-particle theory provided many interesting insights to information theory. For instance, it has been argued [Sou94, Ruj93] that it is more effective for decoding to calculate the local magnetization of the spin glass model defined by H_c at a specific finite temperature instead of evaluating the ground state, because the magnetization at a site provides one with the most probable bit while the ground state is only the most probable bit sequence. Recently, spin glasses have also been considered [TSN05] in the context of quantum error correcting codes which are needed for quantum computing. Since quantum information is not binary, error correction is even more important than in classical computing. Maybe, spin glass theory is also able to provide essential input to this rather modern topic.

1.2.3 Neural networks

The third field of computer science, I want to mention here, in which spin glass theory found interesting applications, are neural networks. The human brain, as a famous example of a neural network, is certainly one of the most complex and also one of the most fascinating objects we know of. The implications of insight into the functionality of the brain are unusually widespread, ranging from biology and medicine over physics and computer science to philosophy and theology. Especially the question whether something like a soul really exists or if all thoughts and emotions are 'only' a feature of a complex biological machine touches not only scientists. The immense complexity of the human brain, however, prevents direct answers to those fundamental questions. Toy models and thorough investigations of the collaborative effects which emerge from the interaction of many simple units (neurons) might eventually lead to a full understanding, but we will probably have to wait a long time until this will happen. Many of those simpler models, however, have properties which allow for interesting and even non-academic applications. For instance, neural networks can learn and recognize complex patterns [Zel94] or they can even be trained to play games - actually they play quite well, compared to the average human player [LS05].

When looking at neural networks, one can distinguish two main types. There is the feedforward network, which represents the simplest type of neural networks. Its topology is such that there is an input layer, a specific number of hidden layers and an output layer so that to each input vector, an output vector is calculated. Such a network is relatively easy to analyze because it is nothing else than a deterministic function. By properly adjusting the strengths of the synapses, the network can learn a desired function from a teacher[12]. The second important class of neural networks are the recurrent networks. Here, the topology does not allow to define a direction as in the feedforward net. The reason is that there exist feedbacks in those networks, as they also exist in a real brain. The analysis of those recurrent networks are considerably more complicated compared to the feedforward networks, but they are also much richer, and this makes them interesting also for physicists. In general, neural networks may be mapped to Ising spin systems such that the neurons correspond to the spins and the synapses are represented by the spin-spin interactions.

Already in the beginning of the 1980s J. J. Hopfield investigated a full recurrent neural network [Hop82, Hop84], consisting of a set of neurons which are completely interconnected by synapses with randomly chosen weights. He described this net by means of the statistical physics of the SK-model. The idea of many metastable states lead him to a kind of associative self-correcting memory device. Because of this construction, replica symmetry breaking clearly exists in the Hopfield net, but it has been shown that the difference of the solution from the replica symmetry approximation is not that severe [AGS87]. However, interesting *exotic* RSB properties have been observed in modified models of neural networks [DT92]. Still today, replica theory and the investigation of neural networks are intimately interconnected fields [HKN02, SY04, HHO06].

1.3 Ergodicity breaking

Phase transitions in statistical mechanics are generally due to a specific spontaneous symmetry breaking which forbids the access to parts of the phase space by the formation of energy barriers between the different domains of the phase space. As a result, the system is trapped in one 'valley' of the free energy landscape. These valleys are called ergodic components of the system. In the simplest case of a classical Ising ferromagnet, one can save oneself by introducing a symmetry breaking field $h > 0$ and let it go to zero after the thermodynamic limit has been performed. By this trick, one of the two ergodic components (spin-up or spin-down) are explicitly chosen.

[12] The learning procedure is typically implemented as a gradient descent in the space of the weights of all synapses.

In a spin glass, there is no such obvious symmetry breaking. The spins, though they are frozen at low temperatures, are randomly aligned. This fact prohibits the introduction of an artificial symmetry breaking field as for a ferromagnet. As a result, the mean-field theory must appropriately consider the whole phase space.

1.3.1 Quenched disorder vs. annealed disorder

One of the central questions at the beginning of the theory of disordered systems is how to incorporate disorder in a thermodynamic formalism. Theoretically, an observable $\mathcal{O}$, which is a function of the statistical variables, is measured in a system described by a Hamiltonian H by evaluating the trace

$$\langle \mathcal{O} \rangle_T = \frac{\text{tr } \left[e^{-\beta H} \mathcal{O} \right]}{\text{tr } \left[e^{-\beta H} \right]} \tag{1.1}$$

with respect to the statistical degrees of freedom. In a disordered system, however, beside the statistical degrees of freedom, one has to deal with 'disorder degrees of freedom' which also need to be averaged somehow[13]. The question is now, what quantity should be averaged. If the characteristic time of disorder fluctuation is much smaller than the observation time, i.e. $t_{\text{obs}} \gg \tau_{\text{dis}}$, then one can directly average the density matrix $\rho = \left\langle e^{-\beta H} \right\rangle_d$. This type of disorder is called *annealed disorder*.

In the opposite limit $t_{\text{obs}} \ll \tau_{\text{dis}}$ a different treatment, called *quenched disorder*, is in order. It turns out, that in this case one must average the natural logarithm of the partition function instead of the partition function itself. The crucial point of the argumentation leading to the quenched average [Bro59] is that in an experiment one measures an observable for one particular disorder realization. Since the sample is large, however, one effectively performs many measurements over sub-samples and implicitly averages over all those sub-measurements[14]. One only must assure that the coupling between the sub-systems is small - and this is typically justified by a surface to volume argument. Obviously, in such a system, which is called self-averaging, the observables must be averaged over disorder directly, i.e. the result of the measurement O of the observable $\mathcal{O}$ is given as

$$O = \langle \langle \mathcal{O} \rangle_T \rangle_d \tag{1.2}$$

where $\langle \cdot \rangle_T$ corresponds to a thermodynamic average and $\langle \cdot \rangle_{\text{dis}}$ corresponds to the disorder average. The thermodynamic average of an observable is typically proportional to the free energy f, or is a derivative of f. Since the free energy is proportional to $\log Z$, and a derivation commutes with the disorder average, it is clear that $\log Z$ should be averaged when dealing with the quenched case.

1.3.2 Replica trick

In spin glass theory one is especially interested in the quenched disorder average. It is obtained by averaging the natural logarithm of the partition function $Z = \text{tr } e^{-\beta H}$ of a system described by the Hamiltonian H. One method to cope with this kind of disorder average would be to write a theory which depends on a large set of random variables $\{J_{ij}\}$, calculate observables which depend parametrically on $\{J_{ij}\}$ and perform the average over the randomness of J_{ij} at the very end. This leads to a diagrammatic expansion of the free energy which is known as the TAP-theory of spin glasses [TAP77].

Another approach has been proposed by Edwards and Anderson [EA75] which enables the theorist to integrate the disorder distribution at the *beginning* of all calculations. The resulting theory does not depend on the large set of random variables anymore. This so-called replica trick is based on the identity

$$\log Z = \lim_{l \to 0} \frac{1}{l} (Z^l - 1). \tag{1.3}$$

Assume that the Hamiltonian $H = H[\{S_i\}, \{J_{ij}\}]$ can be written as a function of a set of dynamical variables $\{S_i\}$ and coupling parameters $\{J_{ij}\}$[15]. The trace operator acts on the dynamical variables only. In the lth

[13] This statement is not at all obvious and depends on the size of the spin glass system. In the macroscopic regime, where a spin glass is self-averaging [BY86], the disorder fluctuations indeed vanish. In a mesoscopic regime, however, the situation might well be different. The present work, however, focuses on large systems in which the thermodynamic limit $N \to \infty$ is applicable.

[14] This point is easily understood by considering the measurement of the magnetization in a large sample, consisting of many sub-samples.

[15] I start to use the common notation of J_{ij} as a random coupling constant and S_i as a dynamical spin-variable already here. Of course, the replica trick is not restricted to this kind of Hamiltonian. Another example of its application is an elegant proof of the linked-cluster theorem for Feynman diagrams (see e.g. [NO98]).

power of $Z = \mathrm{tr}\, e^{-\beta H}$, the dynamical variables must be labeled by a second index - the replica index $a = 1, ..., l$ - which denotes the membership of a specific S_i^a in replica a, because Z^l is formally identical to the partition function $Z_{(l)}$ of an l times replicated system without interactions between the different replicas. The configuration of the random variables $\{J_{ij}\}$ is the same in each replica. Thus, the quenched average of $\log Z$ can be written as

$$\langle \log Z \rangle_d = \lim_{l\to 0} \frac{1}{l} \left(\mathrm{tr} \left\langle \exp\left(-\beta \sum_{a=1}^{l} H\left[\{S_i^a\}, \{J_{ij}\}\right] \right) \right\rangle_d - 1 \right), \tag{1.4}$$

where tr is meant to act in the whole replicated space of all dynamical variables S_i^a. The disorder average now acts directly on the density matrix of the replicated system and can be performed by integrating with respect to J_{ij} with a specific distribution function of the random variables in the integral measure. The price for this convenience is the appearance of inter-replica couplings of higher order, the decoupling of which leads to the spin glass order parameter.

In equation (1.4) the conceptual difficulty within the replica trick can be observed: The parameter l which symbolizes the number of replicas and as such should be integer-valued, is, on the other hand, sent to zero in the replica limit $l \to 0$ and thus assumed to be a continuous parameter. This formal contradiction is resolved by explicitly rewriting the l-dependence of the replicated partition function $Z_{(l)}$ in such a way that it can be regarded as a continuous variable. Some steps in this procedure are by no means mathematically rigorous and therefore replica theory has earned much criticism over the years. It is only seen *a posteriori* that the results are physical[16] and so it is assumed that the replica trick appropriately incorporates the important physics. Nevertheless, it is a very appealing and widely accepted method which is deeply engrained and indispensable in the theory of glassy systems.

1.4 Mean-field theory: from ferromagnetism to RSB

In this section, I present a qualitative introductory discussion of the concept of replica symmetry breaking (RSB) in spin glass theory, starting with an application of the replica trick to a simple mean-field model of ferromagnetism [NO98]. The aim is to fix some notations used later by discussing their analogues in a theory in which the meaning of several terms is much clearer. Further, a first impression of the replica trick shall be conveyed to the reader before discussing it in all detail in Chapter 2. It turned out that refering to this simple model is useful for developing some physical intuition for the replica formalism and the quantities arising there.

Consider the Hamiltonian $H = -\frac{J_0}{2N} \sum_{i,j} S_i S_j$ of N Ising spins $S_i = \pm 1$. Instead of following the usual steps [NO98], however, I apply the replica trick, as introduced above, by writing

$$\log Z = \lim_{l\to 0} \frac{1}{l} \left(\mathrm{tr}\ \exp\left(-\beta \sum_{a=1}^{l} H[\{S_i^a\}] \right) - 1 \right) = \lim_{l\to 0} \frac{1}{l} \left(\mathrm{tr}\ \exp\left(\frac{\beta J_0}{2N} \sum_{a=1}^{l} \left(\sum_i S_i^a \right)^2 \right) - 1 \right). \tag{1.5}$$

The quadratic spin sum can be linearized with the help of a Hubbard-Stratonovich transformation by introducing an auxiliary field M_a for each replica. The physical meaning of M_a is a magnetization per replica. This results in the following expression for the replicated partition function:

$$Z_{(l)} = \prod_a \int \mathcal{D}M_a \exp\left(-\frac{\beta J_0 N}{2} \sum_a M_a^2 \right) \underbrace{\mathrm{tr}\ \exp\left(\beta \sum_{a,i} J_0 M_a S_i^a \right)}_{=\prod_{a,i} 2\cosh(\beta J_0 M_a)} \tag{1.6}$$

Since the different replicas are completely independent, one can set $M_a = M$ by symmetry. As a result, the sum and the product over the replica variable a can be replaced by a factor or an exponent l, respectively. The auxiliary field M is fixed in the thermodynamic limit by a saddle point integration so that the partition function becomes

$$Z_{(l)} = \exp\left(-Nl\beta \left(\frac{J_0}{2} M^2 - T \log 2\cosh(\beta J_0 M) \right) \right). \tag{1.7}$$

[16] Meanwhile, the correctness of the replica-treatment of the SK-model has been mathematically been proven with great effort [Tal06].

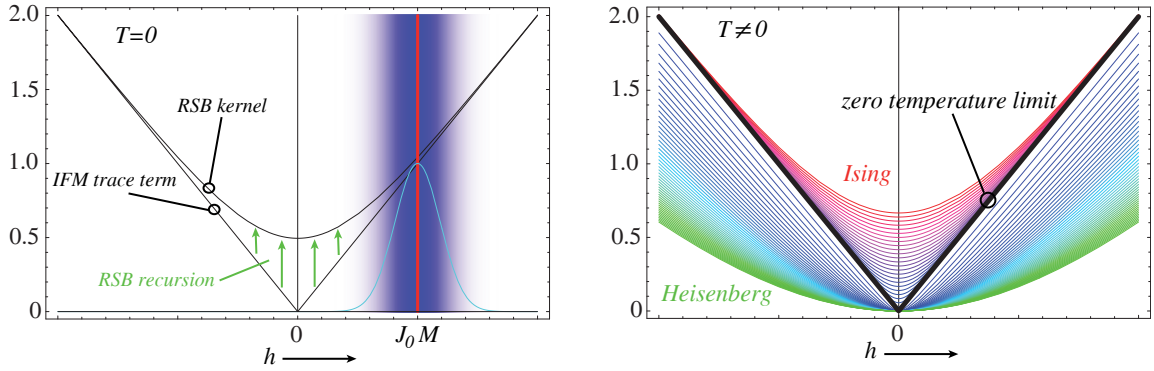

Fig. 1.2: *Left:* From a ferromagnet to a spin glass with replica symmetry breaking at $T = 0$. In the ferromagnet one evaluates the trace term at a single h-value while in a RSB spin glass one averages the RSB-kernel over a definite range in h. *Right:* The zero temperature limit of Ising and Heisenberg kernels. The thick black line is the zero temperature limit of integral kernels with an arbitrary number of components. The red (green) to blue lines are the Ising (Heisenberg) kernels from high to low temperatures, respectively.

In contrast to equation (1.5), the number l of replicas can be considered as a continuous variable in (1.7) and thus the replica limit can be performed to obtain the free energy per spin of an Ising ferromagnet (IFM)

$$f = \frac{J_0}{2}M^2 - \underbrace{T\log 2\cosh(\beta J_0 M)}_{\text{trace term}} \overset{T\to 0}{\longrightarrow} \frac{J_0}{2}M^2 - \underbrace{|J_0 M|}_{\mathcal{T}_{IFM}(J_0M)} \tag{1.8}$$

where the value of M must be found by minimizing f. I call the last term of the expressions *trace term* $\mathcal{T}_{IFM}(J_0M)$, as indicated in the formula, since it originates from the evaluation of the spin trace. The remaining terms result from the introduction of auxiliary fields in order to reduce the order of the spin-terms and therefore will be called field terms[17].

The trace term is the part of the free energy where, from a conceptual point of view, spin glass physics and RSB mainly enters. In the following I will discuss this point with the help of Figure 1.2. Since the effect of RSB is largest at low temperatures, a discussion directly at $T = 0$ is suggestive. At zero temperature, the trace term of the IFM is the absolute value of its argument and it must be evaluated exactly at the magnetization J_0M, as indicated by the red vertical line in Figure 1.2.

A first approximation in spin glass theory is the assumption of replica symmetry (RS). Its detailed derivation for the Ising spin glass considered here can be found in Chapter 2, near equation (2.19). The main effect of the RS treatment is the substitution of the IFM trace term in (1.8) by a Gaussian average of $\mathcal{T}_{IFM}$

$$\mathcal{T}_{IFM}(J_0M) \to \mathcal{T}_{RS}(J_0M) = \int \frac{dz}{\sqrt{2\pi}} e^{-\frac{z^2}{2}} \mathcal{T}_{IFM}(J_0M + J\sqrt{q}z), \tag{1.9}$$

where J is a measure of disorder in the spin glass and q is a spin glass order parameter. Obviously, for a spin glass, the trace term of the clean IFM system must be averaged over disorder in a first approximation and the width of the averaging is given by the amount of disorder J and the spin glass order parameter q[18]. This situation must be interpreted as follows: In contrast to the IFM case, where only one sharp value J_0M of the internal field exists, one must consider a certain *distribution of internal fields* in a spin glass. In Figure 1.2 the averaging is symbolized by the blue cloud and the Gaussian curve.

The proper treatment of the Ising spin glass requires the breaking of replica symmetry - a scheme with a hierarchy of many order parameters. This scheme contains recursion relations which depend on the order parameters and which successively change the integration kernel $\mathcal{T}_{IFM}$ which is averaged in (1.9) to the RSB kernel $\mathcal{K}_{RSB}$, as indicated by the arrows in Figure 1.2. The recursion relations change the kernel mainly at small arguments. At large arguments, there is an exponential cutoff of the RSB action. This fact will later

[17] The identification of the trace and field terms is not always unambiguous. Specific terms can be transformed from the trace term to the field term and vice versa, depending on convention. This ambiguity is immaterial, however. In the context of RSB, the important point is the non-triviality of the trace term which, in contrast to the field term, yields not analytically solvable integrals.

[18] q is also determined self-consistently by an additional term in f which is not discussed here.

be described in terms of a function ker$\mathcal{C}$, the kernel correction function[19], which describes the difference between $\mathcal{T}_{IFM}$ and $\mathcal{K}_{RSB}$. The RSB trace term then reads

$$\mathcal{T}_{RSB}(J_0 M) = \int \frac{dz}{\sqrt{2\pi}} e^{-\frac{z^2}{2}} \mathcal{K}_{RSB}(J_0 M + J\sqrt{q}z). \tag{1.10}$$

The transition from $\mathcal{T}_{IFM}$ to $\mathcal{K}_{RSB}$ again is due to a kind of averaging process in κ hierarchical steps. κ is called the order of RSB and each step i gives rise to two order parameters q_i and a_i. The proper values of those order parameters must be determined self-consistently and this is the main objective of replica-based spin glass theory. Actually, an infinite number of RSB steps is required to obtain the true mean-field solution of an Ising spin glass. As a result, an infinite number of order parameters is obtained, which have to be determined self-consistently. In this limit $\kappa \to \infty$, which is called continuous RSB, the set of order parameters give rise to an order function in terms of which the theory is formulated. In this case, the recursion relation passes over to a partial differential equation as discussed in Chapter 5.

In this work, also the extension of low temperature theory of an Ising spin glass to more than one spin components will be discussed. Already in the ferromagnet, one can see the typical zero temperature simplifications which also appear in replica theory and RSB. The ferromagnetic trace term is always of the form $T \log f(h/T)$ where f is a function with asymptotically exponential behavior. If, e.g. the Ising case is considered $f(x) \propto \cosh(x)$, while for the Heisenberg case one finds $f(x) \propto \sinh(x)/x$. In general, for n spin components, one can express $f(x)$ in terms of modified Bessel functions. One finds that the zero temperature limit of the trace term with a general number n of components is independent of n, i.e.

$$\lim_{T \to 0} T \log f(h/T) = |h|. \tag{1.11}$$

On the right side of Figure 1.2 the $T \to 0$ transition of the Ising ($n = 1$) and the Heisenberg ($n = 3$) kernels are shown. Clearly they become equal at $T = 0$. At zero temperature, the asymptotic behavior of the trace terms are the important regime and this statement remains true for spin glasses and replica symmetry breaking.

[19] In [SO08] it has been termed exponential correction function ker$\mathcal{C}$, because it formally corrects the argument of an exponential function. The author found the present term more appealing, however.

Chapter 2

Formalism at finite RSB

After the important points of the RSB formalism used in this thesis have been intuitively outlined in the introduction, in the present chapter the complete replica formalism, which is needed to properly treat the classical n-component spin glass with infinite range interactions and quenched disorder at low temperatures[1], will be derived. Let $\{\mathbf{S}_r\}$ denote the totality of N vector-spin variables spanning the configuration space. The spin glass system under consideration is described by the Hamiltonian

$$H(\{\mathbf{S}_r\}) = -\sum_{\nu}\sum_{r<r'} J^{\nu}_{rr'} S_{r\nu} S_{r'\nu} - \sum_{\nu,r} h_\nu S_{r\nu} \tag{2.1}$$

where r is a site label, ν labels the spin component, $J^{\nu}_{rr'}$ are random coupling constants and h_ν is a homogeneous external field. Throughout this work, a sum or a product over $x < x'$ (x can be a spatial index, a replica index, etc.) means that each pair of distinct (x, x') is considered exactly once. The classical spin variables $S_{r\nu}$ obey a normalization constraint $\mathbf{S}_r^2 = \sum_\nu (S_{r\nu})^2 = L_S^2$. The model defined by Hamiltonian (2.1) is a generalization of the well-known Sherrington-Kirkpatrick (SK) model of spin glasses [SK75] to an arbitrary number n of spin components. In analogy to the SK model, the probability distribution of the coupling constants is chosen Gaussian with properly scaled[2] mean and standard deviation

$$P^\nu(J^\nu_{rr'}) = \sqrt{\frac{N}{2\pi J_\nu^2}} \exp\left(-\frac{N}{2J_\nu^2}\left(J^\nu_{rr'} - J^\nu_0/N\right)^2\right). \tag{2.2}$$

This most general probability distribution function allows for all possible types of anisotropies. However, the explicit calculations - analytical as well as numerical - become extremely involved for (2.2) in full generality, so that I will restrict the discussion to less general P^ν later. Nevertheless, it is instructive to see where the problems appear which force the analysis to special cases.

The independence of the probability distribution on the spatial index r reflects the infinite-range nature of the interaction or, in other words, the infinite dimensionality of this model. The exactness of mean-field theory for the Hamiltonian (2.1) is a result of this spatial independence of P^ν. As discussed above, the replica trick is convenient for the treatment of quenched disorder, so I introduce a replica label $a = 1, ..., l$ in the spin variables $S^a_{r\nu}$ and translate the disorder averaged[3] free energy $-T\langle \log Z\rangle_d$ with $Z = \mathrm{tr}\, e^{-\beta H}$ to the replica formalism.

In the remainder of the present chapter, I discuss the application of the replica trick to the Hamiltonian (2.1) in detail and introduce the concept of replica symmetry breaking (RSB). Each section starts with the most general case. Simplifying restrictions to the special cases of (quasi-)isotropic n-component spin glasses or Ising spin glasses will also be discussed. In spite of the fact that the important physics of RSB is seen most clearly in the Ising spin glass, I perform the derivation on a higher level of generality, so that the domain of applicability of the formalism is more obvious to the reader. At the end of this chapter, the formulas

[1] The formalism is not restricted to low temperatures, only to temperatures below the spin glass transition temperature T_C. It is, however, especially convenient for $T \ll T_C$ because it allows a smooth transition to $T = 0$, which is not possible in traditional formulations.

[2] The moments of the coupling constant distribution P^ν must scale properly with system size in order to obtain a meaningful thermodynamic limit ($N \to \infty$).

[3] I will use the d-indexed brackets $\langle\cdot\rangle_d$ to denote disorder average while the thermodynamic average with respect to the spin variables $\{\mathbf{S}_r\}$ is expressed by the trace operator tr .

of the important observables are translated to the replica formalism and some simplifications due to zero temperature are discussed.

2.1 The free energy in replica formalism

2.1.1 General formulation

The working plan for this section is to perform the disorder average of the replicated partition function, carry out a first reduction of the power of the spin variables by introducing matrix and vector valued auxiliary fields $\tilde{\mathbf{q}}$ and $\tilde{\mathbf{M}}$, respectively, and finally express the free energy per spin in the thermodynamic limit in terms of the saddle point values $\mathbf{q}$ and $\mathbf{M}$ of the auxiliary fields.

Due to the infinite range character of the interaction, the average over disorder in the coupling constants can be performed exactly in the l times replicated partition function $Z_{(l)}$. The price one has to pay for the convenience of removing the dependence of the theory on the large set of coupling constants $\{J^\nu_{rr'}\}$ is the appearance of fourth order spin couplings between different replicas. By carrying out the integrations over $J^\nu_{rr'}$ one obtains

$$\begin{aligned}\left\langle Z_{(l)}\right\rangle_d &= \left[\prod_{\substack{r<r'\\ \nu}}\int dJ^\nu_{rr'}P^\nu(J^\nu_{rr'})\right]\ \mathrm{tr}\ \exp\left(\beta\sum_{\nu,r,a}h_\nu S^a_{r\nu}+\beta\sum_{\substack{r<r'\\ a,\nu}}J^\nu_{rr'}S^a_{r\nu}S^a_{r'\nu}\right)\\ &= \mathrm{tr}\ \exp\left(\beta\sum_{r,a,\nu}h_\nu S^a_{r\nu}+\sum_{\substack{r<r'\\ \nu}}\left(\frac{\beta J^\nu_0}{N}\sum_a S^a_{r\nu}S^a_{r'\nu}+\frac{\beta^2J^2_\nu}{2N}\sum_{a,b}S^a_{r\nu}S^a_{r'\nu}S^b_{r\nu}S^b_{r'\nu}\right)\right)\end{aligned}\tag{2.3}$$

where tr represents the thermodynamic trace in the nNl-dimensional *replicated spin space* of $S^a_{r\nu}$ which is also restricted to the constraint $(\mathbf{S}^a_r)^2=L^2_S$. The spin sums can be rearranged by collecting powers of sums over spatial indices r:

$$\sum_{\substack{r<r'\\ a}}S^a_{r\nu}S^a_{r'\nu}=\frac{1}{2}\sum_a\left(\sum_r S^a_{r\nu}\right)^2-\frac{1}{2}\sum_{a,r}(S^a_{r\nu})^2\tag{2.4}$$

$$\sum_{r<r'}\sum_{a,b}S^a_{r\nu}S^a_{r'\nu}S^b_{r\nu}S^b_{r'\nu}=\sum_{a<b}\left(\sum_r S^a_{r\nu}S^b_{r\nu}\right)^2-\frac{1}{2}\sum_{a,b,r}(S^a_{r\nu})^2(S^b_{r\nu})^2+\frac{1}{2}\sum_a\left(\sum_r(S^a_{r\nu})^2\right)^2\tag{2.5}$$

When performing the replica limit $l\to 0$ and the thermodynamic limit $N\to\infty$, only terms proportional to lN survive[4] in the replicated partition function. With this knowledge, all other terms can be dropped already at this point. The disorder averaged, replicated partition function then reads

$$\begin{aligned}\left\langle Z_{(l)}\right\rangle_d = \mathrm{tr}\ \exp\Bigg\{&\beta\sum_{r,a,\nu}h_\nu S^a_{r\nu}+\\ &\sum_\nu\left[\frac{\beta J^\nu_0}{2N}\sum_a\left(\left(\sum_r S^a_{r\nu}\right)^2+\frac{\beta^2J^2_\nu}{4N}\left(\sum_r(S^a_{r\nu})^2\right)^2\right)+\frac{\beta^2J^2_\nu}{2N}\sum_{a<b}\left(\sum_r S^a_{r\nu}S^b_{r\nu}\right)^2\right]\Bigg\}.\end{aligned}\tag{2.6}$$

To be able to perform the spin trace, the quadratic and quartic spin terms must be reduced in order. This is done by decoupling the variables $S^a_{r\nu}$ with Hubbard-Stratonovich transformations, which give rise to $nl(l+3)/2$ auxiliary field variables[5] $\tilde{M}^\nu_a$, $\tilde{q}^\nu_{ab}=\tilde{q}^\nu_{ba}$ and $\tilde{q}^\nu_{aa}$. These fields will be fixed shortly by means of a saddle point integration in the thermodynamic limit. The first decoupling step leads to the replicated partition function of a corresponding (exact) effective single site model. The summation over sites r leads

[4] The detailed argument for this can be found in Appendix A.1.

[5] The strict separation of $\tilde{q}^\nu_{ab}$ for $a\neq b$ and $\tilde{q}^\nu_{aa}$ is convenient at this stage to prevent double counting. Later, the two quantities will be merged into a single matrix.

to a factor N, all site indices can be dropped and one obtains

$$\left\langle Z_{(l)}\right\rangle_d = \int \mathcal{D}\tilde{\mathbf{M}} \int \mathcal{D}\tilde{\mathbf{q}} \exp\left(-\beta N \sum_\nu \left(\sum_a \frac{J_0^\nu}{2}(\tilde{M}_a^\nu)^2 + \sum_{a<b}\frac{\beta J_\nu^2}{2}(\tilde{q}_{ab}^\nu)^2 + \sum_a \frac{\beta J_\nu^2}{4}(\tilde{q}_{aa}^\nu)^2\right)\right) \times$$
$$\text{tr } \exp\left(\beta N \sum_\nu \left(\sum_a (h_\nu + J_0^\nu \tilde{M}_a^\nu) S_\nu^a + \beta J_\nu^2 \sum_{a<b} \tilde{q}_{ab}^\nu S_\nu^a S_\nu^b + \frac{\beta J_\nu^2}{2}\sum_a \tilde{q}_{aa}^\nu (S_\nu^a)^2\right)\right), \quad (2.7)$$

where the short hand notations of integrals with respect to the vectors $\tilde{\mathbf{M}} = (\tilde{M}_a^\nu)_{a=1}^l$ and the matrices $\tilde{\mathbf{q}} = (\tilde{q}_{ab}^\nu)_{a,b=1}^l$ of auxiliary fields

$$\int \mathcal{D}\tilde{\mathbf{M}} := \prod_{\nu a} \sqrt{\frac{\beta J_0^\nu N}{2\pi}} \int d\tilde{M}_a^\nu, \qquad \int \mathcal{D}\tilde{\mathbf{q}} := \left[\prod_{\substack{a<b \\ \nu}} \sqrt{\frac{\beta^2 J_\nu^2 N}{2\pi}} \int d\tilde{q}_{ab}^\nu\right] \times \left[\prod_{\nu a} \sqrt{\frac{N}{\pi}} \frac{\beta J_\nu}{2} \int d\tilde{q}_{aa}^\nu\right] \quad (2.8)$$

have been introduced.

The next step is to fix the values of the auxiliary fields in the thermodynamic limit by a multi-dimensional saddle point (SP) integration. In order to clearly point out the relation to the text book version of a SP integral [Nol04], I rewrite equation (2.7) as

$$\left\langle Z_{(l)}\right\rangle_d = \int \mathcal{D}\tilde{\mathbf{M}} \int \mathcal{D}\tilde{\mathbf{q}} \;\; \exp\left(-\beta N g(l, \tilde{\mathbf{M}}, \tilde{\mathbf{q}})\right) \quad (2.9)$$

with

$$g(l, \tilde{\mathbf{M}}, \tilde{\mathbf{q}}) = \sum_\nu \left(\frac{J_0^\nu}{2}\sum_a (\tilde{M}_a^\nu)^2 + \frac{\beta J_\nu^2}{2}\sum_{a<b}(\tilde{q}_{ab}^\nu)^2 + \frac{\beta J_\nu^2}{4}\sum_a (\tilde{q}_{aa}^\nu)^2\right) - T \log \text{tr } \exp L(\tilde{\mathbf{M}}, \tilde{\mathbf{q}}) \quad (2.10)$$

and

$$L(\tilde{\mathbf{M}}, \tilde{\mathbf{q}}) = \beta \sum_\nu \left(\sum_a (h_\nu + J_0^\nu \tilde{M}_a^\nu) S_\nu^a + \beta J_\nu^2 \sum_{a<b} \tilde{q}_{ab}^\nu S_\nu^a S_\nu^b + \frac{\beta J_\nu^2}{2}\sum_a \tilde{q}_{aa}^\nu (S_\nu^a)^2\right). \quad (2.11)$$

As a function of the fields $\tilde{\mathbf{M}}$ and $\tilde{\mathbf{q}}$, $g(l, \tilde{\mathbf{M}}, \tilde{\mathbf{q}})$ is bounded from below and is independent of N. Therefore, the usual SP argument from statistical mechanics is applicable[6] and one can replace the fields $\tilde{\mathbf{M}}, \tilde{\mathbf{q}}$ by their SP values $\mathbf{M}, \mathbf{q}$, i.e. the coordinates in $(\tilde{\mathbf{M}}, \tilde{\mathbf{q}})$-space where g assumes its global minimum. Those coordinates can be found later in terms of self-consistency equations, obtained from the derivatives of the resulting free energy. At this point, the separation of trace term and field term discussed in 1.4 can be observed: the field term depends polynomially on the field variables, while in the trace term $T \log \text{tr } e^L$ the field dependence remains highly nontrivial.

After the SP integration has been carried out, the replicated partition function becomes, up to an irrelevant prefactor,

$$\left\langle Z_{(l)}\right\rangle_d = \exp\left(-\beta N g(l, \mathbf{M}, \mathbf{q})\right). \quad (2.12)$$

Now that the partition function is a function of the saddle point values, the next step is the proper replica limit $l \to 0$. A direct inspection of g as a function of the number of replicas l shows that $g(l = 0, \mathbf{M}, \mathbf{q}) = 0$, because all sums in (2.10) and (2.11) have zero terms. Consequently, the replicated partition function for zero replicas is $\left\langle Z_{(0)}\right\rangle_d = 1$. According to standard rules of calculus, the replica limit in the formula $\langle \log Z\rangle_d = \lim_{l\to 0} l^{-1}(\left\langle Z_{(l)}\right\rangle_d - 1)$ leads to a differentiation of g with respect to the number of replicas l which is assumed continuous from now on[7]:

$$\langle \log Z\rangle_d = \lim_{l\to 0} \partial_l \left\langle Z_{(l)}\right\rangle_d = -\beta N \lim_{l\to 0} \underbrace{\exp\left(-N\beta g(l, \mathbf{M}, \mathbf{q})\right)}_{\to 1} \partial_l g(l, \mathbf{M}, \mathbf{q}) \quad (2.13)$$

[6] See Appendix A.1 for details.

[7] The mindful reader might be intrigued somewhat by the ease of handling the replica and the thermodynamic limit, especially the assumption of their commutativity. With great mathematical effort, it has been strictly proved [Tal06] that this derivation is indeed valid - at least for the SK-model.

The derivative of g with respect to l is again rewritten in terms of a limit $l \to 0$ and one obtains for the free energy per spin $f = -T/N \langle \log Z \rangle_d$ in the replica formalism

$$f = \lim_{l \to 0} \frac{1}{l} \left[\sum_{\nu} \left(\frac{J_0^\nu}{2} \sum_a (M_a^\nu)^2 + \frac{\beta J_\nu^2}{4} \sum_{a,b} (q_{ab}^\nu)^2 \right) - T \log \mathrm{tr}\ \exp L \right] \tag{2.14}$$

with

$$L = \beta \sum_{\nu,a} (h_\nu + J_0^\nu M_a^\nu) S_\nu^a + \sum_\nu \frac{\beta^2 J_\nu^2}{2} \sum_{a,b} q_{ab}^\nu S_\nu^a S_\nu^b. \tag{2.15}$$

The proper parameters q_{ab}^ν and M_a^ν are obtained by finding the point in the $(\tilde{\mathbf{M}}, \tilde{\mathbf{q}})$-parameter space where $g(l, \tilde{\mathbf{M}}, \tilde{\mathbf{q}})$ or equivalently the free energy per spin f is extremal, i.e. where[8] $\nabla g(l, \tilde{\mathbf{M}}, \tilde{\mathbf{q}}) = 0$. One can see that for $l \geq 1$, the free energy is bounded from below as a function of $\mathbf{q}$ and $\mathbf{M}$ and therefore, it has to be minimized in order to obtain the correct saddle point. In the limit $l \to 0$, however, the minimization w.r.t. the matrix elements of $\mathbf{q}$ passes over to a maximization w.r.t. specific subsets of matrix elements. I will further comment on this issue when discussing the replica symmetric approximation, where this min $\leftrightarrow$ max transition is most obvious.

With the help of the extremization principle, a physical meaning can be assigned to the parameters q_{ab}^ν and M_a^ν. Extremization of the free energy with respect to the M_a^ν fields results in

$$\frac{\partial f}{\partial M_a^\nu} = \lim_{l \to 0} \left[\frac{J_0^\nu}{l} M_a^\nu - \frac{1}{\beta l} \frac{\mathrm{tr}\ e^L \frac{\partial L}{\partial M_a^\nu}}{\mathrm{tr}\ e^L} \right] \stackrel{!}{=} 0 \tag{2.16}$$

$$\Rightarrow \qquad M_a^\nu = \frac{1}{\beta J_0^\nu} \frac{\mathrm{tr}\ e^L \beta J_0^\nu S_\nu^a}{\mathrm{tr}\ e^L} = \frac{\mathrm{tr}\ e^L S_\nu^a}{\mathrm{tr}\ e^L} \equiv \langle S_\nu^a \rangle \tag{2.17}$$

Apparently, $\mathbf{M}_a$ has the meaning of a magnetization per replica. This can easily be understood as the analogon of the derivative of (1.8) with respect to M which results in the IFM mean-field equations for the magnetization. Similarly to (2.17) one finds for the *spin glass order parameters* q_{ab}^ν the meaning of a spin overlap between two replicas a and b:

$$q_{ab}^\nu = \frac{\mathrm{tr}\ e^L S_\nu^a S_\nu^b}{\mathrm{tr}\ e^L} \equiv \left\langle S_\nu^a S_\nu^b \right\rangle. \tag{2.18}$$

The usefulness of equations (2.17) and (2.18), especially the identities of the order parameters and derivatives of $\log \mathrm{tr}\ e^L$, will be much appreciated in connection with thermodynamical considerations in Section 2.5, where they considerably simplify the analysis.

Equation (2.14) is the basis of further investigations. However, the conceptual difficulty, mentioned in Section 1.3.2 can clearly be observed there: l is both, a small continuous parameter which approaches zero in the replica limit and an integer valued parameter which denotes the number l or $l(l-1)/2$ of terms in the summations $\sum_a$ or $\sum_{a<b}$, respectively. Due to the absence of any terms in the summations in the square brackets for $l = 0$, there is at least in principle a chance for the limit $l \to 0$ to be finite. The formal way to resolve this contradictory definition is to cancel the $1/l$ prefactor in equation (2.14) with the factor l in the number of terms in the summation over replica indices a, b. This, however, requires further assumptions about the structure of the replica matrix $\mathbf{q}$ or the vectors $\mathbf{M}$. Before discussing possible structures of the order parameters, it is useful to see how the general formulas are simplified for the special cases of Ising spin glasses ($n = 1$) and (quasi-)isotropic spin glasses in which the order parameters $\mathbf{M}$ and $\mathbf{q}$ do not depend on the spin component.

2.1.2 Special case: Ising spin glass

For the special case of the classical Ising spin glass which has only one spin component ($n = 1$) one can drop the component index ν and finds $q_{aa} = L_S^2$ because there is no need to decouple the squared terms

[8] ∇ is defined in the $(\tilde{\mathbf{M}}, \tilde{\mathbf{q}})$-parameter space.

$S^a S^a \equiv L_S^2$ which are fixed by the length of the one component spin vector. Setting $L_S = 1$ yields the SK-model [SK75] and equation (2.14) simplifies to

$$f_{\text{Ising}} = -\frac{\beta J^2}{4} + \lim_{l\to 0}\frac{1}{l}\left(\frac{J_0}{2}\sum_a M_a^2 + \frac{\beta J^2}{2}\sum_{a<b} q_{ab}^2 - T\log\text{tr }\exp(L_{\text{Ising}})\right) \tag{2.19}$$

with[9]

$$L_{\text{Ising}} = \beta\left(\sum_a (h + J_0 M_a)S^a + \beta J^2 \sum_{a<b} q_{ab} S^a S^b\right). \tag{2.20}$$

The Ising spin glass, described by (2.19) and (2.20) is one of the simplest models for studying the physics of glassy systems. Large parts of this work focus on this model an on its low temperature properties, because it is easiest to learn the principles of RSB there. Extensions to more than one component mainly complicate the numerical and analytical treatment without introducing fundamentally new RSB features. The exact solubility of the so called spherical model [KTJ76] with infinitely many spin components, however, renders the investigation of beyond-Ising models interesting from a formal point of view. Moreover, it is important to understand the principles of RSB with many spin components for investigations of quantum spin glass models where more than one spin component is needed to account for quantum dynamics.

2.1.3 Special case: (Quasi-)isotropic n-component spin glass

A slightly more complicated, but still mathematically and especially numerically feasible model is the isotropic n-component spin glass, which is obtained by restricting the parameters of the most general model (2.14) to

$$J_0^\nu = 0, \qquad J_\nu = J, \qquad h_\nu = 0 \tag{2.21}$$

so that the spin system obeys an $O(n)$ symmetry. All spin components, labeled by ν, are equivalent and so there is no reason why the replica overlap q_{ab}^ν should depend on ν. It is further clear from symmetry that the magnetization of a replica $M_a^\nu = 0$: because of $J_0^\nu = 0$ there is no preference of parallel or antiparallel alignment of a pair of spins, and because of $h_\nu = 0$ there is no preferred direction in the system. As a result, the index ν of all quantities except the spin variables can be dropped. The ν-sum in the last term of (2.11) can be performed and is fixed by the normalization condition $(\mathbf{S}^a)^2 = L_S^2$, so it can be pulled out of the trace. Similarly to the Ising model, one obtains a trivial q_{aa}-dependence of the free energy which can be written, up to q_{aa}-independent terms, as

$$f = \frac{\beta J^2}{4}\sum_a (n\, q_{aa}^2 - 2L_S^2\, q_{aa}) + \ldots \tag{2.22}$$

Extremization of the free energy f with respect to q_{aa} yields $q_{aa} = L_S^2/n$ which is exactly what one would expect from the physical meaning of $q_{aa} = \langle (S_\nu^a)^2\rangle$ for $O(n)$ symmetry, namely that the length L_S of the classical spin vector is on average equally distributed over the components. The expression for the free energy in the isotropic spin glass simplifies to

$$f_{\text{Isotropic}} = -\frac{\beta J^2}{4}\frac{L_S^4}{n} + \lim_{l\to 0}\frac{1}{l}\left(\frac{\beta J^2}{2} n \sum_{a<b} q_{ab}^2 - T\log\text{tr }\exp(L_{\text{Isotropic}})\right) \tag{2.23}$$

with

$$L_{\text{Isotropic}} = \beta^2 J^2 \sum_{a<b} q_{ab} \sum_\nu S_\nu^a S_\nu^b. \tag{2.24}$$

Apart from a renormalization of some factors, the expression for the free energy of an isotropic n-component spin glass is very similar to the Ising case. I will show later, that the differences mainly manifest in the detailed form of an initial condition of recursion- or differential equations for the finite or infinite RSB formalism, respectively.

A little less restrictive is the assumption that the external parameters are only independent of ν but J_0 and h need not necessarily be zero. In this case, $O(n)$ symmetry is broken and M_a^ν is not expected to vanish

[9] L_{Ising} is not the same as L in (2.11) for $n = 1$. The q_{aa} term has been pulled out of the trace term. This is an example of the ambiguity in the definition of the trace term mentioned in the introduction.

in general. The crucial simplification, namely the independence of q_{ab}^{ν} on ν, however, is still applicable, because again no spin component is preferred by external parameters. This situation restricts the general case only to the extent that the vectors $\mathbf{J}_0$, $\mathbf{J}$ and $\mathbf{h}$ must point into the same direction. The equality of all components of these vectors can then be accomplished by means of an ordinary coordinate transformation. Throughout this work, the such restricted model will be called the quasi-isotropic n-component spin glass.

The advantage of allowing for finite external fields $h = |\mathbf{h}|$ lies in thermodynamic considerations. Derivatives of the free energy with respect to h are directly related to magnetization and magnetic susceptibilities of the system. The generalization of (2.23) to the quasi-isotropic (QI) case is straightforward and reads

$$f_{\mathrm{QI}} = -\frac{\beta J^2}{4}\frac{L_S^4}{n} + \lim_{l\to 0}\frac{1}{l}\left(\frac{J_0}{2}n\sum_a M_a^2 + \frac{\beta J^2}{2}n\sum_{a<b} q_{ab}^2 - T\log\mathrm{tr}\ \exp(L_{\mathrm{QI}})\right) \tag{2.25}$$

with

$$L_{\mathrm{QI}} = \beta\left(\sum_a (h + J_0 M_a)\sum_\nu S_\nu^a + \beta J^2\sum_{a<b} q_{ab}\sum_\nu S_\nu^a S_\nu^b\right). \tag{2.26}$$

In the remainder of this work, the length of the spin vector L_S will be fixed to $L_S^2 = n$, in order to use the same convention as in the literature [AJK78, KTJ76]. In order to stress the difference of length L_S and number of components n, however, at some points this convention is not made explicit and the quantity L_S is kept.

2.2 The replica symmetric approximation

As mentioned above, assumptions about the structure of $\mathbf{q}$ and $\mathbf{M}$ are necessary in order to proceed with the program of decoupling the spin variables so that the spin trace can be calculated. The simplest possible assumptions[10] about $\mathbf{q}$ and $\mathbf{M}$ are the so called replica symmetric (RS) assumptions. These assumptions state that all pairs of replicas are equal with respect to their spin overlap $q_{ab}^{\nu} = \langle S_\nu^a S_\nu^b\rangle$. Only the self overlap q_{aa}^{ν} is allowed to be different from q_{ab}^{ν}, $a \neq b$. More precisely, one assumes that $\mathbf{M}$ and $\mathbf{q}$, chosen replica symmetric, are saddle points of equation (2.9). In the present section, the RS saddle point, which is obtained by restricting the replica matrices $\mathbf{q}$ and vectors $\mathbf{M}$ to the form

$$q_{ab}^{\nu} = q_\nu,\ \ \forall a \neq b, \qquad q_{aa}^{\nu} = d_\nu, \qquad M_a^{\nu} = M_\nu, \tag{2.27}$$

will be investigated. It must be pointed out, however, that this approximation leads to inconsistencies, e.g. a negative entropy at low temperatures. It has been shown[11] by de Almeida and Thouless that this is due to the instability of the RS saddle point [AT78]. The proper treatment, where a specific kind of breaking of replica symmetry is allowed, will be discussed in the next section.

Within the RS assumption, the sum of q_{ab}^{ν} in the field term of the free energy can be calculated an gives

$$\frac{1}{l}\sum_{a<b}(q_{ab}^{\nu})^2 = \frac{l-1}{2}q_\nu^2. \tag{2.28}$$

The quadratic terms of q are the leading terms in the free energy for large q and from the left hand side of equation (2.28) one finds that f, as a function of any of the parameters q_{ab}^{ν}, is bounded from below. On the right hand side, this is still true as long as $l \geq 2$. This is the case where the matrix $\mathbf{q}$ has off-diagonal terms. For $l = 1$, $\mathbf{q}$ is a 1×1 matrix without off-diagonal terms. For $l = 0$, however, the quadratic q-term changes sign. Loosely speaking, a minimization with respect to a *negative number of equal parameters* results in a maximization with respect to the value of the parameters. This is typical of how the unusual situation appears that one must find a maximum of f with respect to the spin glass order parameters q, while it must be minimized with respect to the magnetization M.

The quadratic spin terms in the trace term (2.11) combined with the assumptions (2.27) can be written as

$$\beta^2\sum_\nu\left(J_\nu^2\sum_{a<b} q_{ab}^{\nu} S_\nu^a S_\nu^b + \frac{J_\nu^2}{2}\sum_a q_{aa}^{\nu}(S_\nu^a)^2\right) = \sum_\nu\frac{\beta^2 J_\nu^2}{2}\left(q_\nu\left(\sum_a S_\nu^a\right)^2 + (d_\nu - q_\nu)\sum_a (S_\nu^a)^2\right) \tag{2.29}$$

[10] Indeed, this was historically the first assumption which has been made about $\mathbf{q}$ by the inventors of the SK-model [SK75].
[11] See also appendix A.1.

and one needs two further decoupling fields $\mathbf{z}$ and $\tilde{\mathbf{z}}$, which are introduced by Hubbard-Stratonovich transformations. The field $\mathbf{z}$ originates from decoupling the S^aS^b terms and the field $\mathbf{z}$ from the $(S^a)^2$ terms. Then the free energy per spin simplifies to

$$f = \sum_\nu \left(\frac{J_0^\nu}{2} M_\nu^2 - \frac{\beta J_\nu^2}{4}(q_\nu^2 - d_\nu^2) \right) - T \int_{\mathbf{z}}^G \log \int_{\tilde{\mathbf{z}}}^G \mathcal{C}_n(\beta |\mathbf{H}_{\text{eff}}|) \tag{2.30}$$

where Gaussian integral operators and an effective field $\mathbf{H}_{\text{eff}}$ have been introduced as

$$\int_{\mathbf{z}}^G = \int_{-\infty}^{\infty} \frac{d^n\mathbf{z}}{(2\pi)^{n/2}} e^{-\frac{\mathbf{z}^2}{2}}, \qquad \mathbf{H}_{\text{eff}} = \sum_\nu (h_\nu + J_0^\nu M_\nu + J_\nu(\sqrt{q_\nu} z_\nu + \sqrt{d_\nu - q_\nu}\tilde{z}_\nu)\mathbf{e}_\nu \tag{2.31}$$

with $\{\mathbf{e}_\nu\}$ a set of orthonormal vectors. The kernel $\mathcal{C}_n(\mathbf{x})$ depends on the number of spin components n and the length of the classical spin vector L_S. It is exactly equal to the trace term of a classical n-component ferromagnet as discussed in the Introduction and is defined by

$$\mathcal{C}_n(|\mathbf{x}|) := \text{tr } \exp(\mathbf{x}\cdot\mathbf{S}) \propto \int d^n\mathbf{s}\; \delta(\mathbf{s}^2 - L_S^2) \exp(\mathbf{x}\cdot\mathbf{s}) \tag{2.32}$$

In general, the kernel can be expressed in terms of the modified Bessel function $I_\alpha(z)$ [Wat95] for $n > 1$:

$$\mathcal{C}_n(x) = \mathcal{N} \frac{I_{\frac{n}{2}-1}(L_S x)}{(L_S x)^{\frac{n}{2}-1}} \tag{2.33}$$

with $\mathcal{N}$ an irrelevant[12] normalization factor. Usually, in the literature one finds a normalization of the kernel such that the trace without a field ($\mathbf{x} = 0$ in equation (2.32)) results in the area of an $(n-1)$ dimensional hypersphere with radius $L_S = \sqrt{n}$, i.e. $\mathcal{C}_n(0) = \Omega_n L_S^{n-1}$, where Ω_n is the full solid angle in n-dimensional space. In this case one finds $\mathcal{N} = (2\pi)^{n/2} n^{(n-1)/2}$. Because of the irrelevance of $\mathcal{N}$, I will use the normalization which is most convenient in the specific situation, but when the free energy is plotted, it is always normalized in consistence with the literature [AJK78, BY86]. In the Ising ($n = 1$) and Heisenberg ($n = 3$) cases[13] the kernel (2.33) can be expressed in terms of hyperbolic functions

$$\mathcal{C}_1(x) = 2\cosh(x) \tag{2.34}$$

$$\mathcal{C}_3(x) = 12\pi \frac{\sinh(\sqrt{3}x)}{\sqrt{3}x}. \tag{2.35}$$

For general n, however, the formulation in terms of $I_\alpha(x)$ must be used. In any case the kernel is easily shown to be an even function of its argument. Further, the asymptotic behavior of $\mathcal{C}_n(x)$ is important for simplifying considerations in context of the numerical analysis as well as in the asymptotic renormalization group discussed later in this work. For general n it is given by

$$\mathcal{C}_n(x) \propto \frac{e^{|L_S x|}}{|L_S x|^{(n-1)/2}}, \qquad |x| \gg 1. \tag{2.36}$$

The parameters M_ν, q_ν and d_ν are defined as the solutions of a set of self-consistence equations, which are obtained by finding the roots of the gradient of the free energy in the $3n$-dimensional (M_ν, q_ν, d_ν)-space. These self-consistence equations for the general anisotropic n-component spin glass read

$$M_\nu = \int_{\mathbf{z}}^G \frac{1}{\int_{\tilde{\mathbf{z}}}^G \mathcal{C}_n(\beta|\mathbf{H}_{\text{eff}}|)} \int_{\tilde{\mathbf{z}}}^G \mathcal{C}_n'(\beta|\mathbf{H}_{\text{eff}}|) \frac{H_{\text{eff}}^\nu}{|\mathbf{H}_{\text{eff}}|} \tag{2.37}$$

$$d_\nu = -\frac{T}{J_\nu \sqrt{d_\nu - q_\nu}} \int_{\mathbf{z}}^G \frac{1}{\int_{\tilde{\mathbf{z}}}^G \mathcal{C}_n(\beta|\mathbf{H}_{\text{eff}}|)} \int_{\tilde{\mathbf{z}}}^G \mathcal{C}_n'(\beta|\mathbf{H}_{\text{eff}}|) \frac{\tilde{z}_\nu\, H_{\text{eff}}^\nu}{|\mathbf{H}_{\text{eff}}|} \tag{2.38}$$

$$q_\nu = \frac{T}{J_\nu} \int_{\mathbf{z}}^G \frac{1}{\int_{\tilde{\mathbf{z}}}^G \mathcal{C}_n(\beta|\mathbf{H}_{\text{eff}}|)} \int_{\tilde{\mathbf{z}}}^G \mathcal{C}_n'(\beta|\mathbf{H}_{\text{eff}}|) \frac{H_{\text{eff}}^\nu}{|\mathbf{H}_{\text{eff}}|} \left(\frac{\tilde{z}_\nu}{\sqrt{d_\nu - q_\nu}} - \frac{z_\nu}{\sqrt{q_\nu}} \right). \tag{2.39}$$

[12] Irrelevant means that the parameters q_{ab}^ν and m_a^ν do not depend on the choice of $\mathcal{N}$. The absolute value of free energy per spin, however, has an additional $T \log \mathcal{N}$ term. This is shown in Appendix A.3 for general orders κ of RSB, including the replica symmetric case $\kappa = 0$.

[13] In general, the kernel can be expressed in terms of hyperbolic functions for odd n. The expressions are a bit lengthy for $n \geq 5$, however.

The irrelevance of the normalization $\mathcal{N}$ of the kernel $\mathcal{C}_n(x)$ is clear from the form of self-consistence equations (2.37) - (2.39). This is because the self-consistence equations are obtained from the derivatives of the free energy with respect to the parameters. A multiplicative change in the normalization $\mathcal{N}$ results in an additive term in the free energy, which is independent of the order parameters, as shown in Appendix A.3. As a result, this term cancels in the derivative of f.

2.2.1 Special case: Ising spin glass

The replica symmetric Ising spin glass corresponds exactly to the original treatment of the SK-model which has been proposed and investigated in [SK75]. For completeness and as a basis for generalizations, the results obtained there are shortly discussed in the present work, too. Because the $(S^a)^2$ terms are trivially fixed by the normalization constraint, they need not be decoupled and thus only one scalar field z is needed for decoupling. The SK free energy becomes

$$f = \frac{J_0}{2}M^2 - \frac{\beta J^2}{4}(1-q)^2 - T\int \frac{dz}{\sqrt{2\pi}} e^{-\frac{z^2}{2}} \log 2\cosh(\beta(h + J_0 M + J\sqrt{q}z)). \tag{2.40}$$

The order parameters q and M are given by the self-consistency equations which result from finding the root of the partial derivatives of f with respect to q, M. The self-consistence equations read

$$q = \int \frac{dz}{\sqrt{2\pi}} e^{-\frac{z^2}{2}} \tanh^2(\beta(h + J_0 M + J\sqrt{q}z)) \tag{2.41}$$

$$M = \int \frac{dz}{\sqrt{2\pi}} e^{-\frac{z^2}{2}} \tanh(\beta(h + J_0 M + J\sqrt{q}z)) \tag{2.42}$$

and can easily be solved numerically. For $J \to 0$ the infinite range Ising ferromagnet described in the introduction and in [NO98] is recovered. In this case the spin glass order parameter trivially gets $q = M^2$. Thus, it is obviously not sufficient to identify a spin glass phase by a non-zero spin glass order parameter $q_{ab} = \langle S^a S^b \rangle \neq 0$. One also has to make sure that $\langle S^a S^b \rangle \neq \langle S^a \rangle \langle S^b \rangle$.

2.2.2 Special case: Quasi-isotropic n-component spin glass

It is convenient to set the length of the classical spin vector of the n-component spin glass to $L_S^2 = n$. With this choice the spin glass order parameter q is - as in the SK-model - mapped to the domain $q \in [0,1]$ because q is the overlap of one single spin component between different replicas. Within this convention the free energy in the RS approximation can be obtained directly from equation (2.25) by evaluating the angular integral, introducing $h_2 = \sqrt{n}(h + J_0 M)$ and transforming to the new integration variable $h_1 = \sqrt{q}z$.

$$f = \frac{J_0 n}{2}M^2 - \frac{\beta J^2 n}{4}(1-q)^2 - \frac{T}{q}\int_0^\infty dh_1 h_1^{\frac{n}{2}} \exp\left(-\frac{h_1^2 + h_2^2}{2q}\right) \frac{I_{\frac{n}{2}-1}\left(\frac{h_1 h_2}{q}\right)}{h_2^{n/2-1}} \log \mathcal{C}_n(\beta h_1). \tag{2.43}$$

As above, $I_\alpha(x)$ is the modified Bessel function. The self-consistency relation for the magnetization M is obtained as usual by differentiating the free energy with respect to M. For the self-consistence equation of the spin glass order parameter q, an additional partial integration is needed in the derivation. After some analysis which involves the exploitation of several identities of Bessel functions [Wat95], one finds

$$q = \int_0^\infty \frac{dh_1}{q} h_1^{\frac{n}{2}} \exp\left(-\frac{h_1^2 + h_2^2}{2q}\right) \frac{I_{\frac{n}{2}-1}\left(\frac{h_1 h_2}{q}\right)}{h_2^{n/2-1}} \left(\frac{I_{\frac{n}{2}}(\beta\sqrt{n}h_1)}{I_{\frac{n}{2}-1}(\beta\sqrt{n}h_1)}\right)^2 \tag{2.44}$$

and

$$M = \int_0^\infty \frac{dh_1}{q} h_1^{\frac{n}{2}} \exp\left(-\frac{h_1^2 + h_2^2}{2q}\right) \frac{I_{\frac{n}{2}-1}\left(\frac{h_1 h_2}{q}\right)}{h_2^{n/2-1}} \left(\frac{I_{\frac{n}{2}}(\beta\sqrt{n}h_1)}{I_{\frac{n}{2}-1}(\beta\sqrt{n}h_1)}\right). \tag{2.45}$$

In the literature [BY86, AJK78], one mostly finds the self-consistence equations (2.44) and (2.45) for the isotropic n-component spin glass. The isotropic equations can be obtained from the more general quasi-isotropic equations by performing the isotropic limit $h_2 \to 0$. The magnetization is exactly zero in this

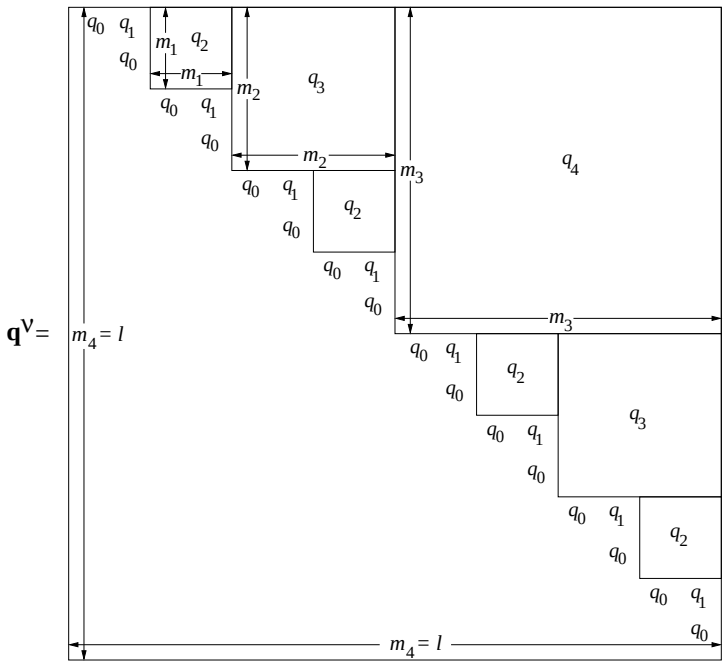

Fig. 2.1: The Parisi scheme of the matrix $\mathbf{q}^\nu$ for 3rd order of RSB ($\kappa = 3$). The blocks with matrix elements q_i are $m_{i-1} \times m_{i-1}$ sub-matrices. The total size of the matrix is $l \times l = m_4 \times m_4$. The index ν in the matrix elements and the block sizes have been omitted as well as the sub diagonal triangle, which is obtained by symmetry $q^\nu_{ab} = q^\nu_{ba}$.

case, because of symmetry arguments. The h_2^{-1} singularities in (2.44) can be cured by expanding the Bessel functions for small arguments.

Similarly, the Ising spin glass is obtained in the limit $n \to 1$. The limit $n \to \infty$ yields the so-called spherical model [KTJ76] for which the RS-approximation is exact in the sense that the saddle point in equation (2.9) is stable. There are, however, other artefacts in this model as e.g. a logarithmically diverging entropy in the zero temperature limit[14].

2.3 Parisi RSB

As already mentioned, it has been shown in Ref. [AT78] that the assumption of replica symmetric matrices $\mathbf{q}^\nu$ is too restrictive and does not represent the correct saddle point in equation (2.9). Thus, a higher number of degrees of freedom in the choice of the replica matrix $\mathbf{q}^\nu$ is required. In the RS approximation, only diagonal and off-diagonal elements have been distinguished. However, possibilities for choosing other degrees of freedom are strongly restricted by the condition that the replica limit $l \to 0$ must remain meaningful on one hand, and by the requirement that the structure of $\mathbf{q}^\nu$ must be sufficiently simple to be mathematically feasible, on the other hand.

A just tractable scheme for the replica matrix structure has been proposed by Parisi [Par79] and it turned out only recently [Tal06] that this proposal in fact yields a correct solution[15]. It amounts to an iterative replacement of matrix elements in quadratic diagonal blocks of size m_i^ν in $\mathbf{q}^\nu$, as indicated in Figure 2.1. More general RSB-schemes than the Parisi scheme are also possible [DGD82], but they are considerably more complicated and not required in most cases. In this section, the Parisi-scheme for $\mathbf{q}^\nu$ will be applied to the classical n-component spin system. The order of RSB κ is the number of block replacement iterations. An RSB scheme of κth order is called κ RSB.

The Parisi scheme for $\mathbf{q}$ is shown for 3rd order of RSB in Fig. 2.1[16]. In this example, one starts with a large $l \times l$ matrix, filled by matrix elements $q_4 = q_{\kappa+1}$. Then, blocks of size $m_3 \times m_3$ on the diagonal of the matrix are replaced by matrix elements q_3. The block sizes m_3 are chosen such that an integer number of

[14] See also Appendix A.6.
[15] In fact there are many equivalent choices of $\mathbf{q}^\nu$. In the Parisi RSB, however, the replica limit can be directly performed.
[16] The index ν is irrelevant in this paragraph and thus will be dropped for convenience.

blocks exactly fit into the $l \times l$ matrix, i.e. the quotient $\frac{l}{m_3}$ must be integer valued. Next, matrix elements on sub-blocks of the m_3 blocks with sizes m_2 are replaced by q_2. Again, the m_2 blocks are chosen such that an integer number of them fit exactly into an m_3 block. This scheme is iterated until one arrives at the diagonal matrix elements (1×1 blocks) which are replaced by q_0.

The magnetization per replica is assumed replica symmetric, i.e. $M_a^\nu = M_\nu$, as in the RS case discussed in the preceding section. With the help of this scheme, the free energy per spin can be written in terms of the block size parameters m_i^ν, the matrix elements q_i^ν and the magnetization M_ν in such a way that the spin trace and the replica limit can be performed. This will be discussed in the following for general orders κ of RSB.

First consider the field term of the free energy per spin in equation (2.14)

$$\lim_{l\to 0} \sum_\nu \left[\frac{J_0^\nu}{2l} \sum_a (M_a^\nu)^2 + \frac{\beta J_\nu^2}{4l} \sum_{a,b} (q_{ab}^\nu)^2 \right]. \tag{2.46}$$

The sum of M_ν^a is trivial and the sum of q_{ab}^ν can be evaluated according to the prescription in Appendix A.5. Within κ RSB the evaluation of the field term (2.46) results in

$$\sum_\nu \left[\frac{J_0^\nu}{2} M_\nu^2 + \frac{\beta J_\nu^2}{4} \sum_{i=1}^{\kappa} m_i^\nu ((q_i^\nu)^2 - (q_{i+1}^\nu)^2) + \frac{\beta J_\nu^2}{4} ((q_0^\nu)^2 - (q_1^\nu)^2) \right]. \tag{2.47}$$

More effort is necessary, however, to handle the trace term of the free energy. The idea on which the treatment is based is similar to the evaluation of the replica sums in the field term, but remember that the spin trace still needs to be performed. This is the point which complicates the analysis considerably. Again, the spin terms must be reduced to linear order.

As a first step in the spin decoupling program, one separates the spin-linear part L_0 from the spin-quadratic part L_1 in expression (2.15)

$$L = \underbrace{\beta \sum_{a\nu} (J_0^\nu M_\nu + h^\nu) S_\nu^a}_{L_0} + \underbrace{\sum_\nu \frac{(\beta J_\nu)^2}{2} \sum_{a,b} q_{ab}^\nu S_\nu^a S_\nu^b}_{L_1}. \tag{2.48}$$

The term L_0 may remain as is because the spin variables already are of linear order. In L_1, however, some more work is in order.

Firstly the quadratic spin terms which correspond to the same value of q_{ab}^ν must be collected. This can be done for each term in the ν-sum separately. To properly collect the spin terms $S_\nu^a S_\nu^b$, it is helpfull to imagine them as being 'projected' onto the matrix $\mathbf{q}^\nu$ by a one-to-one correspondence $S_\nu^a S_\nu^b \leftrightarrow q_{ab}^\nu$. Since $\mathbf{q}^\nu$ consists essentially of quadratic blocks of equal matrix elements[17], the spin term can also be expressed as quadratic spin blocks. I define a short hand expression for such a spin block as the quadratic sum of a specific subset of the spin variables

$$B_\nu(m_i^\nu, j) = \left(\sum_{a=(j-1)m_i^\nu+1}^{jm_i^\nu} S_\nu^a \right)^2. \tag{2.49}$$

Now one must collect the specific combinations of q_i^ν parameters which correspond to each spin block. If one considers, for instance, the largest block $B_\nu(l,1)$ of all spin variables, the corresponding factor is $q_{\kappa+1}^\nu$. However, the spin variables $S_\nu^a S_\nu^b$ which are projected to one of the largest blocks with matrix elements q_κ^ν have been wrongly assigned a factor $q_{\kappa+1}^\nu$ instead of q_κ^ν. This misassignment must be cured with hindsight when considering the spin blocks $B_\nu(m_\kappa^\nu, j)$ by giving them a prefactor $(q_\kappa^\nu - q_{\kappa+1}^\nu)$. At this stage, all terms with a prefactor $q_{\kappa+1}^\nu$ are correctly respected. In the next stage, the misassignment of the parameter q_κ^ν to blocks of size $m_{\kappa-1}^\nu$ must be cured in the same fashion by assinging prefactors $(q_{\kappa-1}^\nu - q_\kappa^\nu)$ to the blocks $B_\nu(m_{\kappa-1}^\nu, j)$. This procedure is iterated until one arrives at the diagonal elements.

According to the above considerations and by introduction of another short hand notation $\Delta q_i^\nu \equiv q_i^\nu - q_{i+1}^\nu$, $\Delta q_{\kappa+1}^\nu \equiv q_{\kappa+1}^\nu$ for the differences of the q-parameters, the sum over replica indices in L_1 can be written

[17] Smaller quadratic blocks are 'cut out' of the blocks, as can be seen in Figure 2.1. This results in non-quadratic arrangements of equal matrix elements. Nevertheless the definition of quadratic spin-blocks is reasonable here, as will be seen shortly.

as

$$\begin{aligned}\sum_{a,b} q_{ab}^{\nu} S_{\nu}^{a} S_{\nu}^{b} &= \Delta q_{\kappa+1}^{\nu} B_{\nu}(l,1) \\ &+\Delta q_{\kappa}^{\nu} \left\{ B_{\nu}(m_{\kappa}^{\nu},1) + B_{\nu}(m_{\kappa}^{\nu},2) + ... + B_{\nu}\left(m_{\kappa}^{\nu}, \frac{l}{m_{\kappa}^{\nu}}\right) \right\} \\ &+... + \Delta q_{i}^{\nu} \left\{ B_{\nu}(m_{i}^{\nu},1) + B_{\nu}(m_{i}^{\nu},2) + ... + B_{\nu}\left(m_{i}^{\nu}, \frac{l}{m_{i}^{\nu}}\right) \right\} + ... \\ &+\Delta q_{0}^{\nu} \left\{ B_{\nu}(1,1) + B_{\nu}(1,2) + ... + B_{\nu}\left(1,l\right) \right\}. \end{aligned} \tag{2.50}$$

Each spin block is a quadratic sum of spin variables and thus can be decoupled by means of Hubbard-Stratonovich transformations. Again, field variables which must be integrated over are introduced by the transformations. In this case, however, no saddle point integration can be utilized in order to fix those fields and get rid of the corresponding integrals. It is this large number of field integrations which makes the treatment of RSB highly nontrivial.

For each block $B_{\nu}(m_i^{\nu}, j)$ a separate field $z_{j,i}^{\nu}$ is needed, where the index j denotes the position of the corresponding block, the index i denotes the size $(m_i^{\nu} \times m_i^{\nu})$ of the block and ν stands for the spin component. The explicit transformation for a particular block reads

$$\exp\left(\frac{(\beta J_{\nu})^2}{2} \Delta q_i^{\nu} B_{\nu}(m_i^{\nu}, j)\right) = \int_{\nu,j,i}^{G} \exp\left(\beta J_{\nu} \sqrt{\Delta q_i^{\nu}} z_{j,i}^{\nu} \sum_{a=(j-1)m_i^{\nu}+1}^{jm_i^{\nu}} S_{\nu}^{a}\right) \tag{2.51}$$

where a short hand notation for the Gaussian integrals has been introduced as

$$\int_{\nu,j,i}^{G} = \int_{-\infty}^{\infty} \frac{dz_{j,i}^{\nu}}{\sqrt{2\pi}} \exp\left(-\frac{\left(z_{j,i}^{\nu}\right)^2}{2}\right) \quad \text{or} \quad \int_{j,i}^{G} = \prod_{\nu=1}^{n} \int_{\nu,j,i}^{G} = \int_{-\infty}^{\infty} \frac{d^n \mathbf{z}_{j,i}}{(2\pi)^{n/2}} \exp\left(-\frac{|\mathbf{z}_{j,i}|^2}{2}\right). \tag{2.52}$$

After decoupling all spin blocks in equation (2.50) one is left with only linear spin variables in L_1. By merging together all prefactors of a spin variable S_{ν}^{a} in a field-like quantity f_a^{ν} one can finally write down an expression for e^{L_1} in which only linear spin terms appear

$$\exp\left(L_1\right) = \int \mathcal{D}(z) \exp\left(\beta \sum_{a\nu} f_a^{\nu} S_{\nu}^{a}\right). \tag{2.53}$$

The integral measure $\mathcal{D}(z)$ means the totality of all integrations over the field variables $z_{j,i}^{\nu}$ as defined in (2.52). Now, the factors f_a^{ν} must be written down explicitly in order to be able to further simplify the expressions in the following. By direct inspection of equation (2.50) in combination with (2.51) and with the definition of a shifted integer part function $\mathrm{ip}(x) := 1 + x - \mathrm{mod}(x, 1)$, it can easily be seen that the factors f_a^{ν} are given by

$$\begin{aligned} f_1^{\nu} &= J_{\nu}\left(\sqrt{\Delta q_0^{\nu}}\, z_{1,0}^{\nu} + \sqrt{\Delta q_1^{\nu}}\, z_{1,1}^{\nu} + \sqrt{\Delta q_2^{\nu}}\, z_{1,2}^{\nu} + ... + \sqrt{\Delta q_{\kappa+1}^{\nu}}\, z_{1,\kappa+1}^{\nu}\right) \\ &\vdots \\ f_a^{\nu} &= J_{\nu}\left(\sqrt{\Delta q_0^{\nu}}\, z_{a,0}^{\nu} + \sqrt{\Delta q_1^{\nu}}\, z_{\mathrm{ip}(a/m_1^{\nu}),1}^{\nu} + \sqrt{\Delta q_2^{\nu}}\, z_{\mathrm{ip}(a/m_2^{\nu}),2}^{\nu} + ... + \sqrt{\Delta q_{\kappa+1}^{\nu}}\, z_{1,\kappa+1}^{\nu}\right) \\ &\vdots \\ f_l^{\nu} &= J_{\nu}\left(\sqrt{\Delta q_0^{\nu}}\, z_{l,0}^{\nu} + \sqrt{\Delta q_1^{\nu}}\, z_{\mathrm{ip}(l/m_1^{\nu}),1}^{\nu} + \sqrt{\Delta q_2^{\nu}}\, z_{\mathrm{ip}(l/m_2^{\nu}),2}^{\nu} + ... + \sqrt{\Delta q_{\kappa+1}^{\nu}}\, z_{1,\kappa+1}^{\nu}\right). \end{aligned} \tag{2.54}$$

At this point, the job of decoupling the spin variables by introducing auxiliary fields is finished and one can perform the spin trace. Before doing this, the linear spin terms from L_0 in (2.48) must be included in expression (2.53) so that all spin variables are respected on equal footing in

$$e^{L} = \int \mathcal{D}(z) \exp\left(\beta \sum_{a} \sum_{\nu} (h_{\nu} + J_0^{\nu} M_{\nu} + f_a^{\nu}) S_{\nu}^{a}\right) = \int \mathcal{D}(z) \exp\left(\beta \sum_{a} \mathbf{F}_a \cdot \mathbf{S}^{a}\right) \tag{2.55}$$

where a replica dependent vector field $\mathbf{F}_a$ with components $F_a^\nu = h_\nu + J_0^\nu M_\nu + f_a^\nu$ has been defined. Recalling the definition of the integral kernel $\mathcal{C}_n(x)$ in (2.32) one can write down a closed expression for the trace term by applying the spin trace operator, which, due to the above rearrangements, can be written directly in front of an exponential function, as usual

$$\text{tr } e^L = \int \mathcal{D}(z) \text{tr } \exp\left(\beta \sum_a \mathbf{F}_a \cdot \mathbf{S}^a\right) = \int \mathcal{D}(z) \prod_a \text{tr } \exp\left(\beta \mathbf{F}_a \cdot \mathbf{S}\right) = \int \mathcal{D}(z) \prod_a \mathcal{C}_n(\beta |\mathbf{F}_a|). \tag{2.56}$$

In order to be able to perform the replica limit $l \to 0$, where the number of factors in (2.56) goes to zero, one must continue with further grouping the factors $\mathcal{C}_n(\beta|\mathbf{F}_a|)$ according to the differences between them. It turns out that there is a hierarchical system of differences between the single terms.[18] Each term is an individual term, on the lowest level different from all other terms. However, families of m_1^ν similar individuals and super-families with $\frac{m_2^\nu}{m_1^\nu}$ similar families, etc. exist.

Exploiting this hierarchy by properly arranging the integral operators $\int_{\nu,j,i}^G$ defined in equation (2.51) together with the individuals, families, ... results in an expression for the trace term in which the replica limit can be performed. At this point, I restrict the discussion to the special cases of an Ising spin glass and a quasi-isotropic n-component spin glass. For the general case of anisotropic spin glasses, the analysis gets extremely involved because of the dependence of the family sizes on the component index ν.

2.3.1 Ising spin glass (n=1) with finite J_0 and finite external field

As usual, the component index ν can be dropped in the Ising case and the integral kernel is given by $\mathcal{C}_1(x) = 2\cosh(x)$. Further, in the Ising spin glass the diagonal elements q_0 of $\mathbf{q}$ are unity for the same reason as in the RS case.

Now one starts at the lowest level in the hierarchy of equation (2.56), i.e. the level of individuals ($i = 0$). At this level, there are l integrals with respect to the fields $z_{a,0}$, $a = 1, ..., l$ which can be performed analytically[19], each giving a factor $\exp((\beta J)^2 \Delta q_0/2)$. Defining $F_a^{(1)} = F_a|_{z_{a,0}=0}$ and noting that $\Delta q_0 = 1 - q_1$, one can write

$$\text{tr } e^L = \exp\left(\frac{(\beta J)^2}{2}(1-q_1)l\right) \left\{ \prod_{i=1}^{\kappa+1} \left[\prod_{j=1}^{\frac{n}{m_i}} \int_{m_i,j}^G \right] \right\} \prod_{a=1}^{n} 2\cosh(\beta F_a^{(1)}). \tag{2.57}$$

Direct inspection of the effective fields $F_a^{(1)}$ which are obtained from (2.54) by setting $z_{a,0} = 0$ shows that they can be grouped into families of identical individuals with m_1 members, each. The differences of the individuals have been integrated out and are now located in the exponential factor in (2.57).

The most important difference between the families is the different auxiliary field $z_{i,1}$. When performing the integration over a specific $z_{1,1}$, say, the m_1 equal individuals of the first family can be treated as the m_1th power of the first individual in the family, i.e. $\left[2\cosh(\beta F_1^{(1)})\right]^{m_1}$. Analogous to that, the kth family gives rise to an integral over $z_{k,1}$ of $\left[2\cosh(\beta F_{1+(k-1)m_1}^{(1)})\right]^{m_1}$. After the integrals over $z_{k,1}$ have been performed, which cannot be done analytically anymore, the index k in $z_{k,1}$ can be dropped because the integrations in all different families are formally the same. Now, the level of families is finished and one continues with the same type of analysis on the level of super-families which consist of m_2/m_1 families. Iterating this procedure $\kappa + 1$ times leads to

$$\text{tr } e^L = \exp\left(\frac{(\beta J)^2}{2}(1-q_1)l\right) \int_{\kappa+1}^G \left[\int_\kappa^G \left[\int_{\kappa-1}^G ... \int_1^G \left[2\cosh\left(\beta H_{\text{eff}}\right)\right]^{m_1} ... \right]^{m_\kappa/m_{\kappa-1}} \right]^{l/m_\kappa} \tag{2.58}$$

$$= \exp\left(\frac{(\beta J)^2}{2}(1-q_1)l\right) \int_{\kappa+1}^G \left[\int_\kappa^{GE} \int_{\kappa-1}^{GE} ... \int_1^{GE} 2\cosh\left(\beta H_{\text{eff}}\right) \right]^{l/m_\kappa} \tag{2.59}$$

[18] A physical meaning can be assigned to this hierarchy. It turns out that the phase space of a spin glass is hierarchically ordered as an ultrametric tree. More information about ultrametricity can be found e.g. in [MPS84].

[19] See Appendix A.2.

where the Gaussian integral operators[20]

$$\int_i^G f(...,z_i,...) = \int_{-\infty}^{\infty} \frac{dz_i}{\sqrt{2\pi}} e^{-\frac{z_i^2}{2}} f(...,z_i,...), \qquad \int_i^{GE} f(...,z_i,...) = \int_i^G [f(...,z_i,...)]^{r_{i-1}} \tag{2.60}$$

have been introduced together with the block size ratios

$$r_i = \frac{m_{i+1}}{m_i}, \qquad r_0 = \frac{m_1}{1} \tag{2.61}$$

and a final effective field variable

$$H_{\text{eff}} = h + J_0 M + J \sum_{i=1}^{\kappa+1} z_i \sqrt{\Delta q_i}. \tag{2.62}$$

With expression (2.59) for $\operatorname{tr} e^L$ one is in a position to perform the replica limit $l \to 0$ of the trace term. Note, however, that with assuming l to be a small continuous variable, one gives up the integer property of the parameters m_i and projects them onto the interval $[0,1]$. Performing the replica limit in equation (2.59) yields

$$\lim_{l\to 0} \frac{T}{l} \log \operatorname{tr} e^L = \frac{\beta J^2}{2}(1-q_1) + \frac{T}{m_\kappa} \int_{\kappa+1}^G \log \left[\int_\kappa^{GE} ... \int_2^{GE} \int_1^{GE} 2\cosh(\beta H_{\text{eff}}) \right]. \tag{2.63}$$

In combination with the field term of the free energy in equation (2.47), specialized to $n = 1$, and with the definition of the non-equilibrium susceptibility[21] $\chi_{ne} = \beta(1-q_1)$ one can write the free energy per particle of an Ising spin glass within κth order of RSB as a function in the $(2\kappa+2)$-dimensional parameter space $\{\mathbf{m}, \mathbf{q}, M\}$

$$f_{\text{Ising}}[\mathbf{m},\mathbf{q},M] = \frac{J_0}{2}M^2 - \frac{1}{4}TJ^2\chi_{ne}^2 + \frac{1}{4}\beta J^2 \sum_{i=1}^{\kappa} m_i(q_i^2 - q_{i+1}^2) - \mathcal{T}(h + J_0 M) \tag{2.64}$$

where the trace term is given by

$$\mathcal{T}(h + J_0 M) = \frac{T}{m_\kappa} \int_{\kappa+1}^G \log \left[\int_\kappa^{GE} ... \int_1^{GE} 2\cosh(\beta H_{\text{eff}}) \right]. \tag{2.65}$$

From expression (2.64) the proper order parameters can be obtained by extremization. For large order parameters q_i and M the field term is dominant because it depends quadratically on them whereas the dependence in the trace term is linear. With this in mind, it is readily seen that f is bounded from below with respect to M, so that extremization with respect to M means minimization, as usual. For the parameters q_i, however, the converse is found, i.e. f is bounded from above with respect to q_i, because of the prefactor $(m_i - m_{i-1}) < 0$ of q_i^2 in the field term (see Appendix C.2). Therefore, extremization of f means *maximization with respect to* q_i. The hand-waving argument of a negative number of parameters from the discussion of the replica symmetric approximation can also be applied here.

The large a_i behavior is not that easily seen and so it is not a priori clear whether f must be maximized or minimized with respect to a_i. Since one must find a saddle point[22], anyway, it is most convenient to calculate the self-consistent order parameters by means of a root search of the f gradient in the order parameter space.

For convenience in notation, the energy scale of the system is usually defined in units of J. This is done by the rescaling

$$\beta J \to \beta, \qquad \frac{f}{J} \to f, \qquad \frac{h}{J} \to h, \qquad \frac{J_0}{J} \to J_0. \tag{2.66}$$

This is equivalent with setting $J = 1$ everywhere in the theory. If not explicitly stated elsewise, this convention is used in the remainder of this thesis.

[20] See also Appendix C.1.

[21] The quantity χ_{ne} will be derived in section 2.5.

[22] Here, not the complex saddle point is meant, but the saddle point which arises at the minimum/maximum of f with respect to M and q_i, respectively.

2.3.2 The quasi-isotropic n-component spin glass

An important condition for the tractability of the Ising spin glass is the possibility to define families, superfamilies, etc. of individual factors in (2.56). In the $n = 1$ case, this was possible because at each hierarchy level i, only one family size m_i existed. For $n > 1$, however, the possibility of different family sizes $m_i^\nu \neq m_i^{\nu'}$ for different spin components $\nu \neq \nu'$ opens up and this scenario would be much harder to treat. To avoid such a complication for $n > 1$, I restrict the further discussion to the treatment of the quasi-isotropic n-component spin glass, i.e.

$$q_{ab}^\nu = q_{ab} \tag{2.67}$$
$$M_a^\nu = M \tag{2.68}$$
$$J_0^\nu = J_0 \tag{2.69}$$
$$h_\nu = h \tag{2.70}$$
$$J_\nu = J. \tag{2.71}$$

In this subsection, I directly define J as the energy scale, like in the preceding subsection, by setting $J = 1$. Within the quasi-isotropic special case all the replica matrices $\mathbf{q}^\nu$ are identical by symmetry so that the index ν can be dropped. As a result, an analysis similar to the Ising case is applicable. This will not be repeated here in detail. I will only point out the main differences.

First of all, the number of fields $z_{j,i}^\nu$ is n times larger than for the Ising case and so one gets n integrals instead of only one from (2.52) at each level of integration. However, these integrals can be lumped together in the definition (see Appendix C.1)

$$\int_i^G f(\{z_j^\nu\}) = \int \frac{d^n\mathbf{z}_i}{(2\pi)^{n/2}} \exp\left(-\frac{|\mathbf{z}_i|^2}{2}\right) f(\{z_j^\nu\}) \tag{2.72}$$

where $\mathbf{z}_i = \sum_\nu \hat{\mathbf{e}}_\nu z_i^\nu$ is defined and $\{\hat{\mathbf{e}}_\nu\}$ is a set of orthonormal vectors. As a result, the form of the trace term (2.65) remains the same. The exponentiated integral operators $\int^{GE}$ are defined in analogy to (2.60) but with $\int^G$ replaced by the n-component version in (2.72). The hierarchical ordering is done in the same fashion, but instead of a scalar H_{eff}, one obtains a vector-valued effective field. A preliminary definition (symbolized by the tilde) corresponding to the situation before the evaluation of the first integral is given by

$$\tilde{\mathbf{H}}_{\text{eff}} = \sum_\nu \hat{\mathbf{e}}_\nu \tilde{H}_{\text{eff}}^\nu, \qquad \tilde{H}_{\text{eff}}^\nu = h + J_0 M + \sum_{i=0}^{\kappa+1} \sqrt{\Delta q_i} z_i^\nu \tag{2.73}$$

with which the (preliminary) trace term, which can be written as

$$\tilde{\mathcal{T}}(h + J_0 M) = \frac{T}{m_\kappa} \int_{\kappa+1}^G \log\left[\int_\kappa^{GE} ... \int_1^{GE} \int_0^G \mathcal{C}_n(\beta|\mathbf{H}_{\text{eff}}|)\right]. \tag{2.74}$$

Following Appendix A.2, the first integral in this sequence is then evaluated and the resulting factor $\exp(\beta^2/2\Delta q_1 L_S^2)$ is pulled through the integrals as described in Appendix A.3, giving a term $-\frac{\beta}{2}(1-q_1)L_S^2$ in the free energy. By combining this term with the field term (2.47) one obtains the final expressions for the free energy

$$f = n\left[\frac{J_0}{2}M^2 - \frac{\beta}{4}(1-q_1)^2 + \frac{\beta}{4}\sum_{i=1}^{\kappa} m_i(q_i^2 - q_{i+1}^2)\right] - \mathcal{T}(h + J_0 M) \tag{2.75}$$

with the trace term

$$\mathcal{T}(h + J_0 M) = \frac{T}{m_\kappa} \int_{\kappa+1}^G \log\left[\int_\kappa^{GE} ... \int_1^{GE} \mathcal{C}_n(\beta|\mathbf{H}_{\text{eff}}|)\right] \tag{2.76}$$

where the effective field components are $H_{\text{eff}}^\nu = h + J_0 M + \sum_{i=1}^{\kappa+1} \sqrt{\Delta q_i} z_i^\nu$. Note that the sum runs from $i = 1$ to $\kappa + 1$ as opposed to (2.73) where the sum starts at $i = 0$.

2.3.3 h-field integration

In the formulation of the trace term in the two preceding subsections, $\kappa+1$ integral operators, each n-dimensional, act on a function of $n(\kappa+1)$ field components z_i^ν. Due to the exponentiation involved in the Gaussian integral operators $\int^{GE}$, these operators are non-linear and essentially non-commutative. Therefore the sequence of integral operators inside of the log in the trace terms (2.65) or (2.76) cannot be transformed to a $n\cdot\kappa$-dimensional Gaussian integral with $O(n\kappa)$ symmetry, which would simplify the computation considerably. Thus, one effectively must integrate numerically over a $\kappa\cdot n$-dimensional space, and in principle the cost of such a task grows exponentially with κ.

Nevertheless, one can gain considerable conceptual and numerical simplification by transforming to a recursive sequence of κ Gaussian convolutions which obey at least an $O(n)$ symmetry for quasi-isotropic n-component glasses. The cost of successive numerical application of κ convolution operators only grows polynomially with κ and thus, the importance of this transformation cannot be overemphasized. This transformation replaces the integration variables $\mathbf{z}_i$ by a sequence of $\mathbf{h}$-fields[23] defined by

$$\mathbf{h}_1=\mathbf{H}_{\rm eff},\qquad \mathbf{h}_i=\sum_\nu \hat{\mathbf{e}}_\nu(h+J_0M)+\sum_{j=i}^{\kappa+1}\sqrt{\Delta q_i}\mathbf{z}_i \qquad\Rightarrow\qquad \mathbf{z}_i=\frac{\mathbf{h}_i-\mathbf{h}_{i+1}}{\sqrt{\Delta q_i}}. \tag{2.77}$$

Within this formulation, at each level of integration[24] i there is a function of one vector valued variable $\mathbf{h}_{i+1}$, whereas in the original formulation one has to deal with a function of $(\kappa+1-i)$ variables $\mathbf{z}_j$ at the ith level. The operators $\int_i^{GE}$ act on functions of a single field variable $\mathbf{h}_i$ and the result of the application of this operator is a function of the next field variable in the sequence. Thus the ith level exponentiated Gaussian operator in $\mathbf{h}$-field formulation is conveniently defined by its action on a general function $f(\mathbf{h}_i)$ of the field variable $\mathbf{h}_i$

$$\int_i^{GE} f(\mathbf{h}_i)\equiv\int\frac{d^n\mathbf{h}_i}{(2\pi\Delta q_i)^{n/2}}\exp\left(-\frac{1}{2\Delta q_i}|\mathbf{h}_i-\mathbf{h}_{i+1}|^2\right)[f(\mathbf{h}_i)]^{r_{i-1}} \tag{2.78}$$

with the usual block-size ratios $r_i=\frac{m_{i+1}}{m_i}$. It is important to note here that, if $f(\mathbf{h}_i)$ is a function of the absolute value $|\mathbf{h}_i|$ only, then the function of $\mathbf{h}_{i+1}$ which results from $\int_i^{GE} f(\mathbf{h}_i)$ is also independent of the orientation of $\mathbf{h}_{i+1}$.

It is now convenient, from an analytical point of view as well as from numerical considerations, to formulate the trace term recursively in terms of a sequence of functions $f_i^{\rm sub}(h_{i+1})$ which are interconnected by the recursion relation

$$f_i^{\rm sub}(h_{i+1})=\int_i^{GE} f_{i-1}^{\rm sub}(h_i), \tag{2.79}$$

and an initial condition $f_0^{\rm sub}(h_1)=\mathcal{C}_n(\beta h_1)$. Since the kernel $\mathcal{C}_n$ in (2.76) is a function of $|\mathbf{H}_{\rm eff}|=|\mathbf{h}_1|=h_1$ only, it is clear by induction that each $f_i^{\rm sub}$ in the sequence is spherically symmetric in $\mathbf{h}_{i+1}$ and the definition of $f_i^{\rm sub}$ as a function of $h_{i+1}=|\mathbf{h}_{i+1}|$ does not cause a loss of generality.

With this recursive sequence of functions, the trace term (2.76) of the quasi-isotropic spin glass[25] can be written in terms of the last function in the recursion sequence $f_\kappa^{\rm sub}$ as

$$\mathcal{T}(h+J_0M)=\frac{T}{m_\kappa}\int_{\kappa+1}^{G}\log f_\kappa^{\rm sub}(h_{\kappa+1}) \tag{2.80}$$

where the dependence on $h+J_0M$ is implemented through the remaining integral operator $\int_{\kappa+1}^G$ by setting $h_{\kappa+2}=\sqrt{n}(h+J_0M)$. Remarkably, by the transformation to $\mathbf{h}$-field integrals, the explicit dependence on the external field and the magnetization has been transformed from level 1, i.e. directly from the kernel $\mathcal{C}_n$ to the highest level, even outside of the logarithm. That this is extremely desireable will be seen in Section 2.5 where partial derivatives of f with respect to M or h must be calculated.

At this point, it is obvious that the form of the recursive theory as introduced above is independent of the number of spin components n. The explicit expressions for $\mathcal{C}_n(x)$ and $\int_i^{GE}$ do depend on n, of course. This,

[23] The h-field transformation is presented here for quasi-isotropic n-component spin systems, in which the fields are initially vector-valued. The Ising case is easily obtained as the special case $n=1$, where h-fields are scalar fields.

[24] With level, I mean the depth in the integration sequence of the trace term from now on. For instance, $\mathcal{C}_n(\beta|\mathbf{H}_{\rm eff}|)$ is the 0th level and after the operator $\int_1^{GE}$ acts, the level number is 1.

[25] Of course, the Ising spin glass is included as a special case.

however, can be regarded as a numerical detail, since solving the recursion relation for finite κ is a task for a computer program, anyway. The important point is that, from a *conceptual* point of view, the theory is formally invariant with respect to a change of n.

The explicit expressions of the initial condition $f_0^{\text{sub}} = \mathcal{C}_n$ have been given in Section 2.2. For the explicit form of the integral operators, one must perform the integration of the angular parts in (2.78). This is straightforward for general n and leads to

$$\int_i^G f(h_i) = \int_0^\infty \frac{dh_i}{\Delta q_i} h_i^{\frac{n}{2}} \exp\left(-\frac{h_{i+1}^2 + h_i^2}{2\Delta q_i}\right) \frac{I_{\frac{n}{2}-1}\left(\frac{h_i h_{i+1}}{\Delta q_i}\right)}{h_{i+1}^{\frac{n}{2}-1}} f(h_i), \tag{2.81}$$

where $I_\alpha(x)$ is the modified Bessel function. $I_\alpha(x)$ has a simple asymptotic form $I_\alpha(x) = e^x/\sqrt{2\pi x}$ for $x \gg 1$, so that in the asymptotic regime, equation (2.81) becomes

$$\int_i^G f(h_i) \simeq \int_0^\infty \frac{dh_i}{\sqrt{2\pi\Delta q_i}} \left(\frac{h_i}{h_{i+1}}\right)^{\frac{n-1}{2}} \exp\left(-\frac{(h_i - h_{i+1})^2}{2\Delta q_i}\right) f(h_i), \qquad \text{for } h_{i+1} \to \infty. \tag{2.82}$$

The asymptotic behavior of the recursion relation is important for numerical simplifications in the Ising spin glass at low temperatures. For the most interesting cases of $n = 1, 2, 3$ equation (2.81) simplifies to

- **Ising spin glass:** $n = 1$

$$\int_i^G f(h_i) = \int_{-\infty}^\infty \frac{dh_i}{\sqrt{2\pi\Delta q_i}} \exp\left(-\frac{(h_{i+1} - h_i)^2}{2\Delta q_i}\right) f(h_i) \tag{2.83}$$

- **XY spin glass:** $n = 2$

$$\int_i^G f(|h_i|) = \int_0^\infty \frac{dh_i}{\Delta q_i} h_i f(h_i)\, e^{-\frac{1}{2\Delta q_i}(h_i^2 + h_{i+1}^2)} I_0\left(\frac{h_i h_{i+1}}{\Delta q_i}\right) \tag{2.84}$$

- **Heisenberg spin glass:** $n = 3$

$$\int_i^G f(|h_i|) = \int_{-\infty}^\infty \frac{dh_i}{\sqrt{2\pi\Delta q_i}} \exp\left(-\frac{1}{2\Delta q_i}(h_i - h_{i+1})^2\right) \frac{h_i}{h_{i+1}} f(h_i) \tag{2.85}$$

For an odd number of components, the index of the modified Bessel function is half-integer. In those cases it can be expressed in terms of hyperbolic functions which are numerically less expensive. For even n, however, one must deal directly with the numerical representation of the Bessel functions.

Remarkably, the Gaussian integral of the Heisenberg spin glass is, similar to the Ising spin glass, equal to its asymptotic form.

2.4 Low temperature formalism

The above formulation of the theory in terms of block size parameters m_i is convenient at temperatures T between about 0.3 and the freezing temperature $T_C = 1$[26]. In this temperature range, the m_i are more or less uniformly distributed over the interval $[0, \bar{x}_1]$, where $\bar{x}_1 \in [0, 1]$ is the so-called break point[27]. For temperatures near $T = 0$, however, all parameters m_i approach zero for finite orders of RSB. At the same time, the factors $\beta = 1/T$ diverge as $T \to 0$. In order to be able to formulate a meaningful theory directly at $T = 0$, these singularities must be accounted for. In the present section, it will be discussed how this is accomplished by means of a singular rescaling of the m_i parameters.

[26] Remember that the energy, as well as the temperature scale has been redefined in units of J. Without setting this energy scale, one obtains $T_C = J$.

[27] In the temperature regime which is investigated in this work, the break point is approximately 0.5. For more informations, see chapters 4 and 5.

2.4.1 Parameter rescaling

The form of the field term in the free energy (2.75), especially the combination in which β and m_i appear in the sum term, is highly suggestive of an absorption of the β divergence into the block size parameters m_i. This is done by a rescaling with temperature and the introduction of *rescaled block size parameters*[28]

$$a_i(T) \equiv \beta m_i(T). \tag{2.86}$$

Since the original Parisi block sizes m_i vanish linearly with temperature, at $T = 0$ the a_i parameters are the linear temperature coefficients in a Taylor series of $m_i(T)$. In other words, the block sizes at zero temperature are trivially zero and thus the leading temperature dependences of the block sizes are the proper order parameters in this case.

At finite temperatures the a-based formalism is equivalent to the m-based formalism. At very low temperatures, however, the quantities which must be handled in the a-formalism remain well behaved[29] in contrast to the m-based quantities. This even allows for calculations at $T = 0$ directly. The free energy in terms of the rescaled block size parameters a_i reads

$$f = n\left[\frac{J_0}{2}M^2 - \frac{\beta}{4}(1-q_1)^2 + \frac{1}{4}\sum_{i=1}^{\kappa} a_i(q_i^2 - q_{i+1}^2)\right] - \mathcal{T}(J_0 M + h) \tag{2.87}$$

with the trace term

$$\mathcal{T}(J_0 M + h) = \frac{1}{a_\kappa}\int_{\kappa+1}^{G} \log\left[\int_{\kappa}^{GE} ... \int_{2}^{GE}\int_{1}^{G} \left[\mathcal{C}_n\left(\beta h_1\right)\right]^{a_1 T}\right]. \tag{2.88}$$

In the field term, the only explicit temperature dependence is found in the term $-\beta(1-q_1)^2$ and this term is even singular at $T = 0$. Thus, this term must be handled analytically before the self-consistence equations are numerically solved.

For $q_1 \neq 1$ this term becomes the dominant contribution to the field term at $T = 0$: the term is $-\infty$ for any $q_1 \neq 1$ in the zero temperature limit. The trace term on the other hand remains finite for any allowed q_1 and thus it follows from the maximization principle of the free energy with respect to q_1 that $\lim_{T\to 0} q_1 = 1$. By expanding q_1 in a Taylor series near $T = 0$ it is obvious that the term $-\beta(1-q_1)^2$ even vanishes at $T = 0$.

Regarding the trace term $\mathcal{T}$ it should be noted that the first Gaussian operator $\int_1^G$ is not the exponentiated version. The exponent has been explicitly assigned to $\mathcal{C}_n$ in order to be able to exploit the linear T dependence of the parameter m_1. This is important for rendering the integrand finite at $T = 0$.

In analogy to equations (2.80) and (2.79), the trace term again can be expressed recursively. The initial condition in a-formulation, however, must be defined in combination with the temperature exponent as $f_0^{\mathrm{sub}}(h_1) = \left[\mathcal{C}_n(\beta h_1)\right]^T$ in order to obtain a meaningful zero temperature limit. Apart from the first ratio r_0 which must be adapted to $r_0 = a_1$, the definition of the block size ratios $r_i = \frac{m_{i+1}}{m_i} = \frac{a_{i+1}}{a_i}$ remains formally invariant when transforming from m_i formulation to a_i formulation. As a result, the same recursion relation (2.79) is valid in m-formulation as well as in a-formulation. With the recursively defined functions f^{sub} in a-formulation, the trace term of the free energy reads

$$\mathcal{T}(J_0 M + h) = \frac{1}{a_\kappa}\int_{\kappa+1}^{G} \log f_\kappa^{\mathrm{sub}}(h_{\kappa+1}). \tag{2.89}$$

Within the a-formulation of RSB, one can directly perform the zero temperature limit of the initial condition of the recursion. If the a_i parameters are assumed to remain finite as $T \to 0$ - and it turns out that this is indeed true for $\kappa < \infty$, the only $1/T$ divergence is located at the argument of the inner integrand $\mathcal{C}_n(\beta h_1)$. However, the integrand is exponentiated by temperature due to the rescaling. Thus one obtains a simple expression for the zero temperature limit of the initial condition[30] by exploiting the asymptotic form of the modified Bessel functions

$$\lim_{T\to 0} f_0^{\mathrm{sub}}(h_1) = \lim_{T\to 0}\left[\mathcal{C}_n(\beta h_1)\right]^{a_1 T} = e^{\sqrt{n} a_1 |h_1|}. \tag{2.90}$$

[28] The implicit temperature dependence of the parameters is made explicit at this point for clarity, only.

[29] Well behaved means especially that the numbers do not exceed the numerical capacity of standard computer arithmetics.

[30] At this point one must distinguish between finite a_1 and $a_1 = \infty$. The first case always happens at finite order of RSB. Then the given zero temperature limit is valid. In the limit $\kappa \to \infty$, however, a_1 also approaches infinity. This case will be discussed in Chapter 5.

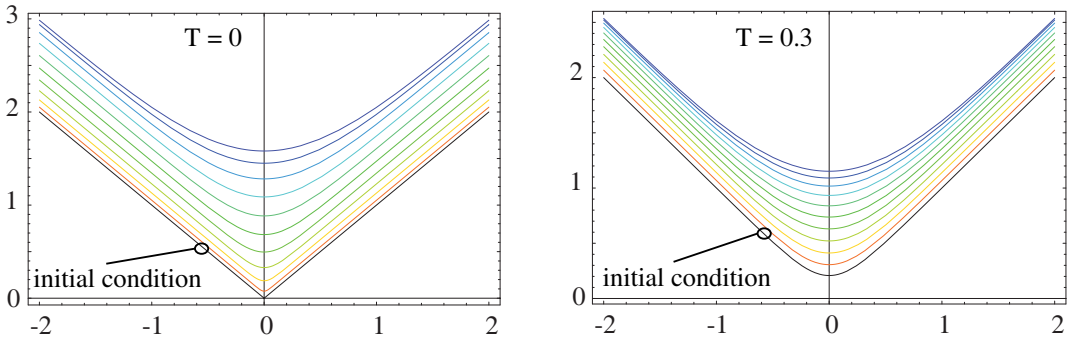

Fig. 2.2: Plots of $\frac{1}{a_i}\log f_i^{\mathrm{sub}}(h)$, $i = 0, ..., 10$ at zero temperature (left) and $T = 0.3$ (right) for 10 RSB in case of an Ising spin glass ($n = 1$). The lowest black curves represent the initial condition of the recursion scheme in both cases.

Remarkably, the zero temperature limit of the inner integrand of an arbitrary n-component spin glass is equal to the asymptotic form of the Ising kernel. This is a typical for classical n-component spin systems and is also encountered in the mean-field theory of n-component models of a ferromagnet, as pointed out in the introduction. In this case, however, the trivial solutions for the magnetization per spin $|\mathbf{M}| = 1$ of the equation $M = \tanh(\beta J_0 M)$ are obtained. Physically, this is reasonable because at zero temperature a classical spin in a ferromagnet does not move at all; the system is and remains in its ground state and all spins point into the same direction, no matter whether different orientations are possible or not. In a spin glass, however, many ground states exist in which the spins point into all possible directions. Thus, the number of possible spin directions matters and so the trace term $\mathcal{T}$ depends on the number n of spin-components, though the initial condition does not: the n-dependence of $\mathcal{T}$ is incorporated only through the different Gaussian integral operators for different numbers of spin components.

At this point, it is useful to discuss the recursive formalism in view of the qualitative introduction to spin glass theory in Section 1.4. The IFM kernel which was discussed there is equal to the initial condition f_0^{sub}. On the left side of Figure 2.2 the sequence of functions $\frac{1}{a_i}\log f_i^{\mathrm{sub}}$ for zero temperature is shown. Obviously, the situation is not quite the same as described in Figure 1.2. In the asymptotic regime, there is an upward shift due to a multiplicative correction to f^{sub}. In the next subsection, it will be seen that this shift is given by a combination of the a_i and q_i parameters and can be removed by transforming it to the field term. However, apart from this shift the situation is as described in the introduction: one starts with the V-like initial condition which is represented by the black line in Figure 2.2. This is the same as if one would look at an Ising ferromagnet model at $T = 0$. Then by successively applying the recursion relation (2.79) the cusp is rounded and the top blue curve is obtained at the end of the recursion scheme. This is the action of RSB on the IFM kernel. Then one last Gaussian average must be performed on $\frac{1}{a_\kappa}\log f_\kappa^{\mathrm{sub}}$ to finally calculate the trace term.

In a $T = 0$ calculation within the replica symmetric approximation (i.e. $\kappa = 0$) the V-like initial condition is set directly in (2.89) and the Gaussian average is performed on the IFM-kernel as described in the introduction. For $\kappa > 0$, however, the hierarchical averaging described by the recursion relations changes the IFM kernel to the RSB kernel. The explicit averaging is to be self-consistently determined by extremizing the free energy with respect to the parameters on which the averaging procedure depends, i.e. q_i and a_i.

At finite temperatures, the initial condition has no sharp cusp at $h = 0$ so that the RSB averaging process only quantitatively changes the degree of rounding. This is shown in the right part of Figure 2.2. Here again, an upwards shift in the asymptotic regime appears. As in the zero temperature case, it will be transformed to the field term of the free energy in the next subsection.

The Parisi block sizes m_i were restricted to the interval $[0, 1]$. Due to the rescaling with β, the domain of the new block size parameters a_i is the interval $[0, \beta]$ which becomes semi-infinite at $T = 0$. Nevertheless, as long as a finite number of RSB steps are considered, all a_i remain finite even at zero temperature. Sometimes, however, boundary values of the sequence of numbers a_i are needed in certain rearrangements of the sum terms which appear in the free energy[31]. This is done by defining $a_{\kappa+1} = 0$ and $a_0 = \beta$. These boundaries are fixed and must not be understand as self-consistent order parameters.

[31] The aim of these rearrangements is mostly, to see the connection to an integral of the form $\int_0^\beta da$.

2.4.2 Asymptotic renormalization group

In general, the recursion relation (2.79) cannot be solved analytically and one has to resort to numerical techniques. In the asymptotic regime, however, the recursion can be written in form of a renormalization group and the behavior for $h_i \to \infty$ at each level of integration can be calculated analytically.

Since prefactors of the inner integrand are irrelevant (see Appendix A.3), I consider only proportionality up to an h-independent factor for now. It is found[32] for finite temperatures in m and a formulation, respectively, that f^{sub} can be written asymptotically as

$$f_i^{\mathrm{sub}}(h_{i+1}) \sim \left[\frac{\exp(\beta L_S h_{i+1})}{h_{i+1}^{(n-1)/2}}\right]^{m_i} = \frac{\exp(a_i L_S h_{i+1})}{h_{i+1}^{\frac{n-1}{2} a_i T}} \tag{2.91}$$

at each level i. In the limit $T \to 0$, where a formulation in terms of m_i becomes invalid, the exponent of the denominator vanishes, provided that a_i is finite. Since this is always the case for $\kappa < \infty$, one obtains - in analogy to the zero temperature initial condition (2.90) - a simple asymptotic form

$$f_i^{\mathrm{sub}}(h_{i+1}) \sim \exp(a_i L_S h_{i+1}). \tag{2.92}$$

Here again, the asymptotic form of f^{sub} is independent of the number of spin components n in the zero temperature limit[33]. The small h regime, however, depends on n and, as it determines the nontrivial spin glass properties, this is the regime where RSB is important and where it changes the physics.

Apart from the conceptual information that RSB does not act on the asymptotic regime of the kernels in the trace term, the asymptotic behavior is important for two further reasons. Firstly, analytical knowledge about the large h regime can be used to fix boundary conditions in a continuous RSB theory[34] where the recursion relation (2.79) passes over to a partial differential equation. Secondly, at finite κ it can be used to dramatically reduce the numerical cost of computing all the functions f_i^{sub} by the recursion relation[35].

To automatically keep track of the asymptotic behavior of f^{sub}, a new set of auxiliary functions - the kernel correction functions - $\{\mathrm{ker}\mathcal{C}_i(h_{i+1})\}_{i=0}^{\kappa}$ is introduced. They describe the evolution of the initial condition due to the RSB recursion in terms of the deviation of f^{sub} from its asymptotic h-behavior near $h = 0$. The kernel correction functions are defined at each recursion level i as

$$f_i^{\mathrm{sub}}(h) = \exp\left[a_i\left(\frac{1-n}{2} T \log(\beta L_S h_{i+1}) + \frac{1}{2}\sum_{j=1}^{i} a_j \Delta q_j + |h| + \mathrm{ker}\mathcal{C}_i(h)\right)\right]. \tag{2.93}$$

The recursion relation of the functions f_i^{sub} can be translated to recursion relations for $\mathrm{ker}\mathcal{C}_i$. The logarithmic term in (2.93) leads to a singularity at small h. However, the term vanishes for an Ising spin glass ($n = 1$) or at zero temperature. This is where the ker$\mathcal{C}$-formalism gets especially convenient. In the $T \neq 0$ and $n \neq 1$ cases, the logarithmic divergence of the first term would have to be compensated by the ker$\mathcal{C}$-term. However, one could save the numerics by introducing an artificial regularization which renders the first term finite at $h = 0$, for instance by replacing $\log(\beta L_S h_{i+1}) \to \log(\beta L_S h_{i+1} + e^{-\lambda h_{i+1}})$ with a parameter λ which can be chosen by numerical convenience.

I will now discuss the most interesting cases of an Ising spin glass at arbitrary temperatures and of an n-component spin glass at $T = 0$. The analysis of these special cases in high RSB orders is sufficient to understand the zero temperature properties of RSB. Of course, calculations of non-Ising spin glasses at non-zero temperature can also be performed. It is may be more convenient, however, to do this by means of the f^{sub}-recursion formulation.

[32] See Appendix A.4

[33] Within the usual convention that $L_S^2 = n$, the form (2.92) does trivially depend on n, of course. This dependence, however, is not fundamental because it could be removed by an integral transformation $dh \to d(L_S h)$.

[34] See chapter 5.

[35] By implementing the knowledge about asymptotic behavior in the numerics the code got faster by about a factor of 10 while numerical accuracy increased considerably at the same time.

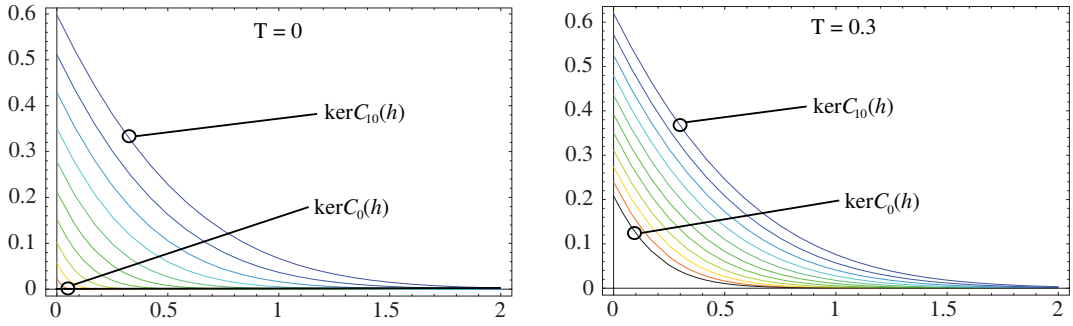

Fig. 2.3: Plots of ker$\mathcal{C}_i(h)$, $i = 0, ..., 10$ at zero temperature (left) and at $T = 0.3$ (right) for a calculation within 10 RSB of an Ising spin glass. In the zero temperature plot, the initial condition ker$\mathcal{C}_0(h)$ is exactly zero, while for finite temperatures it is represented by the lowest black curve.

2.4.3 The kernel correction function for an Ising spin glass

For one spin component the logarithmic term in equation (2.93) has a zero prefactor and the definition of the kernel correction function simplifies to

$$f_i^{\text{sub}}(h) = \exp\left[a_i\left(\frac{1}{2}\sum_{j=1}^{i} a_j \Delta q_j + |h| + \ker\mathcal{C}_i(h)\right)\right]. \tag{2.94}$$

In the last integration of f_κ^{sub} with respect to $h_{\kappa+1}$ in the trace term (2.88), one may combine the sum of $a_i\Delta q_i$ with the sum in the field term of the free energy (2.87). Doing so, one obtains an expression of the free energy per spin of the Ising spin glass at κth order of RSB in terms of the function ker$\mathcal{C}_\kappa$ which results from passing through the whole recursion scheme

$$f = \frac{J_0}{2}M^2 - \frac{\beta}{4}(1-q_1)^2 + \frac{1}{4}\sum_{i=1}^{\kappa} a_i\left((q_i-1)^2 - (q_{i+1}-1)^2\right) - \int_{\kappa+1}^{G}\left(\ker\mathcal{C}_\kappa(h) + |h|\right), \tag{2.95}$$

where the last Gaussian integral must be centered at $h_{\kappa+2} = J_0 M + h$, as usual.

The recursion relation between the kernel correction functions at different levels i can be obtained from the recursion relation of the functions f_i^{sub} given by equation (2.79). According to the the relation between f^{sub} and ker$\mathcal{C}$ given by (2.94) one finds

$$\ker\mathcal{C}_i(h) = \frac{1}{a_i}\log\left[\int_{-\infty}^{\infty}\frac{dh'}{\sqrt{2\pi\Delta q_i}}\exp\left(-\frac{1}{2}a_i^2\Delta q_i + a_i(|h'|-|h|) - \frac{(h-h')^2}{2\Delta q_i}\right)\exp\left(a_i\ker\mathcal{C}_{i-1}(h')\right)\right]. \tag{2.96}$$

The kernel correction functions have been designed such that the initial condition ker$\mathcal{C}_0$ vanishes at zero temperature. At finite temperatures, the initial condition is given by

$$\ker\mathcal{C}_0(h) = \log\left[(2\cosh(\beta h))^T\right] - |h| = T\log\left(1+\exp\left(-\frac{2|h|}{T}\right)\right). \tag{2.97}$$

Already at this point, I want to draw the readers attention to the typical problems that will be encountered in the ∞RSB limit. At each finite temperature, the slope of the initial condition in (2.97) is -1 at $h = 0^+$. At zero temperature, however, where ker$\mathcal{C}_0(h) \equiv 0$, also the derivative of ker$\mathcal{C}_0(h)$ is zero, of course, especially at $h = 0^+$. On the other hand, if one first evaluates the h-derivative at finite temperatures and performs the zero temperature limit of ker$\mathcal{C}_0'$ afterwards, one finds

$$\ker\mathcal{C}_0'(h) = -\frac{2}{e^{2\beta h}+1} \quad \Rightarrow \quad \lim_{T\to 0}\ker\mathcal{C}_0'(h) = \begin{cases} 0 & \text{for } h > 0 \\ -1 & \text{for } h = 0 \end{cases}. \tag{2.98}$$

Consequently, if the limits are performed in this order, i.e. calculation of the derivative before zero temperature limit, the second derivative is singular at $h = 0$ for $T \to 0$.

$$\ker\mathcal{C}_0''(h) = \frac{4\beta}{e^{2\beta h}+e^{-2\beta h}+2} \quad \Rightarrow \quad \lim_{T\to 0}\ker\mathcal{C}_0''(h) = \begin{cases} 0 & \text{for } h > 0 \\ \infty & \text{for } h = 0 \end{cases}. \tag{2.99}$$

The appearance of a non-commutativity of two limits, i.e. in the present case the limit $h \to 0$ and the limit contained in the definition of derivatives, is typical for replica symmetry breaking, especially in the $\kappa \to \infty$ limit. Another example of non-commutativity is met in discussion of the question whether in the limit of zero temperature and infinite order of RSB, all parameters m_i become dense or not.

For the finite RSB technique at zero temperature which has been derived in the present chapter, the issue of the divergency in the second derivative of $\ker\mathcal{C}_0$ is not a problem because one is only concerned with integrals of $\ker\mathcal{C}_i(h)$ in which derivatives do not matter. In the limit $\kappa \to \infty$ which is discussed in Chapter 5, however, a more careful analysis is in order because the derivatives of $\ker\mathcal{C}$ directly enter a partial differential equation (5.10) which describes the a-dependence of $\ker\mathcal{C}$.

2.4.4 The kernel correction function at $T = 0$ for general n

At zero temperature and for general n the logarithmic term in (2.93) vanishes as long as $a_i T = 0$ which is the case for finite κ. Thus, the definition of the kernel correction function is not very different from the Ising case in (2.94). The only difference is a prefactor n in front of the sum term

$$f_i^{\mathrm{sub}}(h) = \exp\left[a_i\left(\frac{n}{2}\sum_{j=1}^{i} a_j \Delta q_j + |h| + \ker\mathcal{C}_i(h)\right)\right]. \tag{2.100}$$

The recursion relation between successive $\ker\mathcal{C}_i$ is different, though. It reads

$$\ker\mathcal{C}_i(h_{i+1}) = \frac{1}{a_i}\log\int_0^\infty dh_i \mathcal{K}_n(h_i, h_{i+1}, \Delta q_i)\exp\left(-\frac{h_i^2 + h_{i+1}^2}{2\Delta q_i} - \frac{n}{2}a_i^2\Delta q_i + a_i(h_i - h_{i+1} + \ker\mathcal{C}_{i-1}(h_i)\right), \tag{2.101}$$

where an additional convolution function

$$\mathcal{K}_n(h_i, h_{i+1}, \Delta q_i) = \frac{I_{\frac{n}{2}-1}\left(\frac{h_i h_{i+1}}{\Delta q_i}\right)}{\Delta q_i h_{i+1}^{n/2-1}} \tag{2.102}$$

has been defined. For $h_{i+1} \to 0$, the convolution function is singular. The singularity can be removed, though, by expanding the modified Bessel function for small arguments $I_n(x) = x^n(c_1 + \mathcal{O}(x^2))$.

$$\mathcal{K}_n(h_i, h_{i+1}, \Delta q_i) \sim \frac{h_i^{n-1}}{(\Delta q_i)^{n/2+1}} + \mathcal{O}(h_{i+1}^2). \tag{2.103}$$

Obviously, the $n > 1$ and $T = 0$ case can be treated numerically in analogy to the Ising case.

2.5 Observables in the replica formalism

In the preceding sections, a powerful formalism has been derived which extends the traditional formulation of replica symmetry breaking in the Parisi gauge [Par80, BY86] to low temperatures in the general case of n-component spin glasses. All the above formulas, however, are only useful for determining the free energy and with it the spin glass order parameters q_i and a_i. In the following section, the above formalism will be connected to the most important observables in context of magnetically ordered systems, namely the free/internal energy and the entropy, as well as magnetization and magnetic susceptibilities.

2.5.1 Free/internal energy and entropy

Let me start with the internal energy per spin u. It is defined as the thermal expectation value of the Hamiltonian (2.1). However, since the Hamiltonian depends on the set of random coupling constants $\{J_{rr'}\}$, again some kind of disorder average must be performed. In the introduction it has been argued that the extensive quantities are the ones which should be directly averaged, and u definitely is an extensive quantity. Therefore one can write

$$u = \left\langle \frac{\mathrm{tr}\, e^{-\beta H} H}{\mathrm{tr}\, e^{-\beta H}} \right\rangle_d = \left\langle -\frac{\partial}{\partial\beta}\log Z \right\rangle_d = \frac{\partial}{\partial\beta}\left\langle -\log Z\right\rangle_d. \tag{2.104}$$

The disorder average is independent of temperature and so one can pull the derivative with respect to β out of the average. Obviously, no complication arises from quenched disorder when considering the internal energy and so it can be obtained by a partial derivative from an expression for the free energy, as usual. A particularly convenient expression for this purpose can be found in equation (2.14) in which no specific form of the $\mathbf{q}^\nu$ matrices has been assumed. Performing the β-derivative leads to

$$u = \frac{\partial(\beta f)}{\partial \beta} = \lim_{l\to 0} \left[\sum_\nu \left(\frac{J_0^\nu}{2} \sum_a (M_a^\nu)^2 + \frac{\beta J_\nu^2}{2} \sum_{a,b} (q_{ab}^\nu)^2 \right) - \frac{\text{tr } e^L \frac{\partial L}{\partial \beta}}{\text{tr } e^L} \right]. \tag{2.105}$$

The derivative of the trace term can be further simplified. A derivative of L with respect to β results in terms proportional to tr $e^L S_\nu^a$ or tr $e^L S_\nu^a S_\nu^b$. These can be evaluated by means of equations (2.17) and (2.18) and one obtains

$$\frac{1}{\text{tr } e^L} \text{tr } e^L \frac{\partial L}{\partial \beta} = \sum_\nu \left[\sum_a (h_\nu + J_0^\nu M_a^\nu) M_a^\nu + \beta J_\nu^2 \sum_{a,b} (q_{ab}^\nu)^2 \right] \tag{2.106}$$

so that the trace term contribution can be combined with the field term contribution and a simple expression for the internal energy is obtained

$$u = \lim_{l\to 0} \frac{1}{l} \sum_\nu \left[\frac{J_0^\nu}{2} \sum_a (M_a^\nu)^2 - \sum_a h_\nu M_a^\nu - \frac{\beta J_\nu^2}{4} \sum_{a,b} (q_{ab}^\nu)^2 \right] \tag{2.107}$$

which only depends polynomially on the parameters q_{ab}^ν and m_a^ν. These parameters must be calculated self-consistently for a specific assumption of the structure of $\mathbf{q}^\nu$ with the help of the formalism, introduced in the preceding sections. However, in contrast to all free energy expressions, no complicated trace term is left in the internal energy. With the help of the formula for replica sums, derived in Appendix A.5, expressions for the RS and the RSB case are easily obtained.

- The replica symmetric case.

$$u = -\sum_\nu \left[\frac{J_0^\nu}{2} M_\nu^2 + h_\nu M_\nu + \frac{\beta J_\nu^2}{2} (1 - q_\nu^2) \right] \tag{2.108}$$

- The RSB case for a quasi-isotropic spin glass.

$$u = -n \left[\frac{J_0}{2} M^2 + hM + \frac{J^2}{2} \sum_{i=1}^{\kappa} a_i (q_i^2 - q_{i+1}^2) + \frac{\beta J^2}{2} (1 - q_1^2) \right] \tag{2.109}$$

At zero temperature, the free energy and the internal energy are equal. It must be remarked at this point, however, that $u = f$ is only true for the self-consistent order parameters q_i, a_i, M. This means that the simple expressions (2.108) and (2.109) cannot be used to derive the self-consistency equations for the order parameters. In any case, the free energy must be used for this task.

The next quantity which is introduced is the entropy per spin s. It is usually defined as the negative slope of the free energy as a function of temperature. It is more convenient, however, to calculate the entropy at finite temperatures from

$$s = \beta(u - f). \tag{2.110}$$

The free energy and the internal energy can be calculated with high accuracy by the above method and the numerical code which has been developed in this work (see Appendix D). As a result, the entropy which is calculated from (2.110) also has only a small numerical error. The combination of equation (2.87) with (2.109) or its RS conterparts to a single expression for s is obvious and will not be stated here explicitly.

At zero temperature, equation (2.110) is singular. The knowledge of the numerical values of f and u at $T = 0$ alone is not any longer sufficient to determine s. Actually, as expected, it is only found that the two energies f and u are equal up to numerical errors at $T = 0$. The straightforward solution to the problem of finding the entropy at $T = 0$ would be to extrapolate $s(T)$ from calculations at finite temperatures to $T = 0$. In 2.5.3, however, an advanced approach for obtaining the zero temperature entropy directly at $T = 0$ without the need for finite T calculations is derived.

2.5.2 Magnetic observables

Like in (anti-)ferromagnetic theories, the magnetic properties of spin glasses are extremely important. They are, however, much less obvious - even in mean-field theory - than the properties of their simpler, disorderless counterparts. I shall start the discussion with the best-known order parameter which is the central quantity in a ferromagnet, i.e. the magnetization vector $\mathbf{M}$. According to thermodynamics, it can be calculated from a partial derivative of the free energy

$$M_\nu = \frac{1}{N}\left\langle \frac{1}{Z}\mathrm{tr}\; e^{-\beta H}\sum_r S_{r\nu}\right\rangle_d = -\frac{\partial}{\partial h_\nu} f \tag{2.111}$$

were H is the fundamental Hamiltonian defined in (2.1). Within the replica formalism, one can plug the free energy given in (2.14) into the right hand side of (2.111) and finds $M_\nu = \lim_{l\to 0}\frac{1}{l}\sum_a M_\nu^a$. The replica order parameter M_ν^a, in turn, must be calculated from the minimization[36] of the free energy. In the limit of $J_0 \to 0$ which will be mostly assumed in this work, the free energy does not depend on M_ν, though. This is physically reasonable because without a finite mean value of the coupling between spins it makes no difference whether the spins are aligned to some extent or not. Nevertheless, a closed self-consistence equation can be given for the magnetization by first differentiating the free energy with respect to M_ν, before the $J_0 \to 0$ limit is performed.

This can be done directly at κth order of RSB by using expression (2.87) for the free energy and differentiating it with respect to M. Some care is needed, however, because of the definition of M as one component of the magnetization vector $\mathbf{M}$. It is best to rewrite terms of the form nM^α with $\alpha = 1, 2$ as the sum over ν-indices from which they originated. Doing so one finds

$$\frac{\partial f}{\partial M_\nu} = J_0 M_\nu - \frac{\partial}{\partial M_\nu}\frac{1}{a_\kappa}\int_{\kappa+1}^{G}\log f_\kappa^{\mathrm{sub}}(h_{\kappa+1}) \stackrel{!}{=} 0. \tag{2.112}$$

The only dependence of the trace term on M_ν is located at the Gaussian integral operator $\int_{\kappa+1}^{G}$ through $h_{\kappa+2}^\nu = h_\nu + J_0 M_\nu$. It is important at this point to not use the simplified formula (2.81) of the Gaussian integral operator in which the angular integrals already have been performed, because an additional angle appears in the integral which cannot be accounted for with hindsight[37]. Instead, the n-dimensional Gaussian integral operator (2.78) must be used. By differentiating the exponential function in its definition $\exp\left[-(2q_{\kappa+1})^{-1}\sum_\nu (h_\nu + J_0 M_\nu + h_{\kappa+1}^\nu)^2\right]$ with respect to M_ν one can cancel down the J_0 factors and finds

$$M_\nu = -\frac{h_\nu + J_0 M_\nu}{q_{\kappa+1}}\mathcal{T}(\mathbf{h}+J_0\mathbf{M}) + \frac{1}{a_\kappa q_{\kappa+1}}\int \frac{d^n\mathbf{h}'}{(2\pi q_{\kappa+1})^{n/2}} h'_\nu \exp\left(-\frac{|\mathbf{h}+J_0\mathbf{M}-\mathbf{h}'|^2}{2q_{\kappa+1}}\right)\log f_\kappa^{\mathrm{sub}}(|\mathbf{h}'|) \tag{2.113}$$

which is meaningful also in the $J_0 = 0$ case. For $\mathbf{h} = 0$ and $J_0 = 0$, the first term becomes trivially zero. In the second term, the integrand becomes spherically symmetric up to the linear dependence on h'_ν. It follows by symmetry in the angular integrations that also the second term vanishes and so, for each order of RSB, $\mathbf{M} = 0$ for zero external field and zero mean of the spin interaction J_0, as expected.

For finite external field and/or J_0, equation (2.113) becomes cumbersome because of the existence of two in general different angles[38] in the integration of the second term. In the special case of $J_0 = 0$, where the free energy does not depend on $\mathbf{M}$, knowledge of the self-consistent magnetization is not needed for calculating the free energy. Thus, there is no need to cope with (2.113) if one is not explicitly interested in the magnetization. The accuracy of the whole computation does not depend on the accuracy of $\mathbf{M}$ so that one can resort to less precise methods for determining $\mathbf{M}$: after the free energy f as a function of the external field h has been calculated, the magnetization can be obtained *a posteriori* by the (numerical) h-derivative of f[39]. This is possible again due to the equality of the fist total and partial derivatives of the self-consistent

[36] In this case it is really a minimization and not a maximization as for the spin glass order parameters q.

[37] Actually, there is a trick which still allows using the simplified Gaussian integral expression: one must sum equation (2.113) over all component indices ν and combine the integrals. By doing this, the two angles which appear under the integral are the same again. This trick has been utilized in the derivation of equation (2.45), for instance. Here, the described method is easier in use, however.

[38] One angle is the angle between $\mathbf{h} + J_0\mathbf{M}$ and $\mathbf{h}'$ and the second angle is the angle between $\hat{\mathbf{e}}_\nu$ and $\mathbf{h}'$.

[39] The accuracy of $\mathbf{M}$ gained by this method, however, is much lower than the accuracy which can be obtained by using equation (2.113). It strongly depends on the resolution of the numerical data in h-direction. Thus, this simpler method is only recommended for $J_0 = 0$.

free energy with respect to the external parameters $\mathbf{h}$ and T: the total derivative of the free energy can be expanded in terms of all partial derivatives

$$\frac{d\,f}{dh} = \frac{\partial f}{\partial h} + \underbrace{\sum_i \frac{\partial f}{\partial q_i}\frac{dq_i}{dh} + \sum_i \frac{\partial f}{\partial a_i}\frac{da_i}{dh} + \frac{\partial f}{\partial M}\frac{dM}{dh}}_{=0}. \tag{2.114}$$

The self-consistent values of the order parameters a_i, q_i and M are defined as the point in the order parameter space in which the gradient of the free energy vanishes. As a result, all terms, but the partial derivative of f with respect to h on the right hand side of (2.114) vanish and thus the first order partial and total derivative of f with respect to h is equal. This statement remains true, of course, also for temperature derivatives of first order.

For more than one spin component, only quasi-isotropic spin glasses, where all components h_ν and M_ν are equal, are considered. Thus, one must be careful in normalizing the total derivative. If one could change the components of $\mathbf{h}$ separately then, by explicitly writing out the dependence of f on the components of $\mathbf{h}$, the magnetization component is

$$M_\nu = -\frac{d\,f(h_1, h_2, ..., h_n)}{dh_\nu}. \tag{2.115}$$

In the case of the quasi-isotropic n-component spin glass, however, all external field components are varied at the same time and one must consider instead

$$-\frac{d\,f(h, h, ..., h)}{dh} = -\sum_\nu \frac{\partial\, f}{\partial h_\nu}\frac{dh_\nu}{dh} = nM \qquad \Rightarrow \qquad M = -\frac{1}{n}\frac{d\,f}{dh}. \tag{2.116}$$

In an n-component spin glass, the length L_S of a spin vector has been normalized to $L_S^2 = n$. Thus for maximum alignment in one direction[40] ν, the magnetization component $M_\nu = \sqrt{n}$ and $|\mathbf{M}|^2 = n$. This situation can be transformed to quasi-isotropy by rotating the magnetization vector such that all components are equal, i.e. $|\mathbf{M}|^2 = \sum_\nu M_\nu^2 = nM^2 = n$. As a result, the maximum magnetization $M = M_\nu$ becomes unity within the conventions used in this thesis.

In the calculation of the magnetization, it was sufficient to consider the total derivative of f instead of its partial derivative, because all remaining terms in the total derivative of f contain first partial derivatives of f with respect to an order parameter and those are zero because of the very definition of the order parameter. For susceptibilities, this simplification is not generally applicable. This is due to the appearance of terms with higher order derivatives of f with respect to order parameters, which do not vanish per definition as the first order derivatives do.

A second complication lies in the interpretation of the susceptibility. Ergodicity breaking plays an important role in the magnetic properties of spin glasses. The question is: how long does the experimentalist wait after having changed the external field h by a small amount until he starts the measurement of the resulting change in magnetization. In other words, the relaxation time is important. In this context, the equilibrium susceptibility χ_e and the non-equilibrium susceptibility χ_{ne} must be defined, corresponding to the long relaxation time and the short relaxation time regime, respectively.

Let me start with the discussion of the equilibrium susceptibility χ_e. Its physical meaning is the linear response of the magnetization M to a small change in the external field h. The measurement of M is performed after an infinitely long time[41] in which the system is allowed to relax back to equilibrium. In other words, the equilibrium susceptibility regards the system as if ergodicity breaking was absent. An analogy with an Ising ferromagnet again helps to understand this concept. The IFM has two ergodic components in the ordered phase, i.e. positive or negative magnetization. Say, the system is in the ergodic component with positive M. Then measuring the magnetization in a 'normal' experiment would yield a positive M, of course, because the system is trapped in one ergodic component and can't escape in a finite time. The experiment which is related to χ_e, however, measures infinitely long, so that the system can switch between the ergodic components and the measurement yields $M = 0$. In a ferromagnet, considering such a measurement does not make sense. It is better to identify the ergodic component, the system is trapped in, and restricting the thermal average to this component.

[40] This is not the quasi-isotropic case, of course.

[41] To be very explicit, infinitely long means to let the time τ after which the measurement starts to to infinity *before* performing the thermodynamic limit.

In a spin glass, however, the identification of ergodic components is not possible. They are not even related by a fundamental symmetry of the Hamiltonian. Thus the order parameters q_{ab} or q_i in a spin glass do not identify single ergodic components but rather correlations between them[42] and so consideration of the whole configuration space cannot be circumvented. As a result, the magnetization discussed above, which is an average over all configuration space in the spin glass phase, must be interpreted as equilibrium magnetization: it can also not be measured in a finite time after the external field has been changed. It is best to imagine M and χ_e as 'field cooled' quantities. Thorough and extensive investigations of these issues can be found for instance in [BY86, MPS84, MPV87]. I will instead continue the discussion from a formal point of view rather than by intuitive arguments.

The equilibrium susceptibility $\chi_e^{\nu\nu}$ is a tensor in spin space and its diagonal elements are the interesting quantities for the quasi-isotropic glasses. They are defined by the total derivative of a magnetization component with respect to the component of the external field in the same direction

$$\chi_e^{\nu\nu} = \frac{d\,M_\nu}{dh_\nu} = -\frac{d}{dh_\nu}\frac{\partial}{\partial h_\nu} f = -\frac{\partial^2 f}{\partial h_\nu^2} - \frac{\partial^2 f}{\partial h_\nu \partial q_{ab}}\frac{dq_{ab}}{dh_\nu} - \frac{\partial^2 f}{\partial h_\nu \partial M_a}\frac{dM_a}{dh_\nu}. \tag{2.117}$$

In general, the mixed second order derivatives do not vanish and cause a considerable complication in the computation of the susceptibility. In Chapter 3 the equilibrium susceptibility is computed by using the analytical equation (2.117) under the assumption of replica symmetry. It is, however, too complicated for using it in the RSB treatment. In general, it is better to calculate χ_e as the numerical second derivative of f with respect to h. For the special case of zero external field $h_\nu = 0$ and zero mean interaction $J_0 = 0$, however, equation (2.117) can be simplified considerably because the terms with mixed partial derivatives of f vanish.

At $h = 0$, the spin glass order parameters $q_{ab} = \langle S_\nu^a S_\nu^b \rangle$ are even under $\mathbf{S}^a \to -\mathbf{S}^a$ and the Hamiltonian (2.1) is invariant under time-reversal symmetry[43] $\mathbf{S}^a \to -\mathbf{S}^a$, $\mathbf{h} \to -\mathbf{h}$. As a result, q_{ab} are even functions of $\mathbf{h}$ and thus its h_ν-derivatives at $h_\nu = 0$ vanish. Furthermore, at $J_0 = 0$ the free energy does not depend on the magnetization at all and thus each derivative with respect to M vanishes as well. As a result, for $\mathbf{h} = 0$ and $J_0 = 0$ the susceptibility is equal to the second partial h-derivative $\chi_e^{\nu\nu} = -\partial^2 f / \partial h_\nu^2$.

To evaluate the partial derivatives, it is most convenient to use the free energy expression (2.14) before applying any assumptions on the structure of the replica matrices, even before applying any simplifications to quasi-isotropic or Ising spin glasses. The field term in (2.14) does not depend on $\mathbf{h}$ and the differentiation of the trace term leads to

$$\chi_e^{\nu\nu} = \lim_{l\to 0} \frac{\beta}{l} \left[\frac{\sum_{a,b} \operatorname{tr}\, e^L S_\nu^a S_\nu^b}{\operatorname{tr}\, e^L} - \left(\frac{\operatorname{tr}\, e^L \sum_a S_\nu^a}{\operatorname{tr}\, e^L} \right)^2 \right]. \tag{2.118}$$

Exploiting equations (2.17) and (2.18) and performing the replica limit leads to the vanishing of the second term, since it is of order l^2. The first term can be evaluated within the assumption of κth order of RSB (including the RS case by $\kappa = 0$) by the method described in Appendix A.5. One finally obtains a simple formula for the equilibrium susceptibility χ_e at $\mathbf{h} = 0$ and $J_0 = 0$ for the quasi-isotropic spin glass

$$\chi_e^{\nu\nu} = \chi_e = \lim_{l\to 0} \frac{\beta}{l} \sum_{a,b} q_{ab} = \beta(1 - q_1) + \sum_{i=1}^{\kappa} a_i (q_i - q_{i+1}). \tag{2.119}$$

At zero temperature, the first term is singular. The singularity can be removed, however, by considering the temperature expansion of q_1. This is explained in detail in the next subsection.

Let me now turn to the susceptibility which can be measured in an actual experiment with finite observation time. The argumentation which leads to the proper equations is rather involved and will not be repeated here in detail[44]. It uses the definition of the so-called 'Edwards-Anderson' order parameter q_{EA}[EA75], the physical content of which is, loosely speaking, the short timescale order of a disordered system. It turns out

[42] These correlations have an ultrametric topology. Much work has been invested to understand this issue and to develop an intuitive understanding of the spin glass phase. To some extent this goal has been reached by Mezard et al. in [MPS84]. Compared to ordered magnetic systems, the physics are rather involved, however.

[43] Here it is assumed that time reversal also affects the external field $\mathbf{h}$. This is rather untypical but can be justified by regarding h as created by a system which is also subjected to the time-reversal.

[44] The complete derivation of the non-equilibrium susceptibility requires a dynamical interpretation of the order parameters $q(t)$. Details can be found in [BY86, p. 854]

[BY86] that q_{EA} is given in the RSB formalism[45] by

$$q_{EA} = \lim_{l\to 0}\lim_{a\to b} q_{ab} = q_1. \tag{2.120}$$

The non-equilibrium susceptibility can be written with the help of the Edwards-Anderson order parameter as

$$\chi_{ne} = \beta(1 - q_{EA}) = \beta(1 - q_1). \tag{2.121}$$

It is also called the single valley susceptibility. This name results from the idea that the system is trapped in a single valley of the coarse-grained free energy during the measurement. Thus, its physical meaning is the susceptibility measured in the short observation time limit. This is the susceptibility which can be measured in a real experiment.

It is important at this point to comment on the connection between a dynamical interpretation of spin glasses and the RSB formalism. It will turn out later that the q_i with the smallest index i have the largest value. The Edwards Anderson order parameter $q_{EA} = q_1$ is thus equal to the largest order parameter q_i which is obtained at a given temperature. Since q_i is a spin overlap between two different replicas, the largest q corresponds to the overlap between those replicas which have the most similar configurations. By means of ultrametricity, this is interpreted as the mean overlap of different instances in one single ergodic component. Overlaps of instances in different components are not considered in q_1. In q_2, however, the definition of the ergodic components is changed: each component now consists of several q_1-components. Thus the mean overlap becomes smaller. The characteristic time, one must wait until a real instance of a spin glass averages over this larger ergodic component which corresponds to q_2, is larger than for the q_1 component.

This scheme iterated until one arrives at the smallest q, i.e. $q_{\kappa+1}$, in which only one ergodic component is defined and the average of the overlap is taken over the whole configuration space. The characteristic time which corresponds to this situation is the largest time scale which is important in spin glasses. For zero external field an $J_0 = 0$, this full Gibbs average should yield a zero mean overlap, i.e. $q_{\kappa+1} = 0$. This is true, however, only in the limit of $\kappa \to \infty$. In this way, one can intuitively understand, why one needs an infinite number of replica symmetry breaking steps in order to respect all important physics, i.e. all important time scales.

In the limit of infinitely large systems ($N \to \infty$), all those time scales diverge. They, however, can still be ordered according to their size by considering $1/a_i$ as a pseudo relaxation time of the ergodic component which corresponds to q_i.

2.5.3 Zero temperature and zero external field

In the remainder of this work, the point in parameter space where $T = J_0 = h = 0$ and $\kappa = \infty$ will be of special interest. It turns out that there are certain types of criticalities connected with approaching this point. In order to be able to investigate this critical point in parameter space directly at zero temperature, some further considerations, which simplify the analysis, are useful.

I start with showing how the non-equilibrium susceptibility at zero temperature $\chi_{ne}(0)$ can be calculated easily by exploiting the equality of internal and free energy at $T = 0$. The zero temperature limit of the internal energy requires a zero temperature limit of $\beta(1-q_1^2)$. Near equation (2.88) it has been derived that $\lim_{T\to 0} q_1 = 1$. By assuming[46] $q_1(T)$ to be expandable in a Taylor series around $T = 0$ it is obvious that the linear temperature coefficient is equal to $\chi_{ne}(T = 0)$. Thus one can write

$$q_1(T) = 1 - \chi_{ne}(0)T + \mathcal{O}(T^2) \tag{2.122}$$

and finds in the zero temperature limit that $\lim_{T\to 0} \beta(1 - q_1^2) = 2\chi_{ne}(0)$. Further, the zero temperature limit of the internal energy at κth order of RSB for $J_0 = h = 0$ is obtained as

$$\lim_{T\to 0} u = -n\left[\frac{1}{2}\sum_{i=1}^{\kappa} a_i(q_i^2 - q_{i+1}^2) + \chi_{ne}(0)\right] \tag{2.123}$$

and because $u = f$ at $T = 0$, the non-equilibrium susceptibility can be calculated with the full accuracy of the free energy and the order parameters by

$$\chi_{ne}(0) = -\frac{1}{2}\sum_{i=1}^{\kappa} a_i(q_i^2 - q_{i+1}^2) - \frac{1}{n}f. \tag{2.124}$$

[45] For replica symmetry, $q_{EA} = q$.

[46] Relaxing this assumption to non-integer temperature exponents would lead to inconsistencies.

$\chi_{ne}(0)$ could also be calculated by differentiating the free energy with respect to q_1. From the field term, only the term $\frac{\beta}{2}(1-q_1) = \frac{1}{2}\chi_{ne}$ survives which, according to the extremization principle, must be equal to the q_1-derivative of the trace term. In the zero temperature limit, one then simply sets $q_1 = 1$ in the trace term derivative. This method, however, requires the storage of an additional quantity. Therefore, equation (2.124) is used to calculate $\chi_{ne}(0)$.

Finally, another method is derived for calculating the zero temperature entropy $s(T=0)$ at any order of RSB without the need for extrapolations from finite temperature. The idea is to analytically remove the singularity in (2.110) so that there is no need for finite T calculations. The approach is based on writing the entropy as the negative total temperature derivative of f. As discussed above, the first total temperature derivative of f is equal to the partial temperature derivative.

The partial derivative of f, can be performed without severe analytical complications. Here, I shortly discuss the idea by means of the Ising spin glass. A more detailed analysis for the general n-component spin glass is given in Appendix A.6.

It is most convenient to use the free energy expression in equation (2.87) with the recursively defined trace term. The only part of the field term which survives the differentiation with respect to temperature is

$$\frac{\partial}{\partial T}\frac{\beta}{4}(1-q_1)^2 = -\frac{\beta^2}{4}(1-q_1)^2 = -\frac{\chi_{ne}^2}{4}. \tag{2.125}$$

This term will be seen to be the only term at all in the zero temperature limit of the entropy. I still have to show, however, that the temperature derivative of the trace term vanishes for $T \to 0$. This is done by deriving modified recursion relations for the temperature derivatives of the recursion functions $\partial_T f_i^{\mathrm{sub}}(h_{i+1})$. Obviously, the temperature derivative of the trace term can be written as

$$\frac{\partial}{\partial T}\mathcal{T}(h + J_0 M) = \frac{1}{a_\kappa}\int_{\kappa+1}^{G} \frac{\partial_T f_\kappa^{\mathrm{sub}}(h_{\kappa+1})}{f_\kappa^{\mathrm{sub}}(h_{\kappa+1})} \tag{2.126}$$

where $\partial_T f_\kappa^{\mathrm{sub}}$ must be calculated recursively from

$$\frac{\partial}{\partial T} f_i^{\mathrm{sub}}(h_{i+1}) = \int_i^G \left[f_{i-1}^{\mathrm{sub}}(h_i)\right]^{r_{i-1}-1} r_{i-1}\frac{\partial}{\partial T} f_{i-1}^{\mathrm{sub}}(h_i). \tag{2.127}$$

Since $f_i^{\mathrm{sub}}(h_{i+1})$ is always finite and positive for $i > 0$ (see Figure 2.2), a vanishing temperature derivative anywhere in the recursion sequence leads to a vanishing temperature derivative of the whole trace term. It turns out that the level at which the vanishing can be directly shown is the lowest one, i.e. directly at the initial condition. With $\mathcal{C}_1(x) = 2\cosh(x)$ one finds

$$\frac{\partial}{\partial T} f_1^{\mathrm{sub}}(h_2) = \int_1^G \partial_T \left[\mathcal{C}_1(\beta h_1)\right]^{a_1 T} = \int_1^G a_1 \left[2\cosh(\beta h_1)\right]^{a_1 T} \left\{\log 2\cosh(\beta h_1) - \beta h_1 \tanh(\beta h_1)\right\}. \tag{2.128}$$

The term $[2\cosh(\beta h_1)]^{a_1 T}$ has a finite zero temperature limit, namely $e^{a_1|h_1|}$ as shown in Section 2.4. It will be argued now that for $h_1 \neq 0$ the term in curly brackets vanishes as T approaches zero.

Because of the $h_1 \to -h_1$ symmetry, it is sufficient to consider positive h_1. As $T \to 0$, the argument of both terms in the curly brackets become large so that $2\cosh(\beta h_1) \simeq e^{\beta h_1}$ and $\tanh(\beta h_1) \simeq 1$. Then the first term becomes $\log e^{\beta h_1} = \beta h_1$ and exactly cancels the second term[47] at $T = 0$. For $h_1 = 0$, instead, no cancellation happens. The first term is $\log 2$ while the second term vanishes. This happens only for $h_1 = 0$, however. The finite jump in the infinitely small region around $h_1 = 0$ does not affect the integration $\int_1^G$ at all. Thus, it is shown that $\partial_T f_1^{\mathrm{sub}}(h_2) \equiv 0$ and as a result the temperature derivative of the trace term vanishes for $T \to 0$.

In the general case of quasi-isotropic n-component spin glasses, the zero temperature limit of the entropy is plagued by an artificial logarithmic divergence $\sim \log T$. This divergence is well known for classical n-component spin systems and can clearly be identified as an artefact of the classical vector spin model. I thus *define* the proper zero temperature entropy of models with more than one component as the non-singular part of the entropy (see Appendix A.6)

$$s(T=0) = -n\frac{\chi_{ne}^2}{4}. \tag{2.129}$$

[47] It could lead to problems that the terms which cancel get infinite at $T = 0$ because $\infty - \infty$ is mathematically ill defined. A more thorough investigation which respects this issue properly can be found in Appendix A.6.

Note, however, that (2.129) is only for $n = 1$ consistent with the zero temperature extrapolation of $s(T) = \beta(u-f)$. It is further remarkable that the divergence is not due to differences of f and u at zero temperature. These would result in a T^{-1} divergence of the entropy.

Already at this point, one can see that $s(0)$ is either zero or negative, since the non-equilibrium susceptibility χ_{ne} is a real, positive quantity. So, for the theory to be meaningful, χ_{ne} can be expected to vanish in the limit $\kappa \to \infty$ and $T \to 0$.

Chapter 3

Analysis of the RS saddle point

The formalism which has been derived in the preceding chapter becomes fairly complicated and numerically expensive for high orders of RSB. The $(2\kappa + 1)$-dimensional space of order parameters a_i and q_i further complicates the analysis of the results obtained by the numerical algorithms and one easily looses the overview. Typically, one then restricts the detailed analysis of replica symmetry breaking to a special choice of the external parameters of the model, e.g. the external field $\mathbf{h}$ or the mean of the random interaction $\mathbf{J}_0$. Such a restricted analysis is sufficient in most cases because one is interested in the region where the effect of breaking of the replica symmetry is largest.

In the present chapter the model which has been introduced in Chapter 2 will be discussed in full generality regarding the external parameters, but in the replica symmetric approximation. With the help of the overview, gained by this analysis, the most interesting regions in the parameter space will be identified for the RSB analysis in the following chapters. A well-funded understanding of spin glasses in the RS approximation is indispensable for the considerably more complex analysis of RSB.

3.1 The Ising spin glass

The replica symmetric treatment of the infinite range Ising spin glass represents the easiest possible method of investigating spin glass behaviour. The self-consistency equations (2.41) and (2.42) can be solved numerically by a relatively simple *Mathematica*® program - numerical performance is not important here. The resulting order parameters q and M in dependence of external parameters are shown in Figures 3.1 and 3.2.

The plot of q and M in the $T - J_0$ plane with zero external field can be used to identify the various magnetic phases which are present in the replica-symmetric SK-model. At low temperatures and small mean interaction J_0 the magnetization completely vanishes. This is the spin glass phase. When approaching higher temperatures, the spin glass order parameter q vanishes at $T = T_C = 1$[1]. Above this critical temperature, a paramagnetic phase is found in which both order parameters are zero for zero external field. On the other hand, when increasing the mean interaction J_0 one enters a ferromagnetic phase where both order parameters are non-zero.

In a ferromagnetic Ising model (i.e. no disorder and positive J_0), the spin glass order parameter is also defined. It is, however, simply the square of the magnetization $q = M^2$ in this case because, due to the absence of inter-replica correlations which arise from the randomness, $q = q_{FM}$ can be written as

$$q_{FM} = \left\langle S^a S^b \right\rangle = \left\langle S^a \right\rangle \left\langle S^b \right\rangle = M^2. \tag{3.1}$$

Thus, the criterion for spin glass behaviour is that the difference between q and M^2 does not vanish. In Figure 3.1(c) this difference is plotted in the $J_0 - T$ plane. It is clearly non-zero in a large region around $T = 0$ and $J_0 = 0$. However, $q - M^2$ does not vanish instantly as the system enters the ferromagnetic phase at low temperatures and increasing J_0. Even in the ferromagnetic phase, one always observes a residual effect of the randomness in the interaction. This effect, however, becomes less and less important for $J_0 \gg J = 1$. At zero temperature and zero mean interaction, spin glass behaviour is most important. Further, inside the spin glass phase, varying J_0 does not change the results considerably so that one can restrict oneself to $J_0 = 0$ in the RSB analysis.

[1] The temperature is defined in units of the variance of the coupling constants J.

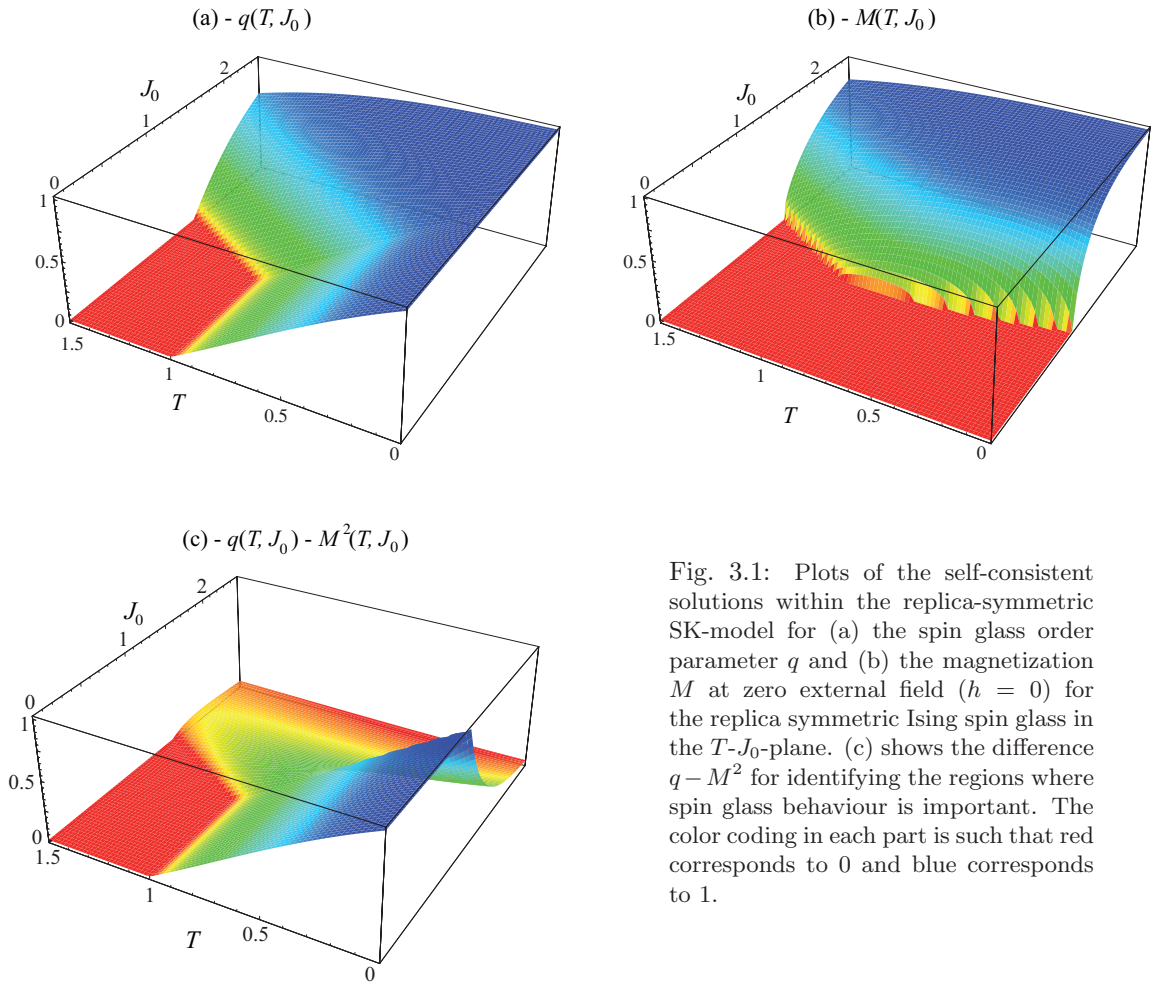

Fig. 3.1: Plots of the self-consistent solutions within the replica-symmetric SK-model for (a) the spin glass order parameter q and (b) the magnetization M at zero external field ($h = 0$) for the replica symmetric Ising spin glass in the T-J_0-plane. (c) shows the difference $q - M^2$ for identifying the regions where spin glass behaviour is important. The color coding in each part is such that red corresponds to 0 and blue corresponds to 1.

A sharp spin glass to ferromagnet phase boundary can be obtained by defining the spin glass phase as the region where $q \neq 0$ and $M = 0$ for vanishing external field. This definition is consistent with defining the phase boundary by a diverging M-susceptibility at the onset of ferromagnetism (see Fig. 3.3). Obviously, at zero temperature, the system is in the spin glass phase for $J_0 \lesssim 1.25$. Thus, disorder in the coupling constants J_{ij} has a similar effect as a finite temperature in that it supresses ferromagnetic ordering of the spins. Nevertheless, the way in which J enters the self-consistency equations is completely different from the way the temperature enters them.

As usual, a finite external field h destroys the sharp phase boundaries and smears out the phase transition FM↔SG. Interestingly, however, it also destroys the sharpness of the PM↔SG transition for $J_0 = 0$ (see Fig. 3.2). This is somewhat intriguing because h is not the field conjugate to the order parameter q. The reason for this is again that a finite magnetization due to an external field leads to a finite q - even without any spin glass features in the model. For large h the spin glass phase is destroyed because the Zeeman term in (2.1) becomes the dominant contribution and aligns all spins into the same direction.

Again, at $T = 0$ the magnetization shows a qualitative similarity with a paramagnet at finite temperatures due to the disorder preventing the system from a ferromagnetic alignment even without thermal fluctuations. The spin glass order parameter q, on the other hand, is not compatible with paramagnetic behaviour. It turns out, however, that the connection to paramagnetism must be discussed within full RSB in order to understand the underlying physical principles. The replica symmetric approximation is simply not capable of describing the difference between thermal fluctuations and disorder properly. While the many RSB order parameters clearly distinguish time scales on which only thermal fluctuations are present and time scales on which also the (effective) disorder fluctuates (and all time scales in between), the single RS order parameter treats all those time scales on average. In full RSB, the largest time scale of the system is described as the small x (or small a) limit of the order function. In this limit, full ergodicity is restored in some sense. For $h = 0$, one finds $q(a = x = 0) = 0$ and with increasing h, a plateau of the order function at small arguments

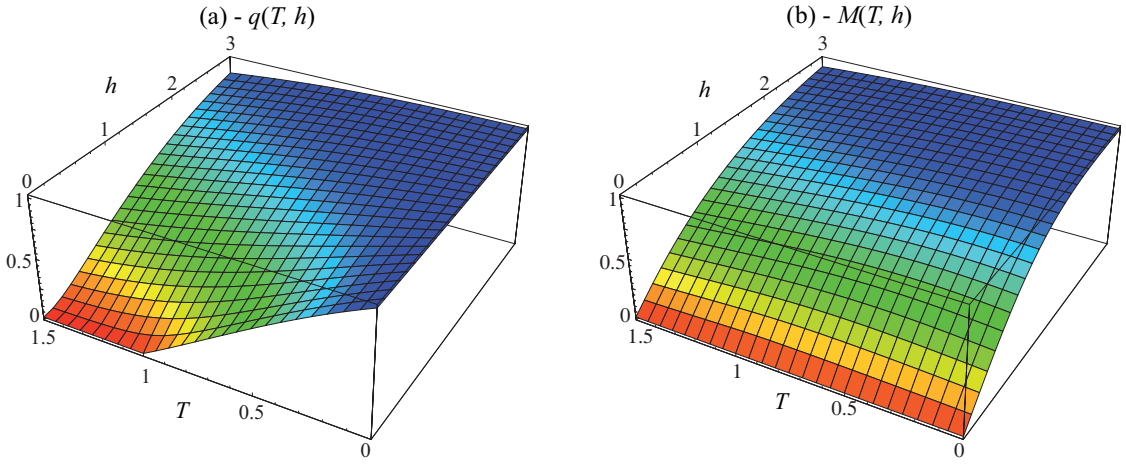

Fig. 3.2: Plots of the self-consistent order parameters $q(T,h)$ (a) and $M(T,h)$ (b) at zero mean interaction J_0 for the replica symmetric Ising spin glass in the T-h-plane. For negative h, the function $q(T,h)$ ($M(T,h)$) has even (odd) parity.

appears, the height of which varies as $h^{2/3}$. Thus, on the largest time scale, also the spin glass order function is qualitatively consistent with a paramagnetic picture.

Now, I turn to a short discussion of linear response to the external field. In the RS approximation, this can be done in full generality, i.e. without restrictions to $h = 0$ and $J_0 = 0$. For RSB, the general case becomes very inconvenient so that certain restrictions will be made later. For a discussion of susceptibilities it is useful to define two different linear response functions, namely the linear response of the magnetization M to a small change in the external field[2]

$$\chi_e^M = \frac{d\,M}{dh} = \frac{1-q}{T - J_0(1-q)} - \frac{\beta\chi_e^q(M-r)}{T - J_0(1-q)} \tag{3.2}$$

and the response of the spin glass order parameter q to an external field

$$\chi_e^q = \frac{d\,q}{dh} = \frac{2(1+J_0\chi_e^M)(M-r)}{T - \beta(1-4q+3s)}. \tag{3.3}$$

Additional quantities have been introduced[3]

$$r = \int_z^G \tanh^3(\beta H_{\text{eff}}), \qquad s = \int_z^G \tanh^4(\beta H_{\text{eff}}) \tag{3.4}$$

for the analysis. Obviously, the formulas are a bit lengthy, even in the RS approximation, and it is obvious that they will become rather cumbersome in the full RSB treatment where a susceptibility must be considered for each of the $2\kappa + 2$ order parameters. At zero external field $h = 0$ and zero mean interaction $J_0 = 0$, however, things can be simplified considerably by noting that M and r become zero because the integrands are odd function of z (see eqns. (3.4) and (2.113)). Thus, $\chi_e^q = 0$ and $\chi_e^M = \beta(1-q)$ for $h = J_0 = 0$.

The vanishing of $\chi_e^q(h = 0, J_0 = 0)$ could have been anticipated because q must be an even function of h at $J_0 = 0$ and should be analytical at $h = 0$. This argument can be extended to the RSB discussion to obtain the simple formula for the equilibrium susceptibility (2.119) at $h = J_0 = 0$ without using the numerical total derivative of a free energy. However, for infinite order RSB the spin glass order parameters are not neccessarily analytical at $h = 0$, as will be seen in the next chapter. In any case, for $h > 0$ the equilibrium susceptibility must be calculated by means of the free energy derivative for any order of RSB $\kappa > 0$.

The susceptibility χ_e^M is plotted in Figure 3.3. One can see how the singularity in χ_e^M at the SG↔FM phase boundary is cut of by a finite external field, irrespective of the sign of h. For zero external field, the position of the singularity defines the phase boundary as shown in the contour plot in Figure 3.3(b). The SG↔FM phase transition is well understood and will not be examined further here. Also the SG↔PM transition, occuring when increasing the temperature, has been analyzed thoroughly in the literature. More details can be found in [BY86].

[2]Note that in the RS approximation, there is no difference between equilibrium and the nonequilibrium susceptibility.
[3]For the definition of the Gaussian convolution operators see Appendix C.1.

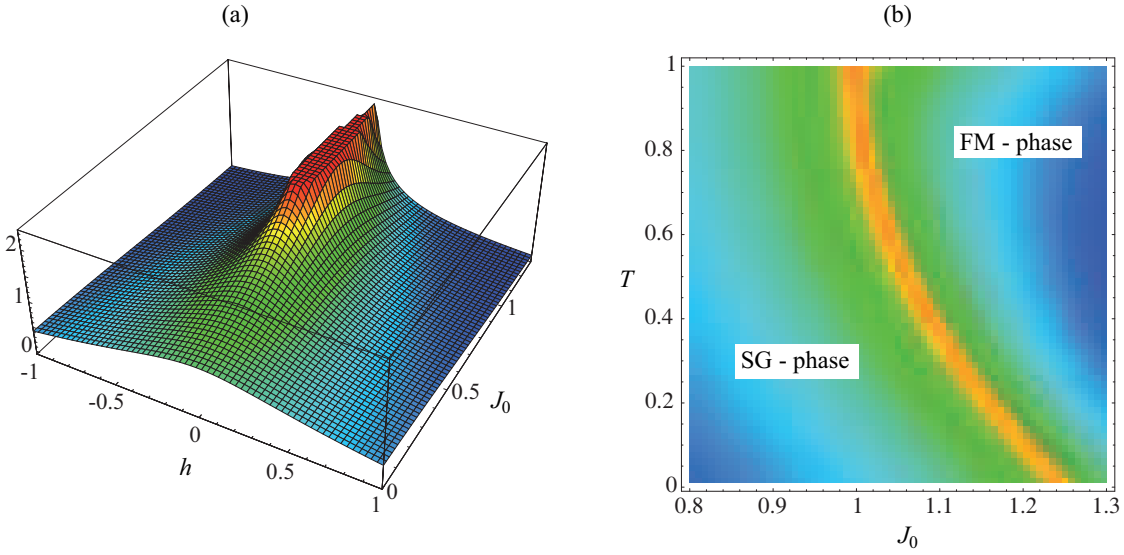

Fig. 3.3: The linear response coefficient χ_e^M of the magnetization to an external field. Part (a) shows how the singularity in χ_e^M for at the FM↔SG phase boundary at $h = 0$ is cutoff by finite h. The temperature in (a) is $T = 0.5$. In part (b), the susceptibility divergence for $h = 0$ is shown. The red line marks the position at which $\chi_e^M = \infty$, or, in other words, the phase boundary.

3.2 Isotropic n-component spin glass

At this point, I want to make only a few comments on the situation in a classical vector spin glass with more than one component, as described in Chapter 2. These are meant as a starting point for an RSB analysis to high orders by a future implementation of the ker$\mathcal{C}$-formalism (see Section 2.4.4). I discuss the differences of the $n > 1$ and Ising case by means of two examples, the order parameter q and the free energy as functions of temperature. The equations which describe a general n-component vector spin glass have the same form as the formulas of the SK-model. Especially in the RS approximation and for isotropic spin glasses, the differences are marginal[4]. Similarly to the Ising case, the self-consistency equations can be solved easily with *Mathematica*® or any other computer algebra system.

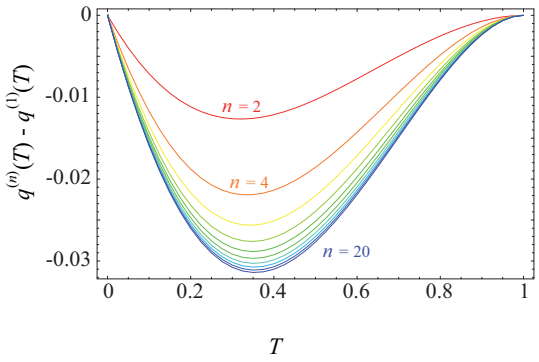

Fig. 3.4: Spin-glass order parameter $q^{(n)}(T)$ for $h = 0$ and $J_0 = 0$ of the isotropic n-component spin glass. The difference $q^{(n)}(T) - q^{(1)}(T)$ is plotted for $n = 2, 4, ..., 20$ (red to blue). The order parameter for an odd number of components shows the same behaviour.

The qualitative behaviour of the replica symmetric spin glass order parameter $q(T, h)$ does not change when varying the number of spin components n. Only a small quantitative change can be observed. In Figure 3.4, the differences of $q^{(n)}(T)$ for different number of components are shown. Obviously, the maximum deviations from the Ising case $n = 1$ are on the order of 3%. For $n \to \infty$, the spherical model is approached where $q(T) = 1 - T$ is linear [KTJ76]. Interestingy, though the spherical model is stable with respect to the breaking of replica symmetry, even the non-singular part of the zero temperature entropy $s_{ns}(T = 0) = -\frac{\chi_{ne}^2}{4}$

[4] In anisotropic spin glasses, one needs more than one spin glass order parameter even in the RS approximation. This fact, of course, changes things considerably.

does not approach zero in the limit $n \to \infty$ but rather approaches a finite negative value. In any case, this non-singular part of the entropy is hidden due to the negative logarithmic singularity (see Fig. 3.5(b)), which is a general issue in classical vector spin systems and not specific to spin glasses. A full quantum mechanical treatment would be in order for resolving this problem [Kop94, SRO95].

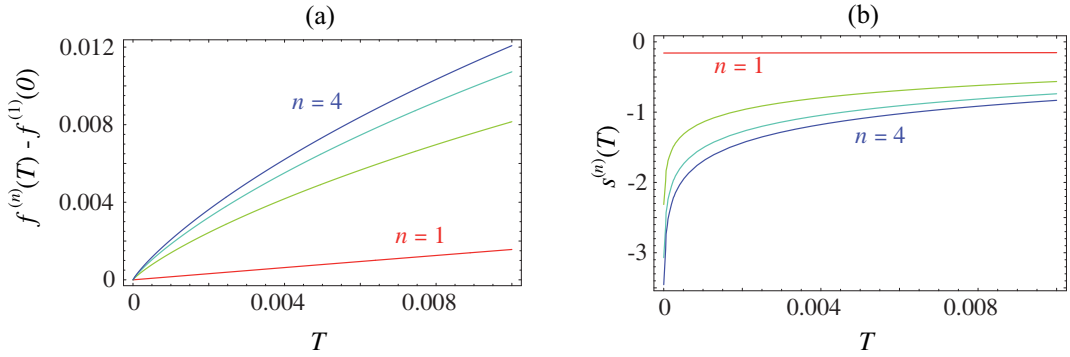

Fig. 3.5: The free energy of isotropic n-component spin glasses in RS approximation. Part (a) shows the temperature dependence of $\frac{f(T)-f(0)}{n}$ near $T = 0$ for $n = 1, ..., 4$ (red to blue). Part (b) shows the entropy as calculated from the derivative of $f(T)$. The color coding of n is the same.

The most striking difference of multiple component spin glasses, compared to the Ising spin glass is observed in the temperature dependence of the free energy near $T = 0$. While the Ising free energy approaches its zero temperature limit linearly and thus has a finite zero-temperature entropy without a singular part, for $n > 1$, there is a $T \log T$-like term in the free energy which leads to the logarithmic divergence of the entropy[5]. In Figure 3.5, the free energy and the corresponding entropy are shown near $T = 0$.

[5]For a general RSB derivation of this statement, which also includes RS ($\kappa = 0$), see Appendix A.6.

Chapter 4

Results and discussion at finite order of RSB

In spite of the fact that for the saddle point in equation (2.9) to be stable one needs an infinite number of replica symmetry breaking steps ($\kappa = \infty$), the finite κ regime is extremely important for understanding the properties of Parisi RSB at low temperatures: first of all, computations can be performed with arbitrarily high accuracy at finite κ and thus the extracted physical quantities exceed the precision of the literature values by several orders of magnitude and, moreover, a thorough understanding of the finite κ regime is inevitable for the construction of a proper continuous theory in the $\kappa \to \infty$ limit at zero temperature.

For moderate temperatures (about $0.1 \lesssim T < 1$) there already exists a formalism, known as continuous RSB, for treating Parisi RSB directly in the limit $\kappa = \infty$. In this formalism the recursion relation (2.79) or its $\ker\mathcal{C}$ pendant is replaced by partial differential equations [Par80, SD84] which depend on an infinite number of order parameters, conveniently expressed as an order function $q(a)$ or $q(x)$. Continuous RSB at finite temperatures has been thoroughly analyzed over the years [CR02, Pan06, Bis90, Nem87]. All investigations relied on the assumption that the parameters m_i (or a_i, equivalently) become dense on their domains as $\kappa \to \infty$. For $T > 0$ this assumption indeed seems valid. At zero temperature, however, it fails as I will show below and thus the traditional formulation of RSB in terms of a differential equation becomes invalid there. At arbitrary small but non-zero temperatures, the traditional continuous RSB still works. It is only numerically inconvenient because of various $1/T$-divergencies arising in the differential equations and their initial conditions.

The aim of the present chapter is to analyze the finite κ domain of the spin glass models defined above at low temperatures and to identify and discuss the specific reasons for the failure of traditional continuous RSB. This is done by a careful analysis of the numerical results at high RSB orders which have been computed from the implementation described in the preceding chapter. Because the influence of disorder can be examined best if the model has no (anti-)ferromagnetic component, the discussion is restricted to the case $J_0 = 0$. It turned out in the discussion under the assumption of replica symmetry that a non-dominant finite J_0 does not change the important physics, anyway.

4.1 Analysis of thermodynamic observables

An important aspect of RSB is the κ-dependence of observables in the large κ limit[1] and the extrapolation of those quantities to $\kappa = \infty$. The finite κ corrections typically decay according to a characteristic power law so that, in order to obtain a confident extrapolation to infinite order of RSB, the numerical data of the observable under consideration is fitted to a function of the form $b_\infty + c(\kappa + \kappa_0)^{-d}$. The sub-leading κ-terms are either addressed by additional terms in the fit function or by multi-flow fits.

[1] The limit $\kappa \to \infty$ is sometimes called the physical limit, because the observables calculated in ∞ RSB coincide with the ones measured in numerical simulations.

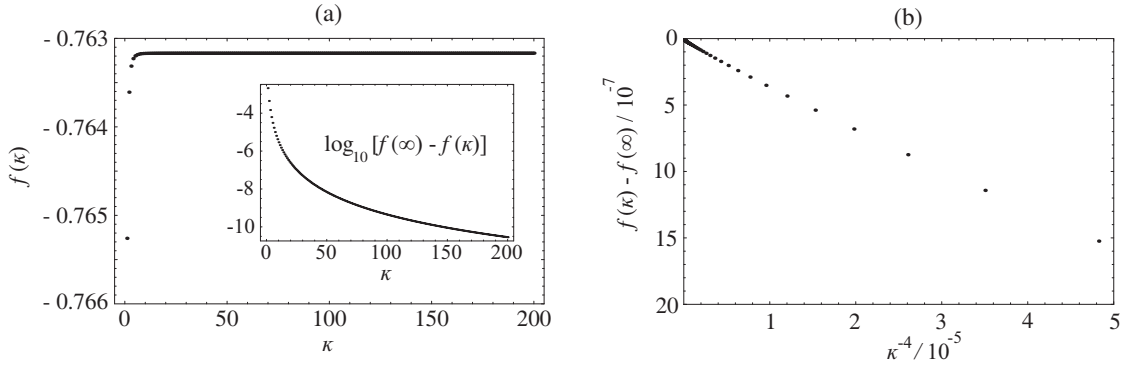

Fig. 4.1: Free energy at zero temperature and zero external field for an Ising spin glass. (a) The plot shows all numerical data in the full range of RSB orders $\kappa = 1, ..., 200$, while the inset shows the digit in which the free energy in finite RSB approximation deviates from its true value $f(\infty)$, i.e. $\log_{10}[f(\infty) - f(\kappa)]$. (b) Plot of $f(\kappa) - f(\infty)$ against κ^{-4} for $\kappa = 12, ..., 200$.

4.1.1 Free energy, internal energy and entropy

The free energy per spin f is the central quantity of statistical mechanics and also plays an important role in spin glass theory. As discussed above, it must be extremized in the space of $2\kappa + 1$ order parameters[2] $\{q_i, a_i\}$ which f depends on. In addition to that, the free energy depends on external parameters like the temperature T or the external field h and on κ, of course. For clarity, those dependences are written out explicitly only if required.

I start the discussion with an investigation of the simplest case, i.e. f at zero temperature and at zero external field. The residual κ-dependence of f is shown in Figure 4.1 in the range $\kappa = 1, ..., 200$. Apparently, the convergence of f with respect to κ is extremely fast so that at $\kappa = 200$, the finite κ approximation to the free energy deviates from its physical limit $f(\infty)$ only in the eleventh digit (see the inset of Fig. 4.1). The extrapolation to $\kappa = \infty$ is found by means of a fit to the function

$$f(\kappa) = f(\infty) + A(\kappa + \kappa_0)^{-\alpha} \tag{4.1}$$

where α is a positive exponent and κ_0 is a shift which helps to enhance the convergence quality[3]. It turns out that $\alpha = 4$ and $\kappa_0 \simeq 1.27$. The numerical error for the exponent α in the fit is of order 0.03. The integer value 4, however, is supported by an analytical analysis near T_C [Par79], so that $\alpha = 4$ can be assumed, confidently[4]. Due to the availability of calculations to up to 200 orders of RSB and the arbitrarily high numerical precision of the results within a given RSB order, the physical free energy $f(\infty)$ at $T = 0$, or, in other words, the ground state energy, can be given with an extraordinary high accuracy. It is

$$E_0 = f(\infty) = -0.763\,166\,726\,566\,547 \tag{4.2}$$

where the numerical error which originates from the fit procedure has been estimated to be of order 10^{-15}. This extrapolation represents the by far most precise numerical value for the ground state energy of the SK-model which can be found in the literature and is consistent[5] with the confidence intervals given there [Par80, CR02].

In Figure 4.2 the temperature dependence of f at various orders of RSB is presented. Obviously, the convergence of f with respect to κ is faster for higher temperatures so that less orders of RSB are needed at higher temperatures to obtain a confident extrapolation to the physical limit. Near T_C, only two RSB steps are even sufficient to obtain fairly good results. The κ convergence being faster at higher temperatures is a general phenomenon which is not restricted to the free energy. It results from the correctness of the

[2]Since $J_0 = 0$ in this chapter, the magnetization M looses some of its importance. It is not a priori needed for finding a self-consistent free energy, but can be calculated from it with hindsight.

[3]A shift κ_0 does not change the coefficient of the leading term. It is, however, proportional to sub-leading terms with exponents $\alpha + 1$, $\alpha + 2, ...$ Allowing for such a shift is a simple way to account for those sub-leading terms *on average*.

[4]It has been checked also in the finite temperature results that the leading term of the finite κ corrections to the free energy is of order κ^{-4}.

[5]There is a typo in the ground state energy given in [CR02]. The correct value found by the authors is $-0.763\,19 \pm 0.000\,03$ (A. Crisanti, priv. commun.).

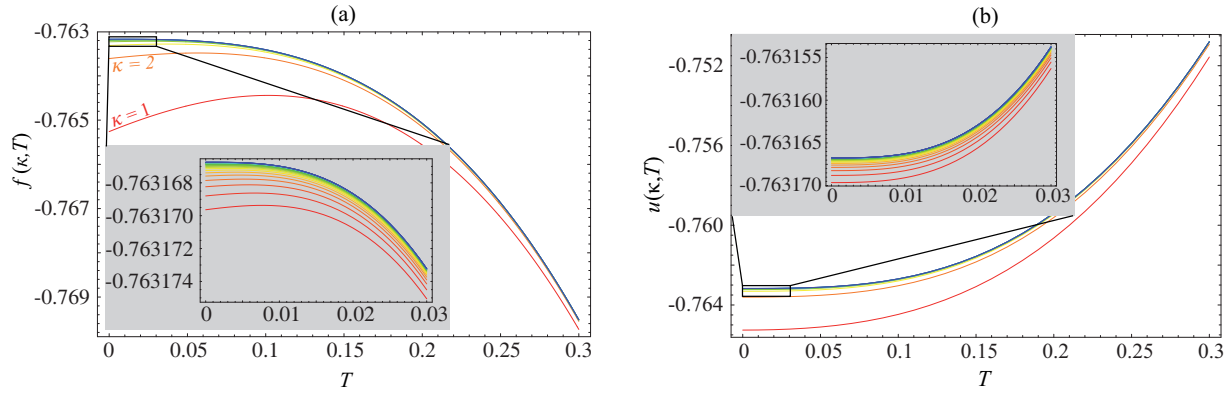

Fig. 4.2: Temperature dependence of the free energy (a) and the internal energy (b) for different orders of RSB. The red lines correspond to the lower RSB orders (κ) while the blue lines represent the higher orders. In the big figures κ ranges from 1 to 10 while in the insets the κ ranges from 10 to 40 are zoomed. Beyond 40 RSB, the improvements are too small to see them on the scale of the plots.

RS assumptions above the AT line[6] and from the similarities of the RS→RSB transition to a second order phase transition in that the deviation of the RSB order function from the (constant) RS order function vanishes smoothly when crossing the AT line. Nevertheless, at finite temperatures the leading term of the κ-corrections is also of order κ^{-4} as for $T = 0$. Only the coefficient of this term becomes smaller for higher temperatures.

From the T-dependence of f at small κ one can directly see why one needs so many RSB steps at low temperatures in order to obtain physically sensible results: a fundamental thermodynamic relation states that the negative slope of f as a function of temperature is equal to the entropy. At low temperatures, however, the finite κ approximations to f show a positive slope in Figure 4.2 and this results in a negative entropy. Of course, negative entropies are physically meaningless and thus finite κ approximations seem unphysical below a specific temperature. The temperature at which $s(T)$ becomes negative for a given RSB order κ can be used as a qualitative border $T(\kappa)$ between validity and invalidity of a κRSB approximation. By inversion of this function, an order of magnitude for the minimum required RSB order $\kappa_{\min}$ at temperature T can be obtained. The resulting function $\kappa_{\min}(T)$ is displayed in the inset of Figure 4.3. It diverges as $\kappa_{\min}(T) \sim T^{-\nu_T}$ where $\nu_T \simeq \frac{3}{5}$ near zero temperature. Here one encounters for the first time a kind of criticality at $T = 0$ where $\kappa_{\min}$ plays the role of a divergent correlation length on a pseudo-lattice of RSB orders [OSS07, OS08].

The constant of proportionality A in (4.1) can be given with high accuracy at $T = 0$ due to the high orders of RSB calculated numerically. The importance of this constant will become clear in Section 4.1.3 where the connection of finite order RSB with finite system sizes is examined. At zero temperature I find $A = -0.046752 \pm 10^{-6}$. At finite T, however, the accuracy is lower due to a smaller range of available data $\kappa = 1, ..., 54$. At temperatures above 0.01 the relative error of $A(T)$ is of order 1%. As the temperature approaches $T = 0$, however, the error increases as discussed in Appendix B. This is another manifestation of the zero temperature criticality of RSB, even though the error bars do not actually diverge at $T = 0$[7]. It is also clear that $A(T)$ should approach zero for increasing temperatures, since the κ-dependence must vanish at and above $T = T_C = 1$ where the RS ($\kappa = 0$) solution is the physical one.

In the context of criticality, it is remarkable that $A(T)$ cannot be expanded in a Taylor series at $T = 0$. The leading term is rather proportional to $T^{\frac{3}{5}}$ (see Appendix B)

$$A(T) \simeq -0.046752 + 0.131 T^{\frac{3}{5}} \quad \text{for } T \ll 1. \tag{4.3}$$

As a result, there exists a term proportional to $T^{\frac{3}{5}}\kappa^{-4}$ in the free energy. However, it is seen below that the thermodynamic quantities can be expanded in a Taylor series at $T = 0$. To be very explicit and in order to stress the fundamental need for scaling concepts in the analysis of the free energy near zero temperature, I

[6] See e.g. Appendix A.1 or [AT78].

[7] Due to calculations of up to 200 orders of RSB at $T = 0$, the error bars are effectively smaller than for finite temperatures, in spite of the fact that the error for a fixed maximum order is largest at $T = 0$.

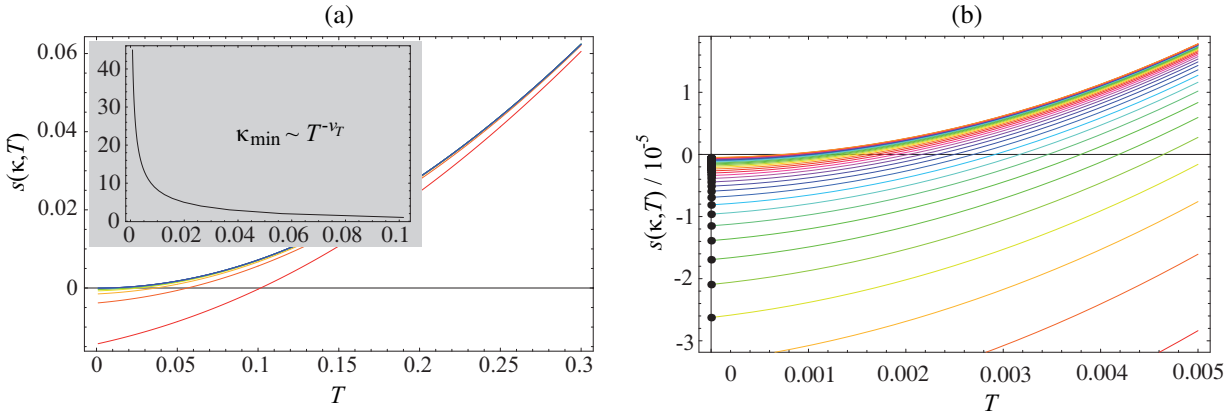

Fig. 4.3: Entropy of the Ising spin glass at low temperatures. (a) Plot of $s(T)$ for $T = 0, ..., 0.3$ for various orders of RSB. The red line corresponds to 1 RSB and the blue line to 10 RSB. The inset shows the minimal order of RSB at a given temperature $\kappa_{\min}(T)$ needed to obtain a positive entropy. (b) A zoom of the $s(T)$ plot to the low temperature region $T = 0, ..., 0.005$ for $\kappa = 10, ..., 45$. The black dots are the zero temperature entropies obtained by $s(0) = -\chi^2_{ne}/4$.

formulate this seeming contradiction[8] as a paradox before I discuss its resolution, i.e. scaling near $T = 0$ and $\kappa = \infty$:

> *It has been checked that the free energy can be expanded in a Taylor series in T at $T = 0$ for all (numerically accessible) fixed κ. On the other hand, the finite κ corrections can be written as $f_4(T)\kappa^{-4} + f_5(T)\kappa^{-5} + ...$ and f_4 is of the form $a + bT^{\frac{3}{5}} + ...$ Thus, at finite κ the term $\kappa^{-4}T^{\frac{3}{5}}$ leads to a diverging T derivative of $f(T, \kappa)$ at $T = 0$, and this is in contradiction with the Taylor expansibility of f near $T = 0$ - especially with the finite entropy $s(T = 0)$.*

This contradiction must be resolved by the introduction of scaling near $T = 0$ and $\kappa = \infty$. There are two scaling variables T and κ^{-1} which define the scaling regimes $\mathcal{R}_1^T = (T \simeq 0, \kappa^{-1} > 0)$ and $\mathcal{R}_2^T = (T > 0, \kappa^{-1} \simeq 0)$. The two regimes are separated by a crossover line $T \sim \kappa^{-\nu_T}$. If one considers the leading κ corrections to the free energy at finite temperatures, i.e. $A(T > 0)$, this analysis is naturally restricted to $\mathcal{R}_2^T$: the fact that the leading κ correction is considered means to analyze the $\kappa \to \infty$ behavior in $\mathcal{R}_2^T$. One indeed finds, that the convergence with respect to κ becomes worse for lower temperatures, because one needs more and more RSB orders to stay away from the crossover line (see Fig. 4.4). This is for instance reflected by the errors in the determination of $A(T)$ which grow as the temperature approaches $T = 0$.

Directly at $\kappa = \infty$, the finite κ corrections vanish and with it the non-analytical T-behavior so that the Taylor expansibility of the physical free energy, i.e. $\lim_{\kappa\to\infty} f(\kappa, T)$, at $T = 0$ is restored even in $\mathcal{R}_2^T$. If one wishes to expand the free energy at finite κ in a Taylor series at $T = 0$, one must rather investigate the regime $\mathcal{R}_1^T$: for each finite κ, one hits the crossover line $T \sim \kappa^{-\nu}$ when lowering the temperature, coming from $\mathcal{R}_2^T$, such that the regime in which e.g. a term $\kappa^{-4}T^{\frac{3}{5}}$ is present is left and the regime in which e.g. a term $\kappa^{-10/3}T$ is present is entered. At the critical point $T = 0$ and $\kappa = \infty$ all terms originating from different scaling regimes are zero. When considering corrections to the critical point, however, the proper regime $\mathcal{R}_1^T$ or $\mathcal{R}_2^T$ must be chosen.

The full structure of scaling near $T = 0$ and $\kappa = \infty$ seems to be quite intricate and is still not completely understood. The further discussion must be delayed to the end of this chapter, when all required analysis is available. Thus I continue with the analysis of the thermodynamic quantities in $\mathcal{R}_1^T$.

At zero temperature, the internal energy equals the free energy and so it has the same convergence properties for $\kappa \to \infty$. At finite temperatures, however, they are different. The temperature dependence of the two energies can conveniently be compared in Figure 4.2. As expected, the internal energy has no linear temperature term like the free energy, because from its definition $u = f + Ts = f - T\frac{df}{dT}$ the linear T term

[8] This is only one example out of many contradictions of a similar sort. Another example would be the $\kappa^{-10/3} \cdot T$ term arising from the negative zero-temperature entropy at finite κ compared to the presence of only integer powers of κ^{-1} in the finite κ corrections of the free energy at $T = 0$ as well as at finite temperatures (see Appendix B).

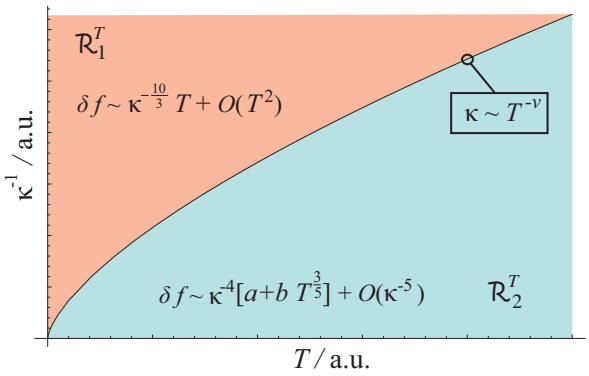

Fig. 4.4: Scaling regimes $\mathcal{R}_1^T$ and $\mathcal{R}_2^T$ are separated by the crossover line $\kappa = T^{-\nu}$. The exponent ν is not explicitly fixed at this point. The typical terms for free energy corrections δf away from the critical point $(\kappa^{-1}, T) = (0, 0)$ which are encountered numerically are shown in the corresponding regimes.

of f is exactly canceled out in u. As pointed out above, it has been checked numerically[9] that f can be expanded in a power series near zero temperature in the scaling regime $\mathcal{R}_1$

$$f(\kappa, T) = E_0(\kappa) - s(\kappa, 0)T - \sum_{k=2}^{\infty} f_k(\kappa) T^k. \tag{4.4}$$

From this series for f it follows for the internal energy $u(\kappa, T)$, the entropy $s(\kappa, T)$ and the heat capacity $C(\kappa, T)$

$$u(\kappa, T) = E_0(\kappa) + \sum_{k=2}^{\infty} (k-1) f_k(\kappa) T^k \tag{4.5}$$

$$s(\kappa, T) = s(\kappa, 0) + \sum_{k=2}^{\infty} k f_k(\kappa) T^{k-1} \tag{4.6}$$

$$C(\kappa, T) = \sum_{k=2}^{\infty} k(k-1) f_k(\kappa) T^{k-1}. \tag{4.7}$$

From the numerical data one finds that $\lim_{\kappa\to\infty} f_2(\kappa) = 0$ and $\lim_{\kappa\to\infty} f_3(\kappa) = 0.24$. As opposed to the free energy, the internal energy u can be calculated as a function of the self-consistently calculated order parameters[10] q_i and a_i and thus has a different formal character in that no complicated trace term must be evaluated (see Sec. 2.5). Nevertheless the two energies together with the entropy s are closely related by thermodynamics, namely by $f - u = Ts$. At finite temperatures this relation has been used to calculate the entropy from the internal and free energy. The temperature dependence of s is shown in Figure 4.3. At zero temperature, where $f = u$, it has been shown in Section 2.5 that the entropy is given by[11]

$$s(\kappa, 0) = -\frac{\chi_{ne}(\kappa, 0)^2}{4} \tag{4.8}$$

where $\chi_{ne}(\kappa, T)$ is the non-equilibrium susceptibility, which is investigated in more detail below. Already at this point it can be concluded that χ_{ne} will vanish in the limit $\kappa \to \infty$ since this is the only chance for the entropy to be non-negative. The black points in Figure 4.3(b) represent $s(\kappa, 0)$ obtained by equation (4.8). Obviously, in spite of the different methods for calculating the entropies, the $T \to 0$ limit of $s(\kappa, T)$ is consistent with $s(\kappa, 0)$. This is only true for the Ising spin glass, however, where the entropy has no singular part (see Appendix A.6).

In the $\kappa \to \infty$ limit, the linear temperature terms of the entropy vanish and the leading term is quadratic in T. This is consistent with predictions of Sommers and Dupont [SD84] and from the calculations I obtain a

[9] The finiteness of the zero temperature entropy is also strong evidence for the existence of this expansion.

[10] This is not quite true for $T = 0$. There one needs to know χ_{ne} in order to compute u in addition to the order parameters. However, χ_{ne} as the linear temperature coefficient of q_1 can also be seen as a rescaled order parameter.

[11] This relation holds only for the case of zero external field.

coefficient for the T^2 term in the entropy of 0.72. Interestingly, the finite κ-corrections of the quadratic term in the entropy seem to vanish according to a power law with the exponent $-\frac{5}{3}$ while the zero temperature entropy vanishes as $\kappa^{-10/3}$ as seen from the analysis of χ_{ne} below. Here again, a contradiction seems to appear: the coefficient of the T-linear term of $f(\kappa, T)$ is proportional to $\kappa^{-10/3}$ on one hand, but the leading κ corrections are κ^{-4}. This is again due to the reference of these statements to different scaling regimes, namely $\mathcal{R}_1^T$ and $\mathcal{R}_2^T$, respectively.

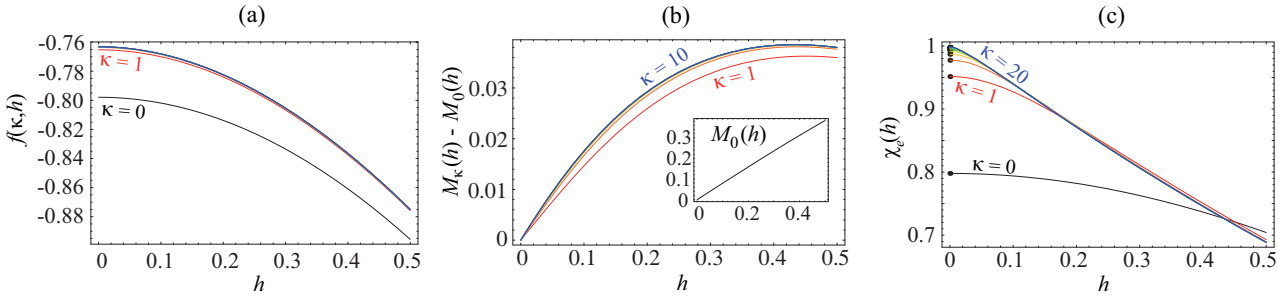

Fig. 4.5: (a) The free energy at $T = 0$ in dependence of an external field h. The black line represents the RS calculation ($\kappa = 0$) and the colored lines represent RSB results from $\kappa = 1$ (red) to $\kappa = 10$ (blue). (b) The magnetization $M_\kappa(h) = -\frac{df(\kappa,h)}{dh}$ at $T = 0$. In the large plot, the difference of the result of κ RSB $M_\kappa(h)$ and the RS result $M_0(h)$ is shown. In the inset one can see the absolute behavior. The different lines for different κ cannot be distinguished. (c) The h-dependence of χ_e at $T = 0$ calculated from numerical f-derivatives. The black line shows the RS result while the colored lines are RSB results for $\kappa = 1, ..., 20$. The black dots represent the results from the analytical formula for χ_e.

Finally, the finite h regime at zero temperature has been investigated. The main results can be observed in Figure 4.5. In addition to the RSB results of the free energy, the simple RS solution has also been plotted. From the deviations one can again see that especially at $T = 0$ and $h = 0$ the breaking of replica symmetry is very important for obtaining correct results, and that this statement is also true for finite h, though the convergence with respect to κ again becomes faster with increasing h.

The magnetization $M_\kappa(h) = -\frac{d f_\kappa(h)}{dh}$ at κ RSB in Figure 4.5 does not depend in such an obvious way on κ. Therefore, only the difference between the RS and the RSB magnetizations are plotted. The inset shows the pure RS result, which is reminiscent of typical finite temperature paramagnetic behavior - even at $T = 0$. This is due to the disorder which has a similar effect on the system as a finite temperature, i.e. a certain randomizing tendency. There is, however, an important difference between those two situations: the paramagnet changes its magnetization *instantly* when an external field is applied. The magnetization curve $M(h)$ in the spin glass, instead, must be understood as the magnetization response, measured after waiting infinitely long, so that the system is in equilibrium again with the altered external field. This is why the corresponding susceptibility χ_e, which is plotted in Figure 4.5(c), is called equilibrium susceptibility. In reality, however, this equilibrium is never reached and the important response function is rather the non-equilibrium susceptibility, which is discussed in the next section. The magnetization in Figure 4.5 must be understood as the *field-cooled* magnetization.

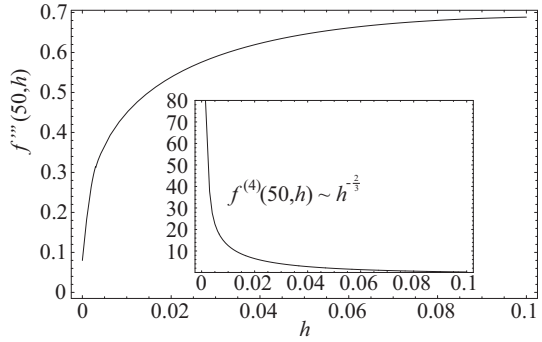

Fig. 4.6: Third and fourth derivative with respect to the external field of the ground state energy. The data is obtained by a direct numerical differentiation of the results of a 50 RSB calculation on a h grid with spacing $\Delta h = 0.001$. This finite spacing is the reason for the loss of accuracy of this plot near $h = 0$.

Next, the expansion of $f(h)$ in powers of h is analyzed in the limit $\kappa = \infty$. From symmetry considerations it is clear that $f(h)$ should not have terms linear in h. The quadratic h term gives rise to the equilibrium

susceptibility and thus should be equal to $-\frac{1}{2}h^2$. Within numerical accuracy, this term is found from the data of the free energy calculations at finite κ. The next h order in the free energy is expected[12] to have an exponent $\frac{10}{3}$ [CRT03]. Indeed, one finds a diverging fourth h-derivative from the numerical results at $T = 0$ as shown in the inset of Figure 4.6. The coefficient of the $h^{\frac{10}{3}}$ term in the free energy can be roughly estimated from the data and thus one can write

$$f(h) = f(0) - \frac{1}{2}h^2 + 0.22h^{\frac{10}{3}} + \mathcal{O}(h^4). \tag{4.9}$$

Anticipating the results for $\dot{q}(a)|_{a=0} = 0.743368$, the coefficient of the anomalous term $h^{10/3}$ in the free energy is in agreement with the analytical result in [PR08] $\frac{3}{20}\left(\frac{9}{4\dot{q}(0)}\right)^{1/3} = 0.216979$, obtained by extremizing the free energy functional with respect to the plateau height.

To further ensure internal consistence of the results, several thermodynamic relations between s, f and u, like e.g. $s = -\frac{df}{dT} = \frac{f-u}{T}$ have been checked. They are all satisfied within numerical accuracy.

4.1.2 Magnetic susceptibilities

Because of its experimental accessibility, the linear response to an external magnetic field is the most important observable of the spin glass phase. The sharp cusp in its temperature dependence at the freezing temperature T_C was the first experimental hint [CM72] for the existence of a new kind of phase transition. This cusp is theoretically well established meanwhile - it can be observed even in the simplest treatment of the SK-model [SK75]. Therefore I will not further go into this 'high temperature' regime $T \lesssim T_C$ but rather discuss linear response at low temperatures.

As explained in Chapter 2, the non-equilibrium (or single-valley) susceptibility χ_{ne} and the equilibrium susceptibility χ_e differ for $\kappa > 0$ since replica symmetry breaking more and more respects the broad spectrum of characteristic time scales as κ is increased. At $\kappa = \infty$, the full spectrum is accounted for. Typically, the effect of finite order of RSB can be seen best at zero temperature and thus I start the discussion of susceptibilities with an analysis of the $T = 0$ results.

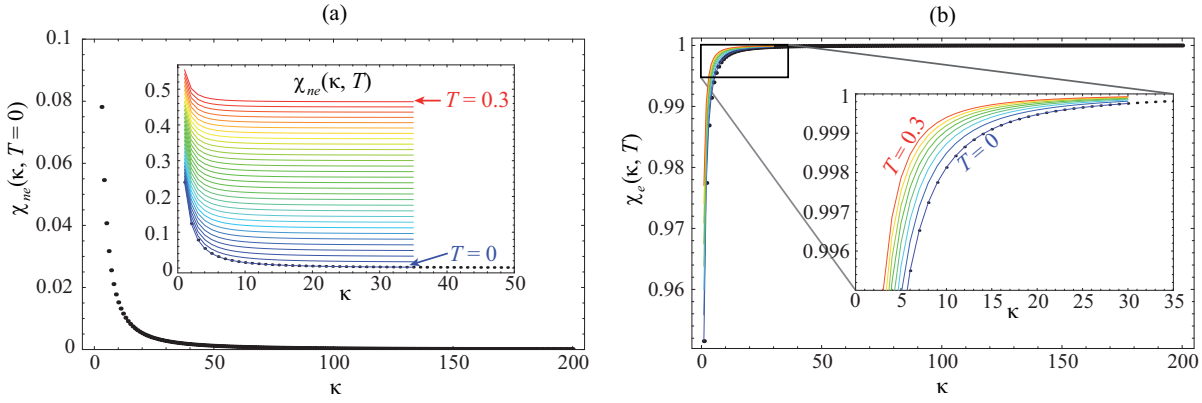

Fig. 4.7: The κ-dependence of the zero field susceptibilities χ_{ne} and χ_e. (a) The $\kappa \to \infty$ approach of χ_{ne} at zero temperature is shown. The colored lines in the inset show the situation at higher temperatures, where the top red line represents $T = 0.3$ and the black points are the $T = 0$ values. (b) χ_e in dependence of κ is represented by the black points at zero temperature. The finite temperature behavior is again symbolized by the colored lines with red corresponding to $T = 0.3$.

In the replica symmetric theory the susceptibilities χ_{ne} and χ_e are identical because of the absence of the hierarchical ordering which characterizes the RSB solution. By allowing for a hierarchical structure of the phase space, one is in a position to distinguish between a susceptibility which is obtained by a measurement with an observation time, short enough to ensure the system to be restricted to one valley of the coarse

[12] It is well known that at finite temperatures there exists an expansion of the free energy of the form $f(h) \simeq f_0 + f_1 p^3 + f_2 p^5 + f_3 p^6 + \mathcal{O}(p^7)$ with $p = h^{\frac{2}{3}}$. Since the h-behavior is represented mainly by the small a regime, where temperature does not lead to singular effects, it is not expected that h powers will appear in the free energy expansion at $T = 0$ which have not been present at finite temperatures.

grained free energy landscape and a susceptibility obtained during an extremely long measurement in which the system moves through the whole phase space. These are the reasons for calling the latter susceptibility equilibrium susceptibility while the former is named the non-equilibrium or single-valley susceptibility. At $T = 0$ and $\kappa = 0$ (RS) one finds $\chi_{ne}(0,0) = \chi_e(0,0) = \frac{2}{\pi}$. The results for $\kappa > 0$ are shown in Figure 4.7. As remarked above, $\chi_{ne}(\kappa, 0)$ must vanish for $\kappa \to \infty$ in order to obtain a non-negative entropy and it indeed does.

In order to investigate the approach to $\kappa = \infty$, the non-equilibrium susceptibility is fitted to the function

$$\chi_{ne}(\kappa, 0) = \chi_{ne}(\infty, 0) + B(\kappa - \kappa_0)^{-\gamma} \tag{4.10}$$

where $\chi_{ne}(\infty, 0)$ is indeed found to be zero within numerical error bars of order 10^{-9} and the exponent is found to be $\gamma = 1.666664 \pm 5 \cdot 10^{-6}$. This for an exponent unusual high accuracy is due to the exact knowledge of the ∞RSB extrapolation, i.e. $\lim_{\kappa\to\infty} \chi_{ne} = 0$ and to the high accuracy of the numerical calculations at finite RSB. Thus I can conclude $\gamma = 5/3$ and so the zero temperature entropy also vanishes as $s(\kappa, 0) \propto -\kappa^{-10/3}$.

For finite temperatures, a linear growth of $\chi_{ne}(T)$ is found. The interpretation of the vanishing of χ_{ne} at zero temperature can be given in terms of ergodicity: consider a spin glass system in one ergodic component at a given temperature T_1. The restriction of the system to one component is due to free energy barriers which surround the phase space volume corresponding to this component. If the temperature is slightly increased $T_1 \to T_2$, but still below the spin glass freezing temperature $T_2 < T_C$, the system is able to transcend some of the free energy barriers. It is, however, not completely free to traverse the whole phase space, but is restricted to a phase space volume which is larger than it was at the lower temperature T_1. This volume is again surrounded by free energy walls which are higher than the walls of the former ergodic component of T_1. In other words, at a higher temperature T_2, subsets of the ergodic components of T_1 merge in order to form the ergodic components of T_2. The non-equilibrium susceptibility describes the behavior of a system which is trapped in one single ergodic component. The size of this component is proportional to the possible change of system properties (magnetization in the present case) by external forces[13]. Since at zero temperature, the system is restricted to one point in the phase, i.e. one of the infinitely many degenerate ground states, it cannot respond to an infinitesimal external field and thus $\chi_{ne}(0)$ must be zero. For describing such a situation, however, infinitely many RSB steps are needed. At finitely many RSB steps the full hierarchy of the states [MPS84] is not properly respected and thus the size of a single ergodic component at zero temperature is overestimated which also leads to an overestimation of the response of the system to an external force. This is the reason for the finiteness of $\chi_{ne}(0)$ at $\kappa < \infty$.

The equilibrium susceptibility χ_e is expected to approach unity in the limit $\kappa \to \infty$, independently of temperature. From Figure 4.7 this is seen to be true. At finite temperatures, however, the convergence with κ is faster. Again, this is a consequence of the zero temperature criticality of RSB. The exponent of the power law decaying finite κ corrections of χ_e is different from γ. This is due to the existence of *two inequivalent critical points* at zero temperature. One is at $a = \infty$ and corresponds to short time behavior. This critical point affects short time quantities like the non-equilibrium susceptibility χ_{ne} or the entropy. The second critical point at $a = 0$ corresponds to long time behavior[14] and affects the equilibrium susceptibility, which is a long time quantity.

It is found that the numerical data at $T = 0$ is well fitted by the power law

$$\chi_e(\kappa, 0) = 1 - \frac{0.238}{(\kappa + \kappa_0)^2} \tag{4.11}$$

with $\kappa_0 \simeq 1.27$ as in the fit of the free energy. At finite temperatures one also finds a power law in κ with leading exponent -2 but with a different coefficient. It can be concluded from the same arguments as in the discussion of $A(T)$ that the coefficient must approach zero for $T \to T_C = 1$.

4.1.3 Connection to systems of finite size

In Ref. [ABM07], Aspelmeier et al. found a relation between finite step replica symmetry breaking and finite size systems. Their argumentation, which works near T_C can be extended down to $T = 0$ by a combination of the results of this work with numerical simulations of the SK-model with finite numbers of spins N. Such

[13] A susceptibility always describes the linear response to a small external field. Thus, the escape of the system from its zero field ergodic component, which would result in a kind of hysteresis, is not described by χ_{ne}.

[14] Long time has to be understood as quasi-infinitely long, i.e. far longer than the age of the universe.

an investigation can be found in [Boe05] where a finite size correction of the ground state energy $\sim N^{2/3}$ is found by extremal optimization.

In this work, it is found that the finite κ corrections to the ground state energy scale as κ^{-4} and the corrections are negative, i.e. $E_\kappa - E_\infty = -0.0468\kappa^{-4}$. The finite size corrections are positive in sign and so both corrections compensate. To be specific, in [Boe05] it has been found that $E_N - E_\infty = 0.70N^{-2/3}$. Both corrections cancel each other if the system size scales with RSB order as

$$\kappa \simeq 0.51N^{\frac{1}{6}} \quad \text{or} \quad N \simeq 58\kappa^6. \tag{4.12}$$

Remarkably, the RSB order grows extremely slow with system size. With 1RSB a system with 58 spins is sufficiently described while with 2RSB systems with over 3000 spins are feasible. With extremal optimization, a fairly advanced algorithm, system sizes of up to 1000 spins are possible. From this point of view, mean-field theory at 200RSB is far beyond the accuracy of numerical simulations.

4.2 The order function

In the description of systems which undergo a critical phase transition of some sort, the concept of order parameters is a central topic [KGH67]. In spin glass theory, however, each finite number of order parameters is insufficient for a satisfactory incorporation of the important physics [Par80, Par79, Par83]. The description only gets formally correct, i.e. the saddle point in equation (2.9) is stable, in the limit of infinitely many order parameters, i.e. in the $\kappa \to \infty$ limit [TAK80]. This rather mathematical fact reflects the existence of a broad spectrum of different time scales instead of only two regimes as, for instance, in a typical ferromagnet. The importance of all those time scales in spin glasses is due to a complicated type of broken ergodicity [Pal82] which complicates the analysis of the spin glass phase in that it is not possible to identify one ergodic component which the analysis can be restricted to. Instead, all components must be respected and this forces the theorist to investigate the infinite hierarchical ordering between them which is expressed as infinitely many steps of RSB.

Nevertheless, a finite number of order parameters can be a very good approximation in some situations. In κ step RSB, the order parameters are the $2\kappa+1$ variables $q_i,\ \ i = 1, ..., \kappa+1$ and $a_i,\ \ i = 1, ..., \kappa$. It has been demonstrated in the preceding Section that, for instance, the free energy in a 200 RSB approximation with $(2 \cdot 200 + 1)$ order parameters deviates only in the eleventh digit from its true ∞RSB value - and this is even the worst case scenario for the convergence at $T = 0$.

The treatment of high orders of RSB is numerically very intricate and the computational cost grows roughly as $\kappa^{3/2}$ as one further increases the number of order parameters. The question is now: *How is it possible to efficiently handle an infinite number of order parameters?* The answer can be found by devising a graphical representation of the set of order parameters at κRSB[15]. As explained in Section 2.4, the domain of the parameters a_i is given by $[a_{\kappa+1}, a_0]$ where additional numbers $a_{\kappa+1} = 0$ and $a_0 = \beta$ have been introduced[16], so that a function $q_\kappa(a)$ can be defined on this domain which consists of $\kappa+1$ plateaus. The height of the plateaus is given by the parameters q_i and the boundaries of the ith plateau are given by the T-rescaled block sizes a_i and a_{i-1}. In Figure 4.8, such a step-like order function for $\kappa = 6$ and $T = 0$ is shown.

As the order of RSB is increased, the number of plateaus also increases while the widths of most[17] plateaus approach zero. The finite κ step function $q_\kappa(a)$ passes over to a smooth function $q_\infty(a) = q(a)$ in the limit $\kappa \to \infty$ and the theory can be expressed in terms of a partial differential equation which depends parametrically on $q(a)$. This differential equation results from the $\kappa \to \infty$ limit of the recursion relations for f^{sub} or for ker$\mathcal{C}$ (see Sections 2.3 and 2.4.3).

At finite κ, the step approximation of the order function can be continued by polynomial interpolation of the center points $\frac{1}{2}(a_i + a_{i-1})$ of the plateaus with height q_i. The so obtained continuous functions for different RSB orders are nearly indistinguishable. There are small systematic deviations of those continuous finite κ order functions from $q_\infty(a)$, the implications of which are not clear by now.

[15] This idea is originally due to G. Parisi [Par80]. He applied it to the finite temperature formalism of RSB, where the block sizes m_i and not a_i are the fundamental variables. At low temperatures, however, the formulation in terms of m_i gets invalid and therefore only the a_i-formalism is discussed here.

[16] a_0 and $a_{\kappa+1}$ must be considered as fixed boundary values for the $a_i,\ \ i = 1, ..., \kappa$ parameters. Therefore the free energy must not be maximized w.r.t. a_0 and $a_{\kappa+1}$.

[17] At finite temperatures, only the width of the plateau at $x > \bar{x}_1$ remains finite in the $\kappa \to \infty$ limit while all other plateau widths vanish. At $T = 0$, however, this is not true anymore. There is a subtle discreteness at $a = \infty$. The implications of those finite plateau widths at zero temperature will be discussed in Section 4.3. If one focusses on the $a < \infty$ domain one can still consider $q(a)$ as a smooth order function even at $T = 0$.

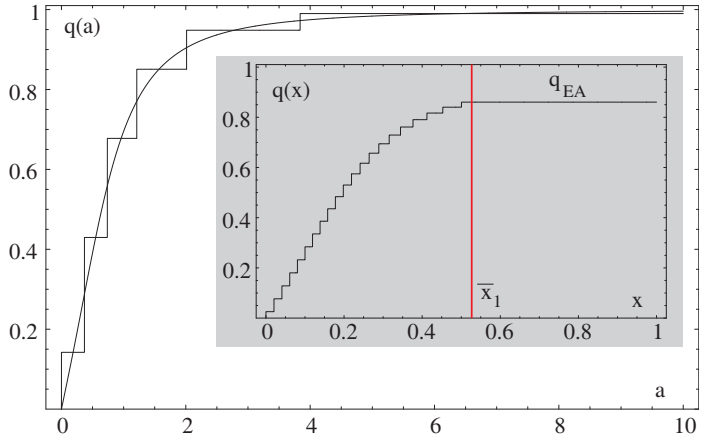

Fig. 4.8: The step-approximation of the order function within a finite number $\kappa = 6$ of RSB steps at $T = 0$. The inset shows an order function for $\kappa = 20$ at $T = 0.3$. The red vertical line marks the break point $\bar{x}_1$.

At finite temperatures, the abscissa of the order function can also be formulated in terms of the variables $x = Ta$, as shown in the inset of Figure 4.8. Obviously there are two different regimes: a plateau regime where $q(x) = q_1 = q_{EA}$ for $x > \bar{x}_1$ and a nontrivial regime for $x < \bar{x}_1$. $\bar{x}_1$ or $\bar{a}_1 = \beta\bar{x}_1$ is the so-called break point which only appears in the finite temperature theory. At $T = 0$, the plateau regime is somewhat more complicated and will be discussed in Section 4.3. For a finite external field h a second break point $\bar{a}_0$ appears in the small a regime. It is important to note that the plateaus are *not* due to the equality of several q_i which correspond to this regime, but rather to the total absence of block size parameters a_i or m_i in the plateau regions.

The various features of the order function have been thoroughly investigated and the results will be discussed subsequently, starting with the special case of zero temperature and zero external field.

4.2.1 $q(a)$ at zero temperature and zero field

The zero-temperature order function is defined on the semi-infinite interval $[0, \infty]$[18]. At finite RSB, the parameters a_i nevertheless remain finite. In Figure 4.12(a) the κ-dependence of all a_i of a $T = 0$ and $h = 0$ calculation is shown on a log-log scale. Obviously, the largest parameter $a_1 \sim \kappa^{5/3}$ diverges according to a power law as $\kappa \to \infty$. Furthermore, it seems that there are three different a regimes: one regime where the block size parameters become dense with increasing κ and two regimes where a finite spacing on a log$a$ scale survives even at $\kappa = \infty$. Those discrete regimes correspond to the two inequivalent critical points $a = 0$ and $a = \infty$. They appear only at exactly $h = 0$ and $T = 0$. The properties of the zero-temperature order function $q(a)$ near these points require a careful analysis.

In the present section, only finite κ approximations of the order function are investigated where $q_\kappa(a)$ is a step function. The continuous function $q_\infty(a)$ can be obtained by polynomial interpolation between the set of κ points which have been obtained at finite order of RSB. Doing so, however, it is not clear whether the resulting function has the same features as the function at infinite order of RSB. It could equally well be that a given feature is a finite RSB effect. If interpolating functions corresponding to different RSB orders are compared one finds, for instance, fixed points at which the functions for different κ coincide and regions where they explicitly deviate from each other.

A better approach to find the proper continuous order function at infinite order of RSB is to plot two different sets of points $\{q_i, a_i\}$ and $\{q_{i+1}, a_i\}$ which serve as upper and lower boundaries for the true ∞ RSB order function. Such a plot is shown in Figure 4.9. This visualization obviously leads to a confidence channel in which the ∞ RSB order function is definitely contained[19]. The width of this channel is smaller than 10^{-2},

[18] In spite of the mathematical ill-definedness, the inclusion of ∞ in the interval is not a typo here. From a certain point of view, the 'point' ∞ is really part of the domain of $q(a)$. This is discussed more thoroughly in section 4.3

[19] Strictly speaking this requires the assumption that beyond 200 RSB, nothing happens which leads to a completely different behavior of the order function for even larger RSB orders. Though this cannot be proven explicitly, the analysis of all data which has been obtained by the numerical calculations does not suggest the existence of an important scale on the κ axis which is beyond 200 RSB. Also the ∞RSB analysis leads to the same results.

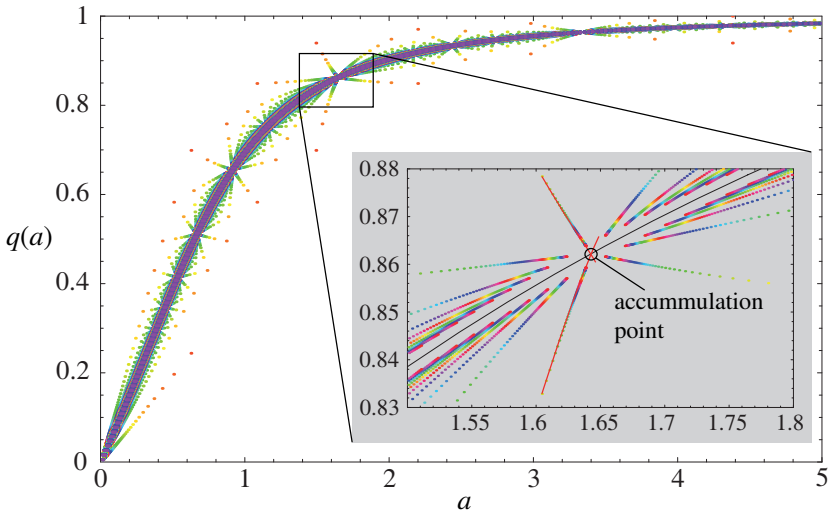

Fig. 4.9: Confidence channel for the zero temperature order function at infinite order of RSB. The points correspond to a range of RSB orders from $\kappa = 10, ..., 200$. The color coding is such that 100 RSB orders correspond to one cycle red - green - blue - red. The inset zooms one fixed point near the region of the most wide confidence channel. The black curve is the interpolating function obtained from a 200 RSB calculation.

the worst accuracy is gained near the maximum curvature of $q(a)$ (see Fig. 4.9). The effective accuracy of the order function, however, is much higher than suggested by the width of the confidence channel. If, for instance, the set of points which is used in the interpolation is obtained by a 'vertical average' $(a_i, \tilde{q}_i)$ with $\tilde{q}_i = \frac{1}{2}(q_{i+1} + q_i)$ instead of a horizontal average $(\tilde{a}_i, q_i)$ with $\tilde{a}_i = \frac{1}{2}(a_i + a_{i+1})$, the two interpolating functions[20] deviate from each other only in the 6th digit.

The above discussion always regarded the point sets obtained at a high RSB order - typically 200 RSB at $T = 0$ - as a sufficiently accurate interpolation set for the order function $q_\infty(a)$. This approximation is obviously not bad, but highly accurate results for $q_\infty(a)$ at a discrete set of points can be obtained by extrapolating the lines which appear in the inset of Figure 4.9. For $\kappa \to \infty$ these point sets approach several accumulation points in the $(a, q(a))$ plane which can be found by means of intersections of Padé fits to those finite κ point sets. The true ∞ RSB order function thus consists of an infinite number of accumulation points.

I now turn to a discussion of the properties of $q(a)$ near the boundary points $a = 0$ and $a = \infty$, starting with the simpler case $a = 0$. In spite of the log-discreteness at $a = 0$ which is observed in Figure 4.12, the analysis of the small a regime of $q(a)$ is rather simple. An equivalent discreteness in the parameters q_i at small a leads, in contrast to the situtation at large a, to an independence of the derivatives of $q(a)$ from the indices of the parameters. For instance, it makes no difference whether one uses the discrete expression $\lim_{\kappa\to\infty} 2\frac{q_{\kappa+1}}{a_\kappa}$ or $\lim_{\kappa\to\infty} 2\frac{q_\kappa}{a_\kappa + a_{\kappa-1}}$ for calculating $q'(0)$[21]. In general, the finite κ corrections to the derivatives $q^{(n)}(0)$ decay as polynomials of κ^{-1} for $\kappa \to \infty$. From the numerical data within 200 RSB one can obtain the first three derivatives with considerable accuracy

$$q'(0) = 0.7433680 \pm 10^{-7}, \qquad q''(0) = 0, \qquad q'''(0) = 4.658 \pm 2 \cdot 10^{-3}. \tag{4.13}$$

Similar results - even though they are less accurate - can be found from extrapolations of the numerical derivatives of the order function interpolation which are plotted as the red lines in Figure 4.11. Obviously, the order function is well behaved near small a and can be expanded in a Taylor series $q(a) \simeq c_1 a + c_2 a^3 + ...$ without a quadratic a term. The vanishing of even terms in this expansion cannot be viewed as a general statement, though, as it has been pointed out by Crisanti and Rizzo who found nonvanishing derivatives $q^{(2n)}(0)$ for $n \geq 2$ in a finite temperature analysis [CR02]. Those non-vanishing even powers of $q(a)$ slightly complicate the interpretation of $q(a)$ in terms of the rescaled[22] overlap probability distribution function (OPDF) $P(q) = \frac{da}{dq}$. For zero external field, this function should be an even function of q because of

[20] The interpolating function is typically constructed by 3rd order polynomials.
[21] This statement is, for obvious reasons, restricted to the $h = 0$ case but is valid at finite temperatures.
[22] The original definition of the OPDF is given in terms of the order function in x-formulation $P(q) = \frac{dx}{dq}$.

symmetry reasons and thus it would be desirable to only have odd powers of a in $q(a)$. The existence of even powers forces one to *define* $P(-|q|) := P(q)$ for negative arguments.

Apart from the subtleties in context of the definition of the OPDF, the behavior of $q(a)$ near $a = 0$ is quite regular. Instead, the analysis of the large a behavior of $q(a)$ is considerably more complicated. The parameters a_i do not become dense on an a-scale and thus one must deal with essentially discrete derivatives. In order to clearly identify the fundamental differences between the small a and the large a behavior, it is useful to perform the analysis in terms of a function $Q(z) = q(1/z)$. The discreteness of the a_i parameters is thus transformed to small z where it vanishes on a z scale in the limit $\kappa \to \infty$[23] in a similar manner as the small a discreteness which can be observed on a $\log a$ scale vanishes on an a-scale. Nevertheless, the behavior of $Q(z)$ near $z = 0$ depends, as opposed to $q(a)$ near $a = 0$, on the indices of the finite RSB parameters from which the derivatives are calculated. Only for the first derivative it can be concluded independently of the parameter indices that $Q'(0) = 0$ within a numerical uncertainty of the order of 10^{-9}. Remarkably, however, the finite κ corrections decay with powers of $\kappa^{-5/3}$ in contrast to the finite κ corrections in the small a regime which vanish as integer powers of κ^{-1}.

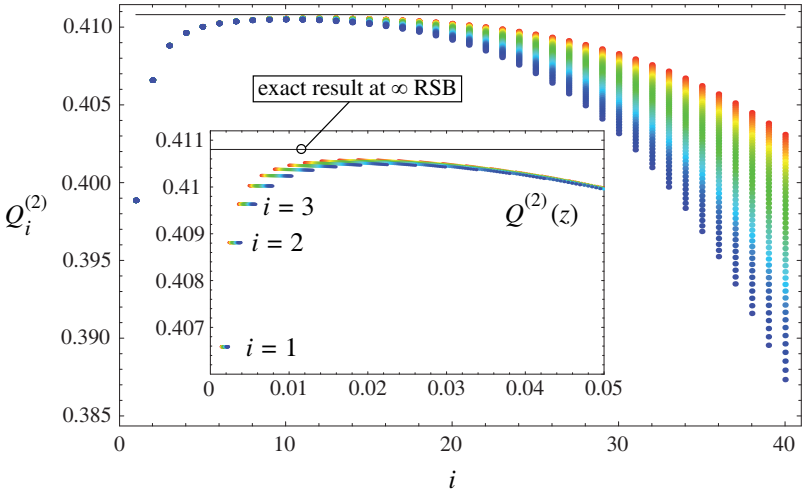

Fig. 4.10: Second derivative of $Q(z) = q(1/z)$ near $z = 0$ calculated from different parameters at large a or small z (see text). The black line represents the numerical value for $Q''(0)$ which is found from the continuous treatment of the finite a regime (see chapter 5 and also [Pan06]). The inset shows the same data but with $z_i^{(2)}$ as abscissa of the value $Q_i^{(2)}$. The color coding is such that blue corresponds to lower RSB orders and red corresponds to higher (up to 200) RSB orders.

At this point, let me discuss only the second derivative of $Q(z)$. The derivatives of $Q(z)$ are calculated as follows: the values of the function $Q(z)$ near $z = 0$ are given at finite κ on a discrete set of points $z_i^{(0)}$

$$z_i^{(0)} = \left(\frac{a_{i-1} + a_i}{2}\right)^{-1} \quad \Rightarrow \quad Q_i^{(0)} = Q(z_i^{(0)}) = q_i. \tag{4.14}$$

The first derivative of $Q(z)$ is also given at a discrete set of different points $z_i^{(1)}$

$$z_i^{(1)} = \frac{z_i^{(0)} + z_{i+1}^{(0)}}{2} \quad \Rightarrow \quad Q_i^{(1)} = Q'(z_i^{(1)}) = \frac{q_{i+1} - q_i}{z_{i+1}^{(0)} - z_i^{(0)}} \tag{4.15}$$

Iterating this procedure, i.e. calculating the $(n+1)$th derivative from a difference quotient of nth derivatives leads to formulas for arbitrary high derivatives. Since for $\kappa \to \infty$ all $z_i^{(n)} \to 0$ for fixed n and i, $\lim_{\kappa\to\infty} Q_i^{(n)} = Q^{(n)}(0)$ would be independent of the parameter index i if the sample points $Q_i^{(0)}$ were taken from an arbitrary regular function $Q(z)$, even if $z_i^{(0)}$ are discrete on a log-scale as described above. This behavior, however, is *not* found from the numerical data. In Figure 4.10, the second derivative is plotted. One clearly observes a dependence of $\lim_{\kappa\to\infty} Q_i''$ on i and thus it can be concluded that there is a certain kind of criticality of

[23] On a log-scale the existence of the discreteness does not depend on whether one considers variables a or $z = 1/a$. On a linear scale, however, discreteness arises only at large a or z, respectively.

the order function near $a = \infty$, not yet having said, what criticality exactly means. In the inset of Figure 4.10 the discretized second derivative of the function $Q(z)$ is shown for various RSB orders. Obviously, the calculation of the second derivative from the finite RSB data is plagued by a non-commutativity of limits

$$\lim_{\kappa\to\infty}\lim_{z\to 0} Q''(z) \neq \lim_{z\to 0}\lim_{\kappa\to\infty} Q''(z). \tag{4.16}$$

If the $\kappa \to \infty$ limit is taken before the $z \to 0$ limit, the second derivative converges to the value which is found from a continuous treatment [Pan06]. These results suggest that there is important information at the point $a = \infty$ which is not completely resolved at $T = 0$ by the a-formulation in a similar manner as the structure at $x = 0$ cannot be resolved by the x-formulation[24]. Obviously, the point $a = \infty$ is fundamentally different from the point $a = 0$ and requires further investigations. Especially for the proper continuous zero temperature theory which is developed in Chapter 5, one must understand the order function at the point $a = \infty$. Because of its importance, a separate Section 4.3 is devoted to this issue.

In [OS05], an analytical model function for $q(a)$ has been proposed which fitted well the available 5 RSB results at zero temperature. The functional dependence implied an error function $\frac{\sqrt{\pi}}{2}\frac{a}{\xi}\mathrm{erf}\frac{\xi}{a}$ and a single fit parameter $\xi \simeq 1.13$. It turned out later [OSS07] that this simple function also fits the results of higher RSB calculations well, but at small a, where the first derivative of the erf-model is nearly constant (see the blue line in Fig. 4.11), a 'wiggle' has been found in the numerical data which could not be represented by the erf-model. This finding called for a more general fit function. It turned out that a generalization of the error function to a confluent hypergeometric function ${}_1F_1(\alpha,\gamma,z)$ yields the desired degree of freedom. The 4-parameter fit-function

$$q(a) = \frac{a}{\sqrt{a^2+w}}\,{}_1F_1\left(\alpha,\gamma,-\frac{\xi^2}{a^2+w}\right) \tag{4.17}$$

fits well the function $q(a)$ and its first derivative as shown in Figure 4.11. The parameters have been fixed by requiring $q'(0) = 0.743368$ and the maximum of the first derivative to be at at $a = 0.3445$. The remaining two parameters are fixed by a least squares fit of $q(a)$ to the numerical data. The simpler erf-model is recovered from (4.17) by setting $\alpha = \frac{1}{2}$ and $\gamma = \frac{3}{2}$.

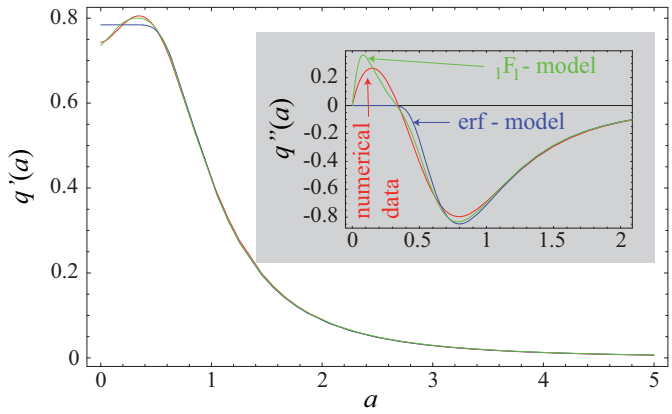

Fig. 4.11: Derivatives of the zero temperature order function. The red line represents the exact numerical results from a 200 RSB computation of the order function. The blue line is the erf-model with $\xi = 1.13$. This model cannot account properly for the small a features. The green line represents the improved order function (4.17) with parameters $\xi = 1.186$, $w = 0.0153$, $\alpha = 0.530$ and $\gamma = 1.73$.

Obviously, the improved model function has considerable deviations in the second derivative. Also the behavior at large a, i.e. the coefficient of the a^{-2} term in the $\frac{1}{a}$ expansion of $q(a)$ near $a = \infty$, cannot be fitted with arbitrary precision to the numerical data. This can be cured, however, by introducing further fit parameters by allowing w to be a function of a. For instance a Padé series instead of a constant w can fit the numerical data arbitrary well, depending on the number of parameters in the series. Also the nonvanishing derivatives $q^{(2n)}(0)$ for $n \geq 2$ can only be accounted for by allowing w to be a-dependent.

[24] The structure at $a = \infty$ is, however, much less important than the structure at $x = 0$ as will be seen later.

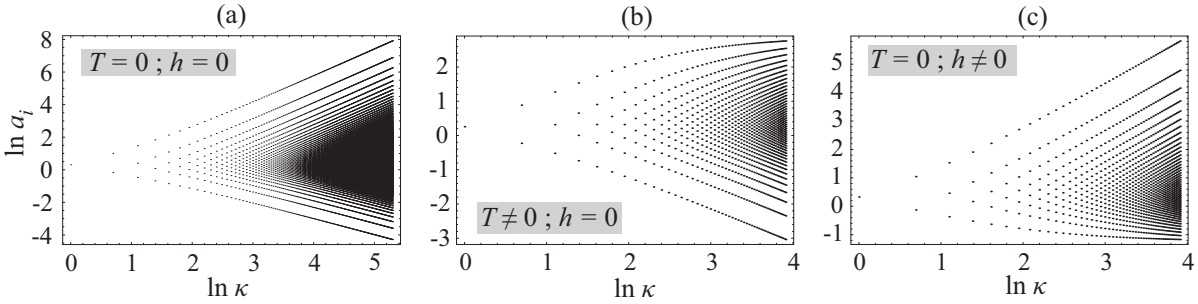

Fig. 4.12: log-log plot of the parameters a_i at $T = 0$ and $h = 0$ (a), $T = 0.03$ and $h = 0$ (b) and $T = 0$ and $h = 0.1$ (c). All values a_i of an RSB order κ given by the abscissa are plotted as points. Ordinate as well as abscissa are log scaled. The RSB orders range from 1 to 200 in the $T = 0$ case and from 1 to 50 for $T = 0.03$ and $h = 0.1$.

4.2.2 $q(a)$ at finite temperatures

At finite temperatures, the domain of the rescaled block-size parameters a_i is restricted to the finite interval $[0, \beta]$. Actually, they even occupy only a sub-interval $[0, \bar{a}_1]$, where $\bar{a}_1 = \beta \bar{x}_1 < \beta$ is the so-called break point in a-formulation or x-formulation, respectively (see inset of Fig. 4.8). In contrast to the zero temperature case, the block size parameters continuously occupy this reduced interval in the limit $\kappa \to \infty$. As a result, the break point equals the largest parameter, i.e. a_1 or m_1, in the limit $\kappa \to \infty$ and thus a further extrapolation of m_1 to infinite order of RSB must be performed. It is convenient to discuss the break point in x-formulation, because the temperature dependence of $\bar{x}_1$ is rather weak for low temperatures. Everything said here about $\bar{x}_1$ can trivially be translated to $\bar{a}_1 = \beta \bar{x}_1$, of course.

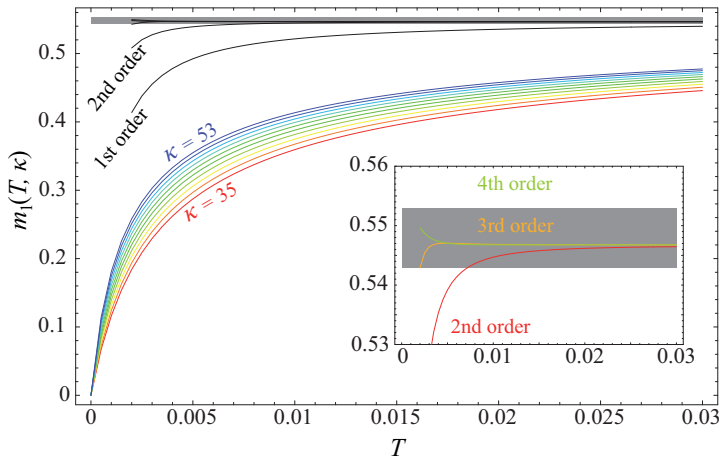

Fig. 4.13: Break point extrapolation at finite temperatures. The colored lines represent the Parisi block size parameter m_1 in the temperature range $T = 0.004, ..., 0.03$ for various RSB orders 35 (red) up to 53 (blue). The black lines show the extrapolations of m_1 to $\kappa = \infty$ for different polynomial orders. The gray area represents the confidence interval of the best estimate 0.548 ± 0.005 for the break point at zero temperature in the literature [CR02].

In Figure 4.13, the parameters $m_1 = Ta_1$ are shown for various orders of RSB in the temperature range $T = 0.004, ..., 0.03$. For each temperature this parameter must be extrapolated to $\kappa = \infty$. This turns out to be not as simple as for the other quantities which have been discussed above, however. The difficulties in the $\kappa \to \infty$ extrapolation of m_1 are due to the importance of sub-leading terms on one hand and, on the other hand, due to the 'distance' between $m_1(\kappa)$ and $m_1(\infty)$ which must be surmounted in the extrapolation. Obviously, this distance even grows with lowering the temperature. Again, the zero-temperature criticality strikes in the present analysis. Compared to the determination of $A(T)$ at low temperatures (see Appendix B), however, the effect of criticality is more severe here: while the error bars of $A(T)$ became larger for lower temperatures but still remained finite at $T = 0$, the error bars of the determination of $\bar{x}_1(T) = \lim_{\kappa \to \infty} m_1(\kappa, T)$ diverge for $T \to 0$. The reason for this is that $\bar{x}_1(T)$ is a pure finite temperature quantity in that the break point is

ill-defined at zero temperature. $\bar{x}_1(T=0)$ can *only* be obtained by extrapolation from finite T calculations to $T=0$[25]. In contrast, $A(T=0)$ has a definite meaning and can be obtained directly from the 200 RSB $T=0$ data. Therefore, it is inevitable for just obtaining an extrapolation $\lim_{\kappa\to\infty} m_1(\kappa,T)$ at a given temperature T to investigate scaling regime $\mathcal{R}_2^T$.

Now that the requirement of restricting the analysis to $\mathcal{R}_2^T$ it is established, it is clear that the κ exponents of the finite κ corrections of the block size parameters is not the irregular $\frac{5}{3}$ which has been found for $a_i(\kappa,T=0)$ before. It rather turned out that the best results can be obtained by fitting polynomials in κ^{-1} of various orders n

$$m_1(\kappa) = m_1(\infty) - \sum_{i=1}^{n} b_i \kappa^{-i} \tag{4.18}$$

to the numerical data. In Figure 4.13 those extrapolations with various polynomial orders are shown independence of the temperature. Obviously, there is a strong dependence of the result on the order n of extrapolation. Compared to the best estimate of the break point in the literature [CR02], however, the results of extrapolations of order $n \geq 3$ already show a much better convergence[26].

The convergence and therewith the accuracy of the estimate of $\bar{x}_1$ from the numerical data can be improved further by utilizing multi-flow fits, the idea of which is as follows: Multiple fits of the numerical data to (4.18) are performed with various sub-ranges $[\kappa_{\min}, \kappa_{\max}]$ of the available data, but with fixed polynomial order n (see Fig. 4.14(a) and (b)). The results of those first extrapolations in dependence of $\kappa_{\max}$ show a flow to a finite limit for $\kappa_{\max}\to\infty$, but the convergence is considerably faster than the convergence of the original data. This flow is then again extrapolated from the available range to $\kappa_{\max}\to\infty$ (see Fig. 4.14(c)). This second extrapolation is performed by fitting to another polynomial $m_1^{(2)}(\kappa) = m_1^{(2)}(\infty) - \sum_{i=n}^{n_2} b^{(2)}\kappa^{-i}$. A further flow which can be extrapolated to infinity can be produced from the results of the second extrapolation by again considering sub-ranges of the available data. This procedure may be iterated until numerical errors become serious. However, a large range of original data is required for many iterations.

In Figure 4.14(c), the result of a two flow fit, i.e. $m_1^{(2)}(\infty)$, is shown for $T=0.0015$. The order $n_2=10$ of the second fit is kept fixed while the order of the first fit is varied from $n=4,...,9$. Obviously, the deviation is relatively small and the break point at $T=0.0015$ can be given with high accuracy $\bar{x}_1(0.0015) = 0.54683 \pm 0.00001$.

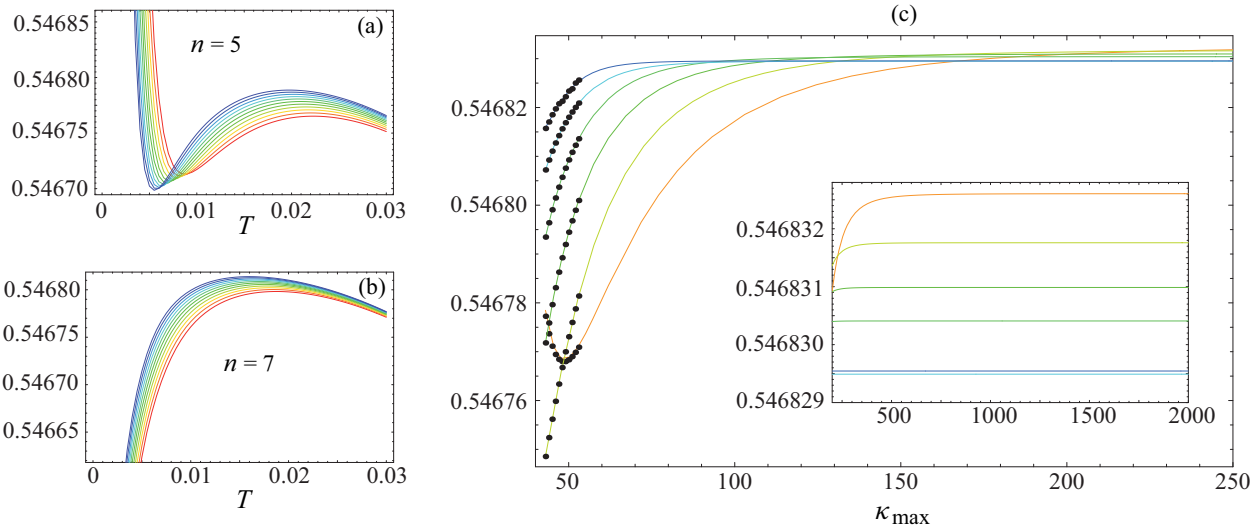

Fig. 4.14: Multi-flow fit of the break point. (a,b) The results of the first extrapolation with different $\kappa_{\max}$ (blue lines represent small $\kappa_{\max}$ and red lines represent large $\kappa_{\max}$) in the temperature range $T=0,...,0.03$ for polynomial orders $n=5,7$. (c) Fits of the second flow at $T=0.0015$ for polynomial orders of the first fit $n=4,...,9$ and $n_2=10$. The black dots are the results from the first fit. The inset shows a zoom to the large $\kappa_{\max}$ region.

[25] The determination of $\bar{x}_1$ in [Pan06] implements this extrapolation by means of a rescaling which allows to perform calculations at $T=0$ in a certain limit.

[26] This statement is true only if one assume the variation of $\bar{x}_1(T)$ for $0<T<0.03$ to be much smaller than the confidence interval (± 0.005) in the literature. This will be seen to be true subsequently

The main problem of those multi-flow fits is that the confidence interval of the result cannot be estimated by standard methods. The best, one can do is to gain an impression of the accuracy of the results by varying the orders of the extrapolation. From the inset in Figure 4.14 one can estimate the order of magnitude of the error of the fit procedure. The error seems to be smaller than 10^{-5}.

In Figure 4.15 the results of the break point extrapolations are plotted together with the estimated errors. One can clearly see the precision loss for low T. From the Figure, the impression can be gained that the value of the break point decreases at low temperatures. I rather believe that this is an artefact of the fit procedure and implemented this belief by means of large error bars.

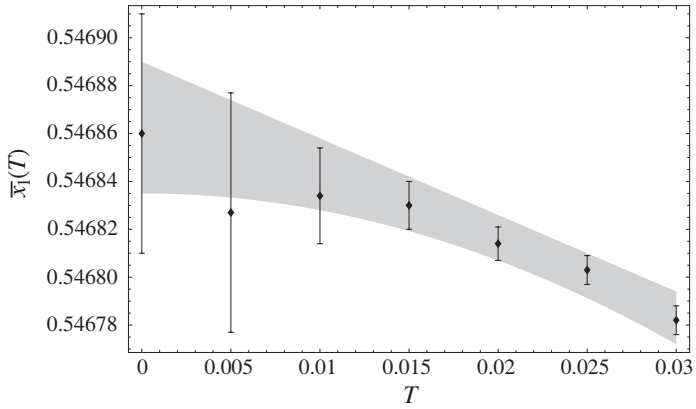

Fig. 4.15: Break points obtained by two-flow fits with estimated errors in the temperature range $T = 0.005, ..., 0.03$. The break point at zero temperature is estimated from the flow of the finite temperature break points to $T = 0$. The gray area shall serve as a 'guide to the eye' for the zero temperature break point estimation.

From the dependence of the break point at temperatures $0.015 \leq T \leq 0.03$ in Figure 4.15, together with the assumption that the break point approaches its zero temperature limit in a well-behaved way, one can obtain a rough estimate of $x_{bp}(T = 0) = 0.54686 \pm 0.00005$. Here, only the results of the break point extrapolations in the range $0.015 \leq T \leq 0.03$ have been respected. Nevertheless, the accuracy of this 'rough' estimate exceeds the best accuracy given in the literature [CR02] by two orders of magnitude.

4.2.3 $q(a)$ at finite external fields

At finite external fields, the lowest a-parameter a_κ does not flow to zero any longer for large κ. Instead, it approaches a finite limit depending on the strength of the field h. The same is true for the lowest q-parameter $q_{\kappa+1}$. Thus, the order function has a plateau at small arguments which is due to finite h in addition to the plateau at large arguments which has been due to finite temperatures. The h-induced plateau is also characterized by a break point $\bar{a}_0(h,T) = \beta\bar{x}_0(h,T)$ below which the order function is constant. In the following, I mainly concentrate on the finite h order function at exactly $T = 0$, since it is, to my best knowledge, investigated for the first time in the present thesis. The zero temperature theory of Parisi RSB has been inaccessible for many years, but with the method derived in Chapter 2 one can investigate this regime at least at finite κ. The continuous limit $\kappa \to \infty$ at $T = 0$ of this method at finite h is also possible and will be discussed in the next chapter.

Figure 4.16 shows the order functions in the range $h = 0, ..., 0.5$. Obviously, the main effect of the external field is that it changes the width and height of the plateau at small a while leaving $q(a,h)$ above $\bar{a}_0$ nearly unchanged. By looking closely to the confidence channels from the step approximation in Figure 4.16(b), however, a small upward correction of $q(a,h)$ above the break point $\bar{a}_0$ is visible for finite $h \gtrsim 0.3$. From this data, it can be conjectured that the PaT projection hypothesis $q(a,h) = q(a,0)$ for $a > \bar{a}$ (see e.g. [PT80, VTP81] or Section 4.4.1) is not exactly but only approximately satisfied even at zero temperature.

The dependence of the plateau height $\bar{q}(\kappa,h)$ is shown in Figure 4.17 for various orders of RSB. The κ convergence of the plateau height appears to be worst at zero external field. Here, another type of criticality arises which calls for a scaling analysis with variables h and κ^{-1} - similar to the (T,κ^{-1})-scaling analysis in Section 4.1. Again, I motivate the scaling analysis by facing two facts which seem to contradict each other and resolve this virtual contradiction by assinging each fact to a different scaling regime. Anticipating some of the results below, one finds:

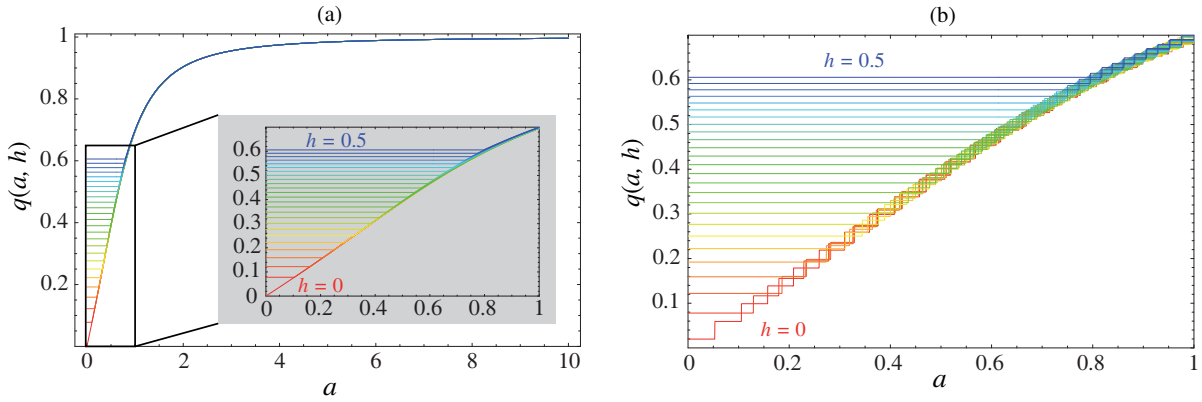

Fig. 4.16: The order function at $T = 0$ and $\kappa = 51$ for finite external fields in the range $h = 0, ..., 0.5$ (red - blue). Part (a) shows the order function obtained from polynomial interpolation. The interpolation point with the smallest abscissa is approximated by substracting half the spacing $a_{\kappa-1} - a_\kappa$ from a_κ. Part (b) shows the step approximation of the order function. From the height of the steps one can extract roughly the confidence channel.

- The order parameters q_i, $i = 1, ..., \kappa + 1$ are even functions of h. It is found from the numerical data of all available finite RSB orders that all those functions are regular at $h = 0$, i.e. they have a Taylor expansion at $h = 0$ with only even terms in h.

- The $\kappa = \infty$ extrapolation of the plateau height $\lim_{\kappa\to\infty} \bar{q}(h)$ at finite h is found to vary as $h^{2/3}$. The finite κ corrections decay as polynomials of κ^{-1}.

Since the plateau height at κRSB is equal to the smallest q-parameter, i.e. $q_{\kappa+1}$, those two facts seem to contradict in that a function $\bar{q}(\kappa, h) \simeq c_1 h^{2/3} + c_2(h)\kappa^{-2} + \mathcal{O}(\kappa^{-3})$ is not Taylor expandable at $h = 0$. From the first derivative of $\bar{q}(\kappa, h)$ which is shown in the inset in Figure 4.17 it is obvious that scaling with respect to the variables h and κ^{-1} is capable of resolving this contradiction: following the curve $\frac{d}{dh}\bar{q}(\kappa, h)$ for a fixed κ coming from large h, a crossover from a diverging behavior (as $h^{-1/3}$) to a vanishing first derivative happens at a certain crossover field $h_{\rm co}(\kappa)$ which depends on κ. This crossover field may be defined[27] as the abscissa of the maximum of $\frac{d}{dh}\bar{q}(\kappa, h)$ for a given κ. One then finds that $h_{\rm co}(\kappa) \sim \kappa^{-3/2}$ which defines the crossover line between the scaling regimes $\mathcal{R}_1^h = (h \simeq 0, \kappa^{-1} > 0)$ and $\mathcal{R}_2^h = (h > 0, \kappa^{-1} \simeq 0)$.

The scaling picture proposed above is only valid if the maximum of $\frac{d}{dh}\bar{q}(\kappa, h)$ really diverges as $\kappa \to \infty$. It is, however, hard to unambiguously determine from the finite RSB numerical calculations whether or not the slope of $\bar{q}(\infty, h)$ is finite at $h = 0$. What one can say is that when the maximum of $\frac{d}{dh}\bar{q}(\kappa, h)$ as a function of κ is fitted to a function which has a finite $\kappa = \infty$ limit, one cannot find optimal fit parameters. With each fit step the fit parameter for the infinite κ limit of the function becomes larger. Instead, if fitted to a function which diverges with some power law in the $\kappa = \infty$ limit, one can easily obtain a set of best fit parameters. I believe that this, together with the analysis in Section 4.4.2 and various publications of different authors [CRT03], is strong evidence for the validity of the scaling picture and for an irregular exponent $\delta < 1$ of $\bar{q}(\infty, h) \propto h^\delta$.

Indeed, a more thorough analysis of the finite h data in which the plateau heights are first extrapolated to $\kappa = \infty$ so that $\bar{q}(\infty, h)$ can be analyzed directly shows that the leading h-term in the regime $\mathcal{R}_2^h$ is proportional to $h^{2/3}$ and the leading κ-term is proportional to κ^{-2}, while in the regime $\mathcal{R}_1^h$ one finds the terms h^2 and κ^{-1}. As in the analysis of the $T = 0$ criticality in Section 4.1 the extrapolation to $\kappa = \infty$ at a fixed h becomes harder as $h \to 0$ in that one needs more and more RSB orders for obtaining a reasonable quality of the extrapolation since any finite RSB order hits the crossover line as $h \to 0$. I found that in $\mathcal{R}_2^h$ the leading terms of the plateau height are

$$(\text{only } \mathcal{R}_2^h) \qquad \bar{q}(\kappa, h) \simeq 1.037\, h^{\frac{2}{3}} - 0.2\, h^2 + 0.3\, h^{-\frac{2}{3}}\kappa^{-2}. \tag{4.19}$$

All the terms with irregular h-exponents are not allowed in $\mathcal{R}_1^h$ and thus must be scaling terms. In scaling

[27] Other definitions as, e.g., the field where the first derivative becomes larger than 3, say, are also possible and lead to the same exponent.

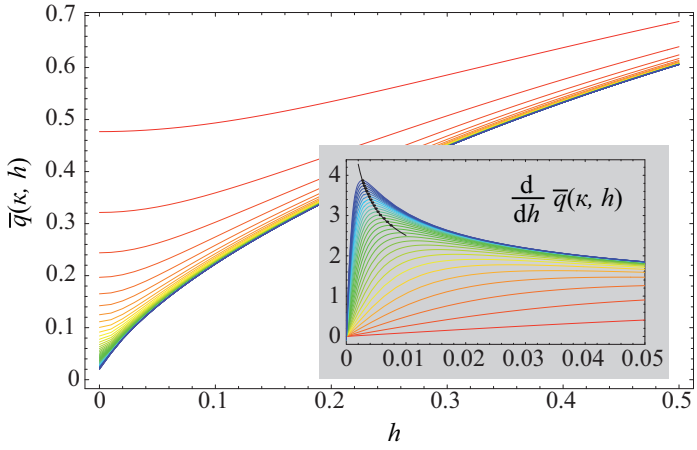

Fig. 4.17: The plateau height $\bar{q}(\kappa, h) = q_{\kappa+1}$ at zero temperature in dependence of an external field h for various orders of RSB. The red line corresponds to 1 RSB and the blue line to 60 RSB. The inset shows the derivative $\frac{d}{dh}\bar{q}(\kappa, h)$ near $h = 0$ for RSB orders $\kappa = 2, 4, ..., 60$. The black curve connects the maxima of $\frac{d}{dh}\bar{q}(\kappa, h)$. It indicates the crossover from a diverging small h behavior above this line to a vanishing small h behavior below this line.

regime $\mathcal{R}_1^h$ the plateau height can be written as

$$(\text{only } \mathcal{R}_1^h) \qquad \bar{q}(\kappa, h) \simeq 1.03\kappa^{-1} - 1.317\kappa^{-2} + \frac{1.03}{2}h^2\kappa^2. \tag{4.20}$$

In this expansion the terms proportional to κ^2 and κ^{-1} are not allowed in $\mathcal{R}_2^h$ and thus they must be scaling terms. The (h, κ^{-1})-scaling picture appears very similar to the (T, κ^{-1})-scaling picture which is illustrated in Figure 4.4. The main differences are the exponents of the crossover lines and the quantities in which scaling has been demonstrated: while (T, κ^{-1})-scaling was found directly in a thermodynamic quantity, i.e. the free energy or the internal energy, the (h, κ^{-1})-scaling has been only discussed by means of a rather unphysical plateau height in the order function.[28] These discussions, however, are only meant to serve as a demonstration of the fundamental need for scaling concepts in the analysis of RSB near $T = h = \kappa^{-1} = 0$ and to introduce the scaling concept. The detailed analysis of those scaling ideas will be presented at the end of this chapter.

4.3 Discreteness at zero temperature

From the plot of the T-rescaled block-size parameters a_i in Figure 4.12 it can be seen that at zero temperature and zero external field certain kinds of discreteness appear on a $\log a$ scale: the difference between $\log a_i$ and $\log a_{i-1}$ does not approach zero in the large a and in the small a regime as $\kappa \to \infty$. In the intermediate regime, which will be seen to extend from $0 < a < \infty$ at ∞ RSB, these differences vanish and the continuous distribution of a_i parameters gives rise to a smooth order function $q(a)$. From the plots at finite temperatures or at finite external field it is also clear that the discreteness at large or small a is temperature or field controlled, in that it is only present at $T = 0$ or $h = 0$, respectively.

The field controlled discreteness at small a must disappear whenever a finite field h is present. Each parameter a_i is larger than the lower break point $\bar{a}_0$, and $\bar{a}_0 > 0$ in case of $h > 0$. Thus the smallest block size parameter is finite. If now the $\log a$ discreteness at small a was present for $\bar{a}_0 > 0$ (i.e. for $h > 0$) then the step character of the order function would survive in the ∞ RSB limit and the order function was not a smooth function. In contrast, the discreteness at $\log a = -\infty$ which is encountered at exactly $h = 0$ does not translate to a discreteness on an a-scale[29] and thus is quite unproblematic as has been discussed in Section

[28] The height of the plateau $\bar{q}(\kappa, h)$ is not a quantity which is in principal accessible in experiments. It is a construct, needed in the mathematical treatment of the SK-model. The difference becomes most obvious when trying to write down the two quantities in terms of the original variables which define the model in (2.1). The internal energy is simply the statistical mechanics average of the Hamiltonian, while for $\bar{q}(\kappa, h)$ one needs the concept of RSB for a proper definition.

[29] Such a behavior would completely invalidate a formulation of the ∞ RSB theory in terms of partial differential equations at small a.

4.2.1. Therefore, this section is devoted to the temperature controlled large a regime of the order function which yields subtle irregular properties. The aim of the following analysis is to understand how the ∞ RSB order function must be represented at zero temperature.

4.3.1 Discrete spectra in the block size ratios

A convenient way of describing the subtleties at $a = 0$ and $a = \infty$ is in terms of ratios of Parisi block size parameters $r_i = \frac{m_{i+1}}{m_i} = \frac{a_{i+1}}{a_i}$. These ratios directly enter the recursion relations in the trace term via the exponentiated Gaussian convolution operator $\int_i^{GE}$ (see Appendix C.1). In Figure 4.18 the ratios are mapped to the interval [0,1] such that the large (small) a regime is projected to 1 (0). To be explicit, a variable $z_l \in [0,1]$ is defined which corresponds to the ratio $\tilde{r}_l = r_i$ with 'inverted' index $l = \kappa - i$ according to

$$z_l = \frac{l}{\kappa} \quad \Leftrightarrow \quad \tilde{r}_l = r_{\kappa - l}. \tag{4.21}$$

For each RSB order, the set of points $(z_l, \tilde{r}_l)$ is plotted in Figure 4.18. The regions where the ratios approach 1 in the ∞ RSB limit are the regions where the points a_i or m_i become dense. This is obviously the case for most of the ratios and thus a partially continuous formulation at zero temperature should be possible. In the following, the situation at $T = 0$ and $h = 0$ (see Fig. 4.18(b)) will be thoroughly investigated. In the limit $\kappa \to \infty$ all ratios $\tilde{r}_l$ corresponding to a $z_l \neq 0, 1$ are unity, whereas at $z = 0$ and $z = 1$ Coulomb-like spectra of ratios which are smaller than 1 appear.

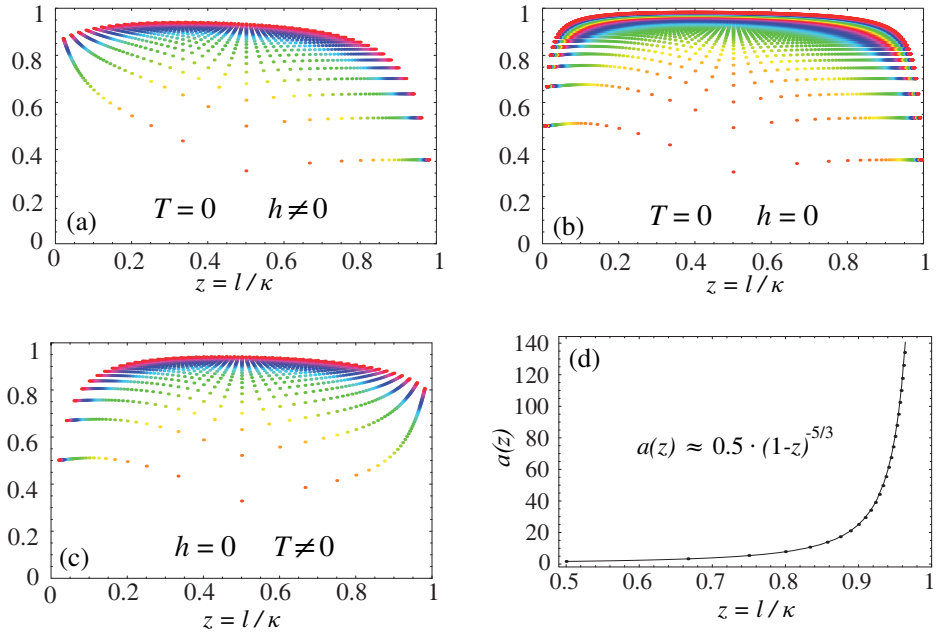

Fig. 4.18: Plots of block size ratios $r_i = \frac{a_i}{a_{i-1}}$ at various RSB orders, mapped to the interval $[0, 1]$. The ratios corresponding to large a_i are near $z = 1$ while the ratios corresponding to small a are near $z = 0$. The part (b) represents the situation at $T = 0$ and $h = 0$ for up to 200 RSB. In parts (a) and (c), results at finite external field $h = 0.1$ and finite temperature $T = 0.03$, respectively, are shown for up to 50 RSB. The colors are chosen such that one cycle red-green-blue-red represents 100 RSB orders in part (b) or 50 RSB orders in parts (a) and (c). In part (d), the mapping $z \leftrightarrow a$ is shown for the $T = 0$, $h = 0$ case.

For the further discussion it is important to establish a connection between the position z_l of a specific ratio $\tilde{r}_l$ and the corresponding a-regime. At ∞ RSB a one-one correspondence between z and a can be given. This correspondence is shown in Figure 4.18(d). It is obtained by extrapolating[30]

$$a(z) = \lim_{\kappa \to \infty} a(z, \kappa), \qquad a(z, \kappa) = a_{(1-z)\kappa}. \tag{4.22}$$

[30] z must be a rational number with relatively small denominator and numerator here. The results of appropriate neighboring rational z give rise to a continuous function $a(z)$.

As expected, the obtained function $a(z)$ which describes the correspondence of block size ratios to different regions of the order parameter $q(a)$ at ∞ RSB diverges near $z = 1$. As a result, the top right corner of the ratio plot at $T = 0$ and $h = 0$ corresponds to $a = \infty$. Similarly, one finds that the top left corner of the ratio plot corresponds to $a = 0$. In other words, the z-interval $]0, 1[$ is mapped to the a-interval $]0, \infty[$ and since the block size ratios which correspond to $z \in]0, 1[$ approach unity in the ∞ RSB limit[31] the regime of finite a is continuously filled with a_i parameters.

The behavior of the order function at $a = 0$ or $z = 0$ is well understood and has been discussed above. It can be incorporated by an order function which is regular in $a = 0$. The large a regime, however, leads to irregularities and cannot be sufficiently incorporated by a continuous function which is regular at $a = \infty$. A first hint for the existence and importance of this issue has been encountered in Section 4.2.1 where a dependence of the derivative of $q(a)$ at $a = \infty$ from the parameter indices has been found. Those issues are located exactly at the point $z = 1$ in the ratio plot of Figure 4.18(b) and intimately correlated with scaling and the zero temperature criticality.

For example, the smallest ratio $r_1 = \tilde{r}_{\kappa-1} = \frac{a_2}{a_1}$, which approaches $\lim_{\kappa\to\infty} r_1 \simeq 0.35$ for ∞ RSB, assures that $a_2 \simeq 0.35a_1$ or $m_2 \simeq 0.35m_1$ for large RSB orders. In the $\kappa = \infty$ limit, however, the parameter a_1 diverges so that also $\lim_{\kappa\to\infty} a_2 = \infty$. Thus, the spacing between successive parameters a_i (with i finite) becomes infinite for $\kappa \to \infty$. The trick is now to characterize all indexed quantities a_i, r_i, q_i by two different scales $a \in [0, \infty]$ and $x \in [0, 1]$ and map the discrete spectrum at $z = 1$ to the finite x domain where $a = \infty$ and the region $z < 1$ where the corresponding ratios are unity to the finite a domain where $x = 0$. In other words, for the discrete region at $a = \infty$ or $z = 1$, the m-formulation of the block size parameters should be used instead of the a-formulation. Doing so one finds, for instance, that[32] $m_2 \simeq 0.19$ and thus $m_1 - m_2 \simeq 0.36$.

In the limit $\kappa = \infty$ there are infinitely many ratios $r_1, ..., r_{\kappa-1}$. In contrast to the finite RSB case, however, there is a sharp separation between three types of ratios: the non-unity ratios at $z = 0$, the unity ratios at $0 < z < 1$ and the non-unity ratios at $z = 1$. Each subset consists of an infinite number of elements (ratios). From a superficial glance at the ratio plots at finite κ one could gain the impression that the number of ratios which become unity is much larger than the non-unity subsets. In the limit $\kappa = \infty$, however, all three subsets have the same cardinality $\aleph_0$, i.e. all of those sets are countably infinitely large[33]. Cardinality is obviously not the proper concept to distinguish those regimes. Instead, I will use a combination of z coordinate as defined in (4.21) and indices i or l: The regime in which the ratios become unity cannot be described by a discrete index but rather by the continuous variable $z \in]0, 1[$. The discrete spectra at $z = 1, 0$, however, are described by the index i and the inverted index l, respectively, in that $r_{i=1}, r_{i=2}, ...$ are the non-unity ratios at $z = 1$ and $\tilde{r}_{l=1}, \tilde{r}_{l=2}, ...$ are the ones at $z = 0$.

At finite temperatures, the finite x and the finite a regime can be mapped onto each other by a transformation $x = Ta$. Thus one may chose one of the variables x or a at will. At zero temperature, this is not possible any longer. Instead one must investigate both scales separately.

4.3.2 Two scales for the order function at zero temperature

It is important at $T = 0$ to resolve the structure of the order function at $a = \infty$ which corresponds to the $x > 0$ regime as well as the structure at $x = 0$ which corresponds to the $a < \infty$ regime. By utilizing this distinction at $\kappa = \infty$, the discrete spectrum of the block size ratios at $z = 1$ (see Fig. 4.18) must be mapped to the $x > 0$ regime. In this way the structure at $a = \infty$ is 'blown up' in a similar manner as the structure at $x = 0$ has been blown up by using the T-rescaled block size parameters a_i instead of m_i, though the resolution of $a = \infty$ is somewhat more subtle because it cannot be directly accessed from finite orders of RSB. As yet, no necessity - neither from the numerical data, nor from conceptual arguments - for mapping the discrete region at small a to another scale has been observed. A description as a regular limit of a continuous function $q(a)$ is sufficient. Here again, the fundamental difference of those two critical points $a = 0$ and $a = \infty$ manifests itself in the different treatments: while $a = \infty$ must be analyzed by means of an additional scale $x \in [0, 1]$, the point $a = 0$ can be incorporated as one single value in a function $q(0)$.

The structure of the discrete regime $x > 0$ must be addressed by investigating extrapolations of several quantities to $\kappa = \infty$ and to $T = 0$. All those extrapolations have been performed in different contexts above and shall be combined now. The first required quantity is the value of the break point at $T = 0$. It has

[31] This can be shown within numerical errors by extrapolation of $r(z, \kappa)$ to $\kappa = \infty$.

[32] Here it has been used that the break point $\bar{x}_1 = m_1 \simeq 0.547$ is finite at $T = 0$.

[33] Figuratively, one could say that the non-unity subsets are only further countably infinite busses which want to check into Hilbert's hotel countably infinity[Cas].

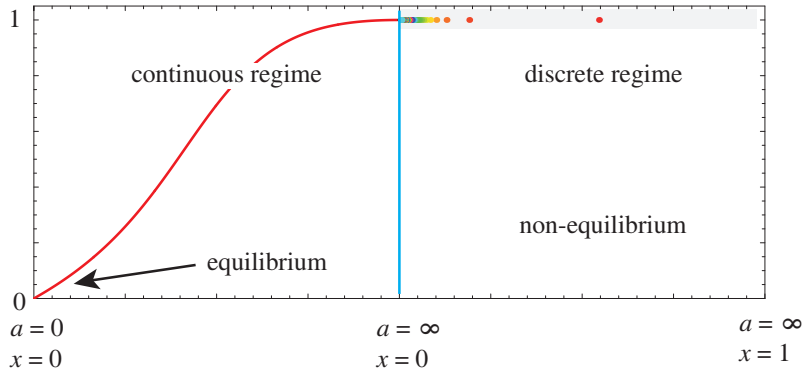

Fig. 4.19: Two regimes of the zero temperature theory at infinite order of RSB. The regime of $0 \leq a < \infty$ on the left hand side gives rise to the continuous part of the order function. On an x-scale this regime is characterized by $x = 0$. The regime of $0 < x \leq 1$ which is characterized by $a = \infty$ does not contain a continuous distribution of block size ratios but rather a discrete set of points a_i at which $q_i = 1$. The red line in the continuous regime is the order function $q(a)$ from a 200 RSB calculation with abscissa transformed to $\zeta = \frac{a}{1+a}$.

been found in section 4.2.2 that $\bar{x}_1$ is finite in the limit $T \to 0$. It should be noted here that the term 'break point' is not completely appropriate in the zero temperature formulation, since there is no kink at $\bar{x}_1$ like in the finite temperature order function. At $T = 0$ the break point is rather defined as the largest block size parameter m_1 in the limit $\kappa \to \infty$. Nevertheless the previous analysis showed that $m_1(T = 0) = 0.54686$. Thus the zero-temperature break point definitely corresponds to $a = \infty$ and $x > 0$.

The second extrapolation which is needed here is the the extrapolation of block size ratios to $\kappa = \infty$ (see Fig. 4.18). At $z = 1$ this leads to the discrete spectrum, starting at $r_1 = 0.36$, which approaches unity for large r_i. The combination of the ratios and the break point allows a construction of the sequence $m_1, m_2, ...$ which is shown in Figure 4.19. Thus it can be concluded that the discrete spectrum at $z = 1$ corresponds in the ∞ RSB limit to an infinite sequence of non-zero Parisi block size parameters m_i. Finally, from the formula for the free energy (2.95) it is easily seen that a $q_i = 1$ corresponds to each $m_i > 0$. This constraint finally fixes the ordinate of the order function in the discrete regime $x > 0$.

From the need for two different scales, it becomes clear why it is difficult to obtain a proper extrapolation the derivatives $\frac{d^n}{d(1/a)^n} q(a)\Big|_{a=\infty} = Q^{(n)}(0)$ from finite RSB data: the discrete derivative $Q_i^{(n)}$ for $i = 1, 2, ...$ as discussed near equation (4.15) does not correspond to the point $(a, x) = (\infty, 0)$ but rather to the finite x regime where the order function is discrete. In Figure 4.10 the correspondence of $Q_1'', Q_2'', ...$ to the discrete regime is reflected by their deviation from the second derivative at $a = \infty$ from the purely continuous treatment which accounts for the distinction of the finite x and the $x = 0$ regime. In a proper $\kappa = \infty$ extrapolation of $\frac{d^n}{d(1/a)^n} q(a)\Big|_{a=\infty}$ from finite RSB data one must not simply follow the largest a parameters, because by doing so one would arrive at the discrete spectrum at $z = 1$ where $r_i < 1$ (see Fig. 4.18). One rather must extrapolate the derivative $\frac{d^n}{d(1/a)^n} q(a)\Big|_{a=a(z)}$ to $\kappa = \infty$ for a fixed z and *afterwards* extrapolate to $z = 1$. By this procedure one arrives at $(a, x) = (\infty, 0)$, as desired.

The physical interpretation of the appearance of two separate scales in the order function is rather subtle. First of all, one can assign equilibrium and non-equilibrium properties of the system to the different scales: non-equilibrium behavior in the sense that the system is trapped in one single ergodic component of the phase space is described by the finite x regime. This can be seen by considering the non-equilibrium susceptibility χ_{ne} at $T = 0$ which is given by the linear temperature coefficient of q_1. Obviously, this non-equilibrium quantity is given by the $x > 0$ regime of the order function. This statement also holds for other non-equilibrium quantities as the susceptibility or the Edwards-Anderson order parameter. On the other hand, equilibrium quantities as e.g. the ground state energy are determined *only* by the $a < \infty$ regime. The integral (sum) over $1 - q(a)^2$ $(1 - q_i^2)$ which appears in the formula for the internal energy at infinite (finite) RSB has only contributions from the finite a regime because $q(a = \infty) \equiv 1$. Besides, $q(a)$ can be interpreted as an autocorrelation function in which $\frac{1}{a}$ parametrizes diverging relaxation times [Som81] and in this interpretation, $a = 0$ corresponds to the longest relaxation time which describes the minimum time

which must be averaged over in a measurement for restoring ergodicity[34].

4.3.3 Criticality of the block size ratios

I have mentioned above that at finite temperatures (external fields) the discreteness at $z = 1$ ($z = 0$) vanishes. This effect shall now be discussed by means of the scaling behavior of the discrete spectra of the block size ratios. In Figure 4.20 the block size ratios from calculations at low temperatures are compared. At $T = 0.0001$ the deviations of the ratios from the $T = 0$ ratios are very small; differences can be seen only for high RSB orders. The deviations of the $T = 0.005$ ratios from $T = 0$, however, can be seen in much lower RSB orders.

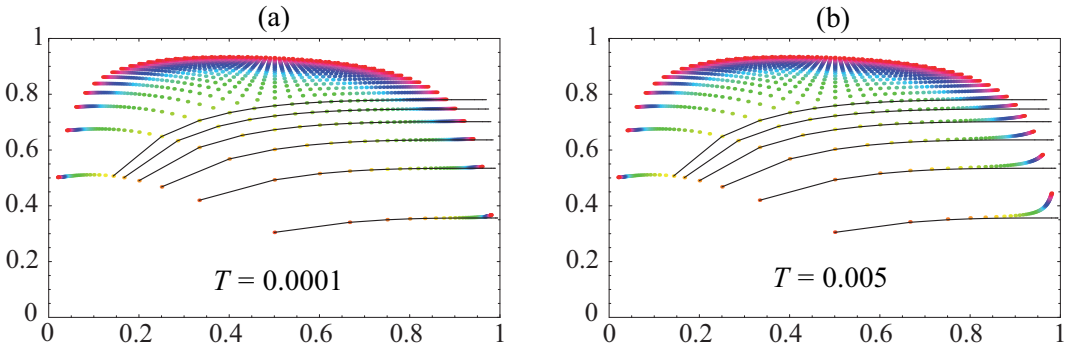

Fig. 4.20: Scaling behavior of the block size ratios for finite temperatures. The black lines are interpolations of the zero temperature ratios $r_1, r_2, ...$ for $\kappa = 2, ..., 200$. The colored dots are ratios from calculations at $T = 0.0001$ (a) and at $T = 0.005$ (b) for $\kappa = 2, ..., 50$.

In order to quantify this statement, I define the following criterion for a finite T result being different from the $T = 0$ result:

> *The ratios at a given RSB order κ and temperature T are different from the $T = 0$ ratios if and only if $r_1(T, \kappa) - r_1(T = 0, \kappa) > \epsilon$, where ϵ is a small number of order 10^{-2} which gives the maximum deviation of an arbitrary ratio $r_i(T, \kappa)$ from its $T = 0$ value.*

This criterion is then used to construct a function $\kappa_{\min 2}(T)$ (cf. $\kappa_{\min}(T)$ in Sec. 4.1) which represents the minimum RSB order needed to resolve finite temperature behavior of the ratio $r_i(T, \kappa)$, i.e. a significant deviation from $r_i(T = 0, \kappa)$, at a specific temperature T. Remarkably, it turns out that $\kappa_{\min 2}(T) \propto T^{-5/3}$ diverges with the same power law as $\kappa_{\min}(T)$ which is defined as the minimum RSB order required to obtain a non-negative entropy at a given temperature. The exponent is independent of the choice of ϵ, as long as it is small enough. A different ϵ only results in a different constant of proportionality. As a result, the same scaling picture which is illustrated in Figure 4.4 is applicable here.

The same analysis has been performed for the h-controlled discreteness in the block size ratios which correspond to small a (see Fig. 4.18 (a) and (b)). The result is that the corresponding $\kappa_{\min 2}(h)$ diverges for $h \to 0$ as $h^{-2/3}$ just like the crossover line between the scaling regimes $\mathcal{R}_1^h$ and $\mathcal{R}_2^h$.

The power laws which describe the scaling of the RSB order with the temperature and the external field are strong evidence for the scaling to be universal in the sense that it is not only restricted to one specific aspect, but rather present in each quantity which is sensitive to changes in the temperature or in the external field. Indeed, all the above findings can be combined to one universal scaling picture as will be argued in the following section.

4.4 Scaling analysis

In the preceding analysis, scaling concepts turned out to be extremely important for a proper understanding of the region in which all parameters κ^{-1}, h, T become small. Several contradictions could only be resolved by assinging conflictive statements to different scaling regimes. In the present section, the scaling concepts, introduced above, will be unified as far as possible.

[34] In this dynamical interpretation which is due to Sompolinsky, all relaxation times τ_a which are parametrized by $\frac{1}{a}$ are divergent in the thermodynamic limit. However, the ratio $\tau_{a=0}/\tau_{a>0}$ also diverges, which means that $a = 0$ corresponds to the largest time scale.

4.4.1 PaT-scaling

In the beginning of the 1980's, the detailed form of the self-consistent solution of Parisi RSB was only poorly understood, because the equations could be solved for arbitrary h and T only with the numerical methods available to that time. One of the first simplifying approaches to gain control over the order function $q(x, T, h)$ for arbitrary temperatures and fields by means of a scaling hypothesis has been proposed by Parisi and Toulouse [PT80, VTP81]. It turned out later [TGL82] that their conjectures lead to a slightly wrong result. Nevertheless, it is a quite good approximation and allows for a relatively simple calculation of the order function.

The PaT-conjecture consists of two main assumptions[35]

1) The *projection hypothesis* states that the Edwards-Anderson order parameter q_{EA} depends only on the temperature and not on the external field. q_{EA} is the height of the large-a plateau in the present formulation. Thus
$$q_{EA}(T, h) = q(\bar{a}_1, T, h) = q_{EA}(T). \tag{4.23}$$
Further, a finite external field induces a plateau at small a in the interval $[0, \bar{a}_0]$ but is assumed to not change the order function for $a > \bar{a}_0$.

2) The *scaling hypothesis* states that between the break points $\bar{x}_0 < a < \bar{x}_1$ the order function $q(x, T)$ is independent of h and can be expressed in terms of a scaling function $f(x/T)$. In the present notation the scaling hypothesis reads
$$q(a, T) = \tilde{q}(a) \quad \text{for} \quad \bar{a}_0 < a < \bar{a}_1. \tag{4.24}$$

With the help of these PaT hypotheses, the scaling function $\tilde{q}(a)$ can be calculated as follows: for each temperature one calculates $q_{EA}(T)$ at the AT-line[36], where the RS-approximation is exact. From the identity $\beta - \int_0^\beta da\, q(a) = 1$[37] the upper break point $\bar{a}_1(T)$ can be calculated (see below). Further, it is clear that the scaling function $\tilde{q}(a)$ evaluated at the point $a = \bar{a}_1(T)$ is equal to the Edwards-Anderson order parameter for the temperature T which has been calculated at the AT-line. Since the break point $\bar{a}_1(T)$ varies between 0 and ∞ as T varies between 1 and 0, respectively, one can construct $\tilde{q}(a)$ for all relevant arguments.

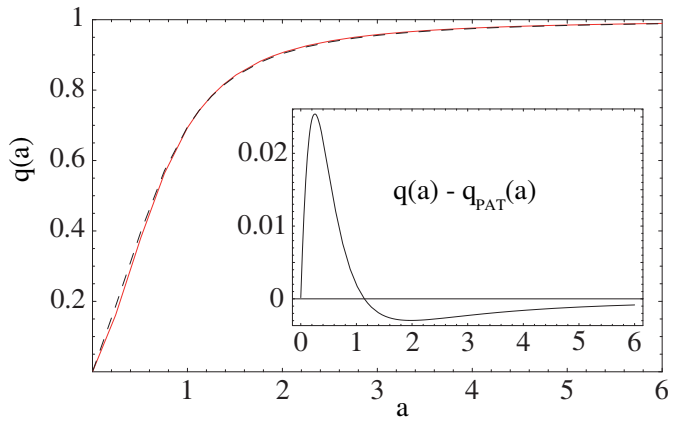

Fig. 4.21: Comparison between PaT scaling prediction (red line) for $q(a)$ at zero temperature and the true order function from a 200RSB calculation (black dashed line). The inset shows the difference between the order functions obtained by the different methods.

In Figure 4.21 the scaling function $\tilde{q}(a)$, calculated from the PaT-hypotheses, is compared to a 200 RSB calculation at $T = 0$, which can be regarded as the exact solution for the accuracy needed here. Obviously the accordance of the two results is remarkably good, especially if one compares the effort for obtaining both solutions - the computer time needed to calculate the 200RSB solution is about $5 \cdot 10^4$ larger than the computation time of the PaT result. There are, however, small but definite deviations of $q_{\kappa=200}(a)$ from the scaling form as illustrated by the inset of Figure 4.21: PaT scaling overestimates the curvature at small a.

[35] The original nomenclature was slightly different. Here the names of the hypotheses are adapted to present needs.
[36] See Appendix A.1.
[37] This identity follows from the equilibrium-susceptibility being unity in the ∞ RSB limit.

In the following I want to discuss PaT-scaling from the $T = 0$ point of view. The reason for doing this is that at $T = 0$ the order function[38] covers the whole a-domain $[0, \infty[$. This is also the domain on which the PaT scaling function is defined. Deviations from PaT-scaling can then be analyzed by means of small corrections to scaling - mainly near $a = \infty$ and $T = 0$. With this type of analysis, exact relations between several quantities can be derived.

In order to discuss the correction to PaT scaling near $T = 0$ and at $h = 0$, the true order function $q(a, T)$ at ∞ RSB is written as the sum of a scaling contribution $q(a, 0)$ and a correction to scaling $\tilde{q}(a, T)$

$$q(a,T) = \begin{cases} q(a,0) + \tilde{q}(a,T) & \text{for} \quad a < \bar{a}_1 \\ q(\bar{a}_1,0) + \tilde{q}(\bar{a}_1,T) & \text{for} \quad a \geq \bar{a}_1 \end{cases} \tag{4.25}$$

From the identity $\chi_e = 1 = \int_0^\beta da(1-q(a,T))$, the correction to the PaT prediction for the zero temperature extrapolation of the break point $\bar{x}_1$ can be derived

$$\bar{x}_1(T=0) = \frac{1}{2} - \frac{1}{2\alpha} \lim_{T\to 0} \int_0^{\bar{a}} da \, \frac{d}{dT} \tilde{q}(a,T) \tag{4.26}$$

where α is the quadratic temperature coefficient of the Edwards-Anderson (EA) order parameter $q_{EA}(T) \simeq 1 - \alpha T^2$. Note that for $\tilde{q}(a, T) = 0$, equation (4.26) reduces to the PaT prediction $\bar{x}_1 = \frac{1}{2}$. Now, if one assumes that $\tilde{q}(a, T)$ can be expanded in a Taylor-series near $(a, T) = (\infty, 0)$, i.e.

$$\tilde{q}(a,T) = \sum_i T^i \, \tilde{q}_i(a), \qquad \text{for } T \ll 1 \tag{4.27}$$

and

$$\tilde{q}_i(a) = \sum_j b_i^j a^{-j}, \qquad \text{for } a \gg 1 \tag{4.28}$$

one can straightforwardly derive relations between the lowest coefficients of the $\tilde{q}(a, T)$ expansion, the quadratic temperature coefficient α of the EA order parameter, the break point and the a^{-2} coefficient c of the expansion of $q(a, 0)$ at $a = \infty$ (see Sec. 5.4.3).

$$b_1^0 = b_1^1 = 0 \tag{4.29}$$

$$\alpha = \frac{c}{\bar{x}_1^2} - b_2^0 \tag{4.30}$$

$$\int_0^\infty da \, \tilde{q}_1(a) = \frac{c}{\bar{x}_1^2}(1 - 2\bar{x}_1) - b_2^0. \tag{4.31}$$

The first relation states that $\tilde{q}_1(a)$ must go to zero faster than a^{-1} as $a \to \infty$. This also ensures that the integral on the left hand side of equation (4.31) converges. The parameters $c, \alpha, \bar{x}_1$ are very well known from the literature and have been obtained from the numerical data of the present work, too. From the above relation, one can thus extract $b_2^0 = -0.22035 \pm 0.00012$ and write the correction to PaT-scaling near $(a, T) = (\infty, 0)$ as

$$q(a,T) = q(a,0) - 0.22 \, T^2 + \mathcal{O}(T, a^{-1})^3. \tag{4.32}$$

Relation (4.31) can be used as a test for $\tilde{q}_1(a)$ extracted from numerics. This, however, should be done directly at $\kappa = \infty$ because the corrections to PaT scaling are on the order of the finite κ corrections.

4.4.2 Scaling in the continuous limit near $h = 0$, $T = 0$

In the previous analysis of the results of the finite RSB calculations, exponents of striking similarity have been found. At several places in the present work and also in the literature [BC03, CRT03] there appeared exponents which are integer multiples of $\frac{1}{3}$ whenever the small a region of the order function and finite external fields have been investigated. In the following, these exponents shall be brought together by considering the h dependence of the ground state energy within PaT approximation.

The ground state energy with finite external field h at $T = 0$ can be written exactly as

$$E_0(h) = -hM(h) - \frac{1}{2} \int_0^\infty da(1 - q^2(a)) \tag{4.33}$$

[38] Here, only the continuous part of the order function is considered.

where $M(h) = \chi_e h + \gamma\, h^{7/3} + \mathcal{O}(h^3)$ is the magnetization. The exponent of the sub-leading term in the magnetization has been chosen such that the first derivative of $f(h)$ in equation (4.9) has the same terms as $M(h)$. The order function for finite external field has a plateau below the lower break point $\bar{a}_0$ with the plateau value $\bar{q}(h) = b_1 h^{\frac{2}{3}} + b_2 h^2$. In the present subsection it is assumed that the order function does not depend on the external field above $\bar{a}_0$. Thus

$$E_0(h) - E_0(0) = -hM(h) - \frac{1}{2}\int_0^{\bar{a}_0(h)} da\, \left[q^2(a, T=0, h=0) - \bar{q}^2(h)\right] \tag{4.34}$$

with $q(\bar{a}_0(h), T=0, h=0) = \bar{q}(h)$. The order function at $T=0$ and $h=0$ may be expanded near $a=0$ up to third order in a (see Sec. 4.2.1)

$$q(a,0,0) = d_1 a + d_2 a^3 + \mathcal{O}(a^4) \tag{4.35}$$

and the integral in equation (4.34) can be solved up to order h^4. Thus, the h dependence of the ground state energy can be written as

$$E_0(h) - E_0(0) = \left(\frac{b_1^3}{3d_1} - \chi\right) h^2 + \left(\frac{b_1^2 b_2}{d_1} - \frac{b_1^5\, d_2}{5 d_1^4} - \gamma\right) h^{\frac{10}{3}} + \mathcal{O}(h^4). \tag{4.36}$$

From the first term in this expansion and from the fact that, due to $\chi_e = -\frac{d^2}{dh^2} E_0(h)$, $E_0(h) = E_0(0) - \frac{1}{2}\chi_e h^2 + \mathcal{O}(h^3)$ one finds that

$$\frac{\chi_e}{2} = \frac{1}{2} = \frac{b_1^3}{3d_1} \qquad \Rightarrow \qquad b_1 = \left(\frac{3d_1}{2}\right)^{\frac{1}{3}} \simeq 1.03697, \tag{4.37}$$

where $d_1 = 0.743368$ from Section 4.2.1 has been used in order to obtain a high accuracy result for b_1. The same type of analysis for the coefficient of the $h^{10/3}$ term in (4.36), however, leads to an inconsistency with the results of the above numerical high precision analysis. This is probably due to the only approximation which has been used here, namely the PaT approximation. A full treatment thus would require to respect the deviation of $q(a,h)$ from $q(a, h=0)$ above the break point. Obviously, PaT scaling is violated at order $h^{10/3}$ in the free energy.

4.4.3 Unified scaling at finite RSB

At several points in the previous analysis, virtual contradictions have been resolved by the introduction of scaling with respect to the variables κ^{-1}, h and T. This has mostly been done by simply assigning a given term to one of the scaling regimes with the argument that it cannot belong to the other regime without violating well established rules (e.g. Taylor-expansibility of the free energy near $T=0$). All those assignments still must be brought together in order to establish one unified picture and to check for consistency of the former statements. This is the aim of the following discussion.

Interestingly, it seems that the scaling variables always appear in pairs (T, κ^{-1}) and (h, κ^{-1}) in that one must consider harmonic functions of a variable T^{ν_T}/κ^{-1} or h^{ν_h}/κ^{-1}. As yet, no need for scaling of T with respect to h has been found. The values of the critical exponents can be extracted from the analysis of the criticality of the block size ratios in Section 4.3.3.

$$\nu_T = \frac{3}{5}, \qquad \nu_h = \frac{2}{3} \tag{4.38}$$

It turns out that these are really the scaling exponents of *all* quantities and not only of the block size ratios. In the following, the quantities in which scaling appears will be discussed. Remarkably, the κ-h scaling and the κ-T scaling can be connected to limiting regimes of the order function, namely $a \to 0$ and $a \to \infty$, respectively.

$\bar{q}(\kappa, h)$ scaling

The plateau height of the order function at small a, given by $\bar{q}(\kappa, h)$, has been investigated in Section 4.2.3 and expansions around $(\kappa, h) = (\infty, 0)$ have been given in the different scaling regimes (eqns. (4.19) and (4.20)). All those terms can be explained by the following Ansatz for the plateau height:

$$\bar{q}(\kappa, h) = \bar{q}_{\rm reg}(\kappa, h) + \bar{q}_{\rm s}(\kappa, h) \tag{4.39}$$

where the regular part is given by

$$\bar{q}_{\rm reg}(\kappa,h) = -0.2h^2 - 1.317\kappa^{-2} + \mathcal{O}(h^3,\kappa^{-3}) \tag{4.40}$$

and the scaling part is written in terms of a function of a single variable $f_{\bar{q}}(x)$. With $x = \frac{h^{2/3}}{\kappa^{-1}}$ it is clear that the scaling regime $\mathcal{R}_1^h$ is equivalent to $x \ll 1$ while $\mathcal{R}_2^h$ corresponds to $x \gg 1$. Thus, the scaling part of the plateau height reads

$$\bar{q}_{\rm s}(\kappa,h) = \kappa^{-1} f_{\bar{q}}\left(\frac{h^{2/3}}{\kappa^{-1}}\right), \qquad f_{\bar{q}}(x) = \begin{cases} 1.03 + \frac{1.03}{2}x^3 + \mathcal{O}(x^4) & \text{for} \quad x \to 0 \\ 1.037x + 0.3\frac{1}{x} + \mathcal{O}(x^{-2}) & \text{for} \quad x \to \infty \end{cases}. \tag{4.41}$$

Interestingly, the terms of the regular part are partially screened by the scaling terms in the two different scaling regimes. For instance, in $\mathcal{R}_1^h$, the regular $h^2 \cdot \kappa^0$ term is hard to observe in the $\kappa \to \infty$ limit, because there is a diverging $h^2 \cdot \kappa^2$ term. Though, careful investigations show that the existence of a $h^2 \cdot \kappa^0$ term in $\mathcal{R}_1^h$ is absolutely consistent with the numerical data.

$\bar{a}_0(\kappa,h)$ scaling

Similarly to the small a plateau height, the plateau width $\bar{a}_0(\kappa,h)$ can be considered. The extraction of the expansions in the different scaling regimes is somewhat more intricate here but is in principle the same. Instead of considering the parameter $q_{\kappa+1}$, the κ and h dependence of a_κ is investigated. One finds in analogy to equations (4.19) and (4.20)

$$(\text{in } \mathcal{R}_1^h) \;\; \bar{a}_0(\kappa,h) = 2.77275\kappa^{-1} - 3.5435\kappa^{-2} - 8.1\kappa^{-3} + \frac{1.4}{2}h^2\kappa^2 + \mathcal{O}(\kappa^{-4}, h^2\kappa, h^{8/3}) \tag{4.42}$$

$$(\text{in } \mathcal{R}_2^h) \;\; \bar{a}_0(\kappa,h) = 1.395h^{2/3} - 3h^2 + 1.35\kappa^{-1} + const.\kappa^{-2}h^{-2/3} + \mathcal{O}(h^{8/3}, \kappa^{-1}h, \kappa^{-2}). \tag{4.43}$$

Again, there are regular contributions and scaling contributions to $\bar{a}_0(\kappa,h)$, namely

$$\bar{a}_0(\kappa,h) = \bar{a}_{\rm reg}(\kappa,h) + \bar{a}_s(\kappa,h) \tag{4.44}$$

with the regular part

$$\bar{a}_{\rm reg}(\kappa,h) = c_1\kappa^{-1} - 3\,h^2. \tag{4.45}$$

Because the term κ^{-1} is present in each scaling regime, it is harder to assign it to the scaling terms or to the regular terms. Thus, this point is left open and a general coefficient c_1 is introduced for the κ^{-1} regular term. Finally, the scaling contribution may be written as

$$\bar{a}_s(\kappa,h) = \kappa^{-1} f_{\bar{a}}\left(\frac{h^{2/3}}{\kappa^{-1}}\right), \qquad f_{\bar{a}}(x) = \begin{cases} c_2 + \frac{1.4}{2}x^3 + \mathcal{O}(x^4) & \text{for} \quad x \to 0 \\ 1.395x + c_3 + const.\frac{1}{x} & \text{for} \quad x \to \infty \end{cases} \tag{4.46}$$

where $c_1 + c_2 = 2.77275$ and $c_1 + c_3 = 1.35$.

Note that there is always some ambiguity in assinging a term to the scaling part or to the non-scaling part on the basis of only numerical data. The ultimate criterion for an assignment to the scaling part is that an assignment to the non-scaling part would lead to contradictions. But also terms which are in principle allowed to be non-scaling terms could arise from the scaling functions. In any case, it has been shown that the scaling picture is consistent for the plateau heights and the plateau widths.

It is further remarkable that the $h^{2/3}$ terms in the plateau region are scaling terms, corresponding to the regime R_2^h. This is also the regime which is addressed by the continuous formulation of ∞ RSB [Par79, CR02, CRT03]. The regime $\mathcal{R}_1^h$, however, is completely inaccessible by the continuous formulation, because an arbitrary small, but finite external field is always assumed implicitly in the method when solving the differential equations numerically[39].

[39] The initial condition of the Lagrange multiplier function $P(x,y)$ at $x = 0$ (see e.g. Chapter 5) is a delta peak for $h = 0$. In a numerical solution, however, one always (even in the pseudo-spectral method [CR02]) assumes a finite width of $P(x,y)$ at $x = 0$, which corresponds to a finite external field.

General small a and small q scaling

The above scaling analysis has been carried out for the smallest a parameter and the smallest q parameter $a_\kappa = \bar{a}_0(\kappa, h)$ and $q_{\kappa+1} = \bar{q}(\kappa, h)$, respectively. The same reasoning is is also applicable for $a_{\kappa-j}$ or $q_{\kappa+1-j}$ with $j \ll \kappa$. From such an analysis, the discrete block size ratios at small a in the scaling regime $\mathcal{R}_1^T$ can be explained. At $\kappa = \infty$ and $h = 0$, though all $a_{\kappa-j}$ are zero, their ratios are different if the critical point is approached from different scaling regimes.

Large a scaling

The large a regime of the order function is connected to (κ^{-1}, T) scaling. In order to support this statement, I now present some evidence.

1. First of all, the large a regime is only meaningful for $T \to 0$, because $q(a)$ is defined on the interval $[0, \beta]$. For finite κ, however, the large a regime is not 'filled', even at $T = 0$, in the sense that no a-parameters are infinitely large. The way, in which the large a regime is filled depends on the order of limits $T \to 0$ and $\kappa \to \infty$: if one performs the $T \to 0$ limit first, the largest a parameter grows with $\kappa^{5/3}$. If, on the other hand, the $\kappa \to \infty$ limit is performed first, then the largest a parameter grows with β. Further increasing a large κ at $T > 0$ leads to only a small grow as $a_1(\kappa, T) \sim a_1(\infty, T) - \frac{const.}{\kappa}$.

2. The discrete block size ratios on the right hand side of Figure 4.18(b) correspond to the large a regime. The discreteness, however, disappears for $T > 0$. More precisely, the discreteness can be observed if one first performs the limit $T \to 0$ and then the limit $\kappa \to \infty$, but it can not be observed for the opposite order of limits.

3. The entropy at $T = 0$ is calculated from the non-equilibrium susceptibility which is given by $\chi_{ne} = \beta(1-q_1)$. q_1, the Edwards-Anderson order parameter, is a short-time quantity and as such corresponds to the large a regime. Further, the entropy was the first quantity (see Sec. 4.1) in which a kind of crossover has been observed. The corresponding crossover line was $\kappa \sim T^{-\nu_T}$.

By again writing scaling parts of certain quantities in terms of a function $f(x)$ with $x = \frac{T^{3/5}}{\kappa^{-1}}$ one can see that a power $T^{3/5}$, as for instance in the coefficient $A(T)$ (see eqn. (4.3)), which is present in scaling regime $\mathcal{R}_2^T$ $(x \to \infty)$ translates to a κ^{-1} term in the scaling regime $\mathcal{R}_1^T$ $(x \to 0)$. As a further example, let me recall the κ dependence of the zero-temperature entropy $s(\kappa, 0) \sim \kappa^{-10/3}$ (see Section 4.1). Obviously, $s(\kappa, 0)$ is located in $\mathcal{R}_1^T$. Such an entropy leads to a term $T \cdot \kappa^{-10/3}$ in the free energy. A finite RSB correction $\kappa^{-10/3}$, however, is not allowed in $\mathcal{R}_2^T$. Thus, the linear temperature $T \to \kappa^{-5/3}$ by scaling arguments which results in a translation $T \cdot \kappa^{-10/3} \to \kappa^{-5}$ as $\mathcal{R}_1^T \to \mathcal{R}_2^T$. The term κ^{-5} in the free energy is in consistence with the numerical results of $\mathcal{R}_2^T$.

If the large a regime of the order function near $(\kappa, T) = (\infty, 0)$ is considered directly, the same concepts are found during the analysis. For instance, since the leading term in the largest a-parameter is $a_1 \sim \kappa^{5/3}$ at $T = 0$ for $\kappa \to \infty$, one may write

$$a_i(\kappa, T) = \kappa^{5/3} f_{a_i}\left(\frac{T}{\kappa^{-5/3}}\right) \tag{4.47}$$

with $f_{a_i}(0) = f_{a_i}^{(0)} > 0$ and $f_{a_i}(x) \sim x^{-1}$ for $x \to \infty$. As a result, the T^{-1} divergence of the largest a-parameter for $\kappa = \infty$ with $T \to 0$ on one hand, and the $\kappa^{5/3}$ divergence for $T = 0$ with $\kappa \to \infty$, on the other hand, is incorporated on the same footing within the scaling formulation (4.47). Note also that the two scaling regimes, resulting from equation (4.47), coincide with the scaling regimes $\mathcal{R}_1^T$ and $\mathcal{R}_2^T$, resulting from the scaling analysis of the thermodynamic quantities. Especially, the crossover lines $\kappa \sim T^{-\nu_T}$ are equal.

Let me conclude this section by stating that it has been demonstrated in the above discussion that scaling with respect to the pairs of variables (κ^{-1}, h) and (κ^{-1}, T) is more than a nice idea, one may think about when looking at 'strange' quantities as, e.g., the smallest order parameter[40]. Scaling is rather an important feature of replica symmetry breaking itself which can be observed in several quantities (order function/parameters, entropy, free energy, magnetization, etc.). The striking point is that in all quantities which have been investigated in the present chapter, the scaling has a universal form, given by the crossover lines $\kappa \sim h^{-\nu_h}$ and $\kappa \sim T^{-\nu_T}$.

[40] Such an order parameter may be called strange at the first sight because it is not a directly measurable quantity. Further, it is - from a more external point of view - a non-physical quantity because the formalism is only correct in the limit $\kappa = \infty$, where no finite number of order parameters exist anymore but rather a pure order function.

Chapter 5

Continuous RSB

Each RSB hierarchy with a finite number κ of steps is unstable against a hierarchy with $\kappa+1$ steps [Par79]. Consequently, infinitely many steps of RSB are needed in order to obtain a stable solution [Tal06]. In this limit the infinitely many order parameters associated with ∞RSB can be written by means of an order function as described in Section 4.2. The continuous theory which results from the $\kappa \to \infty$ limit has a functional form, i.e. the free energy is a functional of the order function $f[q(a)]$, and this functional must be maximized in the space of possible order functions $q(a)$. The functional free energy, however, is not as simple as, for instance, an integral of a specific function of $q(a)$. It will be shown instead that f depends rather implicitly on $q(a)$ through a partial differential equation, the solution of which directly enters f. As a result, the maximization process is difficult and some tricks are needed in order to be able to actually perform the self-consistence calculations.

In the present chapter, I will discuss the $\kappa \to \infty$ transition of the low temperature formulation of RSB which has been derived in Chapter 2. The subtleties of this transition at zero temperature will be analyzed and it is shown how to resolve the issues which made a zero temperature theory directly in the Parisi gauge impossible over years.

In the end, some preliminary computations are presented which have been performed with the help of the computer algebra system *Mathematica*®. They serve as a demonstration of the feasibility of the proposed formalism. A careful programming of numerical differential equation solvers, optimized to the present formalism, is beyond the scope of the present work.

5.1 The continuous RSB transition of $\ker\mathcal{C}$

The central point in the derivation of the continuous RSB formalism is a partial differential equation which arises from the recursion relation (2.96) in the $\kappa \to \infty$ limit. The function which solves this differential equation is the continuous version of the kernel correction function $\ker\mathcal{C}$. For clarity the discussion in the present section is restricted to the Ising spin-glass with $h = J_0 = 0$. The generalization to the non-Ising case, to a finite ferromagnetic component J_0 and to a finite external field h is straightforward, however.

From the expression (2.95) for the free energy of an Ising spin-glass it is easily seen that, in the limit $\kappa \to \infty$, the field term passes over to an integration over the order function $q(a)$. On the other hand, the last Gaussian integration in the trace term becomes infinitely sharp at $h_{\kappa+2} = 0$ because of $\lim_{\kappa\to\infty} q_{\kappa+1} = 0$ so that the free energy can be written as

$$\lim_{\kappa\to\infty} f = -\frac{1}{4}\int_0^\beta da(1-q(a))^2 - \ker\mathcal{C}(0,0) \tag{5.1}$$

where the continuous version of $\ker\mathcal{C}$ has been introduced as follows: the ith function $\ker\mathcal{C}_i(h)$ is related to the ith block size parameter a_i in that it is the only a-parameter which appears in the recursion relation of the ith level. In the continuous limit, the a-parameters become dense on a certain interval $[0, \bar{a}_1]$ where $\bar{a}_1$ is the break point[1] of $q(a)$. The relation of $\ker\mathcal{C}$ to a_i can be exploited to define a continuous function $\ker\mathcal{C}(a,h)$ of two variables

$$\ker\mathcal{C}(a_i,h) = \ker\mathcal{C}_i(h). \tag{5.2}$$

[1] For $a > \bar{a}_1$ the order function $q(a)$ is constant. From the finite RSB point of view, the break point is the $\kappa \to \infty$ limit of the largest block size parameter a_1 (see also the discussion in Sec. 4.2.2).

At finite κ the sequence of functions $\ker\mathcal{C}_i$ is successively calculated from the initial condition $\ker\mathcal{C}_0$ by a recursion relation (2.96) which depends on the parameters q_i and a_i. In the limit $\kappa \to \infty$ this recursion relation passes over to a partial differential equation (PDE) in which the order function enters parametrically. The PDE governs the 'development' of $\ker\mathcal{C}(a,h)$ from an initial condition, which is given at[2] $a = \beta$, down to $a = 0$, where it is required in equation (5.1). In the following this PDE will be derived. The idea is to expand the recursion relation in the differences of successive order parameters $a_i - a_{i+1}$ and $q_i - q_{i+1}$ so that the integral in the recursion relation (2.96) can be solved exactly.

The differences between two neighboring q and a-parameters are written as[3]

$$a_{i+1} - a_i = -da, \qquad q_{i+1} - q_i = -dq, \qquad \text{with } da, dq > 0. \tag{5.3}$$

In the present section it will be assumed that both, dq and also da vanish in the continuous limit $\kappa \to \infty$. While for dq this assumption is always true, for da it is limited to finite temperatures as shown above. At $T = 0$ there is a domain where da does not approach zero in the continuous limit but rather diverges. This, however, happens only at $a = \infty$ and a further restriction to the finite a domain still leads to a valid derivation of the PDE even at $T = 0$. It will be argued below in Section 5.3 that the treatment of the validity domain of the PDE $a \in [0, \infty[$ is sufficient for the calculation of equilibrium quantities, as e.g. the ground state energy, if one introduces a modified initial condition for the PDE at the upper edge of its validity domain.

In terms of the continuous infinite RSB function $\ker\mathcal{C}(a,h)$, the finite RSB recursion relation (2.96) reads

$$a \ker\mathcal{C}(a,h) = \log \int \frac{dh'}{\sqrt{2\pi dq}} \exp\left(-\frac{1}{2}a^2 dq + a(|h'| - |h|) - \frac{(h-h')^2}{2dq} + a\ker\mathcal{C}(a+da,h')\right). \tag{5.4}$$

By a transformation of the integral measure $z = dq^{-1/2}(h' - h)$ and the introduction of an auxiliary function $\gamma(a,h) = \ker\mathcal{C}(a,h) + |h|$ equation (5.4) simplifies to

$$a\,\gamma(a,h) = -\frac{1}{2}a^2 dq + \log \int \frac{dz}{\sqrt{2\pi}} \exp\left(-\frac{z^2}{2} + a\,\gamma(a+da, h + \sqrt{dq}\,z)\right). \tag{5.5}$$

In the continuous limit, dq and da become infinitesimally small and so the Gaussian convolution in equation (5.5) has no effect when setting $da, dq = 0$. In this naive $\kappa \to \infty$ limit, equation (5.5) simply becomes a true statement. One is, however, interested in a description of the development of $\ker\mathcal{C}$ with a and thus has to consider more orders in the small quantities dq and da when performing $\kappa \to \infty$.

An expansion of $\gamma(a + da, h + \sqrt{dq}\,z)$ to up to second order in $\sqrt{dq}$ on the right hand side of (5.5) leads to the desired PDE. In the following, I denote a derivative with respect to h by $\gamma'(a,h)$ and a derivative with respect to a by $\dot\gamma(a,h)$. The expansion reads

$$\begin{aligned} a\,\gamma(a,h) = &-\frac{1}{2}a^2 dq + \\ &\log \int \frac{dz}{\sqrt{2\pi}} \exp\left(-\frac{z^2}{2} + a\left[\gamma(a+da,h) + \sqrt{dq}\,z\,\gamma'(a+da,h) + \frac{dq\,z^2}{2}\gamma''(a+da,h) + \mathcal{O}(dq^{3/2})\right]\right). \end{aligned} \tag{5.6}$$

The z-integration on the right hand side can be performed by completing the square. By further identifying $\gamma(a,h) - \gamma(a+da,h) = da\dot\gamma(a,h) + \mathcal{O}(da^2)$ one can write

$$-a\,\dot\gamma(a,h) + \frac{a^2}{2}\frac{dq}{da} = \frac{a^2 dq(\gamma'(a+da,h))^2}{2\,da(1 - a\,dq\,\gamma''(a+da,h))} - \frac{1}{2\,da}\log\left(1 - a\,dq\,\gamma''(a+da,h)\right) + \frac{\mathcal{O}(dq^{3/2})}{da} + \mathcal{O}(da). \tag{5.7}$$

Now, performing the limit $da \to 0$ while keeping $\dot q(a) = \frac{dq}{da}$ constant (i.e. setting $dq = \dot q(a)da$) leads to a non-trivial PDE for $\gamma(a,h)$

$$\dot\gamma(a,h) = -\frac{\dot q(a)}{2}\left(\gamma''(a,h) + a((\gamma'(a,h))^2 - 1)\right) \tag{5.8}$$

[2]The position $a = \beta$ of the initial condition is the most common one. However, also the initial condition at $a = \bar a_1$ is used sometimes. Those formulations are completely equivalent because the PDE wont change $\ker\mathcal{C}$ beyond the break point $\bar a_1$.

[3]The sign convention results from the finite RSB convention that parameters with higher indices are smaller.

which can be transformed back to a PDE for the continuous kernel correction function $\ker\mathcal{C}(a,h)$:

$$\dot{\ker\mathcal{C}}(a,h) = -\frac{\dot{q}(a)}{2}\left[2\delta(h) + \ker\mathcal{C}''(a,h) + a((\ker\mathcal{C}'(a,h))^2 + 2a\,\mathrm{sign}(h)\ker\mathcal{C}'(a,h))\right] \tag{5.9}$$

The Dirac delta function at $h = 0$ results from the definition of $\ker\mathcal{C}$ as the correction to the asymptotic kernel behavior. Since $\ker\mathcal{C}(a,h) + |h|$ can be shown to be a smooth function with at least one continuous derivative at $h = 0$ it is clear that the first derivative of $\ker\mathcal{C}(a,h)$ must jump down by 2 when crossing $h = 0$ from above. By introducing a boundary condition at $h = 0$ and using the even parity of $\ker\mathcal{C}(a,h)$ with respect to $h \to -h$ one can circumvent the direct treatment of $h = 0$ by restricting oneself to $h > 0$. This further simplifies equation (5.9) to

$$\dot{\ker\mathcal{C}}(a,h) = -\frac{\dot{q}(a)}{2}\left[\ker\mathcal{C}''(a,h) + a((\ker\mathcal{C}'(a,h))^2 + 2a\,\ker\mathcal{C}'(a,h))\right], \qquad \ker\mathcal{C}'(a,0) = -1. \tag{5.10}$$

At this point it is obvious that, for $T > 0$, defining the initial condition at $a = \beta$ is equivalent to defining it at $a = \bar{a}_1$ because between those two positions, $\dot{q}(a) = 0$ (the order function has been defined to be constant above the largest block size parameter) and thus $\ker\mathcal{C}$ is not changed in this range by (5.10). In this way, the validity range $[0, \bar{a}_1]$ of the PDE is artificially extended to $[0, \beta]$ for finite temperatures. At zero temperature, things are slightly more complicated since the above derivation is strictly speaking only valid for $a < \infty$, where $\lim_{\kappa\to\infty} da = 0$ and the initial condition is defined outside of the validity domain.

For finite temperatures, the required initial condition of the PDE can be carried over directly from the initial condition of the recursion relation at finite κ. It reads

$$\ker\mathcal{C}(\beta,h) = \ker\mathcal{C}(\bar{a}_1,h) = T\log(1 + e^{-2\beta h}) \tag{5.11}$$

and completes the continuous formulation.

Equations (5.1), (5.10) and (5.11) represent the complete continuous RSB formalism from which one can in principle calculate the free energy functional $f[q(a)]$ from a given order function $q(a)$ for $T > 0$. Yet, it is in principle nothing else than the reformulated Parisi equations [Par79]. The great advantage of the present formulation, however, is the ability to extend it to $T = 0$. In the limit $T \to 0$ there is still an issue which prevents a direct numerical solution, namely the singularity in the second derivative of $\ker\mathcal{C}$ (see Sec. 2.4). A further rescaling in h resolves this problem.

The rescaling will be seen to still not suffice for constructing a tractable $T = 0$ theory at ∞ RSB. This is due to a singular point in the PDE of the rescaled quantity at $a = \infty$. The analysis of this criticality and the identification of fixed point behavior, however, helps to circumvent the ill-definedness of the PDE and to handle $\ker\mathcal{C}$ by introduction of a new initial condition.

5.2 Continuous RSB at finite temperatures

In order to embed the ideas developed in the present work into the existent formulations which can be found in the literature, the relation to the well-known continuous Parisi RSB [Par80] is shortly discussed in the following. A comment on notation is in order at first: in the traditional formulation of ∞ RSB, the parameters $m_i = Ta_i$ are projected onto the interval $[0,1]$. The continuous variable on this domain is called x. In the low temperature continuous formulation developed here, only the variable a will be used. If it has an index a_i then it is a single, self-consistently calculated order parameter and if it has no index then a is a continuous variable on the interval $[0,\beta]$, the argument of the order function $q(a)$. I will most of the time work with the a-formulation of the order function, i.e. $q(a)$. In the literature, one mostly finds the x-formulation $\tilde{q}(x)$. The two formulations are connected by the transformation $\tilde{q}(x) = q(\beta x)$.

At finite temperatures, the order function $\tilde{q}(x)$ has a plateau, i.e. $\tilde{q}(x) = \tilde{q}(\bar{x}_1)$ for $\bar{x}_1 \le x \le 1$. In this regime, where no finite RSB parameter m_i is located, even in the limit $\kappa \to \infty$, the derivation of the Parisi PDE, which is analogous to (5.10) and governs a function $G(x,h)$ instead of $\ker\mathcal{C}(a,h)$, is *a priori* not valid. In the plateau-region, however, where $\frac{d}{dx}\tilde{q}(x) = 0$, the validity domain of the PDE can be extended *a posteriori* to the whole domain $[0,1]$. This is possible because in the finite κ formalism, $\ker\mathcal{C}(a_0,h) = \ker\mathcal{C}(a_1,h)$ in the limit $\kappa \to \infty$ as long as $a_0, a_1 < \infty$. This can easily be seen from equation (2.96): in the limit $\kappa \to 0$, Δq_1 vanishes and the Gaussian integration becomes an integration over a delta peak. Thus the difference between $\ker\mathcal{C}_0$ and $\ker\mathcal{C}_1$ vanishes as long as $T > 0$.

At finite temperatures, the differential equation which governs ker$\mathcal{C}$ can be translated to the original formalism of Parisi by the transformation to a function $G(x,h)$

$$G(x,h) = \beta(\mathrm{ker}\mathcal{C}(\beta x,h) + |h|) - \frac{\beta^2}{2}\left[\int_x^1 dx'\,\tilde{q}(x') + x\tilde{q}(x) - \tilde{q}(1)\right]. \tag{5.12}$$

From (5.12), the Parisi PDE is obtained

$$\frac{d}{dx}G(x,h) = -\frac{\dot{\tilde{q}}(x)}{2}\left[\frac{d^2}{dh^2}G(x,h) + x\left(\frac{d}{dh}G(x,h)\right)^2\right] \tag{5.13}$$

with an initial condition $G(1,h) = \log 2\cosh(\beta h)$. The functional free energy is then given by

$$f[\tilde{q}(x)] = -\frac{\beta}{4}\left(1 - 2\tilde{q}(0) + \int_0^1 dx\,\tilde{q}(x)^2\right) - TG(0,0). \tag{5.14}$$

There are many techniques for maximizing $f[\tilde{q}(x)]$ with respect to the order function [Nem87, Bis90, MPV87, SD84]. The most advanced is probably the approach which uses high order expansions of $\tilde{q}(x)$ on the analytical side and pseudo-spectral codes for a direct numerical solution of differential equations [CR02]. Details about those methods can be found in the references as I don't want to go into more detail at this point, but rather continue with investigating the zero temperature limit where the traditional x-formulation does not work.

5.3 The proper zero temperature continuous theory

The zero temperature limit of the continuous formalism derived in Section 5.1 is somewhat more challenging than the treatment of zero temperature within a finite number of RSB steps (see Chapters 2 and 4). First of all, for $T \to 0$, the domain of $q(a)$ extends to the semi-infinite interval $[0,\infty]$. For $a < \infty$ the PDE (5.10) is valid because the a-parameters are dense there in the $\kappa \to \infty$ limit. At $a = \infty$, however, discreteness in a must be respected properly.

The position at which the initial condition is defined is $\lim_{\kappa\to\infty} a_1 = \bar{a}_1 = \infty$ for $T = 0$. The next smaller parameter a_2 is infinitely far away from a_1. Nevertheless $a_2 = \infty$ at ∞ RSB. It is not surprising that it is hard to surmount this infinite distance $a_1 - a_2$ by means of a differential formulation which assumes this distance to vanish for $\kappa = \infty$. On the other hand, a superficial look to high order RSB data of the discrete ker$\mathcal{C}_i$ functions shows that they are nearly the same for $i = 0,1,2$. Thus one might be tempted to conclude that the arguments for extending the validity domain of the PDE from $[0,\bar{a}_1]$ to $[0,a_0]$ at finite temperatures would be directly applicable here. This argumentation, however, neglects the singular second derivative of the initial condition (5.11). The above formulation still hides some important structure at $h = 0$ in the limit $a \to \infty$. This will be cured subsequently.

5.3.1 Replacement of the initial condition

First of all one needs to get rid of the divergence in the second derivative of the initial condition (5.11) in the zero temperature limit. This is easily done by a rescaling in h-direction and the introduction of a new function[4]

$$g(a,y) = (a+1)\mathrm{ker}\mathcal{C}\left(a, \frac{y}{a+1}\right). \tag{5.15}$$

In contrast to ker$\mathcal{C}(a,h)$, the function $g(a,y)$ resolves the point $h = 0$ at $a = \infty$. The initial condition of $g(a,y)$ is given at $a = \beta$ and the zero temperature limit of $g(\beta,y)$ as well as all its derivatives with respect to y are well behaved. One finds

$$g(\beta,y) = (1+T)\log\left(1 + \exp\left(-\frac{2y}{1+T}\right)\right). \tag{5.16}$$

[4]The reason for rescaling with $a+1$ instead of a is that one wants a rescaling which is singular at $a = \infty$ while being non-singular at $a = 0$.

Especially the first and the second derivatives are given by $\frac{d}{dy}g(\beta,y)\Big|_{y=0} = -1$ and $\frac{d^2}{dy^2}g(\beta,y)\Big|_{y=0} = \frac{1}{1+T}$, respectively. Further, the boundary condition of $\ker\mathcal{C}(a,h)$ at $h=0$ can be adopted to $g'(a,0) = -1$. The differential equation for the function $g(a,y)$ can also be obtained from the $\ker\mathcal{C}$ PDE and reads

$$\dot{g}(a,y) = -\frac{\dot{q}(a)}{2}(a+1)\left[(a+1)g''(a,y) + 2ag'(a,y) + a(g'(a,y))^2\right] + \frac{g(a,y) - yg'(a,y)}{a+1} \tag{5.17}$$

where again the dot signals a derivative with respect to a and the prime means a derivative with respect to y. Due to the rescaling a term appeared which is independent of $\dot{q}$. As a result, $g(a,y)$ is not constant with respect to a above the break point, in contrast to $\ker\mathcal{C}(a,h)$. This is due to the definition (5.15) in which $g(a,y)$ changes with respect to a even in the case of an a-constant $\ker\mathcal{C}$.

Obviously, the only point where the temperature enters is at the initial condition and so one is tempted to formulate the zero temperature limit of continuous RSB by simply taking the well defined $T=0$ version of (5.16) at $a=\infty$ as an initial condition and using PDE (5.17) to obtain $g(0,y)$ from it. This approach, however, disregards an important point which has been emphasized in the preceding chapter, namely the discreteness at $a=\infty$. To understand this issue, it is favorable to investigate the order function in the a-formulation as well as in the x-formulation at the same time. In doing so, the analysis and the ideas introduced in Section 4.3.2 are employed, namely the two different scales of the order function.

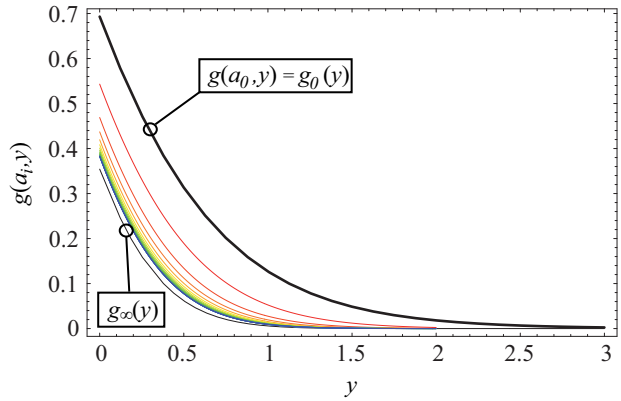

Fig. 5.1: The first 15 functions $g(a_i,y) = (a_i+1)\ker\mathcal{C}_i(y/(a_i+1))$ for $i=1,...,15$ (red to blue) resulting from a 200 RSB calculation at zero temperature. The thick, top black line is a graph of the initial condition $g(a_0,y) = \log\left(1+e^{-2y}\right)$ and the bottom black line is the new initial condition $g_\infty(y)$ at $a=\infty, x=0$ as obtained from the ordinary differential equation (5.20). By further increasing the order of RSB, the functions do not become dense.

The finite x domain, which corresponds to $a=\infty$, is the region in which the order function is trivial at the first sight in that $q(a=\infty) = \tilde{q}(x>0) \equiv 1$. $\tilde{q}(x)$ is, however, not a function of a continuous variable at zero temperature. Instead, it is given only at discrete points. In this sense, the finite x domain is hardly trivial because, though $\dot{\tilde{q}}(x) = 0$[5] in this region and the PDE seems to predict constant $\ker\mathcal{C}$ for $0<x<1$, something happens there. What exactly happens, is hard to catch at ∞ RSB and $T=0$ because it is not possible to do calculations in this regime for $x>0$[6]. The best one can do for now is to investigate the finite x region at $\kappa=\infty$ and $T=0$ from two limiting cases in, i.e. finite κ at $T=0$ and finite T at $\kappa=\infty$ (see Sect. 4.3.2). Luckily, as will be shown below, the following qualitative description of the $x>0$ regime is sufficient to derive an exact formulation for the zero temperature continuous theory.

In the discrete regime of the order function (see Fig. 4.19), the assumption $da \to 0$ or equivalently $dx \to 0$ needed in the derivation of the PDE which governs $\ker\mathcal{C}(a,h)$ or $g(a,y)$ is wrong. This means that it is not *a priori* clear that the initial condition which is given at $x=1$ can propagate to $x=0$ by means of a PDE[7]. This statement is further supported by an investigation of the first few functions $g(a_i,y)$, $i=1,...$ of a calculation within 200 orders of RSB at $T=0$. In regions where the a_i become dense, the difference

[5] If calculated from a difference quotient instead of a differential quotient.

[6] At least not within the formulation used here.

[7] Nevertheless, it is seems that a PDE description of $0<x\leq 1$ can be established. Pankov [Pan06] found that it is possible by a proper rescaling of the differential equations, to do exactly this. The idea behind his treatment, however, is completely different from the present argumentation.

between successive function $g(a_i, y), g(a_{i-1}, y)$ approaches zero for $\kappa \to \infty$. The functions corresponding to the largest a_i, however, remain finitely spaced at zero temperature in the large κ limit. This is shown in Figure 5.1 where the first 15 functions which result from the recursion relation are plotted. As a result, in this region one must still use the recursion relation and so the initial condition $g_0(y) = g(a_0, y)$ is not connected to the validity domain of the PDE $0 \leq a < \infty$. This discreteness is extremely inconvenient for actual calculations because in principle one must maximize the free energy with respect to the function $q(a)$ in the finite a domain and, in addition to that, with respect to infinitely many parameters m_i which enter the recursion relation at $a = \infty$.

There is, however, a simpler and much more convenient approach to circumvent the explicit treatment of the infinitely large set of m_i with $0 < m_i \leq 1$. It is well established (see e.g. Chap. 4 or [Pan06]) that, up to second order in a^{-1}, the order function $q(a)$ can be expanded near $a = \infty$ as

$$q(a) = 1 - c\, a^{-2} + \mathcal{O}(a^{-3}) \tag{5.18}$$

with $c \simeq 0.401$. Utilizing this expansion of $q(a)$, the PDE (5.17) can also be expanded near $a = \infty$. Doing so, one finds to first order in a^{-1} (dropping the y- and a-dependence of $g(a, y)$ for notational convenience)

$$\dot{g} = \frac{1}{a}\left[g - yg' - c(g'' + 2g' + (g')^2)\right]. \tag{5.19}$$

Obviously, there is a singularity in the PDE which governs $g(a, y)$ at $a = \infty$. Typically such an equation leads to a logarithmic divergence in its solution at $a = \infty$[8]. The only way to avoid such a divergence, which is obviously not allowed in the present case, is that the term in brackets in (5.19) vanishes at least with a^{-1} for $a \to \infty$. This means, that $g(\infty, y) = g_\infty(y)$ must satisfy the ordinary differential equation

$$g_\infty - yg'_\infty - c(g''_\infty + 2g'_\infty + (g'_\infty)^2) = 0 \tag{5.20}$$

for the remaining part of $g(a, y)$ at $a < \infty$ to be meaningful. Thus, the central claim of the continuous zero temperature RSB is:

> *At zero temperature, the initial condition (5.16) can be replaced by the initial condition $g(\infty, y) = g_\infty(y)$ which is the solution of the ordinary differential equation (5.20).*

By this replacement, the detailed analysis of the $0 < x \leq 1$ regime has been circumvented in that one can be sure that after the finite x recursion starting at $x = 1$, the function $g(x, y)$ has been driven to $g(x = 0, y) = g_\infty(y)$. The further evolution of $g(a, y)$ from $a = \infty$ to $a = 0$ can now be performed by means of the full PDE (5.17).

The new initial condition $g_\infty(y)$ is plotted in Figure 5.1. Obviously, the recursion relation indeed drives $g(a_i, y)$ to the function $g_\infty(y)$ which is needed for rendering the remaining part (i.e. $0 \leq a < \infty$) of the theory meaningful.

In order to gain better overview of the functions $q(a)$ and $g(a, y)$ on their whole domains, it is convenient to map the a-interval $[0, \infty]$ to $[0, 1]$ by means of a transformation to a new variable

$$a \to \zeta = \frac{a}{1 + a}. \tag{5.21}$$

In Figure 5.2 the functions $g(\zeta, y)$ are shown for three different temperatures. The kink line reflects the position of the break point at finite temperatures. Above the break point, $g(\zeta, y)$ trivially decreases until the break point is reached. The decrease is termed trivial, because one could get rid of it by transforming g back to $\ker\mathcal{C}$ at and only at finite temperatures. In Figure 5.3(a), this triviality at finite temperatures becomes obvious: there is no data point defined in the trivial-decrease region between the location of the initial condition $\zeta = (1 + T)^{-1}$ and the location of the first $\ker\mathcal{C}$ from the recursion relation at $\zeta = \frac{a_1}{1+a_1}$. In this range, the detailed shape of the ζ-dependence of $g(\zeta, y)$ is a matter of definition - in Figures 5.2 and 5.3(a) it has been chosen linear. The numerical solution of the finite T differential equations is difficult near the break point. With some effort, however, a solution with considerable accuracy is possible [CR02]. At zero temperature, the direct numerical solution is not possible due to the singularity at $\zeta = 1$ which cannot be represented by one single function $g(\zeta = 1, y)$. At $T = 0$ and $\kappa = \infty$, $g(\zeta = 1, y)$ is not single-valued[9]

[8] Compare to the simple case of an ordinary differential equation of the form $\dot{f} = f/a$.

[9] This is similar to the situation for $q(a)$ at $a = \infty$, discussed in Section 4.2.1. The second derivative of the order function is also multiple-valued at $a = \infty$.

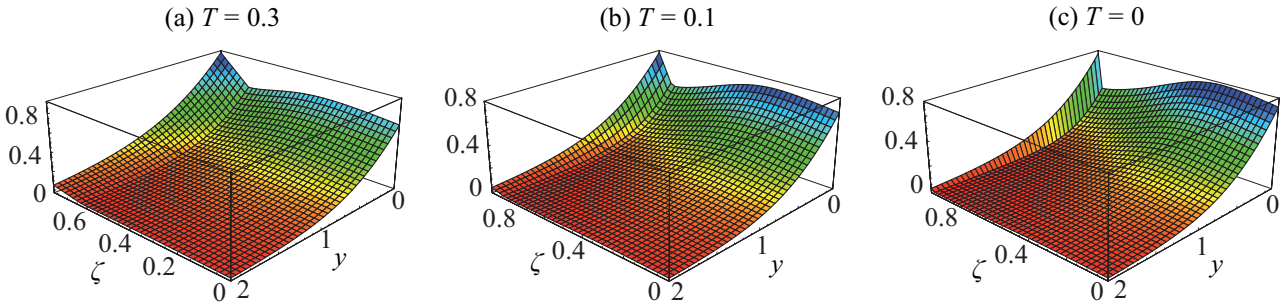

Fig. 5.2: Plots of the function $g(\zeta, y)$ at various temperatures $T = 0.3$ (a), $T = 0.1$ (b), $T = 0$ (c). The functions have been extracted from a 200RSB calculation in case of the $T = 0$ plot and from 35 RSB calculations for $T = 0.1, 0.3$.

as can be seen in Figure 5.3(b). Obviously, the finite spacing between successive iterations for the largest a parameters does not vanish. However, one may *define* the function $g(\zeta, y)$ single-valued at $\zeta = 1$ by setting $g(1, y) = g_\infty(y)$. Doing so and solving the PDE (5.17) numerically, one obtains the red line in Figure 5.3(b). The convergence of the points from the finite RSB calculation, representing the discrete function $g(a_i, 0)$ to the red line, obtained by solving the ∞ RSB differential equation, strongly supports the validity of the approach, proposed here.

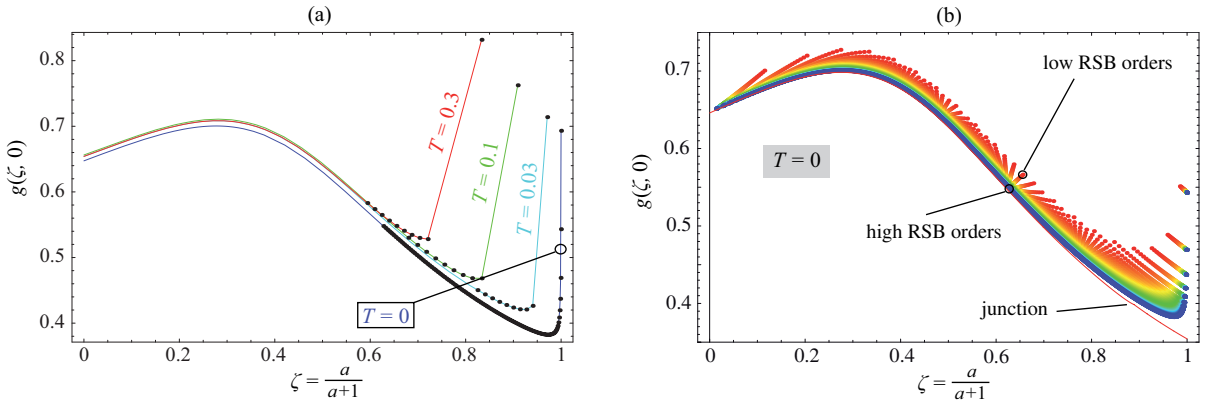

Fig. 5.3: (a) Plots of $g(\zeta, 0)$ for $T = 0, 0.03, 0.1, 0.3$. The black dots represent the numerical data of the large a region as extracted from 200 RSB ($T = 0$) and 35 RSB ($T > 0$) calculations. Part (b) shows more details of the $T = 0$ situation. The red dots correspond to the finite RSB versions of $g(\zeta, 0)$ of lower RSB orders and the blue dots to higher RSB orders. The total range is $\kappa = 30, ..., 200$. The red line corresponds to a numerical solution of the ∞ RSB differential equation (5.17).

The differential equation of the function $g(\zeta, y)$ is obtained directly from the differential equation (5.17), governing $g(a, y)$:

$$\dot{g}(\zeta, y) = \frac{g(\zeta, y) - y\, g'(\zeta, y)}{1 - \zeta} - \frac{\dot{q}(\zeta)}{2(1-\zeta)^2}\left[g''(\zeta, y) + 2\zeta g'(\zeta, y) + \zeta (g'(\zeta, y))^2\right] \tag{5.22}$$

Now that the singular point at $a = \infty$ or equivalently at $\zeta = 1$ is identified and a new initial condition has been given, one must find a way to numerically solve the differential equation (5.22) in the ζ interval $[0, 1]$ with the initial condition $g(1, y) = g_\infty(y)$. The straightforward numerical solution is, however, prevented by the singular point of (5.22) at $\zeta = 1$.

5.3.2 Solving the differential equations

Usually, singular points in differential equations can be managed by expanding around them. This leads to differential equations with reduced dimensionality - one for each order in the expansion parameter. It is

interesting to consider the expansions around $a = \infty$ and around $\zeta = 1$ at the same time, because they seem to be inequivalent with respect to their convergence properties.

For the $\frac{1}{a}$ and $(1-\zeta)$ expansions, one can write

$$g(\zeta, y) = g_\infty(y) + (1-\zeta) g_1^{(\zeta)}(y) + (1-\zeta)^2 g_2^{(\zeta)}(y) + \mathcal{O}(1-\zeta)^3, \tag{5.23}$$

$$g(a, y) = g_\infty(y) + \frac{1}{a} g_1^{(a)}(y) + \frac{1}{a^2} g_2^{(a)}(y) + \mathcal{O}(a^{-3}) \tag{5.24}$$

and $Q(\zeta) = \dot{q}(\zeta)(1-\zeta)^{-1}$ or $Q(a) = \dot{q}(a)(1+a)^3$, respectively. This expansion leads to ordinary differential equations in y for the functions $g_i^{(\zeta)}(y), g_i^{(a)}(y)$, supplemented by the boundary conditions

$$\left.\frac{d}{dy} g_i(y)\right|_{y=0} = 0, \qquad g_i(\infty) = 0. \tag{5.25}$$

Figures 5.4 and 5.5 show the results of the numerical solutions of the differential equations arising from the $\frac{1}{a}$-expansion and from the $(1-\zeta)$-expansion, respectively. The underlying[10] model function for $q(a)$ is the erf-model with parameter $\xi = 1.13$ (see Section 4.2.1). It is not a big surprise that the convergence regions of the expansions do not extend down to the point $\zeta = a = 0$ at which the function $g(\zeta, y)$ enters the free energy, because the convergence of an expansion of the order function at the critical point also stops at $\zeta \simeq 0.3$ due to singularities in the complex plane. Near the singular point, however, one can gain an arbitrary well approximation by the expansion.

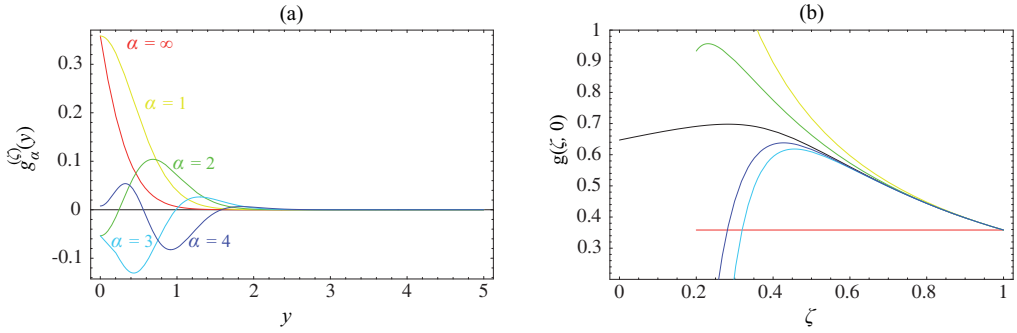

Fig. 5.4: $\frac{1}{a}$-expansion of the PDE (5.17). Part (a) shows the functions $g_\infty(y), g_1^{(a)}(y), ..., g_4^{(a)}(y)$ (red to blue). Part (b) shows the resulting expansion (5.24) transformed to the interval $[0, 1]$ by $a \to \zeta$. The colors refer to the inclusion of the term with the same order as in part (a). The black line is a numerical solution of the full PDE (5.17).

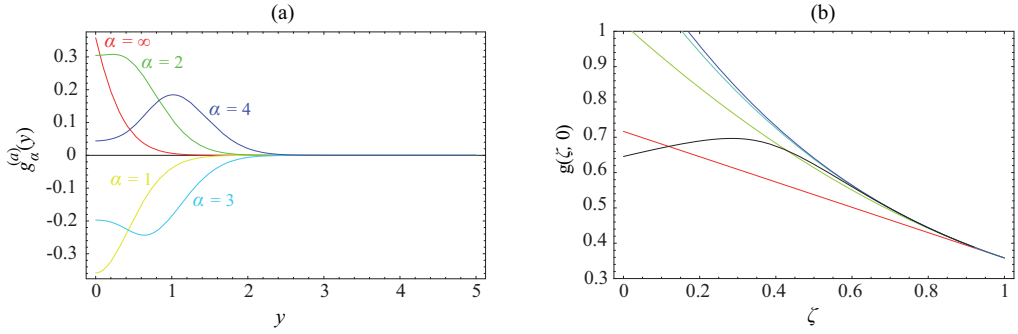

Fig. 5.5: $(1-\zeta)$-expansion of the PDE (5.22). Part (a) shows the functions $g_\infty(y), g_1^{(\zeta)}(y), ..., g_4^{(\zeta)}(y)$ (red to blue). Part (b) shows the resulting expansion (5.23). The colors refer to the inclusion of the term with the same order as in part (a). The black line is a numerical solution of the full PDE (5.22).

[10] $q(a)$ is not self-consistently determined here. The present discussion rather aims at the convergence properties of the expansions (5.23) and (5.24).

In parts (b) of Figures 5.4 and 5.5, a numerical solution of the PDEs is plotted together with the expansions. It has been obtained by using the expansions at $a = 10$ and $\zeta = 0.9$, respectively, as initial conditions for the full PDEs[11]. The solution is consistent with the prediction of the finite RSB treatment (see e.g. Fig. 5.3). Though the $\frac{1}{a}$-expansion is equivalent to the $(1-\zeta)$ expansion in that they can be translated into each other, the $\frac{1}{a}$-expansion seems, on the first sight, to have better convergence properties for larger expansion parameters. It turns out, however, that the $(1-\zeta)$ expansion yields better initial conditions for the full PDE.

With the combination of the expansion near the singular point and the numerical integration in the non-singular domain, one is in principle able to calculate the free energy f from an arbitrary model order function at $T = 0$ and maximize f with respect to the model parameters. It turns out, however, that the free energy varies only weakly when changing the order function so that, for such a program to work, one would require rather high precision in the numerics. A more convenient approach for the self-consistence calculations will be presented in the subsequent section.

5.3.3 The fixed point at $a = \infty$

In the present subsection the notion of a repulsive fixed point at $a = \infty$ (or $\zeta = 1$) shall be investigated more closely on the basis of the a formulation. This idea is guided by the fact that it is impossible to numerically integrate equation (5.17) 'upwards'. The reason for this is the presence of a diffusion part in equation (5.17). This diffusion part arises from the successive convolution with a Gaussian (see eqn. (5.4)) in the continuous limit $(da, dq \to 0)$.

Numerically integrating a diffusion equation in the 'wrong' direction leads to an exponential amplification of fluctuations on a scale Δx in a characteristic time $\frac{(\Delta x)^2}{D}$ where D is the diffusion constant. The proper integration direction can be found from the sign of the prefactor of the second derivative in the corresponding PDE. In case of equation (5.17) the proper direction is $\infty \to 0$[12]. Integrating 'upwards' leads to a result as shown in Figure 5.6. Here, the seemingly paradoxial situation is encountered in which increasing the accuracy of the numerical method[13] leads to a worse quality in the solution: in Figure 5.6(a), for high accuracy, the integration starts at $a = 10$ and the solution is completely wrong after $\Delta a \simeq 0.01$. A further increase of the integration interval leads to a total failure of the routine. In Figure 5.6(b), for low accuracy, one can integrate over an interval $\Delta a \simeq 3$ before the method fails. The reason for this curious behavior is that if a fine grid of points with finite precision[14] is used to calculate a derivative, numerical fluctuations may become important for a sufficiently fine grid, corresponding to high accuracy. For lower accuracy, the numerical fluctuations do not matter. Instead, the error due to the truncation of the order in the $\frac{1}{a}$-expansion, used for the initial condition, are the dominant fluctuations. The spatial scale of those errors are much larger, though, and, as a result, they grow less rapidly than the numerical fluctuations.

From this point of view, the integration in negative a direction (also in negative ζ direction) is stable while integration in the opposite direction is highly unstable against any deviations from an optimal function which is defined at any $a \in [0, \infty[$. This gives rise to a fixed point in the space of functions $g(y)$ defined on $y \in [0, \infty[$ with boundary conditions $g'(0) = -1$ and $g(\infty) = 0$. This fixed point is given by $g_\infty(y)$ and the solution of the PDE (5.17) defines an 'optimal line' in the space of the functions $g(y)$.

The ultimate consequence of this fixed point and the optimal line approaching it is that it is impossible to obtain $g_\infty(y)$ by a numerical integration of (5.17) to $a = \infty$, starting at finite a[15]. Since $g_\infty(y)$ is well known as the solution of an ordinary differential equation, such an upwards integration is not required. Actually one is only concerned with an integration in negative a direction. Nevertheless, the existence of this fixed point is important, as will become clear below.

[11] The full PDEs have been numerically solved by the `NDSolve[]` routine of *Mathematica*®. It seems that the methods implemented in `NDSolve[]` have severe problems near the singular points so that one cannot start slightly below $\zeta = 1$ but must surmount a considerable interval $[0.9, 1]$ by the expansion. A descent numerical program, designed for treating eqns. (5.22) and (5.17) is in order here, but this is beyond of the present work's scope.

[12] In the large a regime, the diffusion constant varies as a^{-1} in leading order. As a result, there is a algebraically diverging term for $a \to \infty$ in the solution of the PDE.

[13] Increasing the accuracy means that more samples in y direction are used to calculate the derivatives at a given a.

[14] A `double` variable in machine precision has about 16 significant digits (base 10).

[15] This would be convenient for instance if one wants to check the validity of the expansion (5.24).

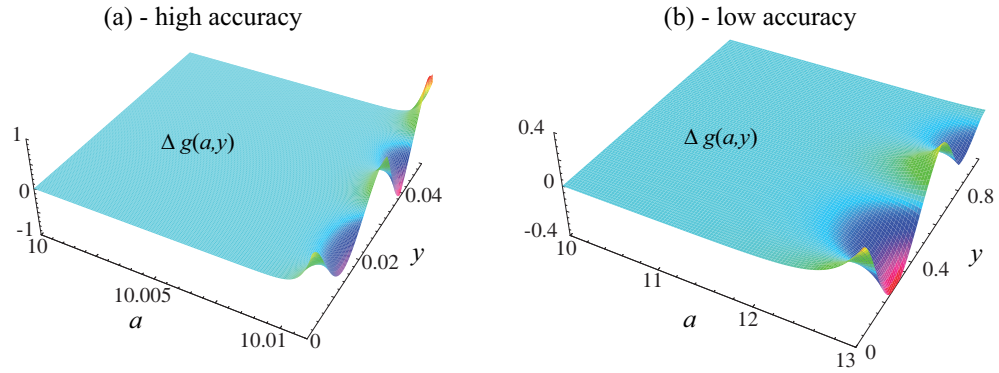

Fig. 5.6: Result of numerical integrations of equation (5.17) with different accuracies, starting at $a = 10$. The initial condition has been taken from a 4th order expansion in a^{-1}, as discussed in 5.3.2. The plots show the difference between the 4th order expansion and the numerical solution, obtained by the routine `NDSolve[]` in *Mathematica*®. The accuracy and precision goal in part (a) have been set to 10, while in part (b) the standard values (8) are used.

5.4 Sommers-Dupont Ansatz

A point which has not been addressed above is the self-consistence of the order function $q(a)$ at $T = 0$. It turned out that a direct maximization of the free energy (5.1) in the space of possible order functions would require an extremely careful programming of the PDE so that the desired precision can be gained. Another problem of the direct maximization is the actual modeling of the order function - one must assure that the model function is sufficiently flexible so that the actual solution of the maximization is contained in the model. All in all, one can say that direct maximization of $f[q(a)]$ is inconvenient and it would be desireable to circumvent it. In the following, I describe a method which makes this possible. It is analogous to [SD84].

5.4.1 The method of functional Lagrange-multipliers

The trick is to view the free energy optimization problem in a larger space, namely in the space of the functions $\{q(a), g(a,y)\}$. The function $g(a,y)$, however, is constrained to fulfill the partial differential equation (5.22). This constraint may be incorporated by introducing a functional lagrange multiplier $p(a,y)$ and redefining the free energy

$$\tilde{f} = -\frac{1}{4}\int_0^\infty da(1-q(a))^2 - g(0,0) + \int_0^\infty da \int_0^\infty dy\, p(a,y)\, F[g(a,y), \dot{q}(a)] \tag{5.26}$$

where (see equation (5.22))

$$F[g(a,y), \dot{q}(a)] = \frac{g - y\,g'}{a+1} - \frac{\dot{q}}{2}(a+1)\left[(a+1)g'' + 2ag' + a(g')^2\right] - \dot{g}. \tag{5.27}$$

According to the usual Lagrange-multiplier formalism, the functional derivatives of $\tilde{f}$ with respect to $q(a), g(a,y)$ and $p(a,y)$ must be zero. Complemented by the initial condition for the differential equation (5.27), one obtains a closed set of equations for $g(a,y), p(a,y)$ and $q(a)$. Rather than rederiving these self-consistency equations from (5.26), I directly want to use the results from Ref. [SD84] and adopt them to the present formulation by rescaling them properly. This is quite instructive because it shows the relation of the present formulation to the traditional formulations which work at finite T only.

5.4.2 The continuous self-consistency equations

In Ref. [SD84], RSB has been investigated by Sommers and Dupont in a generalized gauge [DGD82] at finite temperatures with the help of functional Lagrange-multipliers, as described above. The resulting self-consistency equations, derived in this work, shall be used here in the special case of the Parisi gauge, i.e. the additional Sommers-Dupont gauge order function $\Delta(x)$ is related to $\tilde{q}(x)$ by $\dot{\Delta}(x) = -\beta x \tilde{q}(x)$. The quantity $m(x,h)$, which is related to $G(x,h)$ in equations (5.12) and (5.13) by $\beta m(x,h) = \dot{G}(x,h)$, and

the quantity $P(x,h)$ which is the functional Lagrange-multiplier are given as the solutions of the partial differential equations

$$\dot{m}(x,h) = -\frac{\dot{\tilde{q}}(x)}{2}\left[m''(x,h) + 2\beta x m(x,h) m'(x,h)\right] \tag{5.28}$$

$$\dot{P}(x,h) = \frac{\dot{\tilde{q}}(x)}{2}\left[P''(x,h) - 2\beta x [m(x,h)P(x,h)]'\right] \tag{5.29}$$

with initial conditions

$$P(0,h) = \delta(h), \qquad m(1,h) = \tanh(\beta h). \tag{5.30}$$

Once the functions $m(x,h)$ and $P(x,h)$ are known, the order function can be calculated at each x from them by evaluating the integral

$$\tilde{q}(x) = \int_{-\infty}^{\infty} dh\; P(x,h) m^2(x,h). \tag{5.31}$$

Equations (5.28)-(5.31) define a complete set of equations from which the order function $\tilde{q}(x)$ can be calculated iteratively (see e.g. [CR02]). These equations are valid for any domain of the order function in which the block size parameters are continuous. At finite temperature, this is the whole interval $[0, \bar{x}_1]$. At $T = 0$, however, the block size parameters are dense only at $x = 0$. The a-formulation resolves $x = 0$ and thus is the formulation of choice for $T = 0$. To translate the Sommers-Dupont equations to the formulation, used in the present work, some simple rescalings are in order:

$$x \to a = \beta x, \qquad h \to y = h(1 + \beta x), \qquad P \to p = (a+1)P \tag{5.32}$$

Note that $P(x,h)$ has been normalized $\int_{-\infty}^{\infty} dh\, P(x,h) = 1,\ \forall x$[16] while $p(a,y)$ is normalized to $\int_{-\infty}^{\infty} dy\, p(a,y) = (a+1)^2$. After the rescaling one obtains the desired partial differential equations which are valid at $T = 0$ in the finite a domain.

$$\dot{m}(a,y) = -\frac{\dot{q}(a)}{2}(a+1)\left[(a+1)m''(a,y) + 2a m(a,y) m'(a,y)\right] - \frac{y\, m'(a,y)}{a+1} \tag{5.33}$$

$$\dot{p}(a,y) = \frac{\dot{q}(a)}{2}(a+1)\left[(a+1)p''(a,y) - 2a[m(a,y)p(a,y)]'\right] - \frac{y\, p'(a,y) - p(a,y)}{a+1} \tag{5.34}$$

The form of the corresponding initial conditions requires an analysis similar to the discussion in Section 5.3: the initial condition of $P(x,h)$ is given at $x = 0$ and since $P(x = 0, h) = p(a = 0, y = h)$ and $a = 0$ is not a singular point of the differential equations, one can directly adopt $p(0,y) = \delta(y)$. For the $m(a,y)$ initial condition, however, one must respect the singular point at $a = \infty$ properly. This is done in the next subsection. The equation for the zero temperature order function now reads

$$q(a) = \frac{1}{(a+1)^2}\int_{-\infty}^{\infty} dy\, p(a,y) m^2(a,y). \tag{5.35}$$

5.4.3 Self-consistence at $a = \infty$

At $a = \infty$, equation (5.33) has a singularity of the same type which has been encountered in the discussion of the differential equation, governing the function $g(a,y)$. Again, this singularity leads to an ordinary differential equation which determines $m(a = \infty, y) = m_\infty(y)$. It is derived by expanding equation (5.33) at $a = \infty$, as usual (see Sec. 5.3.2). Similarly, a singular point at $a = \infty$ is found in equation (5.34) and again an ordinary differential equation can be derived for a function $p(a = \infty, y) = p_\infty(y)$ by an a^{-1} expansion. One obtains

$$0 = c\left[m''_\infty(y) + 2m_\infty(y)m'_\infty(y)\right] + y m'_\infty(y) \tag{5.36}$$

$$0 = c\left[p''_\infty(y) - 2(p_\infty(y)m_\infty(y) + m_\infty(y)p'_\infty(y))\right] - y p'_\infty(y) + p_\infty(y) \tag{5.37}$$

Interestingly, the differential equations obtained in the a-formulation from the expansion at $a = \infty$ are completely analogous to equations (5) and (6) in [Pan06] which have been obtained in the x-formulation in the limit $x \to 0$. Obviously, there is a relation between those formalisms. This relation will be discussed

[16] This is easily seen by integrating equation (5.29) over $y = -\infty, ..., \infty$.

in Section 5.4.5. As a result of this relation, the equations (5.36) and (5.37) can be solved as described in [Pan06].

Utilizing the arbitrary precision arithmetics unit of *Mathematica*®, one can easily compute the expansion coefficient c of the a^{-2} term in the order function with many significant digits. Here, I give the result of a computation with 18 significant digits

$$c = 0.410\,802\,099\,693\,446\,683 \tag{5.38}$$

in consistence with [Pan06] but extending the accuracy by several orders of magnitude. With a more advanced programming, 30-60 significant digits of c should be easily achievable.

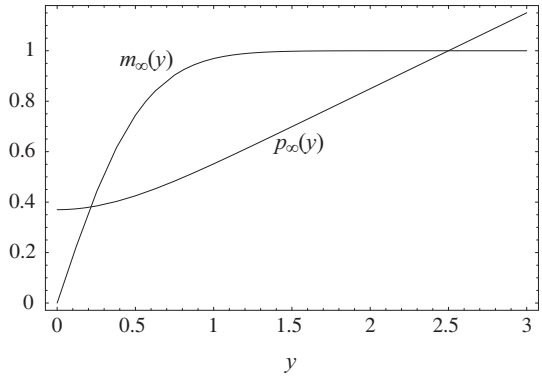

Fig. 5.7: The self consistently calculated 0th order functions $p_\infty(y)$ and $m_\infty(y)$ of the $p(a, y)$ and $m(a, y)$ expansions, respectively, near $a = \infty$. For negative y, $p_\infty(y)$ must be even and $m_\infty(y)$ must be odd.

Given the solubility of the self-consistency equations at $a = \infty$ to 0th order in a^{-1}, it is natural to ask whether it is possible to penetrate the finite a regime by means of self-consistency equations which arise from the higher order a^{-1} expansions. If this was possible, one could calculate an expansion of $q(a)$ at $a = \infty$ to arbitrary order in a^{-1} without knowing about the initial condition of $p(a, y)$ at $a = 0$. This means that an external field $h > 0$, which *only* enters this initial condition, would not affect $q(a)$ wherever the a^{-1} expansion of $q(a)$ converges. Moreover, one could use $p_\infty(y)$ as an alternative initial condition of (5.34) at $a = \infty$ and integrate both differential equations (5.33) and (5.34) starting at $a = \infty$ down to $a = 0$ without knowing something about the existence of an external field. As a result, the PaT projection hypothesis would have to be exact at $T = 0$. However, it has been seen in Section 4.2.3 that this is not true.

To understand the reason why one cannot simply integrate equations (5.33) and (5.34) down to $a = 0$ starting at $a = \infty$ where $m(\infty, y) = m_\infty(y)$ and $p(\infty, y) = p_\infty(y)$ are known, it is helpful to recall the notion of the fixed point in the PDE, governing $g(a, y)$ (see Sec. 5.3.3). Analyzing the PDEs of $m(a, y)$ and $p(a, y)$ in the same manner, one also encounters fixed points at $a = \infty$, but while for $m(a, y)$ the fixed point is repulsive, the $p(a, y)$ fixed point is attractive. This means that, no matter which initial condition one starts from at small a, equation (5.34) always drives $p(a, y)$ to $p_\infty(y)$ as $a \to \infty$. This is obvious from the sign of the $p''(a, y)$ term in (5.34). Thus, it cannot be possible to integrate (5.34) downwards in the same sense as it has not been possible to integrate (5.17) or (5.33) upwards.

A typical objection to the previous argumentation would be: *But I actually can expand the PDE (5.34) around $a = \infty$ and obtain ordinary differential equations!* Indeed, it is not a very striking argument that it is impossible to numerically integrate a differential integration in a specific a direction because one is not able to control the numerical fluctuations. If one only was clever enough, one could eventually solve the PDE analytically, where directions of integrations do not matter[17]. The ultimate reason which prevents the solution of $p(a, y)$ near $a = \infty$ by means of an expansion around $a = \infty$ is that no expansion in the style of (5.24) can exist which obeys the normalization condition $\int_{-\infty}^{\infty} dy\, p(a, y) = (a + 1)^2$ and so the answer to the objection is: Yes, you can expand (5.34), but the expansion is not element of the space of the allowed (i.e. properly normalized) functions $p(a, y)$.

Technically, the solutions of the differential equation (5.34) with an initial condition at $a = \infty$ are nonunique. Because of the complicated type of the differential equation, however, it is hard to analyze its existence and uniqueness properties. The Cauchy-Kowalevski theorem [Fol95] gives a hint. The local existence and uniqueness of a Cauchy initial value problem is only shown for analytical coefficient functions. The coefficient functions of (5.34), however, are singular at $a = \infty$ and so, according to the Cauchy-Kowalevski

[17] Other numerical methods for solving PDEs which reduce the influence of high frequency fluctuations are (pseudo-)spectral codes. They might also be capable of numerically integrating the PDEs in the wrong direction

theorem, the solution need not be unique. Thus, the singularity of (5.34) at $a = \infty$ is responsible for the violation of the PaT projection hypothesis at $T = 0$. But the same argumentation would also be applicable to the $m(a, y)$ differential equation, the solution of which is obviously unique. After all, there is, to my best knowledge, no theorem in the theory of partial differential equations which allows to proof unambiguously the uniqueness of the solution of (5.33) and the nonuniqueness of the solution of (5.34) so that this statement can only be tested numerically.

5.4.4 Self-consistence in the full continuous a interval

For the full solution of the zero temperature continuous RSB one must solve the self-consistence equations numerically for $0 \leq a < \infty$. The initial condition for $m(a, y)$ can be obtained at finite a by means of the expansion technique of Section 5.3.2. The initial condition for $p(a, y)$ is a Dirac delta function which is numerically inconvenient. The dominant part of (5.34) for nearly delta peaked functions, however, is a diffusion equation which can be solved analytically. Thus one can use a properly rescaled Gaussian distribution (which is the solution of the diffusion equation with a $\delta(y)$ initial condition) at $a > 0$ as an initial condition for $p(a, y)$.

The remaining integrations must be performed numerically. This has been done in the present work only to the extent that the practical solubility can be checked. The differential equations have been integrated by the `NDSolve[]` routine of *Mathematica*®. It turns out that the differential equations can indeed be solved numerically with considerable accuracy. However, again a much larger accuracy is needed in order to obtain a self-consistent order function $q(a)$ at infinite RSB which is comparable in accuracy to the high precision computations of Chapter 4. One only can say that, within a numerical error of $\epsilon \simeq 0.005$, the 200 RSB order function is reproduced by the present infinite RSB method. In Figure 5.8, the numerical solutions of the functions $m(a, y)$ and $p(a, y)$ are shown.

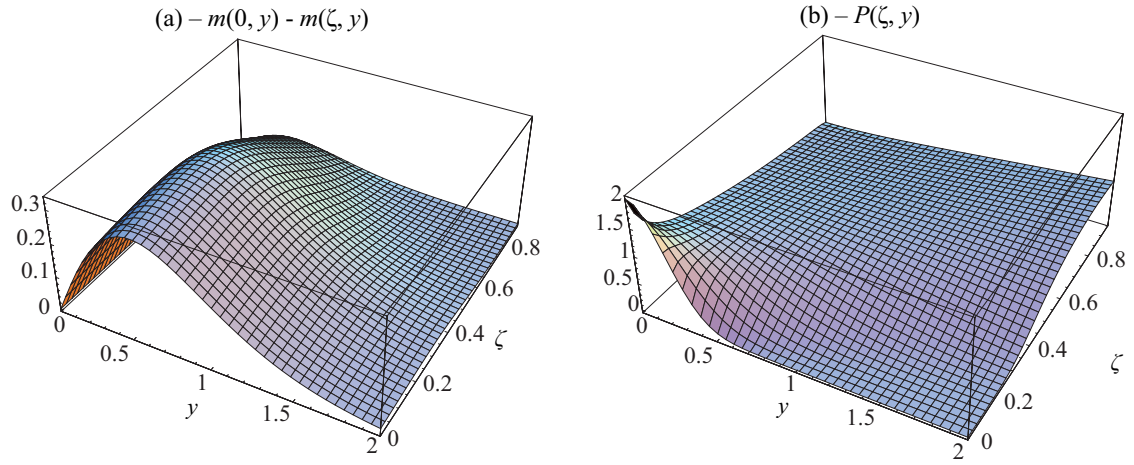

Fig. 5.8: Numerical solutions of the partial differential equations (5.33) and (5.34). Part (a) shows the difference $m(0, y) - m(\zeta, y)$ in order to resolve the variations on the ζ or a scale. In Part (b), the absolute $p(a, y)$ is shown.

Much better accuracy can probably be achieved by utilizing the method of pseudo-spectral codes [For98]. These have been used with great success for the solution of the finite T differential equations [CR02]. The biggest issue at finite temperatures, i.e. the determination of the location of the break point, is absent at $T = 0$ so that it is indeed very likely that such a careful treatment of the PDEs leads to a considerable gain in precision. This, however, is beyond the scope of the present work.

From Figure 5.8 one can see that the nontrivial y-domain in which $p(a, y)$ is non-zero becomes large for $a > 1$, compared to the non-trivial domain of $m(a, y)$ where $m(a, y) < 1$. As a result, the integration (5.35) requires the explicit treatment of a large y-region. Using the normalization condition of $p(a, y)$ this problem can be circumvented and one can write

$$q(a) = 1 - \frac{1}{(a+1)^2} \int_{-\infty}^{\infty} dy\, p(a, y)(1 - m^2(a, y)). \tag{5.39}$$

The integrand in (5.39) is non-zero only in the restricted nontrivial domain $|y| \lesssim 5$ of $m(a, y)$ and one can restrict the treatment of the differential equations to this domain.

5.4.5 Relation to Pankov scaling

It has been pointed out above that the $a = \infty$ expansion of the rescaled Sommers-Dupont partial differential equations in the a formulation leads to the same ordinary differential equations for 0th order in a^{-1} as Pankov obtains for his x-formulation. In the following, I will discuss the relation between those two zero temperature formulations.

As explained in Section 4.3.2, the finite x scale and the finite a scale are inequivalent at zero temperature, while at $T > 0$ there exists a one-one mapping between them. For a complete description of the SK-model at $T = 0$, both scales must be considered. However, the scales are strictly separated by the fixed point at $(a, x) = (\infty, 0)$. This separation allows one to look at one of the two scales without considering the other.

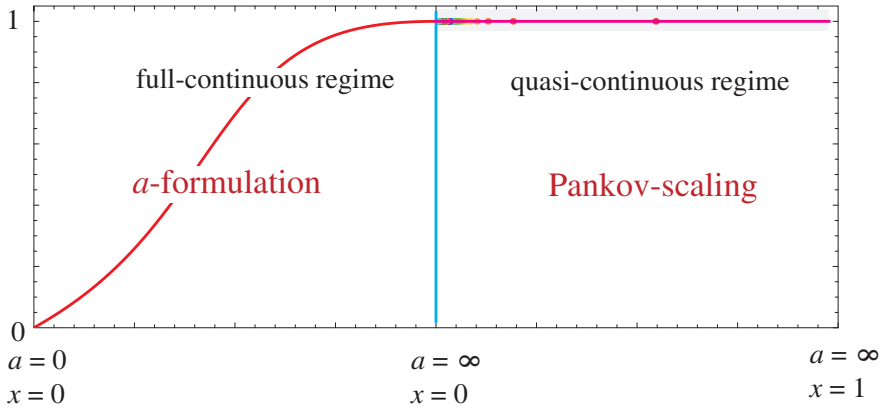

Fig. 5.9: The regimes of Pankov-scaling [Pan06] and of the a-formulation derived in the present work. Both regimes are connected at $a = \infty$ and $x = 0$.

In each of the two formulations, structure is hidden in (or better beyond) the critical point. While the a-formulation mainly resolves the equilibrium properties of the SK-model and the nonequilibrium properties are hidden, it is clear that Pankov-scaling resolves only the nonequilibrium properties and has no access to the fully continuous part of $q(a)$ at $T = 0$.

Another interesting fact is that Pankov describes the finite x regime at $T = 0$ by differential equations. From the point of view of the above discussion, where $x > 0$ has been termed the 'discrete regime', this is rather intriguing. Nevertheless, the resolution of this discrepancy is quite simple: For all finite temperatures one may treat $x > 0$ as a continuous regime. On the other hand, the calculated observables are all continuous in the zero temperature limit as well as in the $\kappa \to \infty$ limit. Thus the order of limits makes no difference for them. For the order function[18], however, the limits do not commute as has been seen in the scaling analysis of Chapter 4. Thus, whether one calls the $x > 0$ regime discrete or continuous is a matter of the order of limits.

[18] Also the finite κ approximation by means of a step function.

Chapter 6

Conclusion and outlook

In this thesis, the low-temperature regime of replica symmetry breaking in the SK-model has been thoroughly investigated. In order to access this regime and to perform self-consistence calculations with high accuracy at high orders of replica symmetry breaking, a formalism has been developed which reduces the numerical effort to the absolute minimum. The central idea of its derivation is the identification of asymptotic regions in which the recursion relations can be solved analytically. The new object in the numerical treatment is then the correction to this asymptotic regime, represented by a sequence of so-called kernel correction functions $\mathrm{ker}\mathcal{C}_i(h)$. This method increased the efficiency of the numerics considerably so that up to 200 orders of RSB could be calculated at zero temperature and zero external field, and up to 60 (65) orders of RSB for finite temperature (external field). The remarkable high precision of these calculations allowed the extraction of several quantities with accuracy exceeding the literature values by several orders of magnitude. For instance, the ground state energy extracted from the $T = 0$ and $h = 0$ calculations

$$E_0 = -0.763\,166\,726\,566\,547$$

exceeds the accuracy of the best literature value [CR02] by 10 orders of magnitude.

The results of the numerical calculations have been analyzed in great detail. Especially the convergence behavior of various observables and of the order function with respect to the RSB order has been investigated since the high but finite RSB regime has been addressed in the present work for the first time. Several unexpected features of finite order replica symmetry breaking have been observed.

- *Discrete spectra* in the Parisi block size ratios at $T = 0$ and $h = 0$ have been found. Normally, it is expected that all block size ratios $\frac{a_i}{a_{i-1}}$ approach unity in the $\kappa \to \infty$ limit and at finite temperature most[1] of them indeed follow this expectation. At zero temperature, however, the large a ratios are smaller than one and thus there is a large spacing between successive block size parameters. The impact of this fact on the continuous $\kappa = \infty$ formulation has been thoroughly investigated and led to a new continuous formulation of Parisi RSB.

- *Scaling* in the variables κ^{-1}, T and h turned out as an important concept for resolving virtual contradictions in the data analysis. The scaling variables always appear together in pairs (κ^{-1}, T) and (κ^{-1}, h) and give rise to temperature vs. RSB order and external field vs. RSB order scaling, respectively. The universal exponents of the crossover lines $\kappa \sim T^{-\nu_T}$ and $\kappa \sim h^{-\nu_h}$ have been extracted and are consistent for all investigated quantities.

- At zero temperature, *two different scales* of the order function are important. The $a < \infty$ regime and the $x > 0$ regime, which are completely equivalent at finite temperatures, become fundamentally different at $T = 0$. While the $x > 0$ regime is trivial in the sense that the order function $q(x > 0) \equiv 1$ there, the $a < \infty$ regime yields nearly all important informations about, e.g., the ground state energy or the effects of a non-zero external field.

The findings from the finite RSB analysis were used to develop a proper continuous zero temperature theory for infinite order replica symmetry breaking in the $a < \infty$ regime. A partial differential equation for the continuous version of the kernel correction function, analogous to the original Parisi equation, has been

[1] The $h = 0$ discreteness which survives at finite temperatures is not as essential as the $T = 0$ discreteness (see Sec. 4.3).

derived in the $\kappa \to \infty$ limit. The discreteness at large a invalidates[2] the treatment of Parisi RSB in the $x > 0$ regime in terms of a differential equation directly at $T = 0$. The initial condition of the $a < \infty$ differential equation, however, is defined in this invalidity domain. An analysis of the $a \to \infty$ limit of the continuous formulation led to the introduction of a new initial condition. It has been argued that in the discrete $x > 0$ regime, the kernel correction function is driven to this initial condition at the point $(a, x) = (\infty, 0)$ by the discrete recursion sequence. Some preliminary solutions of the proposed zero-temperature continuous RSB formalism have been given and they are in excellent agreement with the finite order RSB calculations at $T = 0$.

Though, many features of the low-temperature regime of Parisi RSB have been identified and analyzed, according to the well known adage *"The more you know, the more you know you don't know."* [TOP97], lots of new questions appeared during this work which have not been answered, yet. One of the most fundamental questions is whether the zero temperature discreteness in the block size ratios and in the $x > 0$ regime can actually be detected within numerical simulations of the ground state of classical spin glass models. Since the discrete regime corresponds to short time scale behavior, there is at least in principle a chance to observe such behavior in Monte-Carlo simulations. The lack of a satisfactory interpretation of this discreteness, however, hampers the design of such an experiment. Thus, translating the formal statements about the $x > 0$ regime from the present work as well as from Ref. [Pan06] to 'real space' would be the first step for addressing this issue.

Another, maybe more straightforward task is the systematic numerical analysis of the classical n-component glasses according to the formalism which has been proposed in the present work. Those results for $n = 2, 3$ are needed for a successfull investigation of dynamics in quantum glasses at low temperatures. This task turned out to be extremely intricate at low temperatures [Bec04] because in the limit $T \to 0$, the number of Matsubara frequencies, which must be considered, diverges. At $T = 0$ and $\kappa = \infty$ directly, however, there could be the hope that at least the equilibrium part ($a < \infty$) of the problem can be treated with the continuous formalism which has been proposed in this work.

In any case, the continuous $T = 0$ formalism, derived in Chapter 5, deserves a thorough investigation with the help of advanced techniques for solving partial differential equations. The high precision ground state energy which has been found in this work can serve as a benchmark for such a program. More knowledge about the singular points in the differential equations at $(a, x) = (\infty, 0)$, gained from the further analysis, would also be extremely useful for the topics pointed out above.

[2] It seems, however, that a continuous treatment of the $x > 0$ regime is possible. For a discussion of this issue, see Section 5.4.5.

Zusammenfassung

In der vorliegenden Dissertation wurden die Eigenschaften der Replikasymmetriebrechung (RSB) im Sherrington-Kirkpatrick-Modell bei tiefen Temperaturen gründlich untersucht. Um entsprechend tiefe Temperaturen und sogar $T = 0$ zu erreichen und gleichzeitig die Selbstkonsistenzrechnungen mit hoher numerischer Genauigkeit und bei hohen RSB Ordnungen durchzuführen, wurde ein Formalismus entwickelt, welcher den numerischen Aufwand auf ein absolutes Minimum reduziert. Das zentrale Konzept der Ableitung dieser Formulierung ist die Identifikation asymptotischer Bereiche, in denen die Rekursionsgleichungen der Replikasymmetriebrechung bei endlichen Ordnungen analytisch gelöst werden können. Das neue Objekt, welches numerisch behandelt werden muss, ist die Korrektur zu diesen asymptotischen Bereichen, welche durch eine Reihe von Funktionen, den sogenannten *kernel correction functions* $\ker\mathcal{C}_i(h)$ beschrieben wird. Diese Methode hat die Effizienz der numerischen Behandlung erheblich verbessert, so dass bis zu 200 RSB Ordnungen bei verschwindender Temperatur und bei verschwindendem Magnetfeld und bis zu 60 (65) RSB Ordnungen bei endlichen Temperaturen (Magnetfeldern) berechnet werden konnten. Die ungewöhnlich hohe Genauigkeit dieser Rechnungen erlaubte die Bestimmung vieler Observablen mit einer Genauigkeit, die mehrere Größenordnungen über den Literaturwerten liegt. Zum Beispiel wurde die Energie des Grundzustandes aus den Ergebnissen der RSB Rechnungen bei verschwindender Temperatur und bei verschwindendem Magnetfeld zu

$$E_0 = -0.763\,166\,726\,566\,547$$

bestimmt. Dieser Wert übertrifft die Genauigkeit des besten Literaturwertes [CR02] um 10 Größenordnungen.

Die Ergebnisse der numerischen Rechnungen wurden im Detail analysiert. Speziell das Konvergenzverhalten der Ordnungsfunktion und der interessanten Observablen als Funktionen der RSB Ordnung wurde untersucht. Dieser Bereich hoher, aber endlicher RSB Ordnungen wurde in der vorliegenden Arbeit das erste mal analysiert und viele unerwartete Eigenschaften wurden gefunden. Die wichtigsten sind:

- *Diskrete Spektren* in den Parisi Blockgrößenverhältnissen bei verschwindender Temperatur und verschwindendem Magnetfeld wurden beobachtet. Normalerweise würde man erwarten, dass bei unendlich hoher RSB Ordnung alle Blockgrößenverhältnisse $\frac{a_i}{a_{i-1}} = 1$ sind. Bei endlichen Temperaturen wird diese Erwartung auch von den meisten[3] Blockgrößenverhältnissen erfüllt. Bei $T = 0$ sind die Verhältnisse, welche zu großen a gehören, jedoch kleiner als eins, was zu einem großen Abstand zwischen den Parisi Blockgrößen führt. Die Konsequenzen dieser Diskretheit wurden ausführlich untersucht. Diese Untersuchung führte zu einer neuen kontinuierlichen Formulierung der Parisi Replikasymmetriebrechung.

- *Skalenverhalten* in den Variablen κ^{-1}, T und h ist ein wichtiges Konzept um scheinbare Widersprüche in der Analyse der Daten aufzulösen. Die Skalenvariablen treten immer in Paaren (κ^{-1}, T) und (κ^{-1}, h) auf und führen zum Skalenverhalten der Temperatur mit der RSB Ordnung, bzw. des Magnetfeldes mit der RSB Ordnung. Die universellen Exponenten der Übergangslinien $\kappa \sim T^{-\nu_T}$ und $\kappa \sim h^{-\nu_h}$ wurden bestimmt und sind konsistent für alle untersuchten Größen.

- Bei verschwindender Temperatur wurden *zwei verschiedene relevante Skalen* der Ordnungsfunktion gefunden. Der Bereich $a < \infty$ und der Bereich $x > 0$, welche bei endlichen Temperaturen equivalent sind, sind bei exakt $T = 0$ grundlegend verschieden. Während der $x > 0$ Bereich trivial ist, in dem Sinne, dass die Ordnungsfunktion $q(x > 0) \equiv 1$ ist, beschreibt der $a < \infty$ Bereich nahezu alle wichtigen Eigenschaften des Modells, wie z.B. die Energie des Grundzustandes oder die Wirkung eines endlichen Magnetfeldes.

[3] Die durch endliche Magnetfelder kontrollierte Diskretheit, welche auch bei endlichen Temperaturen auftritt ist nicht so fundamental wie die Diskretheit, welche durch endliche Temperaturen kontrolliert wird.

Die Resultate der Analyse der endlichen RSB Ordnungen wurden für die Entwicklung einer kontinuierlichen $T = 0$ Theorie bei unendlichen RSB Ordnungen benutzt. Eine partielle Differentialgleichung für die kontinuierliche Version der *kernel correction function* wurde, in Analogie zur Parisidifferentialgleichung, abgeleitet. Die Diskretheit bei großen a führt dazu, dass die Behandlung der Parisi RSB bei $T = 0$ für $x > 0$ nicht in Form einer Differentialgleichung möglich ist. Da die Anfangsbedingung der partiellen Differentialgleichung für die kernel correction function aber im Bereich $x > 0$ definiert ist, musste diese durch eine Anfangsbedingung bei $(a, x) = (\infty, 0)$ ersetzt werden. Diese wurde durch eine Analyse der $a \to \infty$ Verhaltens der partiellen Differentialgleichung gefunden. Einige vorläufige numerische Lösungen der vorgeschlagenen kontinuierlichen $T = 0$ Theorie der Parisi RSB wurden angegeben, welche mit den Rechnungen bei endlichen RSB Ordnungen sehr gut übereinstimmen.

Acknowledgments

- First of all I want to express my deep gratitude to my supervisor Prof. Dr. Reinhold Oppermann. Thank you for giving me the opportunity to participate in such an interesting research project, for your support, for all the stimulating discussions about physical topics and especially for the discussions about things beyond our actual project.
- I am also indebted to Prof. Dr. Laurens W. Molenkamp, Prof. Dr. Björn Trauzettel and Prof. Dr. Werner Hanke for additional financial support of this work.
- Especially, I would like to emphasize my thankfulness for all the discussions with Prof. Dr. Björn Trauzettel and Prof. Dr. Laurens W. Molenkamp. It has always been delightful to talk with you about all kinds of things - physical and non-physical.
- Special thanks go to Dr. Charles Gould. Thank you very much for all the help with publications, the English tips, the funny chats, the latest news and last but not least the nice anecdotes from your conferences.
- I also want to thank my colleagues Jutta Ortloff and David Luitz for interesting discussions about nearly everything one can talk about. It really has been a privilege for me to share an office with you.
- Last but not least, I want to thank my family and especially my wife Elisabeth for her support and her patience particularly during the last few months. Thank you also for patiently listening to me talking about spin glasses and RSB, even if you probably didn't understand a word.

Appendix A

Proofs and derivations

A.1 Steepest descent and replica limit

In Chapter 2 the field variables $\tilde{\mathbf{q}}$ and $\tilde{\mathbf{m}}$ in equation (2.9) are to be fixed by a saddle point argument. This shall be discussed in some detail here in connection with the replica limit. The system size N is assumed to be sufficiently large so that the finite size error vanishes. In order to streamline notation, I define a d-dimensional vector $\mathbf{v}$ of field variables with $d = nl\frac{l+3}{2}$. Within this notation, equation (2.9) reads

$$\int \mathcal{D}\tilde{\mathbf{m}}\, \mathcal{D}\tilde{\mathbf{q}}\, e^{-\beta N g(l,\tilde{\mathbf{m}},\tilde{\mathbf{q}})} = A_l \int d^d\mathbf{v} e^{-\beta N g(\mathbf{v})} \tag{A.1}$$

with

$$A_l = \prod_\nu \left[\left(\frac{N\beta J_0^\nu}{2\pi}\right)^{\frac{l}{2}} \left(\sqrt{\frac{N}{2\pi}}\beta J_\nu\right)^{l\frac{l-1}{2}} \left(\sqrt{\frac{N}{\pi}}\frac{\beta J_\nu}{2}\right)^{l} \right] \sim \sqrt{N}^d. \tag{A.2}$$

It is assumed that $g(\mathbf{v})$ has a global minimum at $\mathbf{v} = \mathbf{v}_0$ and that it can be expanded in a Taylor-series near this point. One can then evaluate the integral to second order in $\delta\mathbf{v} = \mathbf{v} - \mathbf{v}_0$ and obtains

$$\left\langle Z_{(l)} \right\rangle_d = A_l e^{-\beta N g(\mathbf{v}_0)} \underbrace{\int d^d(\delta\mathbf{v}) \exp\left(-\beta N \frac{(\delta v)^T \mathbf{H} \delta v}{2}\right)}_{=\sqrt{\frac{(2\pi)^d}{\det[\beta N \mathbf{H}]}}} = B_l e^{-\beta N g(\mathbf{v}_0)} \tag{A.3}$$

where $\mathbf{H}$ is the Hessian of $g(\mathbf{v})$ at $\mathbf{v}_0$. The N-dependence of the Gaussian integral cancels the N-dependence of A_l. Further, since B_l is of the form $[...]^l$, the replica limit of B_l is $\lim_{l\to 0} B_l = 1$. The disorder-averaged free energy per spin is

$$f = -\frac{T}{N}\lim_{l\to 0}\frac{1}{l}\left(\left\langle Z_{(l)}\right\rangle_d - 1\right) = -\frac{T}{N}\lim_{l\to 0}\frac{d}{dl} B_l e^{-\beta N g(l,\mathbf{m},\mathbf{q})} = \lim_{l\to 0}\frac{1}{l} g(l,\mathbf{m},\mathbf{q}) - \underbrace{\frac{T\frac{d}{dl}B_l}{N}}_{\to 0}. \tag{A.4}$$

At this point, one can easily understand why the terms neglected in equation (2.6) are irrelevant. These terms are of the form

$$\exp\left(\frac{1}{N}\sum_r\sum_\nu \alpha_\nu \left(\sum_a (S^a_{r\nu})^2\right)^k\right) \tag{A.5}$$

with $k = 1, 2$ and N-independent α_ν. Reconsidering those terms in (2.6) results in the replacement

$$g \to \tilde{g} = ... - T\log\mathrm{tr}\, e^{\tilde{L}}, \qquad \tilde{L} = L + \frac{l^k}{N} a \tag{A.6}$$

where $L_S^{2k}\min_\nu \alpha_\nu \le a \le L_S^{2k}\max_\nu \alpha_\nu$[1]. Since L is of order 1, the terms vanish in the limit $N \to \infty$ and so the free energy per spin is

$$f = \lim_{l\to 0}\frac{1}{l} g(l,\mathbf{m},\mathbf{q}). \tag{A.7}$$

[1] L_S is the length of the classical spin vector.

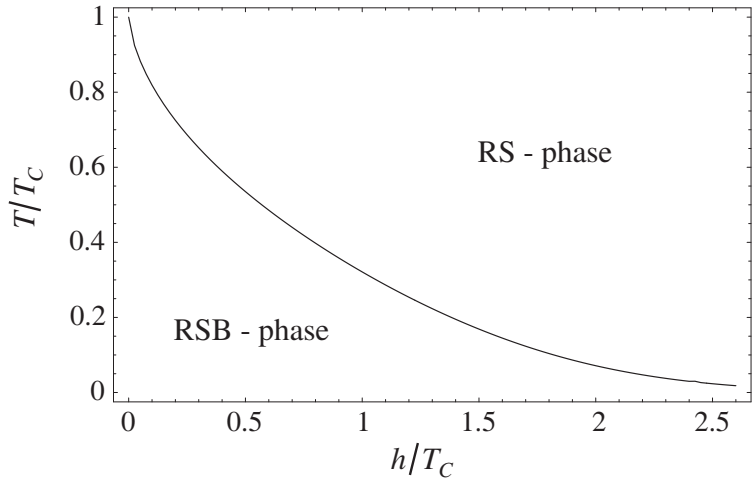

Fig. A.1: The AT-line in the T-h plane. Above the line the RS saddle point is stable while below the line it is unstable and breaking of replica symmetry is required. The AT-line is found by the requirement of only positive eigenvalues of the Hessian $\mathbf{H}$ (see text) in the replica limit $l \to 0$.

An extension of the above argument has been used in [AT78] to investigate the domain of validity of the RS assumption. The authors considered the eigenvalues of the Hessian of $g(\mathbf{v})$ at the replica symmetric saddle point by expressing them in dependence of the number of replicas l. It has been argued that the saddle point is only stable if all eigenvalues of $\mathbf{H}$ are positive in the limit $l \to 0$. The failure of this requirement marks the transition from a RS phase to a RSB phase. This phase boundary in the T-h diagram is called Almeida-Thouless-line (AT-line) and is shown in Figure A.1.

A.2 First integration in the recursion sequence

In the following it is shown that the first integration, i.e. the 0th level of the recursion sequence can be analytically integrated for the quasi-isotropic case and for a general number of components n. The idea is to evaluate the integral by exploiting the definition (2.32) of $\mathcal{C}_n$

$$\int_0^G \mathcal{C}_n(\beta|\tilde{\mathbf{H}}_{\text{eff}}|) = \int_0^G \text{tr } \exp(\beta\, \tilde{\mathbf{H}}_{\text{eff}} \cdot \mathbf{S}) = ... \tag{A.8}$$

and separating the spin components ν

$$... = \text{tr} \prod_\nu \int_{-\infty}^{\infty} \frac{dz_0^\nu}{\sqrt{2\pi}} \exp\left(\beta \tilde{H}_{\text{eff}}^\nu S_\nu\right) = ... \tag{A.9}$$

The components of $\tilde{\mathbf{H}}_{\text{eff}}$ were given by (see equation (2.73))

$$\tilde{H}_{\text{eff}}^\nu = \sqrt{\Delta q_0} z_0^\nu + \underbrace{h + J_0 M + \sum_{i=1}^{\kappa+1} \sqrt{\Delta q_i} z_i^\nu}_{=H_{\text{eff}}^\nu} \tag{A.10}$$

so that the integral can be solved by completing the square

$$... = \text{tr} \prod_\nu \exp\left(\beta H_{\text{eff}}^\nu S_\nu\right) \int_{-\infty}^{\infty} \frac{dz_0^\nu}{\sqrt{2\pi}} \exp\left(-\frac{(z_0^\nu)^2}{2} + \beta\sqrt{\Delta q_0} S_\nu\right) = \text{tr} \prod_\nu \exp\left(\beta H_{\text{eff}}^\nu S_\nu\right) \exp\left(\frac{\beta^2}{2} \Delta q_0 S_\nu^2\right). \tag{A.11}$$

The quadratic spin variable can now be expressed by the normalization constraint *before* performing the spin trace again and one gets

$$\int_0^G \mathcal{C}_n(\beta|\tilde{\mathbf{H}}_{\text{eff}}|) = \text{tr } \exp\left(\beta \mathbf{H}_{\text{eff}} \cdot \mathbf{S}\right) \exp\left(\frac{\beta^2}{2} \Delta q_0 \sum_\nu S_\nu^2\right) = \exp\left(\frac{\beta^2}{2} \Delta q_0 L_S^2\right) \mathcal{C}_n(\beta|\mathbf{H}_{\text{eff}}|). \tag{A.12}$$

The crucial condition for being able to perform the first integration analytically is the independence of J_ν and of Δq_0^ν on the spin component label ν. If the model was anisotropic, then the sum of quadratic spin

components in (A.12) must be replaced by[2]

$$J\Delta q_0 \sum_\nu S_\nu^2 \quad \longrightarrow \quad \sum_\nu J_\nu \Delta q_0^\nu S_\nu^2 \tag{A.13}$$

and the normalization constraint $\mathbf{S}^2 = L_S^2$ could not be exploited. As a result, one must also cope with this first integration numerically.

A.3 Irrelevance of the kernel normalization

The normalization of the kernels (2.32) is shown to be irrelevant in the sense that it only changes the free energy by an additional constant term. This is done for the most general case of κth order of RSB in the quasi-isotropic n-component spin glass model. For this argument, the trace term expression in equation (2.80) is used and all $f_i^{\mathrm{sub}}(h)$ are explicitly written out. Renormalizing $\mathcal{C}_n(\beta h_1) \to \mathcal{N}\mathcal{C}_n(\beta h_1)$ results in

$$\mathcal{T}(h + J_0 M) = \frac{T}{m_\kappa} \int_{\kappa+1}^{G} \log \int_{\kappa}^{GE} ... \int_{2}^{GE} \int_{1}^{G} \left[\mathcal{N}\mathcal{C}_n(\beta h_1)\right]^{m_1} . \tag{A.14}$$

The application of the non-linear Gaussian integral operators $\int_i^{GE}$ imply an exponentiation with $r_{i-1} = \frac{m_i}{m_{i-1}}$ and so the constant $\mathcal{N}$ can be pulled through the integral operators in the fashion

$$... \int_3^{GE} \mathcal{N}^{m_2} \int_2^{GE} \int_1^{G} \left[\mathcal{C}_n(\beta h_1)\right]^{m_1} = ... \int_4^{GE} \mathcal{N}^{m_3} \int_3^{GE} \int_2^{GE} \int_1^{G} \left[\mathcal{C}_n(\beta h_1)\right]^{m_1} = ... \tag{A.15}$$

Pulling $\mathcal{N}$ between the first $\int^{GE}$ operator and the log results in a power m_κ of $\mathcal{N}$ and this cancels with the quotient in front of the trace term. As a result, the replacement $\mathcal{C}_n(\beta h_1) \to \mathcal{N}\mathcal{C}_n(\beta h_1)$ leads to

$$\mathcal{T}(h + J_0 M) \to \mathcal{T}(h + J_0 M) + T \log \mathcal{N} \tag{A.16}$$

This only changes the free energy by a temperature dependent term which vanishes in the derivatives with respect to the order parameters from which the self-consistency equations are obtained.

Also the internal energy u is independent of $\mathcal{N}$. This can be seen from the definition $u = f - \frac{df}{dT}T$ in which linear temperature terms in the free energy cancel. For the entropy $s = -\frac{df}{dT}$, however, the kernel normalization matters. Further, a renormalization of the kernel can be traced back to the original Hamiltonian. It is equivalent of adding a temperature dependent but otherwise constant term of the form $\beta \log \mathcal{N}$ to the Hamiltonian.

A.4 Asymptotic regime of the recursion relations

In this section, it is assumed that the kernel normalization has been chosen such that the asymptotic form of $\mathcal{C}_n(x)$ is given by $e^{L_S x}/(L_S x)^{\frac{n-1}{2}}$. In order to further streamline the notation, I define $l = \beta L_S$. In this case the recursion starts with the initial condition

$$f_0^{\mathrm{sub}}(h_1) = \sqrt{2\pi} \frac{I_{\frac{n}{2}-1}(l h_1)}{(l h_1)^{\frac{n}{2}-1}} \quad \overset{h_1 \to \infty}{\longrightarrow} \quad \frac{e^{l h_1}}{(l h_1)^{\frac{n-1}{2}}} . \tag{A.17}$$

I now show by induction that at finite temperatures $T > 0$ the functions $f_i^{\mathrm{sub}}(h_{i+1})$ obey an asymptotic behavior

$$f_i^{\mathrm{sub}}(h_{i+1}) \quad \overset{h_{i+1} \to \infty}{\longrightarrow} \quad \left(f_0^{\mathrm{sub}}(h_{i+1}) \exp\left(\frac{1}{2} \sum_{j=1}^{i} l^2 m_j \Delta q_j \right) \right)^{m_i} . \tag{A.18}$$

[2]Here, the constant J has been reintroduced in order to be able to distinguish between different J_ν in the anisotropic spin-glass.

By assuming that the asymptotic form of $f_{i-1}^{\rm sub}$ is given by (A.18) one can evaluate $f_i^{\rm sub}(h_{i+1})$ in the limit $h_{i+1}\to\infty$ by completing the square:

$$\int \frac{dh_i}{\sqrt{2\pi\Delta q_i}}\left(\frac{h_i}{h_{i+1}}\right)^{\frac{n-1}{2}}\exp\left(-\frac{(h_{i+1}-h_i)^2}{2\Delta q_i}\right)\left[\exp\left(\frac{m_{i-1}}{2}\sum_{j=1}^{i-1}l^2m_j\Delta q_j\right)\left(\frac{e^{lh_i}}{(L_S\beta h_i)^{\frac{n-1}{2}}}\right)^{m_{i-1}}\right]^{\frac{m_i}{m_{i-1}}}$$
$$=\frac{\exp\left(m_i\left(\frac{1}{2}\sum_{j=1}^{i}l^2m_j\Delta q_j+lh_{i+1}\right)\right)}{l^{\frac{n-1}{2}m_i}h_{i+1}^{\frac{n-1}{2}}}\int\frac{dh_i}{\sqrt{2\pi\Delta q_i}}h_i^{\frac{n-1}{2}(1-m_i)}\exp\left(-\frac{(h_{i+1}-h_i+lm_i\Delta q_i)^2}{2\Delta q_i}\right)\quad\text{(A.19)}$$

The remaining Gaussian integral can be evaluated in the limit $h_{i+1}\to\infty$. Up to terms of order $h_{i+1}^{\frac{n-1}{2}m_i}$ one finds $(h_{i+1}+lm_i\Delta q_i)^{\frac{n-1}{2}(1-m_i)}$. Since $m_i<1$ this term is the only important one. Combined with the h_{i+1} term in the denominator one indeed finds

$$f_i^{\rm sub}(h_{i+1})\overset{h_{i+1}\to\infty}{\longrightarrow}\frac{\exp\left(m_i\left(\frac{1}{2}\sum_{j=1}^{i}l^2m_j\Delta q_j+lh_{i+1}\right)\right)}{(lh_{i+1})^{\frac{n-1}{2}m_i}}.\quad\text{(A.20)}$$

In terms of $a_i=\beta m_i$ the asymptotic form reads

$$\frac{\exp\left(a_i\left(\frac{1}{2}\sum_{j=1}^{i}L_S^2a_j\Delta q_j+L_Sh_{i+1}\right)\right)}{(\beta L_Sh_{i+1})^{\frac{n-1}{2}a_iT}}\quad\text{(A.21)}$$

and in the $T\to0$ limit, where $a_i<\infty$ only the numerator survives while the denominator becomes unity.

A.5 Evaluation of replica sums

In replica theory, one often needs to evaluate sums of functions of matrix elements of ultrametric matrices of the form depicted in Figure 2.1. Typically the sums look like

$$\frac{1}{l}\sum_{a,b}f(q_{ab}^\nu)\quad\text{or}\quad\frac{1}{l}\sum_{a<b}f(q_{ab}^\nu)\quad\text{(A.22)}$$

where the quotient $1/l$ originates from the replica identity (1.3). In the following discussion, the index ν is dropped for convenience, the generalization being straightforward.

With the Parisi scheme for l-dimensional ultrametric matrices where m_i are block sizes chosen such that $\frac{l}{m_i}$ is integer valued, the expressions (A.22) can be evaluated by successively adding contributions from smaller blocks. One starts with the whole matrix which has l^2 matrix elements $q_{\kappa+1}$ and replaces $\frac{l}{m_\kappa}$ diagonal blocks with size $m_\kappa\times m_\kappa$ by matrix elements q_κ. As a result, there are $(l^2-\frac{l}{m_\kappa}m_\kappa^2)=l(l-m_\kappa)$ matrix elements with value $q_{\kappa+1}$. In each diagonal $m_\kappa\times m_\kappa$ block, smaller diagonal blocks are replaced by matrix elements $q_{\kappa-1}$ with the constraint that the smaller blocks with size $m_{\kappa-1}\times m_{\kappa-1}$ fit exactly in the m_κ-blocks, i.e. $\frac{m_\kappa}{m_{\kappa-1}}$ is an integer. After this replacement, one is left with $l(m_\kappa-m_{\kappa-1})$ matrix elements with value q_κ.

This procedure is iterated κ times for κth order of RSB and one obtains

$$\frac{1}{l}\sum_{a,b}f(q_{ab})=f(q_{\kappa+1})(l-m_\kappa)+f(q_\kappa)(m_\kappa-m_{\kappa-1})+...$$
$$...+f(q_i)(m_i-m_{i+1})+...+f(q_1)(m_1-1)+f(q_0).\quad\text{(A.23)}$$

Remarkably, this expression does not explicitly depend on l apart from the first term. An implicit dependence, however, is present in form of the assumptions of $\frac{m_i}{m_{i-1}}$ and $\frac{l}{m_i}$ being integer. In the replica limit $l\to0$, these assumptions become meaningless, of course, and so they simply are relaxed in favor of the assumptions

$$1\geq m_1\geq m_2\geq...\geq m_\kappa\geq0.\quad\text{(A.24)}$$

This step is definitely not a strict mathematical derivation. One finds, however, that within these assumption, the free energy has a maximum in the domain of the block size parameters defined by (A.24), as desired.

In the limit $l \to 0$ the sum can be written by collecting m_i terms as

$$\lim_{l\to 0} \frac{1}{l} \sum_{a,b} f(q_{ab}) = \sum_{i=1}^{\kappa} m_i (f(q_i) - f(q_{i+1})) + (f(q_0) - f(q_1)), \tag{A.25}$$

or equivalently in terms of a parameters (see Section 2.4)

$$\lim_{l\to 0} \frac{\beta}{l} \sum_{a,b} f(q_{ab}) = \sum_{i=1}^{\kappa} a_i (f(q_i) - f(q_{i+1})) + \beta(f(q_0) - f(q_1)). \tag{A.26}$$

In the limit of an infinite number of RSB steps ($\kappa \to \infty$) the parameters m_i become dense[3] on the interval $[0, 1]$. The differences of block size parameters in equation (A.23) then becomes negative[4] infinitesimal and the replica sum can be written in terms of an integral of a function $q(x)$ defined such that $q(x) = q_i$ on the infinitesimal interval $[q_{i+1}, q_i]$. In the traditional m-formulation one finds

$$\lim_{\kappa\to\infty} \lim_{l\to 0} \frac{1}{l} \sum_{a,b} f(q_{ab}) = -\int_0^1 dx f(q(x)) \tag{A.27}$$

whereas in the low-temperature formalism the spin-sum reads

$$\lim_{\kappa\to\infty} \lim_{l\to 0} \frac{\beta}{l} \sum_{a,b} f(q_{ab}) = -\int_0^\beta da f(q(a)) \tag{A.28}$$

with $q(a)$ defined analogously.

A.6 The trace term in the entropy

For the entropy, one must evaluate the temperature derivative of the trace term in the free energy

$$\mathcal{T}(h + J_0 M) = \frac{1}{a_\kappa} \int_{\kappa+1}^{G} \log f_\kappa^{\mathrm{sub}}(h_{\kappa+1}). \tag{A.29}$$

Since the recursion relation and the form of the trace term in a-formulation have no explicit temperature dependence, $\partial_T \mathcal{T}(h + J_0 M)$ can be investigated in terms of the derivative of the initial condition of the f^{sub} recursion. For generality, an additional normalization factor $\mathcal{N}'$ is considered. The kernel $\mathcal{C}_n(\beta h_1) = f_0^{\mathrm{sub}}(h_1)$ is assumed to be normalized in consistence with the literature as described in section 2.2.

$$\frac{\partial}{\partial T} \left[\mathcal{N}' f_0^{\mathrm{sub}}(h_1)\right]^{a_1 T} = \left[\mathcal{N}' C_n(\beta h_1)\right]^{a_1 T} a_1 \left[\log \mathcal{N}' C_n(\beta h_1) - \beta h_1 \frac{\mathcal{C}_n'(\beta h_1)}{\mathcal{C}_n(\beta h_1)}\right]. \tag{A.30}$$

First, the Ising case $n = 1$ shall be discussed. Because of the $h_1 \to -h_1$ symmetry, the discussion is restricted to $h_1 \geq 0$. For $n = 1$, the kernel is $\mathcal{C}_1(\beta h_1) = 2\cosh(\beta h_1)$ and the term in brackets in (A.30) can be written as

$$\log \mathcal{N}' + \log(1 + \delta) + \beta h_1 - \beta h_1 \frac{1 - \delta}{1 + \delta} \tag{A.31}$$

where $\delta = e^{-2\beta h_1}$ is small for $h_1 > 0$ and unity for $h_1 = 0$ when $T \simeq 0$. For any finite h_1, (A.31) becomes $\log \mathcal{N}'$ in the zero temperature limit. For $h_1 = 0$, however, the result of $T \to 0$ is $\log \mathcal{N}' + \log 2$. Such a finite discontinuity with infinitely small width is irrelevant, though, since it vanishes in any integral. Thus, the zero temperature limit of the temperature derivative if the initial condition is

$$\lim_{T\to 0} \frac{\partial}{\partial T} \left[\mathcal{N}' f_0^{\mathrm{sub}}(h_1)\right]^{a_1 T} = a_1 e^{a_1 |h_1|} \log \mathcal{N}'. \tag{A.32}$$

Obviously, the convention $\mathcal{N}' = 1$ leads to the simplification that the entropy s_0 at zero temperature only results from the field term contribution in case of an Ising spin glass, i.e.

$$s_0 = -\frac{\chi_{ne}^2}{4}. \tag{A.33}$$

[3] This is at least true for finite temperatures. The situation at $T = 0$ is more subtle and is discussed in section 4.3.
[4] Since $m_i > m_i + 1$, one obtains $\lim_{\kappa\to\infty}(m_i - m_{i+1}) = -dm$.

This is the convention which is used throughout this work and in the literature. One could formally cure the negative entropy by appropriately choosing the additional normalization $\mathcal{N}' \geq \exp(\chi_{ne}^2/4)$.

A considerably more severe problem, namely a logarithmic divergence, arises in the zero temperature entropy for non-Ising spin systems[5]. For general n, the asymptotic form[6] of $\mathcal{C}_n$, given by equation (2.36) can be exploited to evaluate the zero temperature limit of equation (A.30). One finds

$$\lim_{T\to 0} \frac{\partial}{\partial T} \left[\mathcal{N}' f_0^{\mathrm{sub}}(h_1)\right]^{a_1 T} = a_1 e^{a_1|h_1|} \left[\log \mathcal{N}' + \frac{n-1}{2}\left(1 + \log\left(\frac{2\pi T\sqrt{n}}{h_1}\right)\right)\right]. \tag{A.34}$$

Apart from the usual normalization dependence, represented by the $\log \mathcal{N}'$ term, there is for $n \neq 1$ a divergence in the zero temperature limit. Since this divergence is a general artefact of the classical Hamiltonian (2.1) which is even present in a model without disorder ($J = 0$), the entropy's $\log T$ divergence can be ignored and the proper zero temperature limit is defined as the non-singular part of the whole entropy, i.e.

$$s_n(0) = -n\frac{\chi_{ne}^2}{4}. \tag{A.35}$$

Note, however, that this entropy is not equal to the negative slope of the free energy anymore if $n > 1$.

[5] Indeed, this issue is not restricted to spin-glasses. Also in classical n-component models for, say, a ferromagnet the same divergence is encountered.

[6] Again, the kernel normalization is chosen in consistence with literature, as explained in section 2.2.

Appendix B

The temperature dependence of $A(T)$

In the present chapter, the temperature dependence of the finite κ corrections of the free energy will be discussed in some detail because the analysis is a bit involved and a naive and superficial treatment easily leads to wrong results. The subsequent reasoning shall result in understanding the properties of the expansion

$$f(\kappa, T) \simeq f(\infty, T) + A(T)\kappa^{-4} + B(T)\kappa^{-5} + \mathcal{O}(\kappa^{-6}). \tag{B.1}$$

It has been checked numerically that, at $T = 0$ as well as for finite temperatures, the leading κ correction is indeed the κ^{-4} term, so that $A(T)$ is always the coefficient of the leading κ correction term. In the following, the temperature dependence of $A(T)$ will be investigated. First of all, however, some notes on scaling regimes are in order.

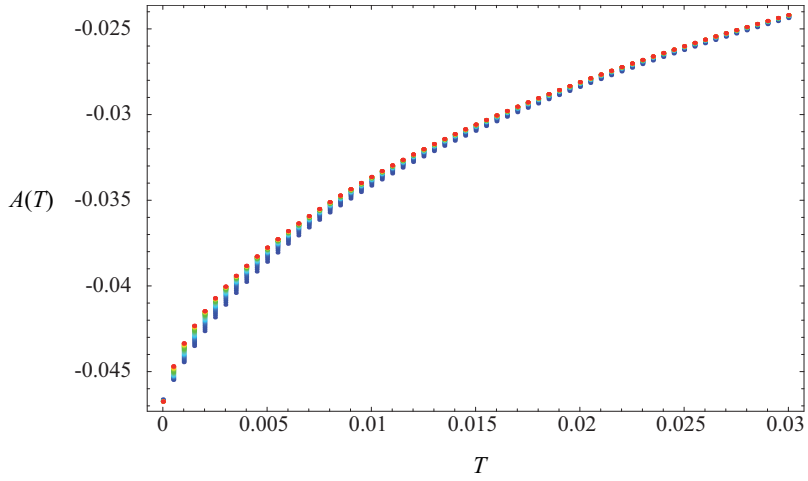

Fig. B.1: The coefficient of the leading κ correction $A(T)$ for temperatures $T = 0, ...0.03$. The different colors correspond to fits to the numerical data in different κ-ranges: the red dots correspond to fits of data between $\kappa = 40, ..., 56$ and the blue dots correspond to a data range $\kappa = 10, ..., 26$. In the fit functions, terms $\kappa^{-4}, ..., \kappa^{-7}$ are respected.

The form of the expansion (B.1) restricts the investigation to the scaling regime $\mathcal{R}_2^T$, because for a fixed temperature $T > 0$ an expansion around $\kappa = \infty$ is considered (see Fig. 4.4). There is, however, only a finite data range $\kappa = 1, ..., 60$ available for finite temperatures. In Figure B.1 one can see the function $A(T)$ as resulting from fits of various κ sub-ranges of the available numerical data to the function $b + A(T)\,\kappa^{-4} + c\,\kappa^{-5} + d\,\kappa^{-6} + e\,\kappa^{-7}$. Obviously, the dependence of $A(T)$ on the data cutoff is stronger for smaller T. This is a result from the scaling terms in the free energy in that the typical RSB orders which are required to stay in scaling regime $\mathcal{R}_2^T$ diverge as $T \to 0$. As a result, only the high T results are really results from the desired scaling regime, while near $T = 0$ the regime $\mathcal{R}_1^T$ is entered. The crossover takes place where the dependence on the data cutoff is largest: while at $T = 0.03$ all investigated data ranges are in $\mathcal{R}_2^T$ and at $T = 0$ all data ranges are in $\mathcal{R}_1^T$, in the intermediate regime $T \simeq 0.005$ the regime affiliation of the data ranges changes with the mean RSB order.

With every finite RSB order calculation one always enters $\mathcal{R}_1^T$ for low temperatures. It is thus quite problematic to obtain a confident prediction of the properties of the expansion coefficient $A(T)$ around $\kappa = \infty$ near $T = 0$. The most straightforward but also most misleading approach might be to fit a function of the form $A(T) \simeq a + bT^z$ to the best available data[1] in Figure B.1. Doing so, one finds $z = \frac{1}{2}$ with a good fit quality as can be observed by comparing the red curve with the data in Figure B.3(a). The exponent $\frac{1}{2}$, however, does not at all fit together with the scaling analysis in Section 4.4. The principal goal is now, to extract a confident value for the exponent z (and maybe also the exponents of the sub-leading terms) from the numerical results.

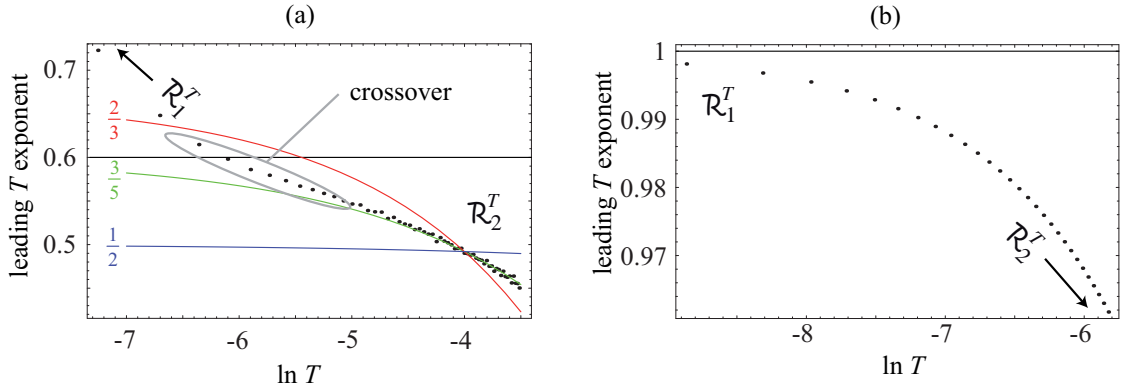

Fig. B.2: The exponent of the leading T-term in $A(T)$ obtained from numerics: Slopes of log-log plots of $A(T)$ in different scaling regimes $\mathcal{R}_1^T$ and $\mathcal{R}_2^T$. The points in Part (a) have been obtained by a fit of data in the range $\kappa = 40, ..., 56$ to a function of the form (B.1). The colored lines are the estimated $T > 0$ corrections of this method under the assumptions of different exponents of the leading term $z = \frac{2}{3}, \frac{3}{5}, \frac{1}{2}$ (see text). Obviously, the $\frac{2}{3}$ exponent fits best in the scaling regime $\mathcal{R}_2^T$. The deviation of the numerical data for lower T signals a crossover from $\mathcal{R}_2^T$ to $\mathcal{R}_1^T$. In Part (b), data in the range $\kappa = 1, ..., 23$ has been used at lower temperatures $T = 0.0001, ..., 0.003$ in order to restrict the analysis to $\mathcal{R}_1^T$. Obviously, the exponent converges to $z = 1$ for $T \to 0$.

Typically, log-log plots are the most robust tool for analyzing the exponents of discrete numerical data which is assumed to originate from a function $f(x) \simeq ax^z$. The slope of $g(t) = \ln f(e^t)$ then approaches z for $t \to -\infty$. In Figure B.2 the slopes of the log-log plot of $A(T) - A(0)$ are plotted as a function of $\ln T$. Obviously, the simple method $z = \lim_{t\to-\infty} \frac{d}{dt} \ln(A(e^t) - A(0))$ for obtaining the leading exponent z is not applicable here. One rather finds that, when considering the region $\ln T > -5$, the exponent seems to converge to $z = \frac{3}{5}$ while for lower T one obtains a larger value for z. The reason for this unusual behavior again lies in the scaling form of the free energy: as indicated in Figure B.2(a), the investigated data in the range $\kappa = 40, ..., 56$ is completely in scaling regime $\mathcal{R}_2^T$ for $\ln T > -5$. The green curve, labeled by the extrapolated exponent $\frac{3}{5}$, serves as a guide to the eye for an extrapolation of z which yields the leading exponent $z = \frac{3}{5}$. It perfectly fits the data for $\ln T > -5$.

For lower T, however, one enters the crossover regime where the numerical data deviates considerably from the green curve. The lowest temperature for which the slope could be obtained for the data range $\kappa = 40, ..., 56$ is $T = 0.0005$. For this temperature, $z \simeq 0.7$ is found. Obviously, this value is still located in the crossover regime, since no convergence for $\ln T \to -\infty$ can be observed when looking at $T \geq 0.0005$. For a proper analysis of the exponent z in the regime $\mathcal{R}_1^T$ in the temperature range $T = 0.0001, 0.0002, ...$ one must reduce the maximum RSB order. In Figure B.2(b) this has been done by analyzing only the range $\kappa = 1, ..., 23$. Obviously, this data range is appropriate for a $\mathcal{R}_1^T$ analysis because the exponent converges to $z = 1$ as $\ln T \to -\infty$. An integer temperature exponent in $\mathcal{R}_1^T$ is consistent with the scaling analysis. Moreover, the integerness of z in $\mathcal{R}_1^T$ is absolutely required by the Taylor-expandability of the free energy near $T = 0$.

The remainder of this section focuses on the determination of z in $\mathcal{R}_2^T$. From Figure B.2(a) one can gain evidence that in the limit $\kappa \to \infty$ and $T \to 0$, the leading T term in $A(T)$ has indeed a leading T exponent $z = \frac{3}{5}$. This is seen by comparing the numerical results to the analytical function[2] $f(x) = ax^z + bx^{2z}$ and the

[1] The best data in this context is the data corresponding to the highest RSB orders.

[2] The reason why I have restricted the sub-leading exponent to twice the leading exponent is that this is a typical situation in scaling theories and, moreover, that it turns out that even with relaxing this constraint, the sub-leading exponent is twice

log-log representation $g(t) = \ln f(e^t)$. The slope of $g(t)$ for large negative t is equal to the leading exponent z, as expected

$$\frac{d}{dt}g(t) \simeq z + 2z\frac{b}{a}e^{zt} + \mathcal{O}(e^{2zt}). \tag{B.2}$$

In addition to the limit $t \to -\infty$ the finite t corrections are respected in the form (B.2). By assuming a fixed exponent z one can fit the remaining parameter $\frac{a}{b}$ in (B.2) to the data set by requiring equality of $\frac{d}{dt}g(t)\big|_{t=t_0}$ with one of the data points at t_0 in the regime $\mathcal{R}_2^T$ as shown in Figure B.2(a). Obviously, only the exponent assumption of $z = \frac{3}{5}$ leads to consistent results: for exponents other than $\frac{3}{5}$, the analytical model only coincides with the data point at t_0 but deviates strongly elsewhere.

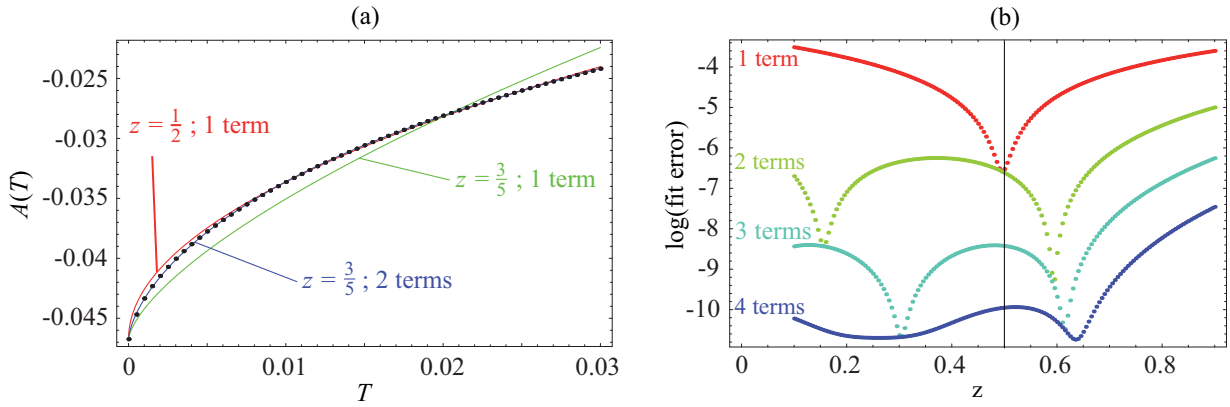

Fig. B.3: Fits of functions $a + bT^z + cT^{2z} + ...$ to the numerical data of $A(T)$: Part (a) shows the quality of the fits with different exponents and different numbers of sub-leading terms. Part(b) shows the error of the best fit (see text) in dependence of the exponent assumption z for different numbers of sub-leading terms.

In Figure B.3 more evidence for a leading T exponent $z = \frac{3}{5}$ in $A(T)$ is presented. In Part (a) one can see the good quality of the $z = \frac{1}{2}$ fit for only one T-term in the fit function which might lead to the *wrong conclusion* of the existence of a $\sqrt{T}$ term in the free energy. With only one term, $z = \frac{1}{2}$ is indeed the only exponent which is capable of fitting the data appropriately (see Part (b)). The $z = \frac{3}{5}$ fit with one term rather suggests that this exponent was wrong. However, the $z = \frac{3}{5}$ fit with two terms shows a nearly perfect reproduction of the numerical data - much better than a two term fit with $z = \frac{1}{2}$. Apparently, the high quality of the $z = \frac{1}{2}$ fit is only a coincidence.

In Figure B.3(b) a systematic analysis of the fit errors $\sum_i \left[A_i - (a + bT_i^z + cT_i^{2z} + ...)\right]^2$, where A_i is the numerical result for $A(T_i)$ from the range $\kappa = 40, ..., 56$, is shown. Obviously, the exponent $z = \frac{1}{2}$ is only stable for restricting the fit to the inclusion of only the leading T-term. When relaxing this restriction, the exponent $z \simeq 0.6$ becomes stable against adding more sub-leading terms to the fit function. The small deviation of the minimum of the fit error from $z = 0.6$ is presumably due to crossover effects because only a finite number of RSB orders are available.

The two independent arguments which have been given above are strong evidence for the leading T exponent in $A(T)$ to be $z = \frac{3}{5}$, rather than $\frac{1}{2}$ as obtained from a naive analysis. Nevertheless, a deviation of z from this prediction cannot be ruled out completely. However, one can be sure that there is an irregular exponent $z < 1$ involved in the $A(T)$ expansion near $T = 0$. From this irregular exponent together with the Taylor expandability of the free energy in $\mathcal{R}_1^T$, one can conclude that this irregular T term must be a scaling term and thus it must fit into the scaling analysis of Section 4.4. The fact that a T^z term with $z \neq \frac{3}{5}$ is hard to include in the scaling picture then gives another indirect evidence for $z = \frac{3}{5}$.

---

the leading.

Appendix C

Definitions and conventions

In the following, the most important definitions and conventions used throughout this work are outlined. Also the convention differences to some of the literature is pointed out, since it often leads to confusion.

C.1 Gaussian integral operators

In the present work, several conventions for the important Gaussian integral operators are used. First of all, they appear in two different forms. One is called the linear Gaussian integral (operator) and is denoted by a G superscript $\int^G$ and the other is the exponentiated Gaussian integral (operator) which is denoted by a GE superscript $\int^{GE}$. Each exponentiated Gaussian integral operator contains its linear counterpart according to

$$\int_i^{GE} f = \int_i^G f^{r_{i-1}} \tag{C.1}$$

where r_i are block-size ratios and f is a general function. The definition of the block-size ratios depends on whether one is in a-formulation or in m-formulation. In m-formulation one has

$$r_i = \frac{m_{i+1}}{m_i}, \qquad r_0 = m_1 \tag{C.2}$$

while in a-formulation the ratios are defined as[1]

$$r_i = \frac{a_{i+1}}{a_i}, \qquad r_0 = a_1. \tag{C.3}$$

Since $a_i = \beta m_i$, the only real difference between the formulations is found for r_0. The linear Gaussian integral operator $\int^G$ is the same for a- and m-formulation. The specific formulation only enters in the exponentiated version. $\int^G$ is used in three different contexts:

- Directly after the replica symmetry breaking scheme is applied, the operator integrates over vector-valued $\mathbf{z}_i$ fields and is defined by (n is the number of spin components)

$$\int_i^G f(\{..., \mathbf{z}_i, ...) = \frac{1}{(2\pi)^{n/2}} \int_{-\infty}^{\infty} d^n \mathbf{z}_i \exp\left(-\frac{|\mathbf{z}_i|^2}{2}\right) f(\{..., \mathbf{z}_i, ...). \tag{C.4}$$

- The transformation to h-field integration leads to a sequence of functions of one vector-valued variable $\mathbf{h}_i$. In this context, the operator reads

$$\int_i^G f(\mathbf{h}_i) = \frac{1}{(2\pi\Delta q_i)^{n/2}} \int_{-\infty}^{\infty} d^m \mathbf{h}_i \exp\left(-\frac{|\mathbf{h}_i - \mathbf{h}_{i+1}|^2}{2\Delta q_i}\right) f(\mathbf{h}_i) \tag{C.5}$$

  with $\Delta q_i = q_i - q_{i+1}$ for $1 \leq i \leq \kappa$ and $\Delta q_{\kappa+1} = q_{\kappa+1}$.

[1] Note the different ratio r_0.

- Exploiting the orientation independence of $f(\mathbf{h}_i)$ in the quasi-isotropic n-component spin glass, the functions of the recursion sequence depend only on $|\mathbf{h}_i| = h_i$ and the operator is

$$\int_i^G f(h_i) = \frac{1}{\Delta q_i} \int_0^\infty dh_i h_i^{\frac{n}{2}} \exp\left(-\frac{h_i^2 + h_{i+1}^2}{2\Delta q_i}\right) \frac{I_{\frac{n}{2}-1}\left(\frac{h_i h_{i+1}}{\Delta q_i}\right)}{h_{i+1}^{\frac{n}{2}-1}} f(h_i) \tag{C.6}$$

  with $I_\alpha(x)$ the modified Bessel function [Wat95].

The context which is used mostly in this work is the a-formulation together with the isotropic h-field integration.

C.2 Parisi block size parameters and matrix elements

The indices of the matrix elements of ultrametric matrices are chosen such that smaller matrix elements and smaller block sizes correspond to higher indices:

$$q_i > q_{i+1}, \qquad m_i > m_{i+1} \tag{C.7}$$

The normalization of $\mathbf{q}^\nu$ is chosen such that the diagonal matrix element of the matrix $\mathbf{q}^\nu$ is q_0^ν (see Fig. 2.1) and is equal to 1 for the quasi-isotropic spin glasses. In the literature, one mostly finds the convention of zero diagonal matrix elements in ultrametric matrices. Also the indices are mostly defined differently in the literature, namely $q_i < q_{i+1}$ and $m_i < m_{i+1}$. Thus, when comparing to the literature, the conventions must be adapted properly.

Appendix D

Numerics of the finite RSB formalism

An important part of the present work was the design of a system of programs which allowed the numerical solution of the self-consistence problem, which has been formulated in Chapter 2 of this thesis, for high orders of RSB. Therefore, I will present a short description of the different parts of the system in the following with the aim of reducing the effort for coming generations of spin glass and RSB researchers in the group of Prof. Oppermann, to assimilate and use this system.

D.1 The program suite

Due to the high numerical cost, it has been indispensable to use more than one computer for the calculations. The need for interactive access to the calculations[1], on the other hand, made the use of supercomputers unattractive for the present problem. The computers which have been used for the numerical solution are the 40 dual-core Opteron 242 computers in the CIP-pool of the Physics Department and the 10 dual-core Opteron 246 computers of the Unix-Cluster of the Department for Theoretical Physics of the University of Würzburg. In addition, some single workstations of our group have been used. All these computers had to be connected appropriately by the system described in the following.

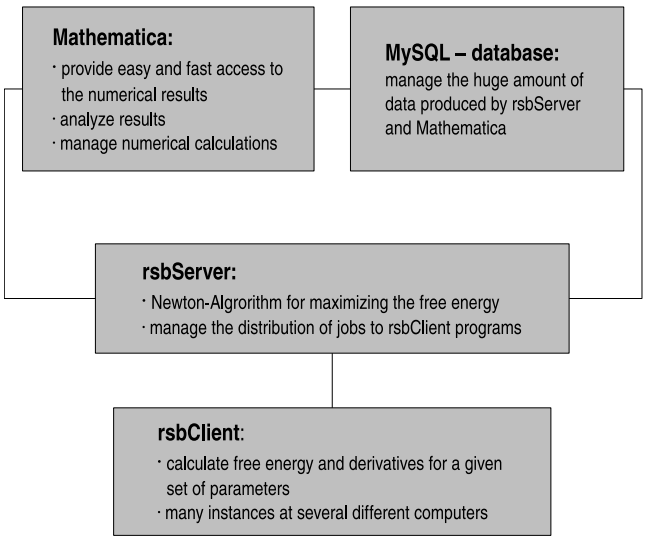

Fig. D.1: Design of the program suite.

The core of the program suite (see Fig. D.1) is the `rsbServer`. This multi-threaded program is responsible for the management of the time consuming calculations of the free energy and its derivatives with respect to the order parameters at a given parameter set as they are needed by the Newton algorithm part of

[1] Interactive access is needed because it is not always clear whether the Newton algorithm, which is used to find the maximum of the free energy, converges. Thus the parameters must be adapted by hand during the calculation.

`rsbServer`. Those calculations are distributed to all attached `rsbClient` programs which run on many different machines (one `rsbClient` for each processor on each computer). The distribution algorithm is such that the free resources of all computers are optimally used. The single calculations are requested by the Newton algorithm part of `rsbServer`, which finds the maximum of the free energy by following the corrected free energy gradient $(\mathbf{H}_f[q(a)])^{-1} \cdot \nabla_{q(a)} f[q(a)]$, where $\mathbf{H}_f[q(a)]$ is the Hessian of the free energy f at $q(a)$. The second derivatives in $\mathbf{H}_f$ are calculated from the $(2\kappa + 1)$ difference quotients of the free energy gradient $\nabla_{q(a)} f[q(a)]$. Thus, for each Newton step one needs $(2\kappa + 2)$ separate calculations from the `rsbClient` program. On the other hand, the main[2] user interface which is written in *Mathematica*® is also connected to the `rsbServer`. From the main user interface, the requests for a self-consistent parameter set with the corresponding free energy are received. The result of a request, after it has been calculated by the Newton algorithm, is stored in a MySQL database which can also be accessed by the user interface so that the results can be analyzed conveniently in *Mathematica*®.

With this system, extensive calculations have been performed for the Ising spin glass. The parameter space which has been covered is

- Up to 200 RSB for $T = 0$ and $h = 0$.
- Up to 30 RSB for $h = 0$ and $T = 0, ..., 0.3$ in steps of $\Delta T = 0.0001$.
- Up to 60 RSB for $h = 0$ and $T = 0, ..., 0.03$ in steps of $\Delta T = 0.0001$ or $\Delta T = 0.00005$.
- Up to 65 RSB for $T = 0$ and $h = 0, ...0.5$ in steps of $\Delta h = 0.001$ or $\Delta h = 0.0005$.

The final results are available in form of a MySQL database dump. For each RSB order κ, there are two tables called `Order`κ`Data` and `Order`κ`FreeEnergy`. In each table, the self-consistent parameters and the free energy are stored, respectively. The (h,T)-coordinates are found in the integer valued columns `hPoint` and `tPoint` from which the real external field and temperature can be obtained by $h = \Delta h \cdot$ `hPoint` and $T = \Delta T \cdot$ `tPoint`. ΔT and Δh are stored in the tables `TemperatureSpacings` and `FieldSpacings`, respectively.

D.2 High precision arithmetics

One main problem, one has to deal with in the numerics, is the weak dependence of the free energy on the order parameters q_i and a_i. Because of this, the usual numerical accuracy of *double* or *long double*[3] variables, which are utilized usually for floating point computations, are not sufficient for higher RSB orders. Because of that, one is forced to use software libraries which implement arbitrary precision floating point arithmetics by using the CPU's exact integer arithmetic unit to emulate high precision floating point operations. This, of course, is much slower than directly using the floating point unit of the CPU. Nevertheless, with the ker$\mathcal{C}$ formulation it is possible to carry out the computations at high RSB orders on a reasonable time scale.

The arbitrary precision implementation, which has been used in the program `rsbClient`, is the MPFR library[4]. It is available on all standard computer architectures, though, for the sake of parallelization and stability, the use of Unix-like systems (all computers which have been used for the numerics had a Linux operating system) is sensible. Also the Newton algorithm in `rsbServer` works with MPFR and thus the network communication between `rsbServer` and `rsbClient` works with MPFR numbers, as well. After the maximum search finished, however, the high precision numbers are truncated to fit in normal double precision variables before they are transfered to the *Mathematica*® user interface and to the MySQL database.

[2] There is also a small user interface in `rsbServer` for the remote computer management.

[3] On standard 64bit CPU's, double variables have a 52 bit mantissa which corresponds to about 16 decimal digits while long double variables have 64 bits to store the mantissa, which corresponds to an accuracy of about 19 decimal digits.

[4] MPFR stands for multi-precision floating-point with correct rounding.

Bibliography

[ABM07] T. Aspelmeier, A. Billoire, E. Marinari, and M. A. Moore. *Finite size corrections in the Sherrington-Kirkpatrick model.* cond-mat/0711.3445 (2007).

[AGS87] D. J. Amit, H. Gutfreund, and H. Sompolinsky. *Statistical Mechanics of Neural Networks near Saturation.* Annals of Physics, **173**, 30 (1987).

[AJK78] J. R. L. de Almeida, R. J. Jones, J. M. Kosterlitz, and D. J. Thouless. *The infinite ranged spin glass with m-component spins.* Journal of Physics C: Solid State Physics, **11**, L871 (1978).

[And70] P. W. Anderson. *Localisation theory and the Cu—Mn problem: Spin glasses.* Materials Research Bulletin, **5**, 549 (1970).

[AT78] J. R. L. de Almeida and D. J. Thouless. *Stability of the Sherrington-Kirkpatrick solution of a spin glass model.* Journal of Physics A: Mathematical and General, **11**, 983 (1978).

[BC03] A. Billoire and B. Coluzzi. *Magnetic field chaos in the Sherrington-Kirkpatrick model.* Physical Review E, **67**, 36108 (2003).

[Bec04] M. Bechmann. *Dynamics in Quantum Spin Glass Systems.* Ph.D. thesis, University of Würzburg (2004).

[Bis90] P. Biscari. *Dynamics of the SK model in the spin-glass phase.* Journal of Physics A, **23**, 3861 (1990).

[Boe05] S. Boettcher. *Extremal Optimization for Sherrington-Kirkpatrick Spin Glasses.* European Physics Journal B, **46**, 501 (2005).

[Bro59] R. Brout. *Statistical Mechanical Theory of a Random Ferromagnetic System.* Physical Review, **115**, 824 (1959).

[BY86] K. Binder and A. P. Young. *Spin Glasses: Experimental facts, Theoretical concepts, and open questions.* Reviews of Modern Physics, **58**, 801 (1986).

[Cas] F. Casiro. *Das Hotel Hilbert.* Spektrum der Wissenschaft Spezial, **2/2005**).

[CGG07] Pierluigi Contucci, Cristian Giardinà, Claudio Giberti, Giorgio Parisi, and Cecilia Vernia. *Ultrametricity in the Edwards-Anderson Model.* Physical Review Letters, **99**, 057206 (2007).

[CLP02] A. Crisanti, L. Leuzzi, and G. Parisi. *The 3-SAT problem with large number of clauses in the ∞-replica symmetry breaking scheme.* Journal of Physics A: Mathematical and General, **35**, 481 (2002).

[CM72] V. Cannella and J. A. Mydosh. *Magnetic ordering in Gold-Iron alloys.* Physical Review B, **6**, 4220 (1972).

[CR02] A. Crisanti and T. Rizzo. *Analysis of the ∞-replica symmetry breaking solution of the Sherrington-Kirkpatrick model.* Physical Review E, **65**, 46137 (2002).

[CRT03] A. Crisanti, T. Rizzo, and T. Temesvari. *On the Parisi-Toulouse hypothesis for the spin glass phase in mean-field theory.* European Physical Journal B, **33**, 203 (2003).

[DGD82] C. de Dominicis, M. Gabay, and B. Duplantier. *A Parisi equation for Sompolinsky's solution of the SK model.* Journal of Physics A: Mathematical and General, **15**, L47 (1982).

[DT92] V. S. Dotsenko and B. Tirozzi. *Replica-symmetry breaking in neural networks.* Physica A, **185**, 385 (1992).

[EA75] S. F. Edwards and P. W. Anderson. *Theory of spin glasses.* Journal of Physics F, **5**, 965 (1975).

[FA86] Y. Fu and P. W. Anderson. *Application of statistical mechanics to NP-complete problems in combinatorial optimization.* Journal of Physics A: Mathematical and General, **19**, 1605 (1986).

[FH86] D. S. Fisher and D. A. Huse. *Ordered Phase of Short-Range Ising Spin-Glasses.* Physical Review Letters, **56**, 1601 (1986).

[Fol95] Gerald B. Folland. *Introduction to Partial Differential Equations.* Princeton University Press (1995).

[For98] B. Fornberg. *A Practical Guide to Pseudospectral Methods.* Cambridge University Press (1998).

[GJ79] M. R. Garey and D. S. Johnson. *Computers and Intractability: A Guide to the Theory of NP-Completeness.* Freeman (1979).

[GP06] G. Gutin and A. P. Punnen. *The Traveling Salesman Problem and its Variations.* Springer (2006).

[HHO06] Kosuke Hamaguchi, J. P. Hatchett, and Masato Okada. *Analytic solution of neural network with disordered lateral inhibition.* Physical Review E, **73**, 051104 (2006).

[HKN02] T. Hosaka, Y. Kabashima, and H. Nishimori. *Statistical mechanics of lossy data compression using a nonmonotonic perceptron.* Physical Review E, **66**, 066126 (2002).

[Hop82] J. J. Hopfield. *Neural networks and physical systems with emergent collective computational properties.* Proceedings of the National Academy of Sciences (USA), **79**, 2554 (1982).

[Hop84] J. J. Hopfield. *Neurons with graded response have collective computational properties like those of two-state neurons.* Proceedings of the National Academy of Sciences (USA), **81**, 3088 (1984).

[KGH67] L. P. Kadanoff, W. Götze, D. Hamblen, R. Hecht, E. A. S. Lewis, V. V. Palciauskas, M. Rayl, J. Swift, D. Aspnes, and J. Kane. *Static Phenomena Near Critical Points: Theory and Experiment.* Review of Modern Physics, **39** (2), 395 (1967).

[Kop94] T. K. Kopec. *Infinite-range-interaction M-component quantum spin glasses: Statistics and dynamics in the large-M limit.* Physical Review B, **50**, 9963 (1994).

[KTJ76] J. M. Kosterlitz, D. J. Thouless, and R. C. Jones. *Spherical Model of a Spin-Glass.* Physical Review Letters, **36**, 1217 (1976).

[LS05] F. Lemmerich and B. Späth. *Evaluation und effiziente Suche in einem 2-Personen-Nullsummen-Spiel am Beispiel von Mühle.* unpublished (2005).

[MP01] M. Müller and S. Pankov. *Mean-field theory for the three-dimensional Coulomb glass.* Physical Review B, **75**, 144201 (2001).

[MPRT04] A. Montanari, G. Parisi, and F. Ricci-Tersenghi. *Instability of one-step replica-symmetry-broken phase in satisfiability problems.* Journal of Physics A: Mathematical and General, **37**, 2073 (2004).

[MPS84] M. Mézard, G. Parisi, N. Sourlas, G. Toulouse, and M. Virasoro. *Nature of the Spin-Glass Phase.* Physical Review Letters, **52**, 1156 (1984).

[MPV87] M. Mezard, G. Parisi, and M. Virasoro. *Spin Glass Theory and Beyond: An Introduction to the Replica Method and Its Applications.* World Scientific Publishing (1987).

[MPZ02] M. Mezard, G. Parisi, and R. Zecchina. *Analytic and Algorithmic Solution of Random Satisfiability Problems.* Science, **297**, 812 (2002).

[MZ96] R. Monasson and R. Zecchina. *Entropy of the K-Satisfiability Problem.* Physical Review Letters, **76**, 3881 (1996).

[MZ97] R. Monasson and R. Zecchina. *Statistical mechanics of the random K-satisfiability model.* Physical Review E, **56**, 1357 (1997).

[MZK99] R. Monasson, R. Zecchina, S. Kirkpatrick, B. Selman, and L. Troyansky. *Determining computational complexity from characteristic 'phase transitions'.* Nature, **400**, 133 (1999).

[Nem87] K. Nemoto. *A numerical study of the pure states of the Sherrington-Kirkpatrick spin glass model - a comparison with Parisi's replica-symetry-breaking solution.* Journal of Physics C, **20**, 1325 (1987).

[NO98] J. W. Negele and H. Orland. *Quantum Many-Particle Systems.* Westview Press (1998).

[Nol04] W. Nolting. *Grundkurs theoretische Physik. Bd.6 : Statistische Physik.* Springer, Berlin (2004).

[OS05] R. Oppermann and D. Sherrington. *Scaling and Renormalization Group in Replica-Symmetry-Breaking Space: Evidence for a Simple Analytical Solution of the Sherrington-Kirkpatrick Model at Zero Temperature.* Physical Review Letters, **95**, 197203 (2005).

[OS08] R. Oppermann and M. J. Schmidt. *Universality class of replica symmetry breaking, scaling behavior, and the low-temperature fixed-point order function of the Sherrington-Kirkpatrick model.* cond-mat/0803.3918 (2008).

[OSS07] R. Oppermann, M. J. Schmidt, and D. Sherrington. *Double Criticality of the Sherrington-Kirkpatrick Model at T=0.* Physical Review Letters, **98**, 128201 (2007).

[Pal82] R. G. Palmer. *Broken ergodicity.* Advances in Physics, **31**, 669 (1982).

[Pan06] S. Pankov. *Low-temperature Solution of the Sherrington-Kirkpatrick Model.* Physical Review Letters, **96**, 197204 (2006).

[Pap94] C. Papadimitriou. *Computational Complexity.* Addison-Wesley (1994).

[Par79] G. Parisi. *Infinite Number of Order Parameters for Spin-Glasses.* Physical Review Letters, **43**, 1754 (1979).

[Par80] G. Parisi. *A sequence of approximated solutions to the S-K model for spin glasses.* Journal of Physics A: Math. Gen., **13**, L115 (1980).

[Par83] G. Parisi. *Order Parameter for Spin-Glasses.* Physical Review Letters, **50**, 1946 (1983).

[PR08] G. Parisi and T. Rizzo. *On Free-Energy Fluctuations in Mean-Field Spin-Glasses.* unpublished (2008).

[PT80] G. Parisi and G. Toulouse. *A Simple Hypothesis for the Spin Glass Phase of the Ininite-Ranged SK model.* Journal de Physique - Lettres, **41**, L361 (1980).

[RS94] Sharad Ramanathan and Eugene Shakhnovich. *Statistical mechanics of proteins with evolutionary selected sequences.* Physical Review E, **50**, 1303 (1994).

[Ruj93] P Rujan. *Finite Temperature Error-Correctiong Codes.* Physical Review Letters, **70**, 2968 (1993).

[RV00] V. G. Rostiashvili1 and T. A. Vilgis. *How to break the replica symmetry in structural glasses.* Europhysics Letters, **49**, 162 (2000).

[Sch03] R. Schilling. *Theories of the Structural Glass Transition.* cond-mat/0305565 (2003).

[SD84] H.-J. Sommers and W. Dupont. *Distribution of frozen fields in the mean-field theory of spin glasses.* Journal of Physics C: Solid State Physics, **17**, 5785 (1984).

[Sho06] A. Shokrollahi. *Raptor codes.* IEEE Transactions on Information Theory, **52**, 2551 (2006).

[SK75] D. Sherrington and S. Kirkpatrik. *Solvable model of a Spin-Glass.* Physical Review Letters, **35**, 1792 (1975).

[SO08] M. J. Schmidt and R. Oppermann. *Method for replica symmetry breaking at and near T=0 with application to the SK-model.* Physical Review E, **77**, 061104 (2008).

[Som81] H. Sompolinsky. *Time-Dependent Order Parameters in Spin-Glasses.* Physical Review Letters, **47**, 935 (1981).

[Sou94] N. Sourlas. *Spin Glasses, Error-Correcting Codes and Finite-Temperature Decoding.* Europhysics Letters, **25**, 159 (1994).

[SRO95] S. Sachdev, N. Read, and R. Oppermann. *Quantum field theory of metallic spin glasses.* Physical Review B, **52**, 10286 (1995).

[SY04] Masatoshi Shiino and Michiko Yamana. *Statistical mechanics of stochastic neural networks: Relationship between the self-consistent signal-to-noise analysis, Thouless-Anderson-Palmer equation, and replica symmetric calculation approaches.* Physical Review E, **69**, 011904 (2004).

[SZ81] H. Sompolinsky and A. Zippelius. *Dynamic Theory of the Spin-Glass Phase.* Physical Review Letters, **47**, 359 (1981).

[TAK80] D. J. Thouless, J. R. L. de Almeida, and J. M. Kosterlitz. *Stability and susceptibility in Parisi's solution of a spin glass model.* Journal of Physics C: Solid State Physics, **13**, 3271 (1980).

[Tal06] M. Talagrand. *The Parisi formula.* Annals of Mathematics, **163**, 221 (2006).

[TAP77] D. J. Thouless, P. W. Anderson, and R. G. Palmer. *Solution of a 'Solvable Model of a Spin Glass'.* Philosophical Magazine, **35**, 593 (1977).

[TGL82] G. Toulouse, M. Gabay, T. C. Lubensky, and J. Vannimenus. *On the order of the spin glass transitions in mean field theory.* Journal de Physique - Lettres, **43**, L109 (1982).

[TOP97] Tower of Power, *Rhythm & Business* (1997).

[TSN05] Koujin Takeda, Tomohiro Sasamoto, and Hidetoshi Nishimori. *Finite-dimensional spin glass and quantum error correcting code.* Physica E, **29**, 720 (2005).

[VTP81] J. Vannimenus, G. Toulouse, and G. Parisi. *Study of a simple hypothesis for the mean-field theory of spin-glasses.* Journal de Physique, **42**, 565 (1981).

[Wat95] G. N. Watson. *A Treatise on the Theory of Bessel Functions.* Cambridge University Press (1995).

[Wes96] D. B. West. *Introduction to Graph Theory.* Prentice-Hall (1996).

[Zel94] A. Zell. *Simulation Neuronaler Netzwerke.* Addison Wesley Longman (1994).

Manuel J. Schmidt - Curriculum Vitae

Institut für Theoretische Physik u. Astrophysik	Phone: ++49 931 888-5892
Lehrstuhl für Theoretische Physik I	Fax: ++49 931 888-5141
Universität Würzburg	
Am Hubland	Manuel.Schmidt@physik.uni-wuerzburg.de
97074 Würzburg, Germany	http://wpfx05.physik.uni-wuerzburg.de

Personal information

Born	02.12.1980 in Schweinfurt, Germany.
Nationality	German.
Marital status	Married, no children.

Education

1991 - 2000	Celtis Gymnasium Schweinfurt.
May 2000	Abitur.
2000 - 2001	Civilian service and participation at the FiPS-project (Früheinstieg ins Physik Studium) of the University of Kaiserslautern (Germany).
2001 - 2005	Study of Physics at the University of Würzburg.
Apr. 2005 - Feb. 2006	Diploma student at the Chair of Prof. Dr. L.W. Molenkamp in Würzburg. Supervising Professor: Prof. Dr. R. Oppermann
Feb. 2006	Physik Diplom with distinction.
since Mar. 2006	Ph. D. student in the group of Prof. Dr. R. Oppermann.

Publications

Method for replica symmetry breaking at and near $T = 0$ with application to the SK-model
Manuel J. Schmidt and R. Oppermann, Phys. Rev. E. 77, 061104 (2008).

Construction and purpose of effective field theories for frustrated magnetic order
R. Oppermann and M.J. Schmidt, Phys. Stat. Sol (c), 4, 3347 (2007).

Bound hole states in a ferromagnetic (Ga,Mn)As environment
M.J. Schmidt, K. Pappert, C. Gould, G. Schmidt, R. Oppermann, L.W. Molenkamp, Phys. Rev. B 76, 035204 (2007).

Control of magnetic anisotropy in (Ga,Mn)As by lithography-induced strain relaxation
J. Wenisch, C. Gould, L. Ebel, J. Storz, K. Pappert, M.J. Schmidt, C. Kumpf, G. Schmidt, K. Brunner, L.W. Molenkamp, Phys. Rev. Lett. 99, 077201 (2007).

Magnetization-Switched Metal-Insulator Transition in a (Ga,Mn)As Tunnel Device
K. Pappert, M.J. Schmidt, S. Hümpfner, C. Rüster, G.M. Schott, K. Brunner, C. Gould, G. Schmidt, L.W. Molenkamp, Phys. Rev. Lett. 97, 186402 (2006).

Double Criticality of the Sherrington-Kirkpatrick Model at T=0
Reinhold Oppermann, Manuel J. Schmidt, David Sherrington, Phys. Rev. Lett. 98, 127201 (2007).